National Library
of Canada

Acquisitions and
Bibliographic Services Branch

395 Wellington Street
Ottawa, Ontario
K1A 0N4

Bibliothèque nationale
du Canada

Direction des acquisitions et
des services bibliographiques

395, rue Wellington
Ottawa (Ontario)
K1A 0N4

Your file Votre référence

Our file Notre référence

NOTICE

The quality of this microform is heavily dependent upon the quality of the original thesis submitted for microfilming. Every effort has been made to ensure the highest quality of reproduction possible.

If pages are missing, contact the university which granted the degree.

Some pages may have indistinct print especially if the original pages were typed with a poor typewriter ribbon or if the university sent us an inferior photocopy.

Reproduction in full or in part of this microform is governed by the Canadian Copyright Act, R.S.C. 1970, c. C-30, and subsequent amendments.

AVIS

La qualité de cette microforme dépend grandement de la qualité de la thèse soumise au microfilmage. Nous avons tout fait pour assurer une qualité supérieure de reproduction.

S'il manque des pages, veuillez communiquer avec l'université qui a conféré le grade.

La qualité d'impression de certaines pages peut laisser à désirer, surtout si les pages originales ont été dactylographiées à l'aide d'un ruban usé ou si l'université nous a fait parvenir une photocopie de qualité inférieure.

La reproduction, même partielle, de cette microforme est soumise à la Loi canadienne sur le droit d'auteur, SRC 1970, c. C-30, et ses amendements subséquents.

Canadä

UNIVERSITY OF ALBERTA

DISTORTIONAL BUCKLING OF STEEL BEAMS

BY

HESHAM S. ESSA

©

A thesis submitted to the Faculty of Graduate Studies and Research in partial fulfillment of the requirements of the degree of Doctor of Philosophy

Department of Civil Engineering

Edmonton, Alberta

Spring, 1993

National Library
of Canada

Acquisitions and
Bibliographic Services Branch

395 Wellington Street
Ottawa, Ontario
K1A 0N4

Bibliothèque nationale
du Canada

Direction des acquisitions et
des services bibliographiques

395, rue Wellington
Ottawa (Ontario)
K1A 0N4

Your file Votre référence

Our file Notre référence

The author has granted an irrevocable non-exclusive licence allowing the National Library of Canada to reproduce, loan, distribute or sell copies of his/her thesis by any means and in any form or format, making this thesis available to interested persons.

L'auteur a accordé une licence irrévocable et non exclusive permettant à la Bibliothèque nationale du Canada de reproduire, prêter, distribuer ou vendre des copies de sa thèse de quelque manière et sous quelque forme que ce soit pour mettre des exemplaires de cette thèse à la disposition des personnes intéressées.

The author retains ownership of the copyright in his/her thesis. Neither the thesis nor substantial extracts from it may be printed or otherwise reproduced without his/her permission.

L'auteur conserve la propriété du droit d'auteur qui protège sa thèse. Ni la thèse ni des extraits substantiels de celle-ci ne doivent être imprimés ou autrement reproduits sans son autorisation.

ISBN 0-315-82189-2

Canada

UNIVERSITY OF ALBERTA

RELEASE FORM

NAME OF AUTHOR: HESHAM SAEID ESSA

TITLE OF THESIS: DISTORTIONAL BUCKLING OF STEEL BEAMS

DEGREE: DOCTOR OF PHILOSOPHY

YEAR THIS DEGREE GRANTED: SPRING, 1993

Permission is hereby granted to the University of Alberta Library to reproduce single copies of this thesis and to lend or sell such copies for private, scholarly or scientific research purposes only.

The author reserves all other publication and other rights in association with the copyright in the thesis, and except as hereinbefore provided neither the thesis nor any substantial portion thereof may be printed or otherwise reproduced in any material form whatever without the author's prior written permission.

(SIGNED)..

PERMANENT ADDRESS:

Department of Structural Engineering
Faculty of Engineering
Ain Shams University
Abbasia, Cairo, Egypt

DATED April 16, 1993

UNIVERSITY OF ALBERTA

FACULTY OF GRADUATE STUDIES AND RESEARCH

The undersigned certify that they have read, and recommended to the Faculty of Graduate Studies and Research for acceptance, a thesis entitled Distortional Buckling of Steel Beams submitted by Hesham S. Essa in partial fulfillment of the requirements for the degree of Doctor of Philosophy.

D.J.L. Kennedy

J.J. Cheng

Theodore V. Galambos

T.V. Galambos

T. Hrudey

T.M. Hrudey

AW Lipsett

A.W. Lipsett

N. Rajaratnam

DATED April 16, 1993

Abstract

In cantilever-suspended span construction, the beams of alternate bays cantilever over the tops of columns and a simple span is suspended between the ends of cantilevers. Secondary framing members such as open-web steel joists can enhance the stability of these beams markedly. The joist-beam connection may enable the joists to provide both lateral and torsional restraints to the beam top flange at discrete locations which in turn is transmitted to the compression flange through the web. With practical sizes of joists, essentially complete (infinite) lateral restraint is provided. The effective torsional restraint, depending on the joist's bending stiffness, the moment-rotation characteristics of the joist-beam connection, the twisting of the braced flange between braces, and local web distortions, is limited. While such restraints have a significant stabilizing effect, the joist loads, which are applied directly at the level of the top flange of the beam, result in a destabilizing effect.

Thirty-three full-scale tests were conducted on two different hot-rolled W-shaped steel cross sections to investigate the effects of different loading conditions and bracing systems on the buckling stability of the beams. The results of these tests show that torsional bracing enhances the stability of the beam much more than the lateral bracing. Also, the favourable residual stress patterns with most of the flanges under tension proved to be beneficial in enhancing the buckling resistance within the elastic range.

A finite element model, featuring plate elements for the web and line elements for the flanges, was adopted to predict the distortional buckling capacity of steel beams under any combination of loading and restraint conditions. This model takes into account inelastic material behaviour, residual stresses and web distortions. The predicted buckling capacities are in good agreement with the experimental results.

Based on the finite element model, a simple design approach was developed for steel beams in cantilever-suspended span construction. In addition, other design procedures are presented for cantilever beams, overhanging beams, suspended beams and simply supported back span beams under lateral and torsional restraints applied at discrete locations to the top flange.

Acknowledgements

This research was completed under the supervision of Dr. D.J.L. Kennedy. His guidance, encouragement, and unlimited help are greatly appreciated.

I would like to thank C. Albert, who worked as a research associate on this project, for his sincere assistance in completing both the analytical and experimental investigations. I would also like to thank E.Y.L. Chien, from the Canadian Institute of Steel Construction, for his technical assistance. The cooperation of the technical staff of the I.F. Morrison Structural Engineering Laboratory is greatly acknowledged. Thanks are also extended to Dr. D.W. Murray for his interest and assistance.

Funding for this research project was provided by the Canadian Institute of Steel Construction supplemented with funds granted to Dr. Kennedy by the Natural Science and Engineering Research Council of Canada.

Finally I wish to express my sincere thanks to the members of my family for their encouragement and support throughout the course of this work.

Table of Contents

Chapter Page

1. INTRODUCTION 1
   - 1.1 General 1
   - 1.2 Objectives 2
   - 1.3 Scope 2
2. LITERATURE REVIEW 4
   - 2.1 General 4
   - 2.2 Distortional buckling 4
   - 2.3 Stability of uniform beams restrained along one flange 6
     - 2.3.1 General 6
     - 2.3.2 Analytical investigations 8
     - 2.3.3 Experimental investigations 13
   - 2.4 Stability of cantilever and overhanging beams 15
   - 2.5 Stability of suspended beams 18
   - 2.6 Stability of steel beams in cantilever-suspended span construction 19
   - 2.7 Comparisons 22
3. BEAM CHARACTERISTICS 27
   - 3.1 General 27
   - 3.2 Beam types, dimensions and geometric properties 27
   - 3.3 Measurement of initial geometric imperfections 29
   - 3.4 Tension coupons 31
   - 3.5 Residual stresses 32
   - 3.6 Stub columns 34
4. EXPERIMENTAL PROGRAM 57

4.1 General 57
4.2 Test setup 58
4.3 Loading and restraint configurations 60
4.4 Simulation of boundary conditions 62
  4.4.1 Top flange restraint 63
  4.4.2 Bottom flange loaded with no restraints 65
  4.4.3 Restraint at the columns 65
4.5 Instrumentation 66
4.6 Testing procedure 68
5. DISTORTIONAL BUCKLING TESTS OF STEEL BEAMS 87
5.1 Introduction 87
5.2 Results of experimental and finite element analyses 88
5.3 General observations 89
  5.3.1 Test-to-predicted ratios 89
  5.3.2 Effects of residual stresses 90
  5.3.3 Double cantilever beams 93
  5.3.4 Buckled shapes 93
  5.3.5 Effect of lateral and torsional restraints 96
  5.3.6 Web distortion and effect of stiffeners 100
  5.3.7 Effect of lack of lateral restraint at column locations 103
  5.3.8 Effect of shape of bending moment diagram 105
  5.3.9 Load-strain behaviour and strain distributions 107
  5.3.10 Load-deflection behaviour 109
  5.3.11 Experimental errors 112
6. FINITE ELEMENT ANALYSIS 155
6.1 General 155

6.2 Basic assumptions 157
6.3 Material properties 159
6.4 Structural element stiffnesses 160
  6.4.1 Flanges 160
  6.4.2 Web 162
  6.4.3 Stiffeners 166
6.5 Geometric element stiffnesses 166
  6.5.1 Flanges 166
  6.5.2 Web 168
6.6 Restraints 172
6.7 Solution technique 173
6.8 Computer program 176
  6.8.1 Introduction 176
  6.8.2 Mesh characteristics 176
  6.8.3 Input data 177
  6.8.4 Solution methodology 181
7. DESIGN PROCEDURES FOR LATERALLY UNSUPPORTED BEAMS 199
7.1 Introduction 199
7.2 Built-in cantilever beams 199
  7.2.1 Cantilevers with free tips 200
  7.2.2 Lateral restraint at top flange 201
  7.2.3 Lateral restraint of top and bottom flanges 201
  7.2.4 Effect of load position 202
7.3 Overhanging beams 203
7.4 Stability of suspended and spreader beams 206
  7.4.1 Suspended beams under self-weight 206

7.4.2 Spreader beams ... 209

7.5 Stability of restrained beams ... 210

7.5.1 Simply supported beam under uniform moment ... 211

7.5.2 Simply supported beam under nonuniform moment ... 214

7.6 Design of beams in cantilever-suspended span construction ... 217

7.6.1 Basic assumptions ... 220

7.6.2 Critical bending moment diagrams ... 221

7.6.3 Design of beams with fork supports ... 224

a) Case 1 ... 224

b) Case 2 ... 227

c) Case 3 ... 228

d) Resistance factors ... 229

7.6.4 Design of beams without fork supports ... 231

8. CONCLUSIONS ... 258

8.1 Observations and conclusions ... 258

8.2 Areas of further research ... 262

REFERENCES ... 264

APPENDIX A ... 274

APPENDIX B ... 294

APPENDIX C ... 306

APPENDIX D ... 308

List of Tables

Table Page

3.1 Cross-sectional dimensions of W360x39 specimens.................. 37

3.2 Cross-sectional dimensions of W310x39 specimens.................. 38

3.3 Cross-sectional properties of test beams.................................... 39

3.4 Average initial imperfections in different studies........................ 40

3.5 Mechanical properties of W360x39 tension coupons.................. 41

3.6 Mechanical properties of W310x39 tension coupons.................. 42

3.7 Stub column test results... 43

5.1.a Test and predicted loads for tests 1 through 12............................ 118

5.1.b Test and predicted loads for tests 13 through 24.......................... 119

5.1.c Test and predicted loads for tests 25 through 33.......................... 120

5.2.a Theoretical predictions demonstrating the beneficial effects of residual stresses on tests 1 through 12......................... 121

5.2.b Theoretical predictions demonstrating the beneficial effects of residual stresses on tests 13 through 24....................... 122

5.2.c Theoretical predictions demonstrating the beneficial effects of residual stresses on tests 25 through 33....................... 123

5.3 Finite element predictions, effect of shape of bending moment diagram... 124

7.1 Effective length factors for built-in cantilevers........................... 233

7.2 Ratios of maximum to minimum factored loads......................... 234

D.1 Verification of design procedure, Case 1.................................... 309

D.2 Verification of design procedure, Case 2.................................... 313

D.3 Verification of design procedure, Case 3.................................... 318

Table Page

D.4 Verification of design procedure, Beams without fork supports.......... 322

List of Figures

Figure Page

2.1 Effective length factors for cantilever and overhanging beams given by the SSRC Guide (Galambos 1988) 24

2.2 Comparison of restraint conditions at cantilever tip 25

2.3 Cantilever-suspended span construction 26

2.4 Open-web steel joists with bottom chord extension 26

3.1.a Initial sweep of W360x39 specimens 44

3.1.b Initial sweep of W310x39 specimens 45

3.2.a Initial twist of W360x39 specimens 46

3.2.b Initial twist of W310x39 specimens 47

3.3.a Initial camber of W360x39 specimens 48

3.3.b Initial camber of W310x39 specimens 49

3.4 Identification and location of tension coupons for W360x39 50

3.5 Identification and location of tension coupons for W310x39 51

3.6 Test specimens for residual stress determination 52

3.7 Sectioning scheme of cross sections for residual stress determinations 53

3.8 Residual stresses 54

3.9 Stub column stress-strain curve for W360x39 55

3.10 Stub column stress-strain curve for W310x39 56

4.1 Schematic diagram of test setup 70

4.2 Overall test setup 71

4.3 Loading frame 72

Figure Page

4.4 Schematic diagram of a typical loading frame.............................. 72

4.5 Loading jack and load cell.. 73

4.6.a Loading and restraint configurations for tests
1 through 12.. 74

4.6b Loading and restraint configurations for tests
13 through 24.. 75

4.6c Loading and restraint configurations for tests
25 through 33.. 76

4.7 Determination of the height of load application
and the height of lateral restraint.. 77

4.8 Details of two different arrangements for free top
flange at a loading point.. 78

4.9 Top flange loaded freely using ball bearings.................................. 79

4.10 Details of lateral restraint condition of top flange......................... 79

4.11 Details of lateral and torsional restraint for top flange.................. 80

4.12 Details of torsional restraint for top flange.................................... 80

4.13 Details of bottom flange loaded with no restraint.......................... 81

4.14 Fork support at column location equivalent to joist
connection with bottom chord extension...................................... 82

4.15 Details of torsional restraint for bottom flange
at column location.. 83

4.16 Stations for measuring displacements... 84

4.17 Details of a measuring displacement station.................................. 84

4.18 Locations of strain gauges on the cross section
at a typical station.. 85

Figure Page

4.19 Strain gauge identification numbers and locations along a beam specimen........ 86

5.1 Finite element mesh used to predict buckling loads for tests 1 through 32........ 125

5.2 Finite element mesh used to predict buckling load for tests 33........ 125

5.3 End view of buckled specimen in test 33........ 126

5.4 Buckling displacements of test 3........ 127

5.5 Buckling displacements of test 4........ 128

5.6 Buckling displacements of test 7........ 129

5.7 Buckling displacements of test 27........ 130

5.8 Buckling displacements of test 28........ 131

5.9 Predicted normalized buckled shape, test 3........ 132

5.10 Predicted normalized buckled shape, test 4........ 132

5.11 Predicted normalized buckled shape, test 7........ 133

5.12 Predicted normalized buckled shape, test 27........ 133

5.13 Predicted normalized buckled shape, test 28........ 134

5.14 Measured and predicted buckled shapes, test 3........ 135

5.15 Plan view of longitudinal buckled shape in test 5........ 136

5.16 Deflected shape of the cross section at the interior support and the cantilever tip in test 26........ 136

5.17 End view of distorted cross section at the cantilever tip, test 4........ 137

5.18 End view of distorted cross section at the cantilever tip, test 11........ 137

Figure Page

5.19 End view of distorted cross section at the cantilever tip, test 20 138

5.20 End view of distorted cross section at the cantilever tip, test 31 138

5.21 Restraint and loading conditions used to investigate the effect of bending moment diagrams 139

5.22 Load versus longitudinal flange strains, strain gauges 3 and 6, test 4 140

5.23 Load versus longitudinal flange strains, strain gauges 4 and 5, test 4 141

5.24 Load versus longitudinal flange strains, strain gauges 7 and 10, test 4 142

5.25 Load versus vertical web strains, strain gauges 1 and 2, test 4 143

5.26 Strain distributions obtained from gauges 38 through 45 at buckling load of test 3 144

5.27 Load versus strains, gauges 38 and 41, test 21 145

5.28 Load versus strains, gauges 42 and 45, test 21 146

5.29 Lateral deflection behaviour of bottom flange at one-third point of back span, test 17 147

5.30 Lateral deflection behaviour of bottom flange at one-third point of back span, test 5 148

5.31 Lateral deflection behaviour of bottom flange at one-third point of back span, test 19 149

5.32 Load-vertical deflection curve of the cantilever tip, test 5 150

Figure Page

5.33 Lateral deflection of bottom flange at cantilever tip, tests 1 and 2 151

5.34 Lateral deflection of bottom flange at cantilever tip, tests 8 and 28 152

5.35 Lateral deflection of bottom flange at cantilever tip, first and second loadings of test 17 153

5.36 Lateral deflection of top flange at one-third point of back span, tests 6 and 7 154

6.1 Coordinate system and finite element model 182

6.2 Idealised stress-strain relationship 183

6.3 Residual stress model 184

6.4 Structural stiffness matrix of flange element 185

6.5 Rectangular plate bending element 186

6.6 Stress resultants in a sub-element of plate bending 186

6.7 Structural stiffness matrix of stiffener element 187

6.8 Geometric stiffness matrix of flange element 188

6.9 Vertical displacements used to obtain the work done by vertical loads, applied at different positions 189

6.10 Geometric stiffness matrix of web element due to vertical stresses caused by a load P applied at a distance a above the shear centre but between flanges 190

6.11 Geometric stiffness matrix of web element due to vertical stresses caused by a load P applied at a distance a_2 above the top flange 191

Figure Page

6.12 Geometric stiffness matrix of web element due to vertical stresses caused by a load P applied at a distance a below the shear centre but between flanges 192

6.13 Geometric stiffness matrix of web element due to vertical stresses caused by a load P applied at a distance a_2 below the bottom flange 193

6.14 Simulation of lateral restraint applied at a point other than nodal points 194

6.15 Addition of restraint conditions to the global structural stiffness matrix when lateral restraint is applied at a other than nodal points 194

6.16 Measurement of eigenvalues from a shifted origin 195

6.17 Optimum location for eigenvalue shift 195

6.18 Flow chart for the main program 196

6.19 Flow chart for the main routine 197

6.20 Mesh characteristics 198

7.1 Comparison of design rules with finite element solution for unrestrained tip, top flange loading 235

7.2 Comparison of design rules with finite element solution for unrestrained tip, shear centre loading 235

7.3 Comparison of design rules with finite element solution for laterally restrained tip top flange at tip, top flange loading 236

7.4 Comparison of design rules with finite element solution for laterally restrained tip top flange at tip, shear centre loading 236

Figure Page

7.5 Comparison of design rules with finite element solution for laterally restrained top and bottom flanges at tip.................. 237

7.6 Restraint conditions at the cantilever tip of overhanging beams.. 238

7.7 Loading and geometry of suspended flexural member............... 238

7.8 Buckling load parameter for different lift points........................ 239

7.9 Unique curve of buckling load parameter for members lifted near midspan.. 239

7.10 Buckling load parameter for members lifted near ends............... 240

7.11 Spreader beam lifted at midspan.. 240

7.12 Buckling load parameter for spreader beam lifted at midspan.. 241

7.13 Simply supported restrained beam under uniform moment.. 241

7.14 Simply supported restrained beam under nonuniform moment.. 242

7.15 Effective buckling coefficient for beams under uniform moment.. 242

7.16 Effective buckling coefficient for free-to-warp back span.. 243

7.17 Double overhanging beam with symmetrical geometry, loading and restraint conditions.. 244

7.18 Case studies, effect of shape of bending moment diagram.. 244

7.19 Effect of shape of bending moment on the buckling capacity of forked system.. 245

Figure Page

7.20 Critical loading condition for beams with fork supports............. 246

7.21 Effects of shape of bending moment on the buckling capacity of unforked system.. 247

7.22 Effects of shape of bending moment and torsional restraint on the buckling capacity of unforked system.. 248

7.23 Loading conditions for beams without fork supports.. 249

7.24 Design cases for beams with fork supports................................. 250

7.25 Design curves for beams with fork supports, case 1................... 251

7.26 Design curves for beams with fork supports, case 2................... 252

7.27 Design curves for beams with fork supports, case 3 with $L_c/L = 0.25$.. 253

7.28 Design curves for beams with fork supports, case 3 with $L_c/L = 0.20$.. 254

7.29 Design curves for beams with fork supports, case 3 with $L_c/L = 0.167$.. 255

7.30 Geometry of beams without fork supports.................................. 256

7.31 Design curves for beams without fork supports.......................... 257

B.1 Beam with two overhangs.. 301

B.2 Cross-sectional dimensions, material properties and residual stresses.. 302

B.3 Mesh characteristics of worked example...................................... 303

B.4 Normalized buckling displacements, predicted for the worked example... 304

Figure Page

B.4 Normalized buckled shape, predicted for the worked example........ 305

C.1 Open-web steel joist........ 307

C.2 Equivalent beam model........ 307

List of Symbols

a = height of load application above or below the shear centre
A = Cross-sectional area
$2a_1$ = longitudinal dimension of the web element
a_2 = height of load application above or below the middle surface of the top or bottom flange, respectively
a_3 = height of lateral restraint above the middle surface of the top or bottom flange
A_1 = a coefficient in the expression for the lateral deflection of a flange element
A_2 = a coefficient in the expression for the lateral deflection of a flange element
A_3 = a coefficient in the expression for the lateral deflection of a flange element
A_4 = a coefficient in the expression for the lateral deflection of a flange element
A_f = cross-sectional area of flange element
A_w = cross-sectional area of web element
b = flange width
$[B]$ = a matrix which serves to express the curvatures in terms of nodal degrees of freedom
$2b_1$ = vertical dimension of the web element
C = constant, determined to be 7.29
$\{C\}$ = curvature vector for an elemental area dxdy
C_w = warping constant of the I-cross section
d = depth of the I-cross section

$[D]$ = elastic constitutive matrix of web element

$[D]_{in}$ = inelastic constitutive matrix of web element

dr = shortening displacement of an elemental length of the flange

ds = arc length

E = modulus of elasticity

EI = bending stiffness of a fictitious 2-node element used to simulate lateral restraint above the top flange

EI_{yf} = lateral bending rigidity of a flange section

$(EI_{yf})_i$ = lateral bending rigidity of flange section at node i

$(EI_{yf})_j$ = lateral bending rigidity of flange section at node j

F = interaction factor

$f_1(x)$ = cubic interpolation function associated with w_i

$f_2(x)$ = cubic interpolation function associated with q_{yi}

$f_3(x)$ = cubic interpolation function associated with w_j

$f_4(x)$ = cubic interpolation function associated with q_{yj}

F_j = force in the z direction at node j of the fictitious 2-node element used to simulate lateral restraint above the top flange

F_s = overall safety factor

F_y = yield strength

G = modulus of rigidity

GJ_f = torsional rigidity of a flange section

h = height of load application above the shear centre

h' = distance between the middle surfaces of the flanges

hh = distance between the middle surface of the top flange and the point of lateral restraint

I_1 = moment of inertia of the central portion of the open-web steel joist between end panels

I_2 = moment of inertia of the top chord member of the open-web steel joist

I_s = moment of inertia about the major axis of a stiffener cross section

I_x = moment of inertia about the major axis of the I-cross section

I_y = moment of inertia about the minor axis of the I-cross section

J = Saint Venant torsional constant of the I-cross section

J^* = modified Saint Venant torsional constant of the I-cross section

J_s = Saint Venant torsional constant of a stiffener cross section

k = effective buckling coefficient

k_b = effective length factor

k_s = effective length factor corresponding to shear centre loading

k_t = effective length factor corresponding to top flange loading

K_b = bracing bending stiffness divided by the brace spacing

K_B = bending stiffness of bracing member

K_e = effective continuous torsional restraint stiffness

K_f = effective torsional stiffness of the flange

K_j = stiffness of the beam to brace connection divided by the brace spacing

K_w = web stiffness

$[K]$ = global structural stiffness matrix

$[K_g]$ = global geometric stiffness matrix

$[K_g]_p$ = global geometric stiffness matrix computed at a loading intensity corresponding to a maximum in-plane bending moment along the beam equals to the plastic moment

$[k]_f$ = structural stiffness matrix of a flange element

$[k]_s$ = structural stiffness matrix of a stiffener element

$[k]_w$ = structural stiffness matrix of web element

$[k_g]_f$ = geometric stiffness matrix of a flange element

$[k_g^w]_f$ = geometric stiffness of flange element, associated with lateral displacement, w

$[k_g^{\theta_x}]_f$ = geometric stiffness of flange element, associated with rotation about the longitudinal axis

$[k_g^1]_w$ = geometric stiffness of web element due to longitudinal and shear stresses

$[k_g^2]_w$ = geometric stiffness of web element due to vertical stresses caused by a load applied above the shear centre but between flanges

$[k_g^3]_w$ = geometric stiffness of web element due to vertical stresses caused by a load applied above the top flange

$[k_g^4]_w$ = geometric stiffness of web element due to vertical stresses caused by a load applied below the shear centre but between flanges

$[k_g^5]_w$ = geometric stiffness of web element due to vertical stresses caused by a load applied below the bottom flange

L = span length of the beam; length of the back span

L_c = length of cantilever span

L_f = length of flange element

L_p = length of the end panel span of open-web steel joist

M = end moment applied to the open-web steel joist

$\{M\}$ = moment vector

M_b = critical buckling moment of the back span

M_c = critical buckling moment of the cantilever span

M_{cr} = critical buckling moment of the overall beam

M_{in} = unfactored inelastic buckling moment resistance

M_j = moment about the x axis at node j of the fictitious 2-node element used to simulate lateral restraint above the top flange

M_p = plastic moment of the cross section

M_x = bending moment/unit length on a positive x-face tending to produce a positive displacement w in the plate

M_{xy} = twisting moment/unit length on a positive x-face in the yz plane tending to produce positive rotation about the x axis

M_y = bending moment/unit length on a positive y-face tending to produce a positive displacement w in the plate

M_{yx} = twisting moment/unit length on a positive y-face in the xz plane tending to produce positive rotation about the y axis

n = number of half waves of the buckled compression flange; number of observations

[n] = two dimensional shape function for lateral displacement, w

N = $\int_b \sigma_x \, t \, dz$

$\overline{N}$ = $N_i + N_j$

N_i = N, evaluated at node i

N_j = N, evaluated at node j

P = vertical load or reaction

P_1 = load transmitted from the suspended span to the cantilever tip through a shear connection

P_2 = joist load applied at top flange level within the cantilever span

r = interpolation factor

R = Nethercot's beam parameter; ratio of the maximum static moment given by the interior loads and the maximum end moment

$\{r\}$ = nodal displacement vector

$\{R\}$ = vector of the global out of plane nodal forces

$[r_i]$ = nodal displacements of node i

$[r_j]$ = nodal displacements of node j

$[r_k]$ = nodal displacements of node k

$[r_l]$ = nodal displacements of node l

s = bracing spacing

S_x = elastic section modulus for bending about strong axis

S_y = elastic section modulus for bending about weak axis

t = flange thickness

t_w = web thickness

U_f = strain energy of a flange element

U_p = strain energy of an elemental plate area dxdy

v = displacement along the y axis

V = volume of a flange or a web element; coefficient of variation

V_E = coefficient of variation of the modulus of elasticity

V_{Fy} = coefficient of variation of the yield strength

V_G = coefficient of variation of the geometric property

V_M = coefficient of variation of the material property

V_P = coefficient of variation of the test/design ratio

V_{P1} = coefficient of variation of the test/predicted ratio

V_{P2} = coefficient of variation of the predicted/design ratio

V_R = coefficient of variation of the resistance

v' = dv/dx

w = lateral deflection

$w(x)$ = lateral deflection of a point with a natural coordinate x

w_b = nodal lateral deflection of bottom flange

w_{cr} = critical buckling load intensity

W_{cr} = critical buckling load of spreader beam

W_f = work done by longitudinal stresses in a flange element

w_i = lateral deflection of node i

w_j = lateral deflection of node j

W_p = work done by vertical forces during buckling

w_{sw} = self-weight of the beam

w_t = nodal lateral deflection of top flange

w' = dw/dx

x = cartesian coordinate in the x direction

X = beam torsional parameter

y = cartesian coordinate in the y direction

z = cartesian coordinate in the z direction

Z_a = distance of the cable attachment from the midspan

Z_x = plastic modulus of the cross section

a_q = end rotation of the open-web steel joist

α_R = coefficient of separation

β = $\int_b z^2 \sigma_x \, t \, dz$; end moment ratio; reliability index

$\overline{\beta}$ = $\beta_i + \beta_j$

β_i = β, evaluated at node i

β_j = β, evaluated at node j

δ = initial sweep or camber

Δ = vertical displacement of the load point due to twisting of the cross section

$\{\psi\}$ = vector of linear shape functions for interpolating the displacements between the two nodes of a flange element

ε_y = yield strain

η = natural coordinate of a point with a cartesian coordinate y

η_i = η at node i

η_0 = $\eta\eta_i$

ξ = natural coordinate of a point with a cartesian coordinate x

ξ_i = ξ at node i

ξ_0 = $\xi\xi_i$

ϕ = resistance factor

$\{\phi\}$ = vector of bilinear shape functions for interpolating the displacement, w, between the four nodes of a web element

γ = elastic buckling load parameter

γ_0 = load factor corresponding to the lower bound of the solution

γ_1 = load factor corresponding to the upper bound of the solution

λ = load factor

λ_n = the closest eigenvalue less than μ

λ_{n+1} = the closest eigenvalue more than μ

λ_{n-1} = the closest eigenvalue more than μ, which happens to be negative

μ = shifted origin used in solving the eigenvalue problem; mean value

ν = Poisson's ratio

ρ_E = ratio of the mean value to the nominal value of the modulus of elasticity

ρ_{Fy} = ratio of the mean value to the nominal value of the yield strength

ρ_G = ratio of the mean value to the nominal value of the geometric property

ρ_M = ratio of the mean value to the nominal value of the material property

ρ_P = mean value of the test/design ratio

ρ_{P1} = mean value of the test/predicted ratio

ρ_{P2} = mean value of the predicted/design ratio

ρ_R = ratio of the mean value to the nominal value of the resistance

σ = standard deviation

σ_r = residual stress at an arbitrary point

$(\sigma_{rf})_1$ = residual stress in the flange at the flange-web junction

$(\sigma_{rf})_2$ = residual stress in the flange at a distance 3b/8 from the tip

$(\sigma_{rf})_3$ = residual stress in the flange at a distance b/4 from the tip

$(\sigma_{rf})_4$ = residual stress in the flange at a distance b/8 from the tip

$(\sigma_{rf})_5$ = residual stress in the flange at the tip

$(\sigma_{rw})_1$ = residual stress at mid-height of the web

$(\sigma_{rw})_2$ = residual stress in the web at a distance h'/8 from the mid-height

$(\sigma_{rw})_3$ = residual stress in the web at a distance h'/4 from the mid-height

$(\sigma_{rw})_4$ = residual stress in the web at a distance 3h'/8 from the mid-height

$(\sigma_{rw})_5$ = residual stress in the web at a distance h'/2 from the mid-height

σ_x = longitudinal stress at an arbitrary point

σ_y = vertical stress at an arbitrary point within the web

τ_{xy} = shear stress at an arbitrary point

θ_x = rotation angle about the x axis

$\theta_x(\xi)$ = rotation angle about the x axis of a point with a natural coordinate, ξ

θ_{xb} = nodal rotation angle of bottom flange about the x axis

θ_{xt} = nodal rotation angle of top flange about the x axis

θ_y = rotation angle about the y axis

θ_{yb} = nodal rotation angle of bottom flange about the y axis

θ_{yi} = rotation angle of node i about the y axis

θ_{yj} = rotation angle of node j about the y axis

θ_{yt} = nodal rotation angle of top flange about the y axis

ω_2 = moment modification factor

Chapter 1

INTRODUCTION

1.1 General

The moment capacity of laterally unsupported steel beams and girders may be greatly reduced by lateral-torsional buckling. This arises because of the difference in the major and minor axis flexural stiffnesses of the type of sections that are normally used to resist bending in one plane. The problem is characterized by a laterally unsupported beam, loaded in its stiffer principal plane, that collapses at loads considerably less than those required to reach the cross-sectional strength by pure in-plane bending.

Current design procedures generally consider lateral restraint to be effective only when it is attached to the compression flange. However, in cases where a beam with cantilevers is braced along the top flange only, a significant portion of the unbraced flange may be under compression under some loading conditions. In these circumstances, the effect of lateral restraint applied to the tension flange may be enough to preclude lateral-torsional buckling.

When a beam is torsionally restrained along one flange, local and lateral buckling combine to produce coupled buckling modes called distortional buckling in which simultaneous cross-sectional distortion and deflection occur. In cantilever-suspended span construction, the torsional restraint provided by open-web steel joists welded to the top flange can enhance the stability of the beams significantly. Designers need simple design procedures to estimate the distortional buckling resistance of beams under such restraint conditions and similar ones that may occur in practice.

1.2 Objectives

The objectives of this investigation are:

1. to develop an analytical model for predicting distortional buckling resistances of steel beams under a variety of loading and restraint conditions,

2. to verify the analytical model experimentally,

3. to suggest design procedures for cantilever beams, suspended beams, overhanging beams, restrained beams and beams in cantilever-suspended span construction.

1.3 Scope

A finite element model is presented to predict the distortional buckling resistances of beams with W-shaped cross section under different loading and restraint conditions (Albert et al. 1992). The model uses 4-node plate elements for the web and 2-node line elements for the flanges and is, therefore, capable of simulating the effects of web distortion on lateral-torsional buckling resistances.

A total of 33 full-scale tests were conducted on 11 beams of two different cross sections and with different loading and restraint conditions. These restraint conditions were chosen in such a way that the effect of different bracing systems on the buckling strength of the beams could be investigated.

An effective length concept is presented for predicting the buckling strength of built-in cantilevers, which takes into account the real restraint conditions. Another design procedure is suggested for overhanging beams under certain restraint conditions. A procedure for checking the lateral-torsional buckling of a beam lifted under self-weight during construction is given. A simple design procedure is developed for a beam, free to warp at its ends and subject to transverse loads and end moments when lateral and torsional restraints are applied to the top flange at discrete locations. Design procedures are developed for cantilever-suspended span beams under a variety of loading and restraint conditions based on the distortional buckling finite element model. Resistance factors consistent with the design procedures and the test results are presented.

Chapter 2

LITERATURE REVIEW

2.1 General

The problem of lateral-torsional buckling of simply supported beams with narrow rectangular cross section and loaded by uniform moment was first investigated by Prandtl (1899) and Mitchell (1899). Independently of each other, they published in the same year a theory of lateral-torsional buckling of beams, arriving at substantially the same solution, a differential equation of the second order with variable coefficients which controls the problem. Further development was due to Timoshenko and Gere (1961), who used the energy method to derive the fundamental differential equation of beams with symmetric I-sections by including the effect of warping on the torsional aspect of the problem. Since then many investigators have developed the subject to handle a variety of loading conditions, end and intermediate restraints, monosymmetry, non-uniform sections and inelastic material behaviour. Previous reviews of the topic have been given by Lee (1960), Trahair (1977) and Schmitke and Kennedy (1984).

2.2 Distortional buckling

The elastic stability of an I-section member has generally been classified as either local buckling or overall member buckling. In local buckling, a component plate of the member such as the compression flange buckles locally over a short length of the member with local changes in the cross-sectional shape. On the other hand, an overall buckling analysis (Timoshenko and Gere 1961) assumes that the member deflects from its initially straight configuration, but that the member cross section remains undistorted (rigid) during buckling. An analysis in which lateral-torsional buckling and local buckling are assumed to occur independently and the original shape of the cross section does not distort is called a linear buckling theory. Hancock (1978) has shown that thin walled members may also buckle in an intermediate distortional mode, in which lateral deflection and twisting are combined with general distortions of the cross-sectional shape.

In I-section members, the flanges are composed of relatively thick and narrow plates compared to the web and, therefore, the distortion in the flanges is much less significant than in the web. Hancock (1978) and Roberts and Jhita (1983) showed that for laterally unsupported beams which are restrained laterally and torsionally at the supports, the geometry of most hot rolled I-section members is such that the effects of web distortion are not significant, so that their buckling loads are close to those predicted based on the classical rigid web analysis. However, Hancock et al. (1980) indicated that the effects of web distortion in I-section beam-columns decrease from a maximum for pure beam behaviour to zero for pure column behaviour. Akay et al. (1977) considered, using a distortional finite element approach, an I-section beam which is fixed at both ends and loaded by a single concentrated load at mid-span. They concluded that web distortion caused a reduction of about 25% in the buckling load given by rigid web analysis. However, most of this reduction could be eliminated by the use of web stiffeners at mid-span. Bradford and Trahair (1981), and Bartels and Bos (1973) indicated that the effects of web distortion increases substantially for short and intermediate length beams when displacements or rotations of the flanges are allowed at the supports. An example of this is the lateral stability of beams on seats (Bradford and Trahair 1983 and Bradford 1989) which prevent only one flange from deflecting laterally and the other flange is restrained only through the stiffness of the web.

2.3 Stability of uniform beams restrained along one flange

2.3.1 General

Because the lateral-torsional buckling phenomenon involves two deformation components, lateral deflection and twist, intermediate restraints against either action may be used to increase the stability of a beam. These restraints can be provided to both flanges in such a way that web distortion is prevented (Nethercot 1973a, Kitipornchai and Richter 1978). Another possible arrangement is restraints attached to the compression (critical) flange. In this case the braced beam is designed on the basis of effective lengths equal to the bracing spacing. Frequently in practical structural framing systems, lateral and torsional restraints are applied at discrete locations to the top flange only. For a continuous beam this is the tension flange in the critical portion of the beam where the bending moments are largest. This problem is more complicated and web distortions are of much significance. Many investigators have considered this problem either analytically or experimentally as discussed later.

The effects of continuous and complete tension flange restraint on distortional buckling, as applied to composite steel-concrete beams have been considered by Johnson and Bradford (1983), Svensson (1985), Williams and Jemah (1987) and Goltermann and Svensson (1988). Johnson and Bradford (1983) used the model of Bradford and Trahair (1982) to conduct a finite element parametric study of elastic distortional buckling in laterally unstiffened fixed-ended composite girders with web depth/thickness ratios varying from 39 to 100. Svensson (1985) presented a method to estimate the elastic lateral-torsional buckling stress by treating the unsupported flange as a column with varying axial force, supported on an elastic foundation representing the web. This method neglects the Saint Venant torsional contribution. William and Jemah (1987) suggested a modification to Svensson's method by including 15% of the web with the unsupported flange to constitute the column of the model. Goltermann and Svensson (1988) modified Svensson's model to handle the case of a finite torsional restraint applied to the laterally supported flange and to include the contribution of Saint Venant torsion. The procedure suggested to predict the elastic lateral-torsional buckling stress is somewhat complicated and not considered to be suitable for design purposes.

2.3.2 Analytical investigations

Winter (1941) was the first to investigate the lateral-torsional buckling of a simply supported monosymmetric beam under uniform moment when laterally restrained along the tension flange. For a doubly symmetric section, the given solution reduces to

$$[2.1] \qquad M_{cr} = \frac{GJ}{d} + \frac{2\pi^2 E C_w}{dL^2}$$

where G is the modulus of rigidity, E is the elastic modulus, J is the Saint Venant torsional constant, C_w is the warping constant, d is the depth of the cross section and L is the span length. Roeder and Assadi (1982) considered the same problem and arrived at the same closed form solution.

Horne and Ajmani (1969) extended the solution, using the energy method, to the case of a beam-column under linear moment gradient which is laterally and torsionally restrained by side rails attached to one flange at discrete locations. They suggested the use of an effective continuous torsional restraint stiffness which accounts for the bracing stiffness, the moment-rotation characteristic of the joint between the side rails and beam-column and web distortion. However, no expression was given to relate the suggested effective continuous torsional restraint stiffness to all these variables, and specifically no suggestion was given on how to account for web distortions. They introduced a standard eigenvalue problem to determine the solution for the critical buckling moment. In order to simplify the solution for design purposes, Horne and Ajmani (1971) suggested that the torsional restraint be neglected and only the effect of lateral restraints be considered.

Milner (1975, 1977a) and Milner and Rao (1983) considered, using the energy method, the problem of a simply supported beam under uniform moment which is braced laterally and torsionally through discrete braces attached to the tension flange. Infinite lateral and finite torsional bracing stiffnesses were assumed. The closed form solution for this problem is given as

$$[2.2] \qquad M_{cr} = \frac{GJ}{d} + \frac{2n^2\pi^2 E C_w}{dL^2} + \frac{K_e L^2}{n^2 \pi^2 d}$$

where most terms are as defined previously for [2.1], n is the number of half waves of the buckled compression flange, which may be selected to make the critical moment a minimum, and K_e is the effective continuous torsional restraint stiffness, given as

$$[2.3] \qquad \frac{1}{K_e} = \frac{1}{K_b} + \frac{1}{K_w} + \frac{1}{K_j}$$

where K_b is the bracing bending stiffness divided by the spacing between braces, K_w is the web stiffness which accounts for the web distortion, given as

$$[2.4] \qquad K_w = 0.5\,\frac{Et_w^3}{s}$$

where t_w is the web thickness, s is the spacing between braces and K_j is the stiffness of the beam to brace connection divided by the brace spacing, depending on the moment-rotation characteristic of the joint. Milner (1977a) recommended an infinite value for K_j in cases of friction grip bolted and welded joints. Milner and Rao (1978) presented some recommendations for estimating K_j for bolted joints based on experimental tests.

The expression for web stiffness recommended by Milner (1977a), given by [2.4], which was also used by Nethercot and Trahair (1984), overlooks the depth of the cross section. Goltermann and Svensson (1987) presented the following expression, to take the depth into account :

$$[2.5] \qquad K_w = \frac{Et_w^3}{4(1-v^2)d}$$

where v is Poisson's ratio.

In computing the effective continuous torsional restraint stiffness, using [2.3], the torsional flexibility of the braced tension flange is not taken into account. When bracing is provided only at discrete locations along the tension flange, the flange between the braces tends to twist, causing a reduction in the effectiveness of the torsional restraint of the bracing.

Lindner (1987) investigated the stabilization of supporting I-beams by corrugated sheeting. The effects of lateral and torsional restraints provided to one flange are taken into account. He also used [2.3] and [2.5] to estimate the effective continuous torsional restraint stiffness. The critical buckling moment of the beam is approximated as

$$[2.6] \qquad M_{cr} = \frac{k}{L}\sqrt{EI_y G J^*}$$

where k is the effective buckling coefficient, obtained from a finite element analysis, and J^* is a modified Saint Venant torsional constant, given as

$$[2.7] \qquad J^* = J + \frac{K_e L^2}{\pi^2 G}$$

Early methods of analyzing web distortion were based on the assumption made by Goodier and Barton (1944), that the web could be assumed to be a series of thin walled vertical beams of length equal to the cross-sectional depth, provided that the elastic modulus was changed from E to $E/(1 - v^2)$. This assumption led to the prediction that the variation of the out of plane displacements over the depth of the web could be represented by a cubic polynomial. Suzuki and Okumura (1968) used this assumption in a folded plate analysis.

Exact plate bending theory was used by Goldberg et al. (1964) to obtain closed form solutions in some cases. Horne and Ajmani (1969), Bartels and Bos (1973), Milner (1975), and Bradford (1988) obtained approximate solutions by using energy and variational methods with assumed displacement functions. In some of these solutions a cubic polynomial was used for the web displacements.

Rajasekaran and Murray (1973) presented a finite element analysis of the coupled local and lateral buckling of wide flange beam-columns. Their analysis used one-dimensional beam elements for the flanges and flexural plate elements for the web. This analysis is somewhat complex in that it needs eleven degrees of freedom at each longitudinal node. As well, it does not account for vertical stresses in the web or residual stresses.

Johnson and Will (1974) used plate elements to represent both the flanges and web, and cubic polynomials for the element displacements in deriving their stiffness matrices. Because most of the cross-sectional distortion occurs in the web, this refinement in modelling unnecessarily complicates the analysis.

Akay et al. (1977) idealized the flanges as beam elements, while plate elements, with several divisions over the depth of the section, were used to represent the web. This leads again to a relatively large number of degrees of freedom.

Bradford and Trahair (1981, 1982) presented a method for the elastic distortional buckling of I-beams which alleviated the high computer cost of other studies. They used 2-node beam elements for the flanges and plate elements, extending over the whole depth of the web, to represent the web. Only three degrees of freedom are needed per node.

Bradford (1986) developed a finite element method of analysis for inelastic distortional buckling of determinate, hot rolled I-beams. The method permits an economic computer analysis to be made for members under various conditions of loading, end support and restraint. However, this method gives inaccurate results due to the approximation used in including the destabilizing effects of vertical loads.

A modification of the finite element method is the finite strip method. In certain cases, it can greatly reduce the number of degrees of freedom of an element or strip, as only one set of cross-sectional degrees of freedom are required. This method was used by Hancock (1978) to demonstrate the interaction between the local, distortional, and lateral buckling modes of simply supported beams in uniform bending. Under other loading and support conditions, this method tends to be so complicated that it cannot be used.

2.3.3 Experimental investigations

To date, most of the experimental studies of the lateral-torsional buckling of I-beams, which are either restrained along one flange or with incomplete supports, have been conducted on model specimens. Although models simplify the testing procedure significantly as compared with full-scale beams, they do not simulate the effects of residual stresses or initial imperfections.

Bartels and Bos (1973) investigated, using model specimens, the effect of the boundary conditions, provided at the supports, on the lateral-torsional buckling stability of both simply supported and continuous beams. They took cross-sectional deformations into account. The loading consisted of several equally spaced loads applied to the top flange. The support boundary conditions were: (a) forked bearings, in which lateral deflections and longitudinal twisting of both flanges were prevented; (b) semi-forked bearings, in which lateral deflections of both flanges as well as twisting of bottom flange were prevented; and (c) bottom flange restraint, in which only the bottom flange was laterally and torsionally restrained. They concluded that cross-sectional deformations within the span of the beam have a negligible effect on the lateral-torsional buckling stability if forked bearings are used. On the other hand, a significant reduction in the lateral-torsional buckling capacity resulted when semi-forked bearings or bottom flange restraint only were used.

Milner (1977b) conducted several model tests on simply supported beams with loads applied at the ends of cantilever overhangs to provide a central portion under uniform moment. The beams were braced laterally and torsionally by means of purlins connected to the tension flange. Apparently, no account was taken of the restraining effect provided by the overhanging portions.

Bose (1982) reported a series of tests on universal beams under a single concentrated load applied to the top flange at mid-span. At each support of the simply supported beam, the compression flange was connected to a spring which provided an elastic torsional restraint. The effect of torsional restraint at supports on the buckling strength of the beams was found to be significant.

Wakabayashi and Nakamura (1983) carried out model tests to investigate the effect of lateral bracing by purlins or beams on the lateral-torsional buckling capacity and post-buckling behaviour of H-shaped beams. Beams with two overhangs were used and several loading conditions were investigated. The cantilever tips were restrained laterally and torsionally.

2.4 Stability of cantilever and overhanging beams

The elastic lateral buckling resistance of built-in uniform cantilevers of doubly symmetric I-shaped cross section has been studied by many investigators such as Timoshenko and Gere (1961) and Nethercot (1973b). Although most cantilevers of practical dimensions would tend to buckle inelastically, elastic buckling resistances are also of importance during construction. As well, elastic buckling resistances are needed as one limit of any empirically derived inelastic buckling resistance; the other limit is the full flexural resistance of the cross section.

Currently available solutions for cantilevers under different loading and restraint conditions, as given by the Structural Stability Research Council (SSRC) Guide (Galambos 1988), use an effective length concept as follows

$$[2.8] \qquad M_{cr} = \frac{\pi}{k_b L} \sqrt{EI_y GJ + \frac{\pi^2 E^2 I_y C_w}{(k_b L)^2}}$$

where k_b, the effective length factor (see Fig. 2.1), models the effects of the type of loading, the level of load application and the type of end restraint. These solutions are based on Nethercot (1983). Two problems may be encountered with these solutions which either limit their applicability or completely invalidate them. The first problem is that Nethercot (1973b) set a limit on the beam torsional parameter, R, here redefined as

$$[2.9] \qquad X = \sqrt{\frac{\pi^2 E C_w}{G J L^2}} = \frac{\pi}{R}$$

The limit is given as

$$[2.10] \qquad 0 < X < 1.57$$

This limit, restricting the solution to relatively long span cantilevers ($R > 4$) was not stated in subsequent publications (Kirby and Nethercot 1979, Nethercot 1983). The second problem, as shown in Fig. 2.2, is concerned with restraint conditions at the tip of the cantilever. The conditions given by the Guide and Nethercot (1983) differ from those in the original derivation (Nethercot 1973b, Kirby and Nethercot 1979) where lateral or lateral-torsional restraint at the cantilever tip is considered to be applied only at the shear centre.

Furthermore a cantilever beam frequently exists as the cantilever projection of a simply supported beam over an end support. This is usually called an overhanging beam. The design recommendations given by the SSRC Guide (Galambos 1988) for overhanging beams use the effective length concept [2.8] as recommended by Nethercot (1973b and 1983) combined with the effective length factors given in Fig. 2.1. Nethercot, however, considered only the case of a cantilever span with an equal back span and with no loads or restraints applied to the back span between supports. To account for the fact that the restraining effect of the back span on the cantilever span is reduced as the back span gets longer, Kirby and Nethercot (1979) introduced the restriction that the effective length of the cantilever should not be less than the back span. However, this restriction is not given in Nethercot (1983) and the SSRC Guide. Without its use, nonconservative results are obtained and even with its use inaccurate and nonconservative results are obtained in some cases.

Lindner (1972) studied the stability of an I-shaped cross section cantilever beam with a back span for the case when lateral displacements of the top flange along both spans were restrained. The loading conditions considered were 1) a single concentrated load at the cantilever tip; 2) a uniform load along the cantilever span; 3) a uniform load along both the cantilever and back span and 4) a concentrated moment at the cantilever tip. The concentrated or uniform loads were considered to act at the level of the top flange or shear centre. He suggested that the lateral-torsional buckling resistance can be approximated as [2.6], in which J^* is replaced by the Saint Venant torsional constant and the coefficient k is given graphically in terms of the cantilever beam torsional parameter and the ratio of the back span to the cantilever span.

Trahair (1983a) has shown that the built-in cantilever model overestimates the buckling resistance of an overhanging segment. He also suggested a method to obtain the elastic lateral-torsional buckling resistance for a beam with two similar overhanging segments at each end of a central segment based on interaction buckling (Nethercot and Trahair 1976) between the different segments. The only loading case considered is that of concentrated loads acting at the cantilever tips. In this method, the buckling load is estimated using the buckling loads of both cantilever and central segments which are free to warp at the ends and the buckling load of a cantilever built-in at the root. Although this method is strictly only applicable to the loading case described, it gives unconservative results when the loads are applied to the top flanges of cantilever tips.

2.5 Stability of suspended beams

A stability problem which has not received much attention from researchers is the lateral-torsional buckling of I-shaped beams acted upon by their self-weight when being lifted by cables or chains. This situation is frequently encountered in construction. Because the cables provide lateral restraint only when they are attached to the top flange of the beam, the lateral-torsional buckling resistance of the beam can be relatively low. Furthermore, the unusual restraint conditions make the classical buckling solutions inapplicable. The dominant loading in a lifting operation is the beam self-weight acting as a uniformly distributed load along the centroidal axis. For relatively short beams, the crane picks the beam up at mid point of the top flange. When the beam is relatively long, a spreader beam is likely used and the cables are attached to the top flange at two symmetrical locations. The beams may be relatively slender, and being lightly loaded, lateral-torsional buckling likely occurs within the elastic range.

Dux and Kitipornchai (1988) derived the governing differential equations of minor axis flexure and torsion for symmetrically loaded suspended beams. Using the finite integral method, they investigated the influence of many variables such as the cable angle, loads and cable attachment positions on the buckling resistance. The theoretical predictions of elastic buckling loads compared favorably with the results obtained from a series of small-scale experiments on aluminum I-beams.

Dux and Kitipornchai (1989) developed buckling capacity charts in a non-dimensional format to check the stability of I-beams under self-weight lifting for different cable angles and attachment positions.

2.6 Stability of steel beams in cantilever-suspended span construction

Cantilever-suspended span beams are commonly used in low-rise industrial and commercial roof construction, especially where regular joist spacing and equal beam spans can be used. Because the cantilever span length can be adjusted to balance the positive and negative bending moments, under the critical loading condition, most of the advantages of continuous construction can be realized and beam sizes can be minimized. This type of construction also leads to reduced erection time as only simple connections are required. The beams of alternate bays cantilever over the top of columns and a simple span is suspended between the ends of the cantilevers, as shown in Fig. 2.3. Secondary framing members such as open-web steel joists, welded to the top flange as shown in Fig. 2.4, can provide lateral and torsional restraints to the top flange. By extending the bottom chord of the joist and attaching it to the bottom flange, lateral bracing is provided to the bottom flange as well. The restraint of the joist attachment to the beam enhances the lateral-torsional stability of the beam dramatically but taking these restraints into account complicates the solution considerably. Frequently the effect of torsional restraints has been neglected.

Mehta (1981), and White and Salmon (1987) presented charts or tables for the preliminary selection of member sizes and cantilever lengths. These charts and tables were obtained by equating the maximum positive and maximum negative moments for each member under different loading conditions. The selection of a member size is based on its maximum bending capacity. They suggested, in a lateral-torsional stability check, to use the unsupported length as the spacing between joists. However, this procedure is unconservative unless all the bottom chords of all joists are connected to the bottom flange of the beam, a condition which is rarely encountered in practice.

The Canadian Institute of Steel Construction (1989) presented another design procedure which puts much more emphasis on the lateral-torsional stability criterion in selecting the member sizes. This procedure appears to be based on the approach given in the Guide to stability design criteria for metal structures (Galambos 1988) for overhanging beams. Two stability checks are suggested; one for the cantilever which takes into account the lateral restraint conditions (if any) and continuity of the cantilever with the back span, and the other for the back span, taking into account the lateral restraints as well as the bending moment diagram. However, both of these stability checks may be unconservative. The stability check of the cantilever, based on Galambos (1988) and in turn on Kirby and Nethercot (1978), reverses the limitation (not stated in the Guide) that the effective length of the cantilever should not be less than the back span. The stability check of the back span uses the expression given by Roeder and Assadi (1982), derived for a simply supported beam under uniform moment and laterally restrained along the tension flange [2.1]. In order to account for the effect of nonuniform bending, a moment modification factor as given by Kirby and Nethercot (1978) is introduced. This factor was originally suggested for unrestrained beams apparently loaded at the shear centre and a modification for restraint to the compression flange had been earlier proposed by Horne and Ajmani (1973). Nonconservatism in this approach, depending on the ratio of the central moment to the end moments, may arise when the loads are applied above the shear centre even though the top flange is laterally supported. On the conservative side, the procedure does not account for the torsional restraint provided by the welded connection between the top flange and the open-web steel joist which significantly enhances the lateral-torsional stability of the beam.

2.7 Comparisons

Bradford's analytical work (1986), the most similar to the work presented herein, differs however in that it uses the consistent approach in deriving the structural and geometric stiffness matrices whereas this work uses cubic shape functions for deriving the structural stiffness matrices and more simplified shape functions for deriving the geometric stiffness matrices. This simplifies the formulation significantly. Bradford as well did not consider the effect of web distortion on the destabilizing effect of loads applied above the top flange as is considered here.

In this study, the determination of the effective torsional restraint stiffness is similar to that proposed by Milner (1975) except that the web stiffness used is that given by Goltermann and Svensson (1987) and furthermore the twisting of the braced flange between bracing points is considered.

Because the experimental work cited above was chiefly conducted on models and not full-scale specimens or further that it did not consider a spectrum of practical loading and restraint conditions or that the boundary conditions were not well defined, a series of full-scale tests with precisely defined boundary conditions were carried out in this study to verify the analytical model experimentally.

Design procedures for cantilever and overhanging beams mark a significant improvement over that of Nethercot (1973b). The approach to suspended beam stability is, in some aspects, considerably simplified as compared to that of Dux and Kitipornchai (1989). The design procedures for restrained beams and beams in cantilever-suspended span construction are novel.

Restraint conditions		Effective length factor, k_b	
At root	At tip	Top flange loading	All other cases
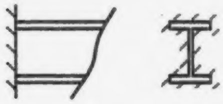	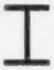	1.4	0.8
	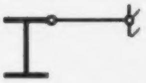	1.4	0.7
	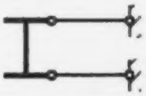	0.6	0.6
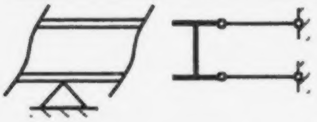	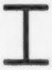	2.5	1.0
	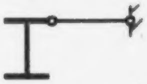	2.5	0.9
	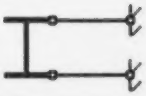	1.5	0.8
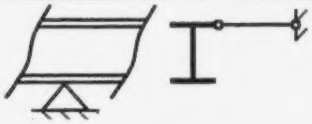	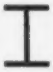	7.5	3.0
	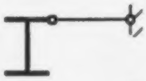	7.5	2.7
	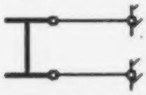	4.5	2.4

Fig. 2.1 Effective length factors for cantilever and overhanging beams given by the SSRC Guide (Galambos 1988)

SSRC guide (Galambos 1988)	Kirby and Nethercot (1979)
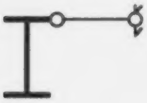	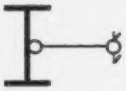
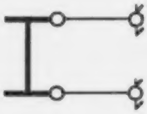	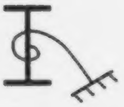

Fig. 2.2 Comparison of restraint conditions at cantilever tip

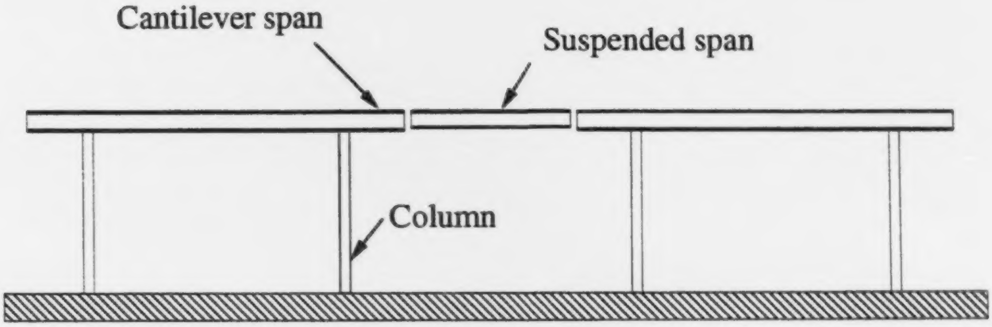
Cantilever span
Suspended span
Column

Fig. 2.3 Cantilever-suspended span construction

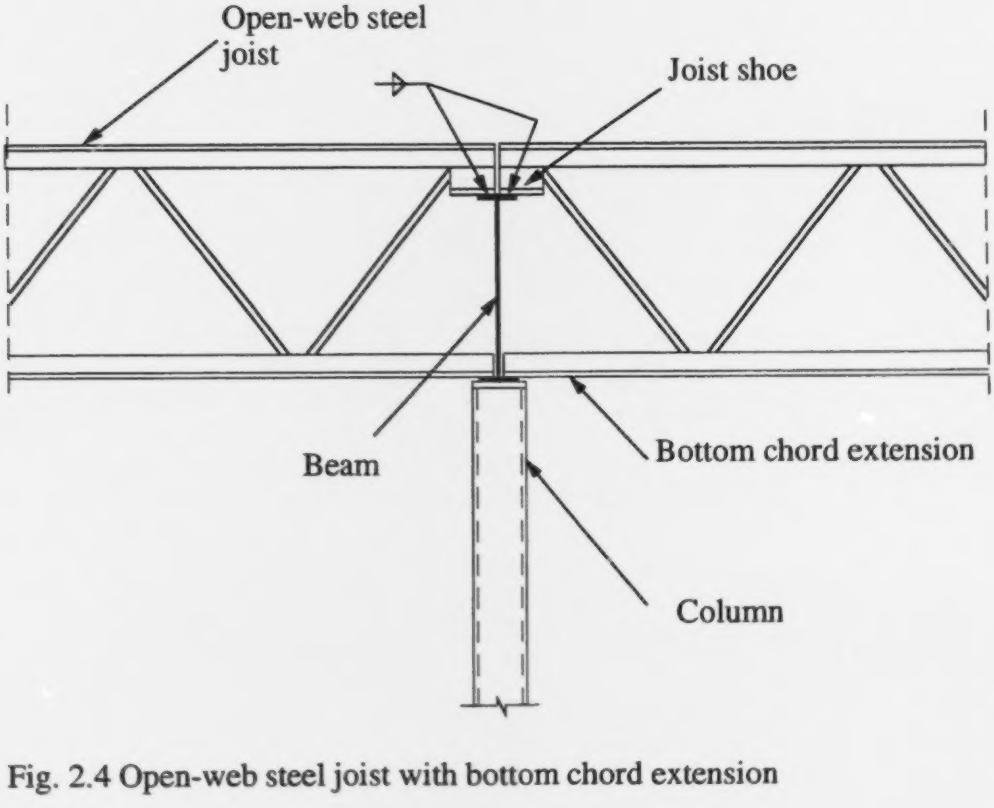
Open-web steel joist
Joist shoe
Beam
Bottom chord extension
Column

Fig. 2.4 Open-web steel joist with bottom chord extension

Chapter 3

BEAM CHARACTERISTICS

3.1 General

The results of measurements of the cross sections, sweep and camber of the beams used in buckling tests, and of the ancillary tests including tension coupon tests, residual stress determinations and stub column tests are presented in this chapter. These results are used in predicting the buckling behaviour and strength of the beam tests based on the finite element model.

3.2 Beam types, dimensions and geometric properties

Eleven different test beams were used in the full-scale buckling tests. Seven beams were W360x39s and the remaining four were W310x39s. Each group of beams of the same cross section came from a single heat. These relatively light beam sections were selected so that the testing frames would be neither too heavy nor too large. Based on the geometry of the test floor, available with reaction points at 610 mm on centre, they also provided reasonable span to depth ratios for cantilever-suspended span construction, and width to depth ratios of the beams (0.36 and 0.53) in the proportions of beams used in real structures. The W360x39 was nominally a class 1 section and the W310x39 a class 2 section. Eight beams were approximately 9 m long while three beams were ordered in 11 m lengths (3A, 3M and 3K) to provide two metres of material each for the ancillary tests.

Because some beams were used to perform as many as seven tests, the sequence of the tests was planned so that elastic tests preceded the last test that could be used to demonstrate significant inelastic behaviour. It follows that any elastic test was stopped shortly after the occurrence of buckling to avoid any inelastic straining in so far as possible or to limit it to a relatively small zone of the beam.

Before any of the major buckling tests were conducted, the cross-sectional dimensions were measured. Measurements of the depth, d, flange width, b, and flange thickness, t, were made at ten equally spaced stations along the beam, while measurements of the web thickness, t_w, were made near the ends. Fillet radii were measured once for each cross section for specimens used in stub column tests. The identification numbers of the beams, the number of observations, n, the mean value, μ, and the coefficient of variation, V, of measured cross-sectional dimensions of the W360x39 and W310x39 specimens are listed in Tables 3.1 and 3.2, respectively. The nominal cross-sectional dimensions are also given in these tables as are the mean/nominal ratios. For all beams, the differences between the measured and nominal dimensions are small and well within the allowable tolerances set by CSA Standard G40.20-M81. In general the mean/nominal ratios are essentially 1.00 and the coefficients of variations are very small, indications of extremely good control of the rolling process.

The cross-sectional area, A, major and minor axes moments of inertia (I_x and I_y, respectively), major axis plastic modulus, Z_x, and major and minor axes elastic moduli (S_x and S_y, respectively) are given in Table 3.3 based on the mean measured cross-sectional dimensions. The contribution of fillets are taken into account. The measured/nominal ratios of the cross-sectional properties are also given in Table 3.3. The ratios for the W360x39 are essentially 1.00 while those for the W310x39 are up to 6% below the nominal value, even though that for the cross-sectional area is 0.993. This is because the flange thickness is about 3% low while the web thickness is 7% high.

3.3 Measurement of initial geometrical imperfections

After measuring the cross-sectional dimensions of a beam specimen, initial geometrical imperfections (sweep of the shear centre axis, twist and camber) were measured at one-metre intervals.

Initial sweep or lateral bow at the elastic shear centre was calculated based on measurements of flange tip deviation from fine lines stretched between the beam ends. Assuming a perfect web, the sweep at the shear centre was calculated as the average of the bows of both flanges. The sweep distributions are given in Figs. 3.1.a and 3.1.b for W360x39 and W310x39 specimens, respectively. The non-dimensionalized initial sweeps (sweep/length) are generally small and below the limit of 0.001 of the length specified by the CSA Standard G40.20-M81 except for specimen 3B where this limit was exceeded slightly. The sweeps of the W310x39 specimens were exceptionally small and did not exceed 0.00055.

To obtain the initial twist, the test specimen was placed with the lower surface of its bottom flange in the horizontal position. A straight edge with a level was positioned vertically just touching the bottom flange tip. The distance of the top flange tip from the straight edge was then measured to determine the twist angle. This procedure was repeated at one-metre intervals along the beam. The initial twist distributions are shown in Figs. 3.2.a and 3.2.b for W360x39 and W310x39, respectively. The data for specimen 3A are not available. In all specimens, the values of initial twist are less than about 1.5°.

Initial camber or vertical bow was measured with the beam specimen placed such that the web was in the horizontal position. Measurements were taken of the deviations of the flange surface from a fine line stretched between the beam ends. The distributions of camber are given in Figs. 3.3.a and 3.3.b for W360x39 and W310x39 specimens, respectively. The maximum values of non-dimensionalized camber (camber/length) in all beam specimens are generally small and significantly less than the limit of 1/1000 given in CSA Standard G40.20-M81.

Table 3.4 gives a comparison between the average measured initial sweep and twist in this study and those reported by Dux and Kitipornchai (1981) on one cross section, Fukumoto et al. (1980) on one cross section and Hechtman et al. (1955) on four cross sections.

Generally, the imperfections reported here, although small, are greater than those reported by other investigators. Fukumoto's beams were however relatively short. Hechtman measured the initial twists and sweeps only at mid-span. The average twists he obtained are considerably more than those reported by Dux and Kitipornchai, and Fukumoto.

3.4 Tension coupons

A total of 22 coupons, 14 from the flanges and eight from the webs, were tested in uniaxial tension to determine the mean flange and web yield stresses as well as elastic moduli for the two W-shaped cross sections used in the distortional buckling tests. The locations and identification marks of the 10 coupons from the W360x39 (Beam 3K) and the 12 coupons from the W310x39 (Beam 3P) are shown schematically in Figs. 3.4 and 3.5. The surfaces of the coupons cut from flanges of W310x39 were milled to give parallel surfaces in order to eliminate a change in thickness across the width of the specimen. In two tests where this was not done, uneven gripping of the test specimen by the testing machine resulted in eccentric loading and unreliable results. The cross-sectional areas of the coupons were determined prior to testing.

The tension coupons were tested in an MTS 1000 testing machine. The results for the W360x39 and W310x39 cross sections are given in Tables 3.5 and 3.6, respectively. The W360x39 coupons had an average modulus of elasticity of 204 500 MPa with a coefficient of variation of 0.021, an average flange static yield strength of 287.9 MPa with a coefficient of variation of 0.025 and an average web static yield strength of 317.8 MPa with a coefficient of variation of 0.040. The results from the W310x39 coupons gave an average modulus of elasticity of 209 300 MPa with a coefficient of variation of 0.025, an average flange static yield strength of 352.2 MPa with a coefficient of variation of 0.014 and an average web static yield strength of 367.4 MPa with a coefficient of variation of 0.017. These variations are not unexpected.

3.5 Residual stresses

Residual stresses in the flanges and webs were determined by the sectioning method (Galambos 1988). The technique and procedure followed closely that reported by Dux and Kitipornchai (1981). Residual strain measurements were taken once for each cross section of the W-shapes. The locations of residual stress test specimen are shown in Fig. 3.6. These residual stress specimens are at least twice the depth away from the ends of the overall specimens so that residual stresses are fully developed in them.

Before cold sawing the residual stress specimen from the overall specimen, a gauge length of 100 mm was defined on each side of the strips, except for the strip at the web-flange junctions where five gauge lengths were used, by steel balls punched into the positions, as shown in Fig. 3.7. The gauge lengths were measured before and after sectioning using a mechanical extensometer (Bam-Setzdehnungsmesser). All cuts were made by slow band-sawing at the locations shown in Fig. 3.7. After cutting, no ball separation was evident but significant bowing occurred in the web portions nearest the flange-web junctions. This phenomenon was also observed by Dux and Kitipornchai (1981). Because measurements were recorded on both sides of a strip, no correction due to bowing was necessary (Galambos 1988).

Residual strains were calculated as the change in the gauge length after longitudinal sectioning divided by the original gauge length. Three measurements were recorded for each gauge length. A gauge length on a steel bar was also measured for temperature compensation. Because the laboratory temperature varied only within a range of 1.5^{o} Celsius, the correction due to temperature was found to be negligible. The repeatability of the measuring device was excellent with deviations from the mean not exceeding +/- 0.002 mm.

The residual stresses in Fig. 3.8 have been obtained using the mean moduli of elasticity of 204 500 MPa and 209 300 MPa for W360x39 and W310x39, respectively, and the mean residual strains from matching gauge lengths on opposite sides of each strip of the flanges and webs. The measured patterns show high compressive residual stresses of about 0.63 to 0.38 of the yield strength for the W360x39 and W310x39, respectively, over most of the web and high tensile residual stresses at the flange-web junctions. The flanges of the W360x39 section were entirely in tension with a maximum residual stress of 0.69 F_y at the web-flange junction. The tensile residual stresses at the web-flange junction of the W310x39 were considerably less at 0.21 F_y and at the flange tips, the average stress was about 20 MPa compression equivalent to 0.06 F_y. These features conforms to that reported by other researchers (Dux and Kitipornchai 1981 and Wong-Chung and Kitipornchai 1987) for beam sections with relatively narrow flanges. For the W310x39, the residual stress pattern appears to be disturbed in the flanges due to the effect of roller straightening. The main specimen length exhibited continuous yield line pattern extending well into the flanges.

3.6 Stub columns

Stub column tests were made on the two W shapes to obtain the average stress-strain characteristics for the cross section as a whole, and to confirm the residual stresses and material properties which were obtained from the other tests. Following the guidelines of the Structural Stability Research Council (SSRC) (Galambos 1988), the W360x39 and W310x39 stub columns were both sawn to a length of 995 mm, and the ends were milled plane. The stub columns were white washed and tested according to the SSRC guidelines in an MTS 6000 testing machine.

The stress-strain curves obtained from the stub column tests on the W360x39 and W310x39 are given in Figs. 3.9 and 3.10, respectively. As indicated in these figures, the load reduced appreciably due to local buckling of the webs just after the maximum load was attained. This was not unexpected due to the high compressive residual stresses extending virtually constant over about 60% of the web height. The moduli of elasticity, average yield strengths of the cross sections and stresses at which first yielding was observed are given in Table 3.7 for the stub column tests. The resulting average yield strengths of the W360x39 and W310x39 cross sections are 96% and 98%, respectively, of the corresponding values from tension coupon tests.

In the W360x39 stub column test, the average stress at first yield as indicated by flaking of the white wash which occurred precipitously over the central 200 mm of the web depth was 229 MPa. This implies, based on the web yield stress of 318 MPa, that a residual compressive stress of about 89 MPa existed. This agrees reasonably with the computed residual stress of about 100 MPa which exists at the limit of the area where flaking occurred. At the mid depth of the web, the computed compressive residual stress was about 200 MPa. Apparently, the white wash, even though probably separated from the steel in this area, dislodged as a unit.

In the W310x39 stub column test, the average stress at which first flaking of white wash occurred (in the web at mid-depth) was 250 MPa. This implies, based on a yield stress of the web of 367 MPa, that the maximum compressive residual stress at that location was at least 117 MPa, a value which agrees well with the computed residual stress of 138 MPa obtained by sectioning.

In both stub column tests, the compressive residual stresses in the web were underestimated, a result of stub column tests also reported by Dux and Kitipornchai (1981). It should be noted that the first deviation from a straight line of the average stress-strain curve is difficult to assess. This happens because yielding actually starts only at a point, in this case the middle of the relatively thin web. Opposed to this, when a W-shaped cross section has significant compressive residual stresses at the flange tips, yielding starts at the four flange tips almost simultaneously causing a noticeable deviation of the inelastic curve from the elastic straight line of the average stress-strain curve.

Beam designation	Depth, d			Flange width, b			Flange thickness, t			Web thickness, t_w		
	n	μ	V	n	μ	V	n	μ	V	n	μ	V
3D	20	352.95	.0055	20	127.46	.0028	40	10.73	.013	6	6.72	.017
3G	20	352.19	.0041	20	127.83	.0050	40	10.69	.014	6	6.68	.023
3K	20	352.87	.0051	20	126.75	.0029	40	10.62	.012	6	6.52	.023
3A	20	353.00	.0042	20	126.89	.0028	40	10.72	.015	6	6.61	.024
3H	20	352.59	.0049	20	127.19	.0037	40	10.73	.012	6	6.76	.027
3C	20	352.82	.0041	20	126.72	.0038	40	10.70	.015	6	6.65	.022
3B	20	352.91	.0051	20	127.08	.0022	40	10.70	.014	6	6.57	.020
Overall	140	352.76	.0048	140	127.13	.0045	280	10.70	.014	42	6.65	.025
Nominal	-	353.00	-	-	128.00	-	-	10.70	-	-	6.50	-
Mean/Nominal		0.999	.0048		0.993	.0045		1.000	.014		1.023	.024

where n = number of observations, μ = mean value and V = coefficient of variation

Table 3.1 Cross-sectional dimensions of W360x39 specimens

Beam designation	Depth, d			Flange width, b			Flange thickness, t			Web thickness, t_w		
	n	μ	V	n	μ	V	n	μ	V	n	μ	V
3M	20	308.81	.0077	20	163.39	.0009	40	9.38	.013	6	6.24	.009
3P	20	308.99	.0086	20	163.27	.0013	40	9.39	.011	6	6.19	.009
3V	20	308.48	.0066	20	163.38	.0008	40	9.35	.014	6	6.20	.011
3T	20	309.03	.0075	20	163.40	.0011	40	9.38	.012	6	6.24	.011
Overall	80	308.83	.0077	80	163.36	.0011	160	9.38	.012	24	6.22	.011
Nominal	-	310.00	-	-	165.00	-	-	9.70	-	-	5.80	-
Mean/Nominal		0.996	.0077		0.990	.0011		0.967	.012		1.072	.011

where n = number of observations, μ = mean value and V = coefficient of variation

Table 3.2 Cross-sectional dimensions of W310x39 specimens

Beam property	Section			
	W360x39		W310x39	
	Measured	$\frac{\text{Measured}}{\text{Nominal}}$	Measured	$\frac{\text{Measured}}{\text{Nominal}}$
A (mm^2)	5007	1.005	4903	0.993
I_x (mm^4)	102 x 10^6	1.000	82.1 x 10^6	0.965
I_y (mm^4)	3.67 x 10^6	0.979	6.82 x 10^6	0.938
Z_x(mm^3)	661.5 x 10^3	0.999	595 x 10^3	0.975
S_x (mm^3)	578.3 x 10^3	0.997	532 x 10^3	0.969
S_y (mm^3)	5.77 x 10^3	0.985	83.5 x 10^3	0.948

Table 3.3 Cross-sectional properties of test beams

	Number of beams	Length, m	$\frac{\text{Sweep}}{\text{Length}}$	Twist, rad.
This study	11	9	0.000508	0.0212
Dux and Kitipornchai (1981)	9	6-11	0.000300	0.0023
Fukumoto et al (1980)	75	1.5-2.6	0.000080	0.0013
Hechtman et al (1955)	33	1.5-15	0.000209	0.0044

Table 3.4 Average initial imperfections in different studies

Coupon no.	Location	Modulus of elasticity, MPa	Static yield stress, MPa
C1	Flange	202 340	291.3
C2	Flange	203 320	277.9
C3	Flange	201 730	287.1
C4	Flange	198 600	292.8
C5	Flange	206 920	281.3
C6	Flange	206 240	296.9
			$\mu = 287.9$ $\sigma = 7.22$ $V = 0.025$
C7	Web	208 740	301.1
C8	Web	200 240	318.8
C9	Web	203 420	318.8
C10	Web	213 230	332.5
	Overall	$\mu = 204500$ $\sigma = 4358$ $V = 0.021$	$\mu = 317.8$ $\sigma = 12.87$ $V = 0.040$

Table 3.5 Mechanical properties of W360x39 tension coupons

Coupon no.	Location	Modulus of elasticity, MPa	Static yield stress, MPa
C11	Flange	220 600	351.7
C12	Flange	208 610	347.4
C13	Flange	215 290	351.5
C14	Flange	207 740	350.8
C15	Flange	212 610	347.9
C16	Flange	204 990	351.5
C17	Flange	206 540	353.9
C18	Flange	214 010	362.9
			$\mu = 352.2$ $\sigma = 4.81$ V = 0.014
C19	Web	204 590	371.5
C20	Web	203 360	361.8
C21	Web	208 710	362.1
C22	Web	204 690	374.0
	Overall	$\mu = 209\,300$ $\sigma = 5265$ V = 0.025	$\mu = 367.4$ $\sigma = 6.32$ V = 0.017

Table 3.6 Mechanical properties of W310x39 tension coupons

Property	Section	
	W360x39	W310x39
Modulus of elasticity, MPa	214 240	208 350
Static yield strength, MPa	289.1	350.5
First observed yield stress, MPa	229	250

Table 3.7 Stub column test results

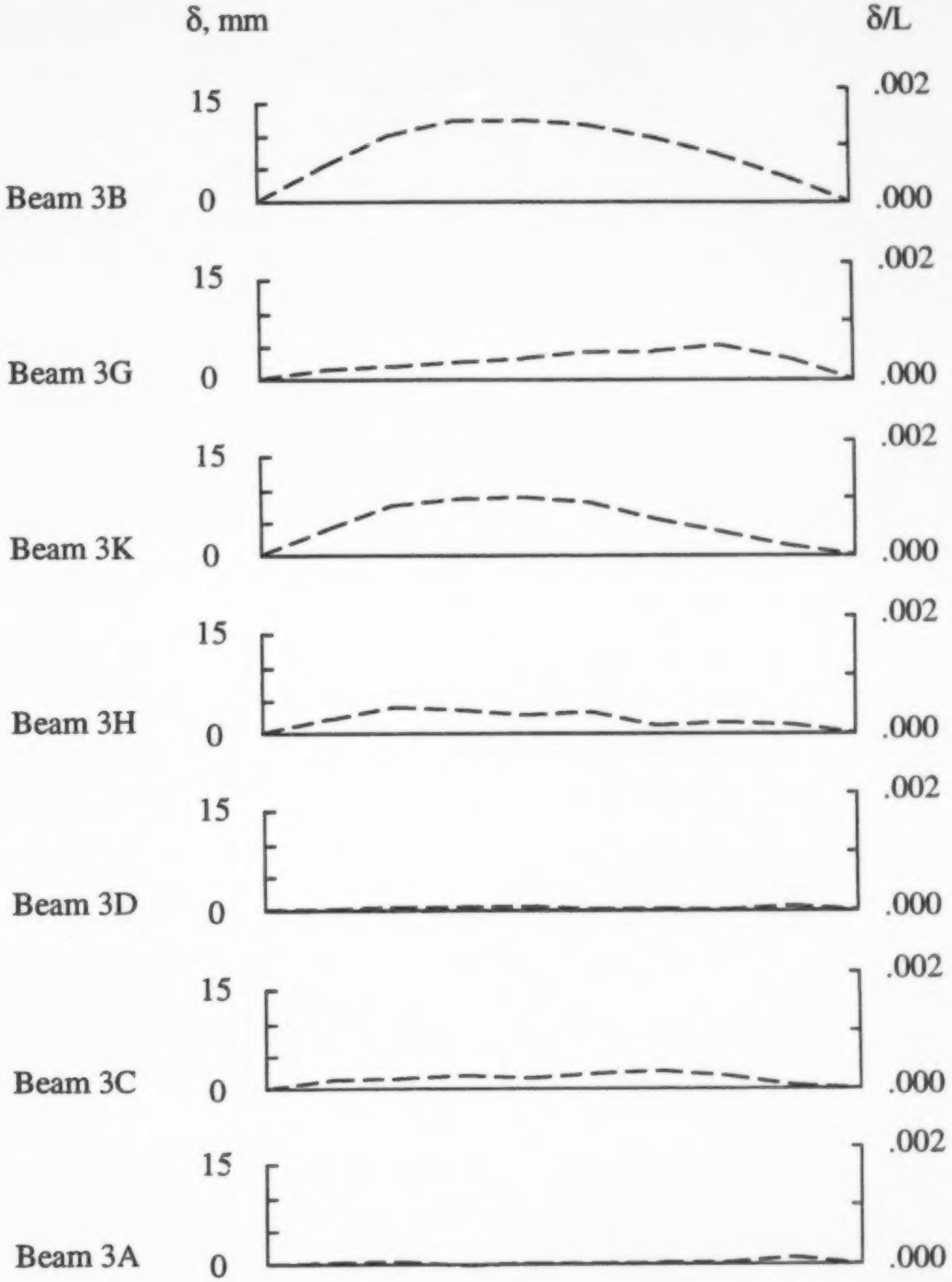

Fig. 3.1.a Initial sweep of W360x39 specimens

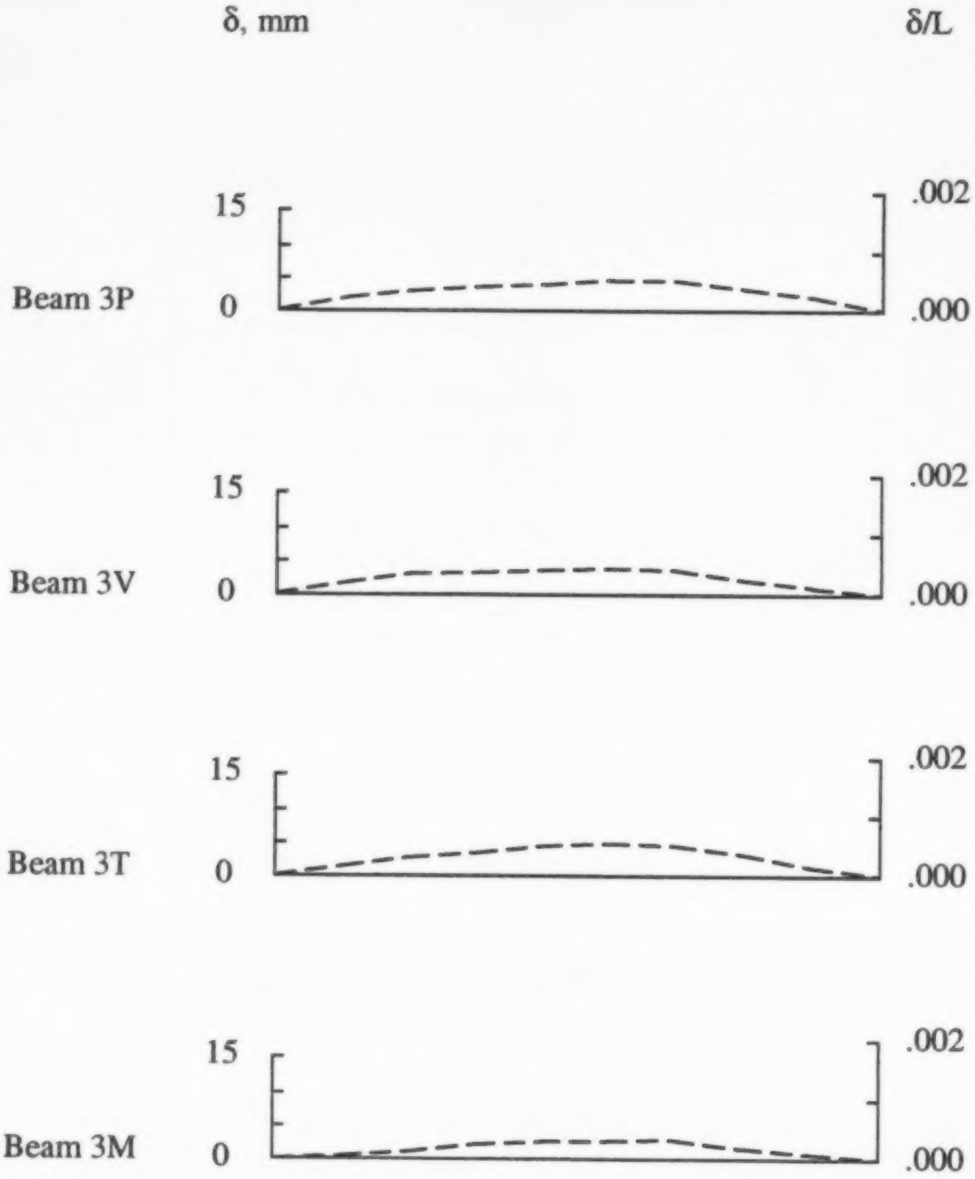

Fig. 3.1.b Initial sweep of W310x39 specimens

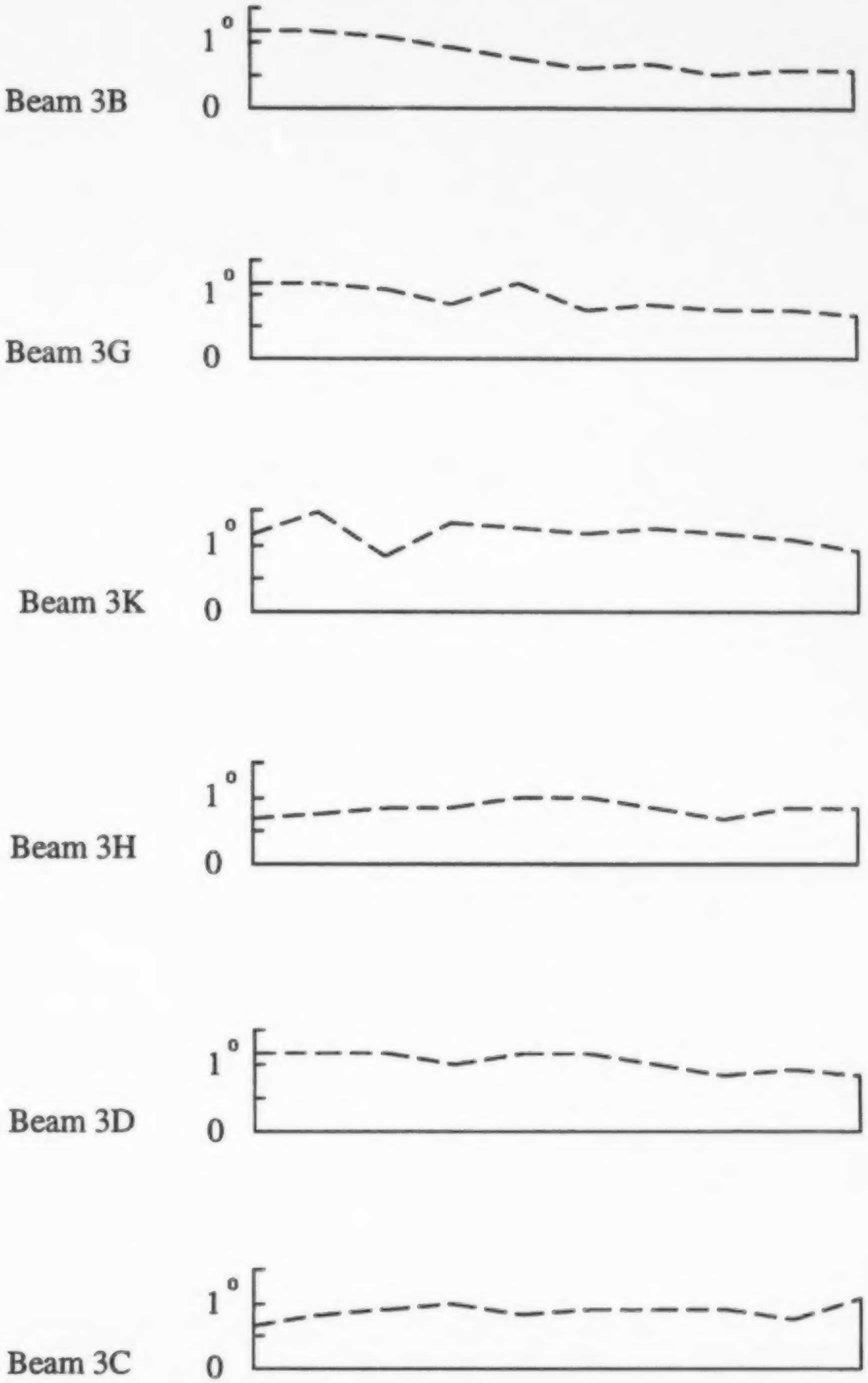

Fig. 3.2.a Initial twist of W360x39 specimens

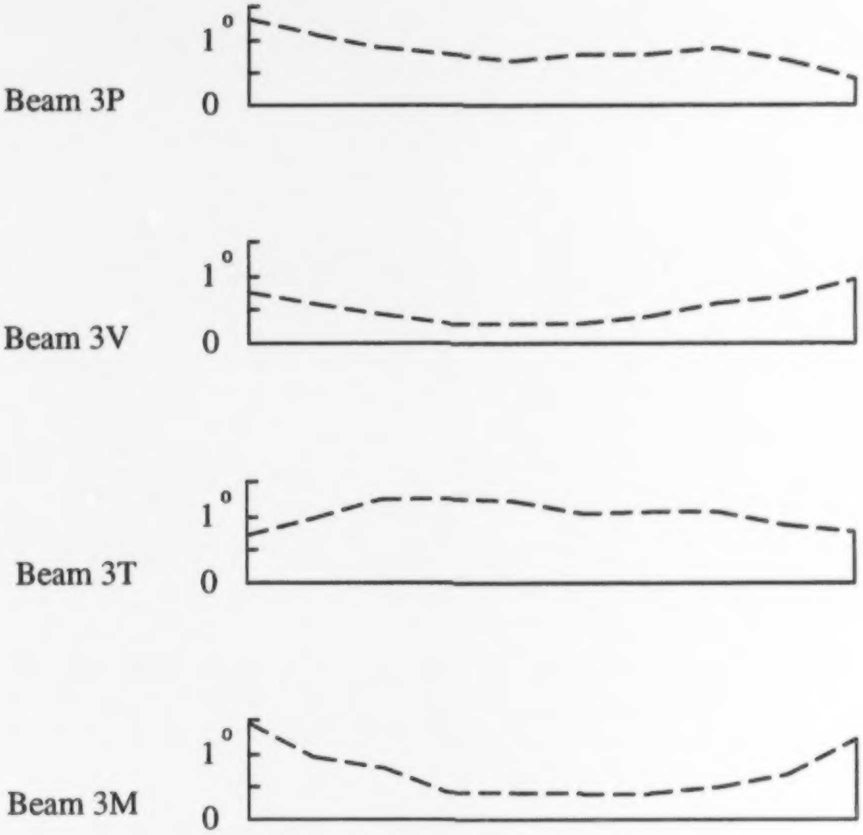

Fig. 3.2.b Initial twist of W310x39 specimens

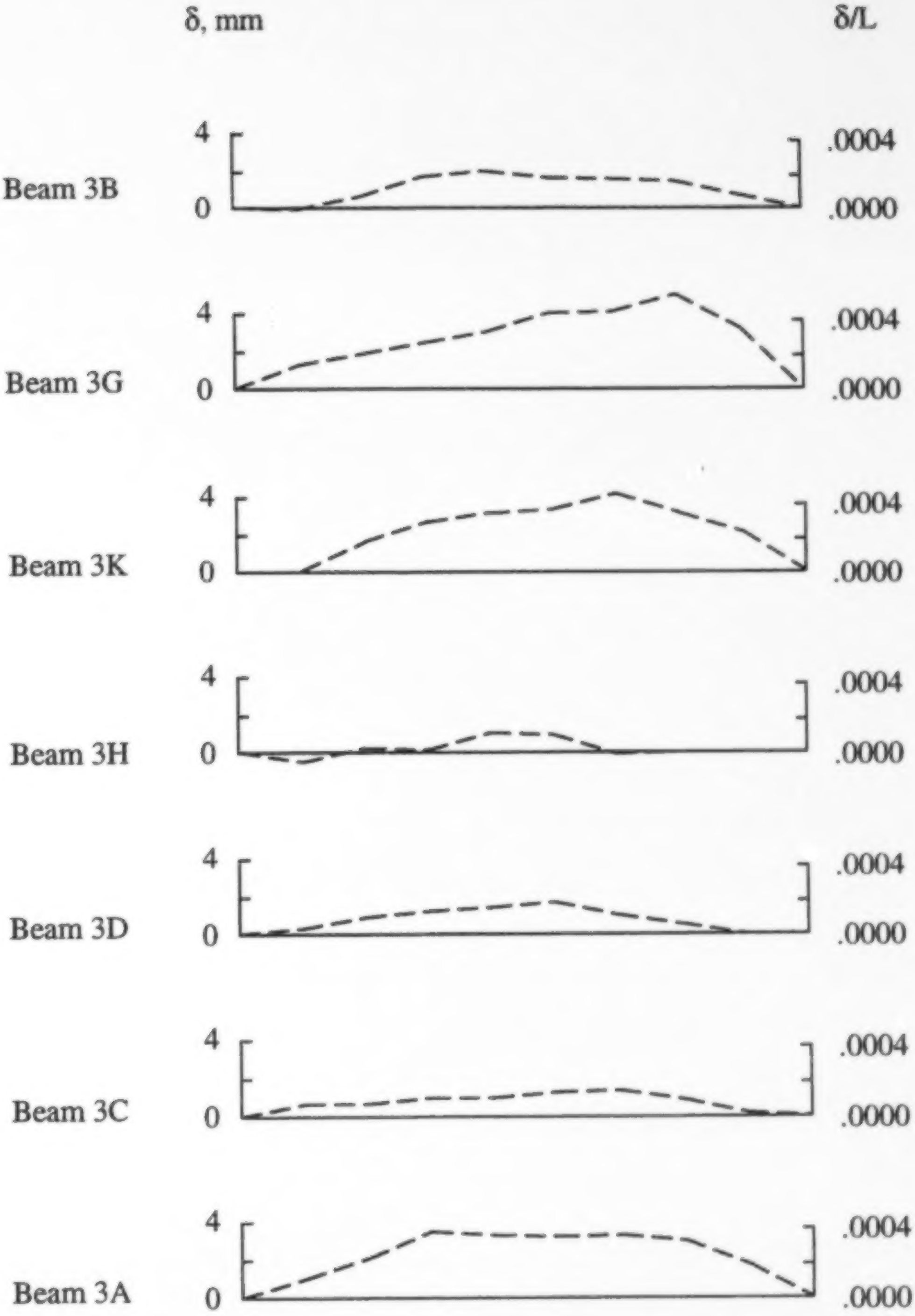

Fig. 3.3.a Initial camber of W360x39 specimens

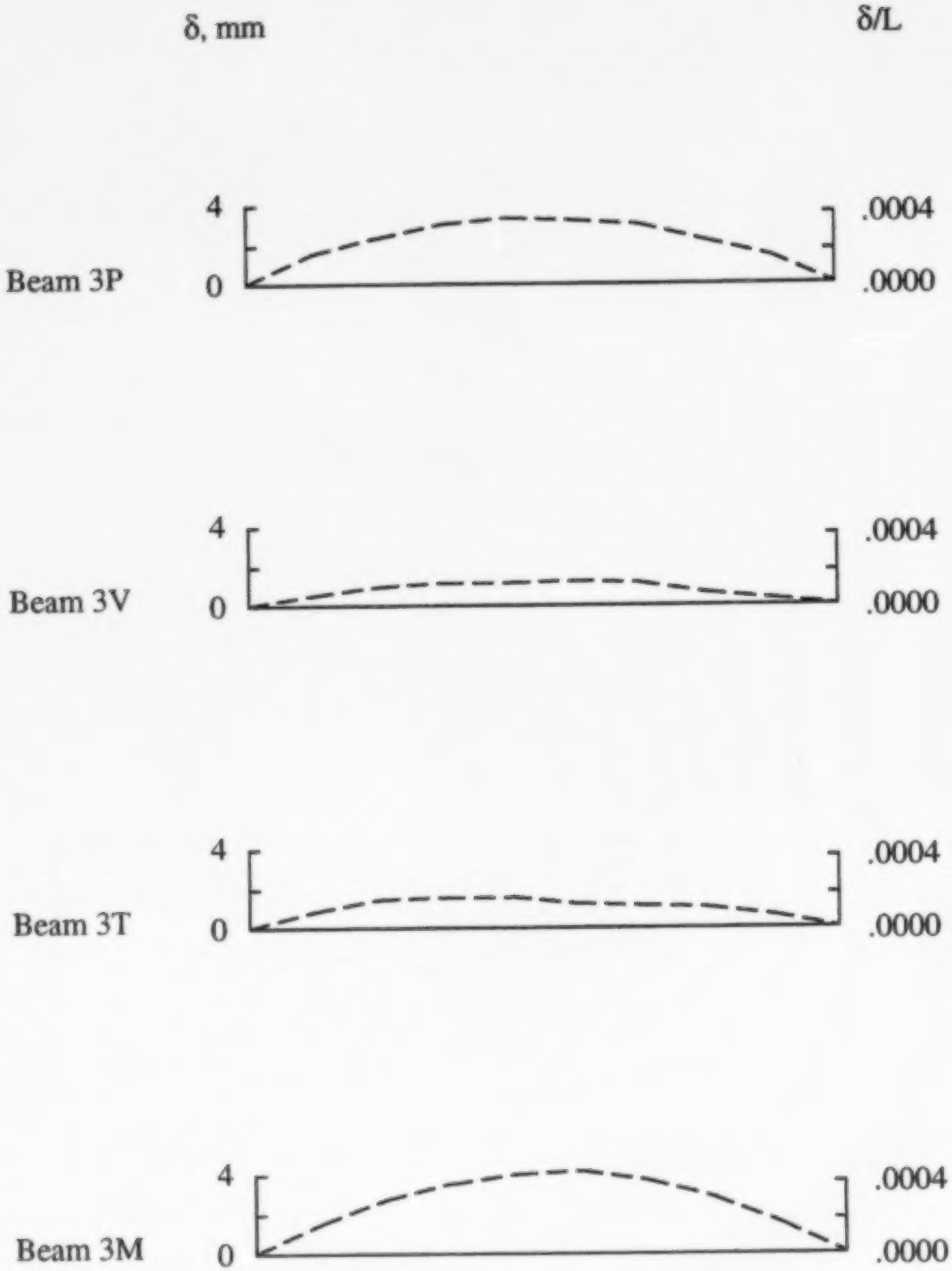

Fig. 3.3.b Initial camber of W310x39 specimens

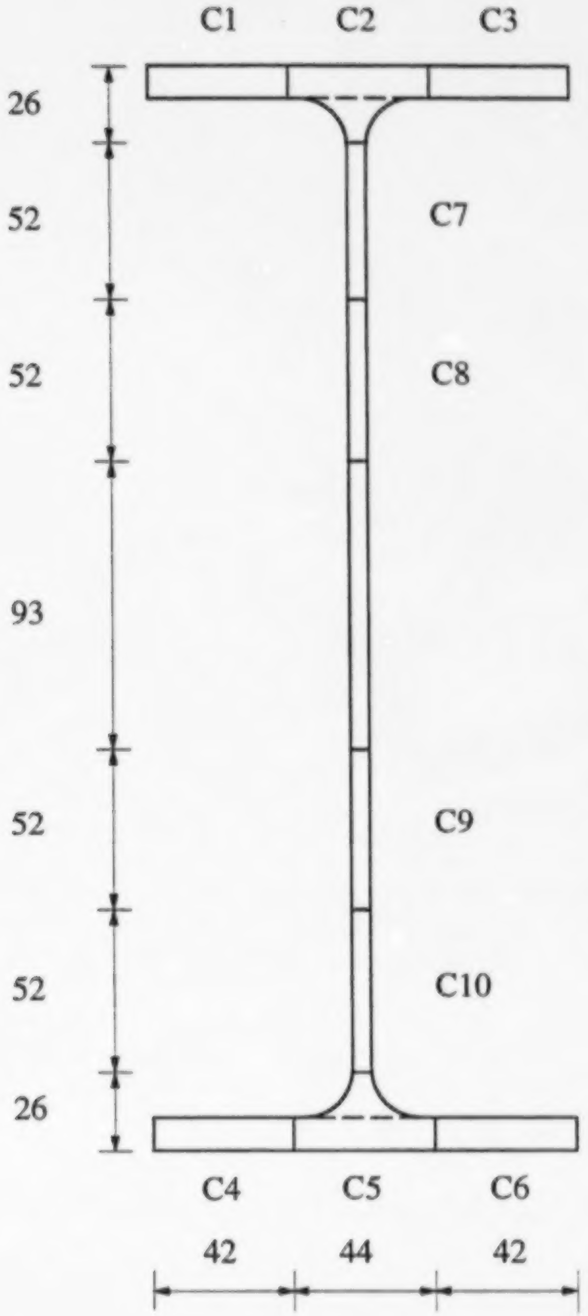
C1
C2
C3
26
52
C7
52
C8
93
52
C9
52
C10
26
C4
C5
C6
42
44
42

Fig. 3.4 Identification and location of tension coupons for W360x39

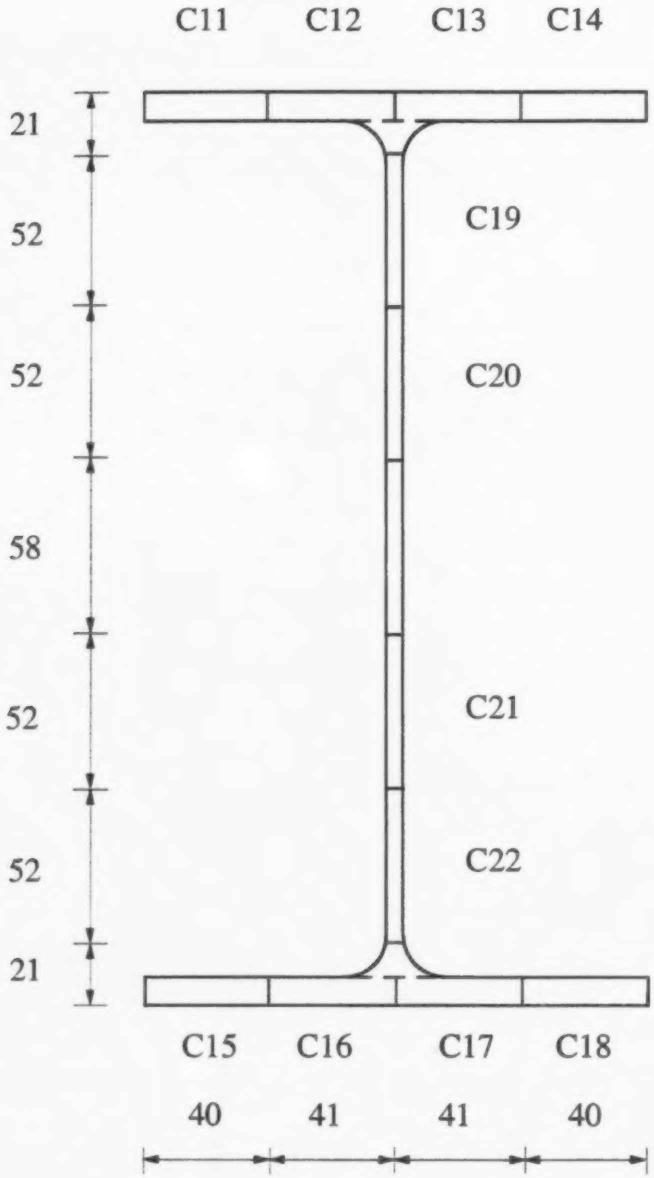
C11
C12
C13
C14
21
52
C19
52
C20
58
52
C21
52
C22
21
C15
C16
C17
C18
40
41
41
40

Fig. 3.5 Identification and location of tension coupons for W310x39

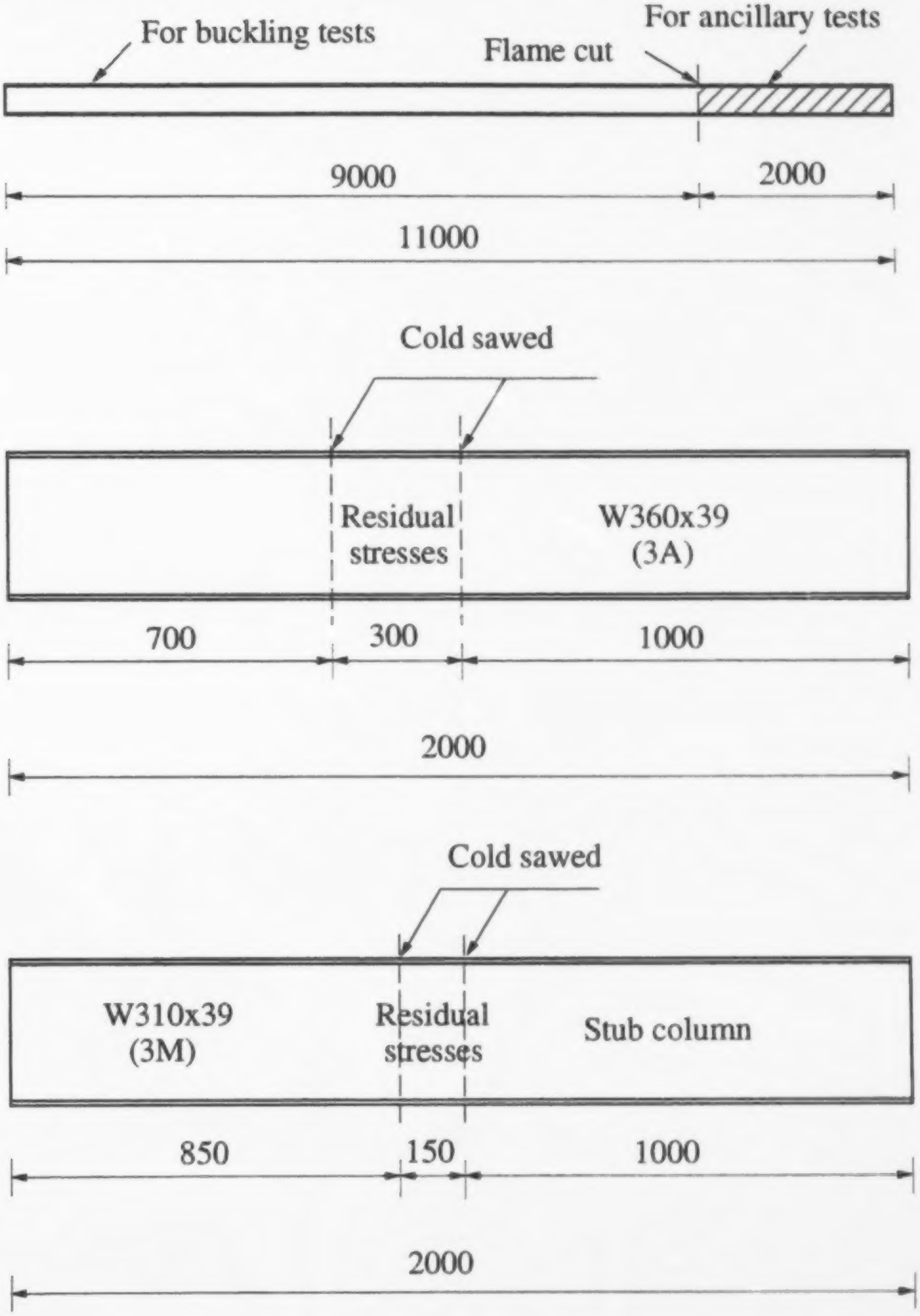
For buckling tests
Flame cut
For ancillary tests
9000
2000
11000
Cold sawed
Residual stresses
W360x39
(3A)
700
300
1000
2000
Cold sawed
W310x39
(3M)
Residual stresses
Stub column
850
150
1000
2000

Fig. 3.6 Test specimens for residual stress determination

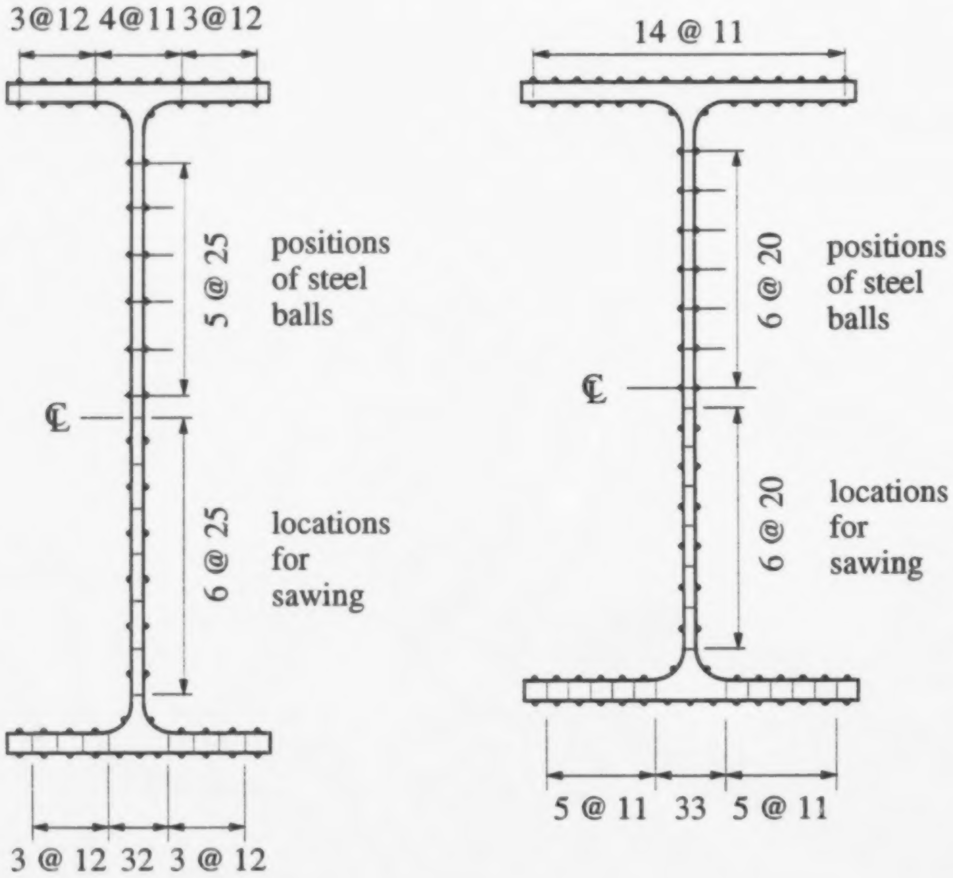
3@12 4@11 3@12
5 @ 25
positions of steel balls
℄
6 @ 25
locations for sawing
3 @ 12 32 3 @ 12
14 @ 11
6 @ 20
positions of steel balls
℄
6 @ 20
locations for sawing
5 @ 11 33 5 @ 11

W360x39

W310x39

Fig. 3.7 Sectioning scheme of cross sections for residual stress determinations

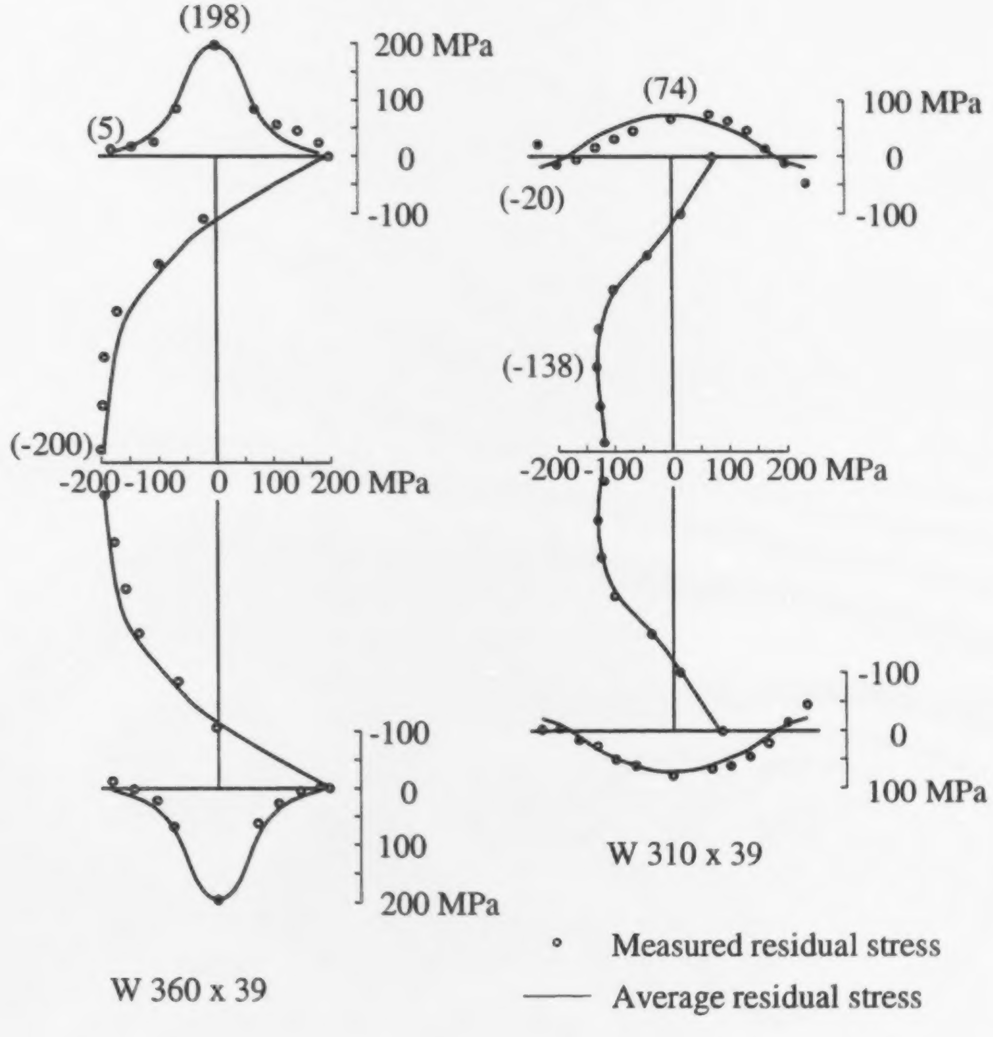

Fig. 3.8 Residual stresses

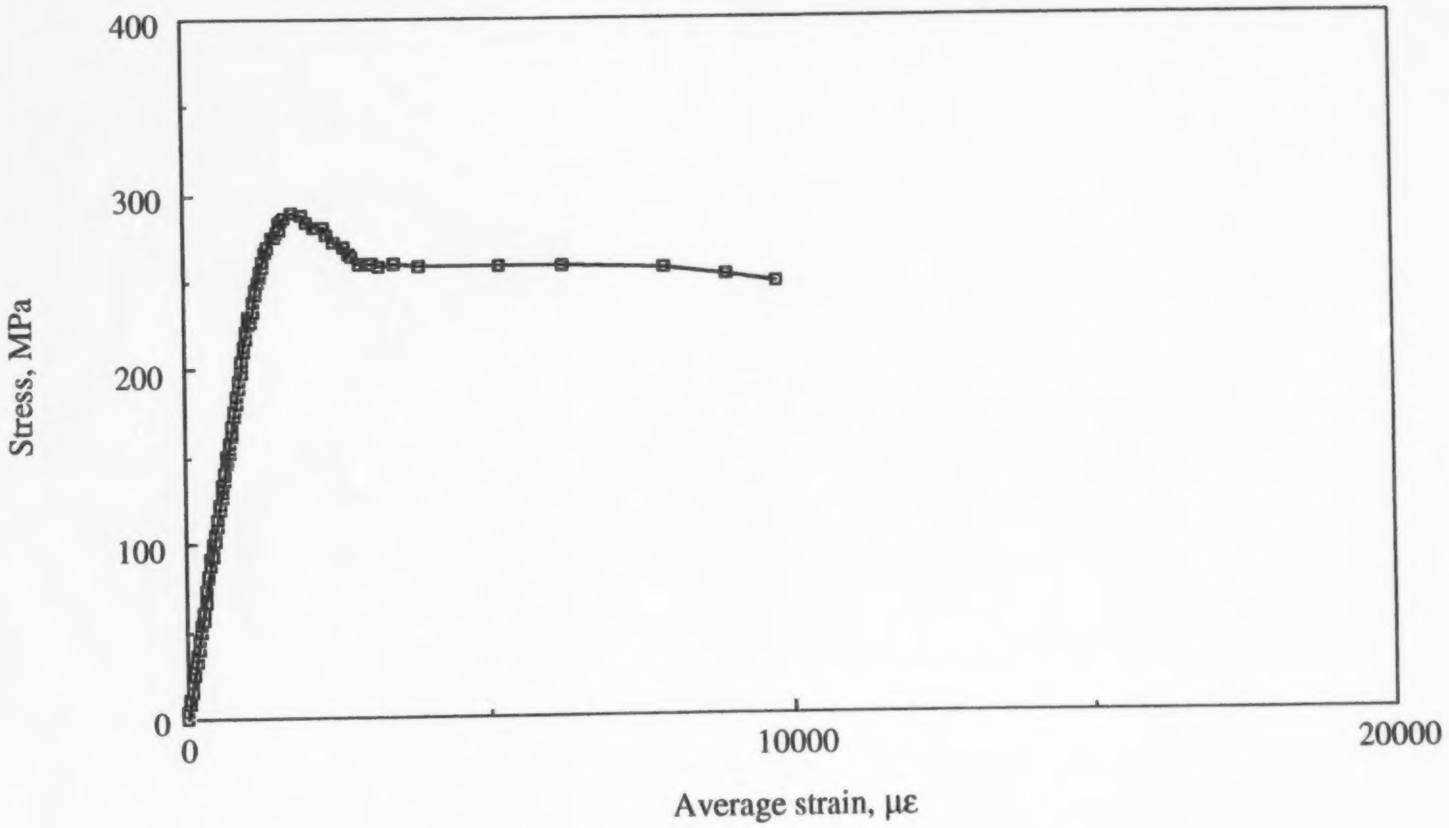

Fig. 3.9 Stub column stress-strain curve for W360x39

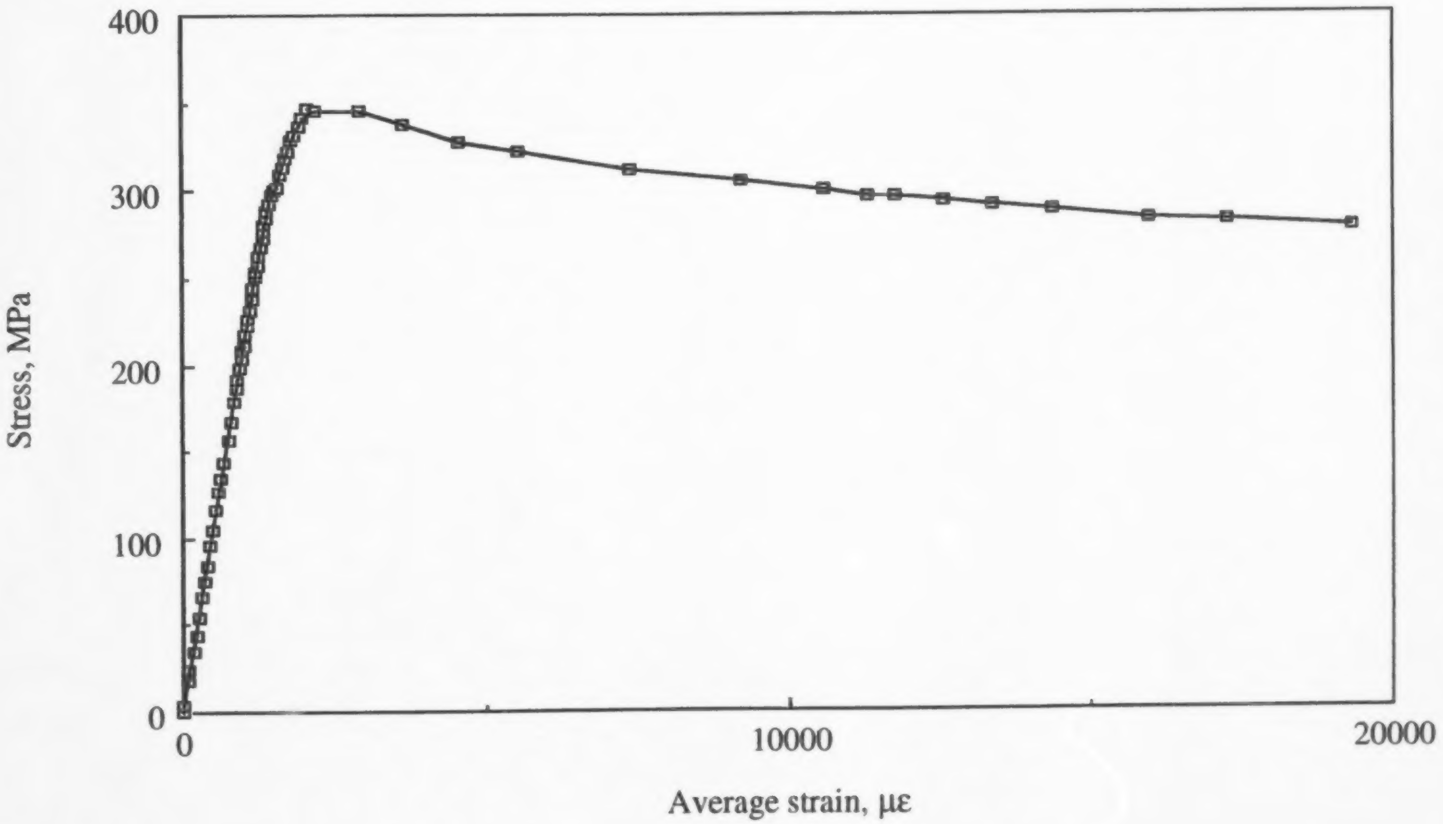

Fig. 3.10 Stub column stress-strain curve for W310x39

Chapter 4

EXPERIMENTAL PROGRAM

4.1 General

Thirty-three full-scale tests were conducted using eleven W-shaped steel beams of two different cross sections in a single overhang configuration, as shown schematically in Fig. 4.1. The sequence of tests performed on a single beam was planned to avoid increasing the initial imperfections due to inelastic deformations in all tests except the last one in the sequence. Aspects of the behaviour of steel beams investigated included:

1. the elastic and inelastic lateral-torsional buckling capacity of steel beams in cantilever-suspended span construction, taking into account the restraining effects provided by open-web steel joists supported on the beams,

2. the effects of web distortion on the buckling capacity of steel beams,

3. the effect of the height of load application above the shear centre as well as bottom flange loading,

4. the effect of the loading arrangement on the buckling capacity,

5. the effect of torsional restraint of the bottom flange of the beam at a column location which may be provided by a rigid connection between the bottom flange and the column,

6. the effect of lateral bracing of columns which support steel beams in cantilever-suspended span construction,

7. the effect of the height at which lateral restraint is provided,

8. the buckling modes and determination of the ratio of the test-to-predicted buckling loads to check the analytical model.

4.2 Test setup

The test setup, shown in Figs. 4.1 and 4.2 was designed to load beams, with a single cantilever, at up to 5 locations between 2 supports and at the cantilever tip. The five loading frames between the supports were spaced at 1.22 m on centers to match the strong floor geometry and the sixth frame was at the tip of a 1.22 m long cantilever.

Load cells were provided at every load or reaction point so that statics was confirmed in each test. As well, any combination of translational and rotational restraints could be provided at the reactions or load points by using assemblies of rollers, knife edges, and thrust bearings as discussed subsequently. When the test beam is laterally unrestrained at a load point, the beam may move laterally and causes an eccentric load on the loading system. The typical loading frame shown in Figs. 4.3 and 4.4 shows how this eccentric load is accommodated while maintaining the load in a nearly vertical position. The inner frame moves smoothly and essentially without friction in the vertical direction guided by four roller bearings between it and the outer frame. The roller bearings, by providing equal and opposite forces at diagonally opposite corners, maintain the equilibrium of the inner frame against eccentric loading that may occur either due to the initial placement of the test specimen or due to the lateral movement of the specimen.

When the test beam is laterally restrained, the lateral restraining force provided by the top horizontal member of the inner frame is transmitted to the outer frame through the set of roller bearings. Because the outer frame is relatively stiff and because the clearance between the two frames is only 2 mm, the deviation of the test loads from the vertical does not exceed about 1/600 rad.

Vertical loads are applied to the test beam by the inner frames which are pulled downward by the pair of loading rods attached to the frame and passing through the floor. The lower ends of the rods are attached to a yoke. As shown in Fig. 4.5, a jack pushes between the yoke and the lower surface of the strong floor and a load cell is provided to measure the jack reaction.

The five frames between supports allow loads to be applied as they would be by open-web steel joists in an actual structure while the single frame at the cantilever tip applies the load simulating that of a suspended span. The frame at the cantilever tip was designed for greater loads than the other five frames.

Because the six loading frames are independent, loading and restraint conditions can be different one from another and from one test to another.

4.3 Loading and restraint configurations

In Fig. 4.5, the load cell used to measure the load applied by the jack is shown. Load cells were also provided at each column support. All load cells were calibrated before usage. In some tests, the end reaction at the start of the test was upwards due to the self-weight of the test specimen but reversed with increasing cantilever tip load. It was necessary, in these cases, to use a temporary load cell under the beam and then a permanent one on top of the beam. In tests where the bottom flange at a column location was allowed to move laterally (as in test 23), it was necessary to use two load cells (one beside the other) to provide a stable condition and to measure the eccentric reaction due to torsional restraint provided to the beam by the support column.

Figs. 4.6.a, b and c show the points of load application and the restraint conditions for each test. The test number, test specimen number and beam cross section designation are also given. In all tests except test 33, the beam specimen was approximately 9 m long as shown in Fig. 4.2. In test 33, the dimensions were as indicated in Fig. 4.6.c.

In Fig. 4.6.a, b and c, the different restraint conditions provided to the flanges of the test beams at load and reaction points are represented by different symbols. A white dot represents a point where only lateral restraint was provided to a flange; a white square where only torsional restraint existed; and a black dot where both lateral and torsional restraints existed. When no restraint was provided, none of these symbols appear. Reactions are denoted by triangles pointing upward or downward in the direction of the reaction. As a fork support, at column locations, provides lateral restraint to both flanges, it is represented by a white dot at each flange.

Full-depth stiffeners as provided in tests 5 and 19 at the cantilever tip are indicated by a pair of vertical lines. The stiffeners had a thickness of 10 mm, an overall width out to out of the pair equal to the flange width and were welded symmetrically to both sides of the web.

The nominal relative values of the applied loads are indicated by the designations P, P/5 or P/2. The numbers in parentheses following the load designation indicate, in order, the height in millimetres above the top flange where the load was applied and the height where lateral restraint was provided. When the flange is unrestrained, only the height of load application is shown and, where no numbers are given, the loads, reactions and restraints were applied directly to the flange surface. In general, the points of load application and lateral restraint are at the same distance above the top flange. This occurs when torsional restraint is provided or, as shown in Fig. 4.7.a, when the freedom of rotation about the longitudinal axis is ensured by a longitudinal knife-edge. In some cases, as indicated in Fig. 4.7.b, the point of lateral restraint is above the point of load application. This occurs when a semi-cylindrical or hemispherical rocker is used to ensure rotational freedom about the longitudinal axis. Lateral restraint is provided through friction at the top of the rocker but rotation of the rocker causes the point of load application to be at the top of the flange.

4.4 Simulation of boundary conditions

At all load or reactions points on a flange, special care was taken to ensure the boundary conditions were accurately modelled. Of the six degrees of freedom at a load or reaction point, that associated with vertical movement was not an issue because the vertical displacement was either that of the loading frames or nil at a reaction point. Devices used to provide the other five degrees of freedom included knife edges, rockers, roller assemblies and thrust bearings. All of these devices had to have capacities sufficient for the loads to be sustained.

Longitudinal and lateral translational freedom was generally provided by using a nest of lateral or longitudinal rollers (These devices, made of hardened steel, have coefficients of rolling friction in the order of 0.0003 at the load levels encountered). To eliminate any longitudinal thrust in the specimen, lateral rollers were provided at all load and reaction points except one.

Rotational freedom about longitudinal or transverse axes was generally provided by using hardened steel knife edge assemblies although in some cases a semi-cylindrical rocker proved to have sufficient capacity and in others a hemispherical rocker provided rotational freedom about both orthogonal axes. Assuming a static coefficient of about 0.3, rotations about a longitudinal axis were limited to about 17° when using longitudinal rockers. A hemispherical rocker was also considered to allow rotation of a beam to occur about a vertical axis at a load point because of the very limited torsional restraint that could be developed over the small contact area. When the point load exceeded the load capacity of a hemispherical rocker, crossed knife edge assemblies coupled with a thrust bearing were used to provide three degrees of rotational freedom.

4.4.1 Top flange restraint

The four distinct top flange restraint conditions provided were those of no restraint (free), lateral restraint only, lateral and torsional restraints, and torsional restraint only.

The free condition was achieved, as shown in Fig. 4.8.a for relatively small loads by permitting lateral and longitudinal displacements by means of longitudinal and lateral rollers, respectively, and allowing rotations about the longitudinal, lateral, and vertical axes by means of a hemispherical rocker. For greater loads, the stresses at the contact points were reduced by replacing the hemispherical rocker with two semi-cylindrical rockers oriented longitudinally and laterally, and a thrust bearing, as shown in Fig. 4.8.b, to allow rotations about the longitudinal, lateral, and vertical axes, respectively. In tests 6 and 7, the free condition of the top flange at the five interior span loading points was achieved, as shown in Fig. 4.9, by using a hemispherical rocker for the rotational degrees of freedom and a nest of ball bearings between two bearing plates to allow translational movement.

By omitting longitudinal rollers but retaining all the other elements, as shown in Fig. 4.10, lateral restraint was achieved through friction between the several elements and the inner loading frame.

In Fig. 4.11, one further degree of restraint is achieved by removing the longitudinal semi-cylindrical rocker and the top flange is both laterally and torsionally restrained.

The condition of torsional restraint about the longitudinal axis only was achieved by using lateral rollers, longitudinal rollers, a thrust bearing, and a lateral semi-cylindrical rocker, as shown in Fig. 4.12.

It is recognized that the only two restraint conditions of the top flange likely to be encountered are those of lateral restraint alone and combined lateral and torsional restraint. The other two conditions were investigated however so that the separate effects could be assessed.

As well, in practice, the torsional restraint offered to the top flange is limited by the in-plane bending stiffness of the joists welded to the top flange, a condition intermediate to the test conditions of zero and complete torsional restraint but much closer to the latter as discussed subsequently.

4.4.2 Bottom flange loaded with no restraints

Test 32 was tested in a double cantilever configuration. The bottom flange at the end of the longer cantilever span was loaded, as shown in Fig. 4.13 to ensure that it was essentially free. The weight of the heavy object was shared by the beam and the crane. The load carried by the beam, determined as the difference in the weight of the heavy object and the load cell reading, was increased gradually by lowering the crane, reducing the tension in the crane cables. Because the distance to the crane was large, the lateral restraining effect of the crane on the specimen was considered to be negligible.

4.4.3 Restraint at the columns

To model the practical situation where, at a column location, an open-web steel joist is welded to the top flange of the supporting beam and has its bottom chord extended and connected to either the bottom flange of the beam or the column, a fork support was used as shown in Fig. 4.14. This ensured that the beam cross section was restrained from twisting and moving laterally whilst remaining free to warp, to move longitudinally and to rotate about the major and minor axes. The fork support consisted of a pair of T-sections, to which were welded two short cylindrical stubs. The T-sections were shimmed to just bear against the web on both sides. It was assumed that longitudinal translation and rotation about a lateral axis were not impeded by the stubs as the normal forces exerted by them and hence the longitudinal frictional forces are small and were further reduced by lubrication.

When there is no joist at a column, both flanges of the beam may move laterally. A rigid connection between the bottom flange and the supporting column provides torsional restraint to the bottom flange and the buckled shape will be accompanied by web distortion. This situation was achieved, as shown in Fig. 4.15, by providing a longitudinal set of rollers under the bottom flange to allow the bottom flange to move sideways. A pair of load cells was used to measure the reaction and to provide a sufficiently broad base to develop the restraining moment on the bottom flange. With the lateral rollers removed from this location only, a single point of longitudinal fixity is provided along the length of the beam. The efficiency of torsional restraint achieved near ultimate loads was better in the tests with the W310x39 beam than in the tests with the W360x39 beam because of the broader flange width of the former.

In those tests where the cantilever load was the only applied load, the downward reaction force at the opposite end of the beam was provided by a reaction beam bolted to columns on both sides of the pedestal.

4.5 Instrumentation

Five types of instrumentation were used to measure the loads and reactions, the displacements of the buckled test beams, the lateral roller movements at supports and strains in the steel.

By using calibrated load cells, as described previously, at each load and reaction point, statics could be used to verify the loads applied. In particular, any unwanted frictional losses in the system would be identified. Three linearly variable displacement transducers (LVDTs) were used to measure the vertical movement of inner frame at the cantilever tip and the roller movements at both reaction points. When the test beam was allowed to move laterally at a reaction point, another two LVDTs were used to measure the lateral movements of the top and bottom flanges at that location.

In order to determine the buckled shape including cross-sectional distortion, six cable transducers were used at each of three stations along the test beam, as shown in Fig. 4.16. The details of one station are shown in Fig. 4.17 where three cable transducers were attached to each flange. This arrangement of cable transducers was enough to measure the vertical deflection, lateral displacement and angle of twist of each flange.

Bending strains about the major and minor axes as well as warping strains were monitored by four longitudinal strain gauges mounted on each flange, as shown in Fig. 4.18, at five locations along the test specimen. Lateral bending strains in the web due to distortion were monitored by a vertical strain gauge mounted on each side of the web near the cantilever tip. The sketch of a beam specimen given in Fig. 4.19 identifies the gauges.

Two dial gauges mounted near the cantilever tip were used to monitor the lateral deflection of either the top or bottom flange and the vertical deflection during the course of a test. The load-deflection curves obtained were used to determine the load increments, particularly as the critical load was being approached.

All electronic measuring devices such as load cells, LVDTs, and cable transducers were calibrated before use.

The output from electrical resistance strain gauges, LVDTs, cable transducers, and load cells, amounting to as many as 85 channels, were recorded automatically at each step during the test on the Fluke data aquisition system.

4.6 Testing procedure

Each load was applied by pumping oil manually to the hydraulic loading jacks (Fig. 4.5). All five interior jacks were supplied from the same manifold and therefore were at the same pressure. The jack at the cantilever tip, applying a much greater load, was on a separate manifold. In all tests, the interior jack load was increased before the load at the cantilever tip.

The test load was applied in increments, the size of which depended on the proximity to failure as estimated from the growth of buckling deformations and from the analytical model. Increments were generally as large as 10 kN in the early stages of testing and as small as 0.5 kN near buckling. To decide on the size of a loading increment and to detect any anomalous restraints, the vertical and lateral deflections of the unrestrained flange at the cantilever tip were plotted against the cantilever tip load. In addition, the lateral deflection of the bottom flange determined from a cable transducer station located in the main span was plotted against the cantilever tip load using an X-Y recorder. Each load was held for few minutes until all readings indicated that the beam had stabilized. Buckling was deemed to occur when a load-deflection curve such as the lateral deflection of one of the flanges or the rotation of the cross section at the cantilever tip reached a horizontal asymptote. As the maximum load was approached, the load was increased only to the extent required to reach a predefined deformation.

At every load step, a check of static equilibrium was obtained from the load cell readings, thereby assuring that the system was functioning properly and that frictional losses were a minimum.

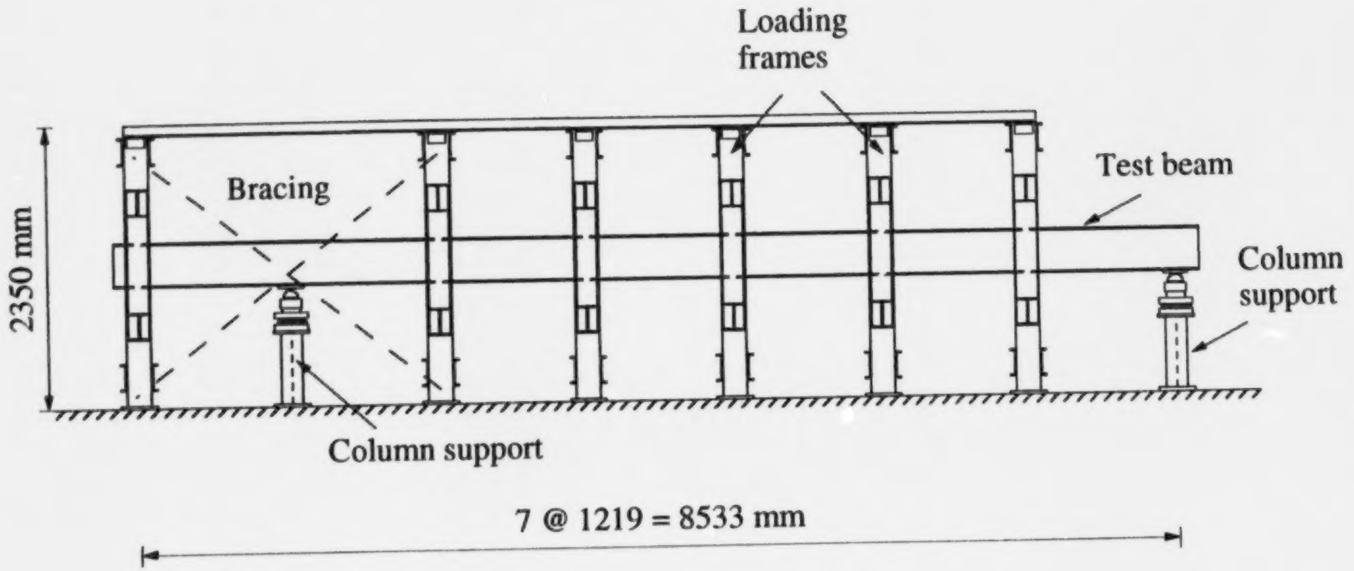
Loading
frames
Test beam
Bracing
2350 mm
Column
support
Column support
7 @ 1219 = 8533 mm

Fig. 4.1 Schematic diagram of test setup

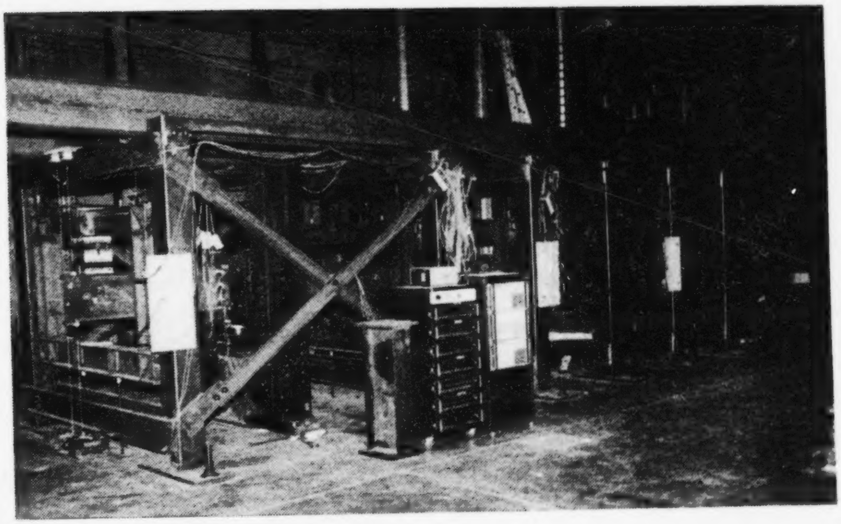

Fig. 4.2 Overall test setup

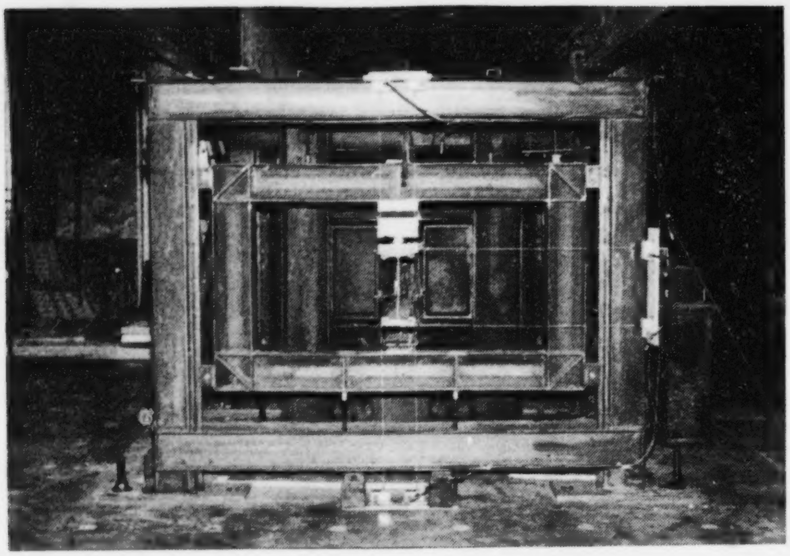

Fig. 4.3 Loading frame

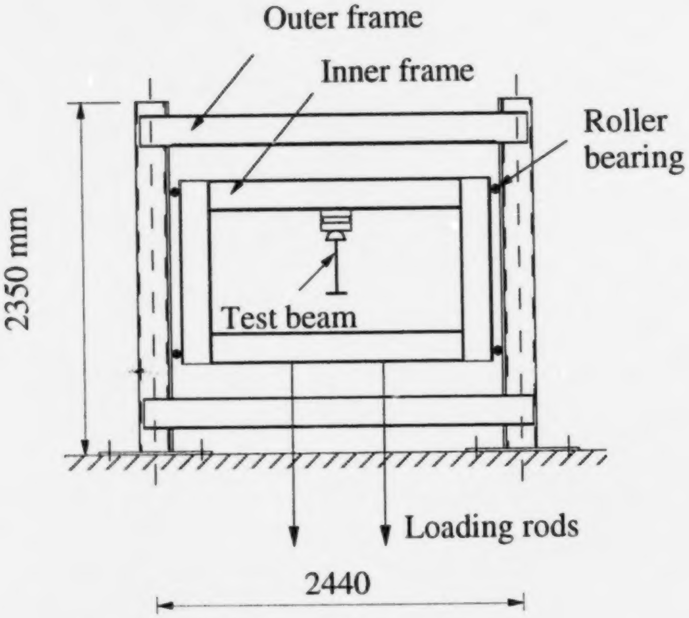
Outer frame
Inner frame
Roller bearing
Test beam
2350 mm
Loading rods
2440

Fig. 4.4 Schematic diagram of a typical loading frame

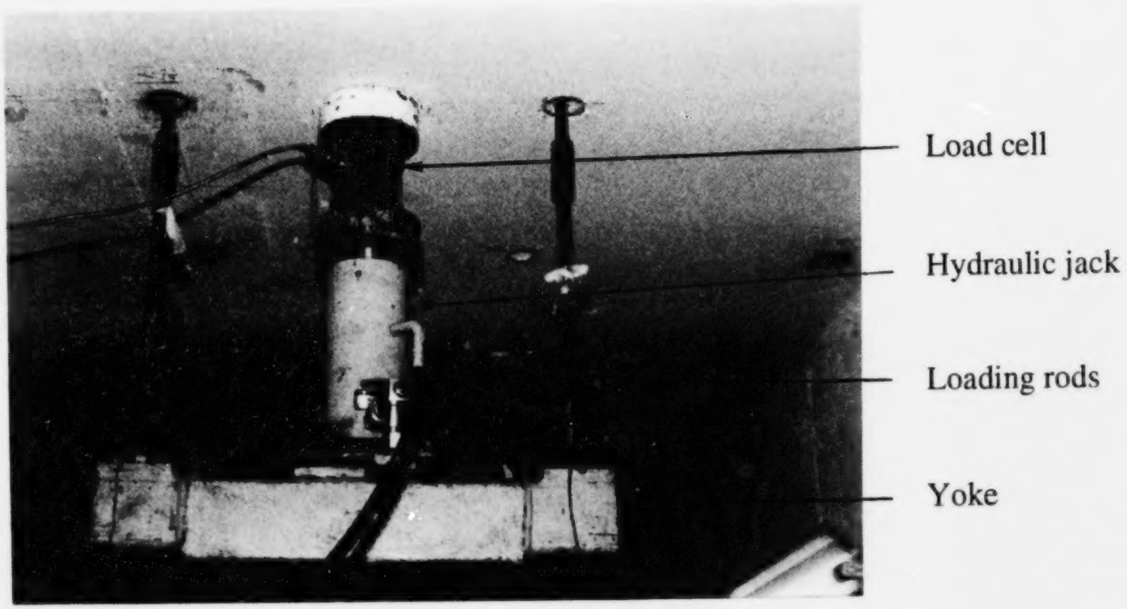
Load cell
Hydraulic jack
Loading rods
Yoke

Fig. 4.5 Loading jack and load cell

Test no.	Loading and restraint diagram	Section	Beam designation
1	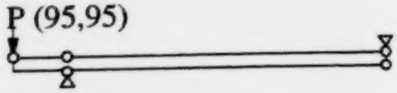	W360x39	3B
2	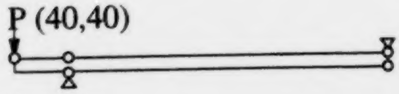	W360x39	3B
3	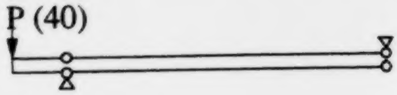	W360x39	3B
4	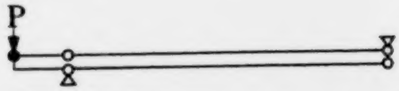	W360x39	3B
5	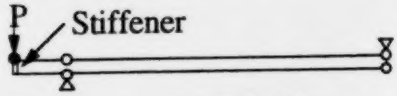 P Stiffener	W360x39	3C
6	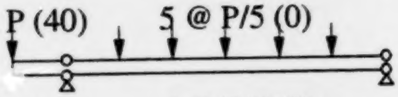	W360x39	3A
7	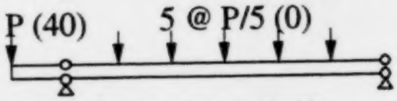	W360x39	3A
8	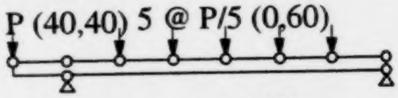 P (40,40) 5 @ P/5 (0,60)	W360x39	3A
9	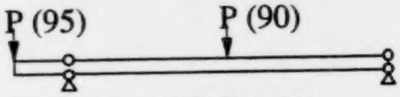	W360x39	3K
10	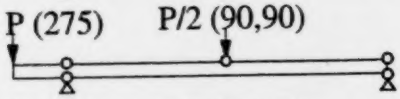 P (275) P/2 (90,90)	W360x39	3K
11	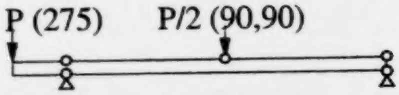 P (275) P/2 (90,90)	W360x39	3K
12	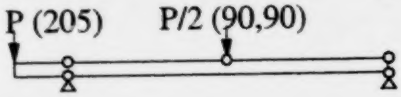 P (205) P/2 (90,90)	W360x39	3K

Note: Loading and restraint symbols are defined in Fig. 4.6.c

Fig. 4.6.a Loading and restraint configurations for tests 1 through 12

Test no.	Loading and restraint diagram	Section	Beam designation
13	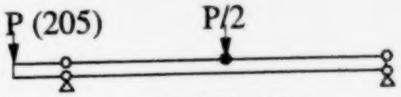	W360x39	3K
14	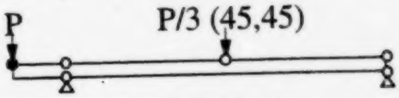	W360x39	3K
15	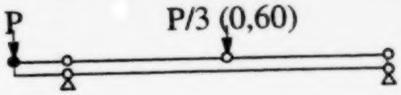	W360x39	3K
16	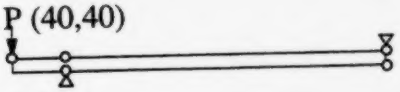	W310x39	3V
17	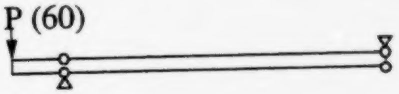	W310x39	3V
18	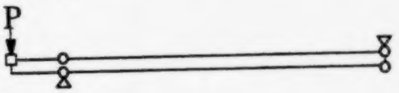	W310x39	3V
19	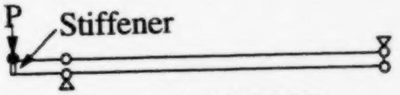 P Stiffener	W310x39	3V
20	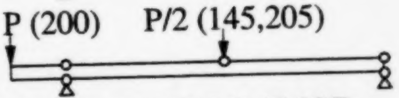 P (200) P/2 (145,205)	W310x39	3T
21	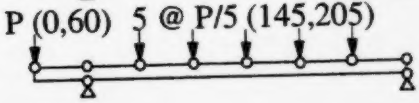 P (0,60) 5 @ P/5 (145,205)	W310x39	3T
22	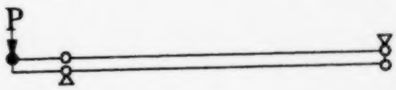	W310x39	3T
23	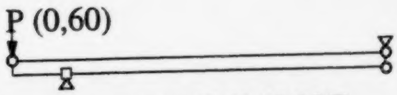	W360x39	3G
24	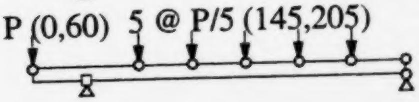 P (0,60) 5 @ P/5 (145,205)	W360x39	3G

Note: Loading and restraint symbols are defined in Fig. 4.6.c

Fig. 4.6.b Loading and restraint configurations for tests 13 through 24

Test no.	Loading and restraint diagram	Section	Beam designation
25	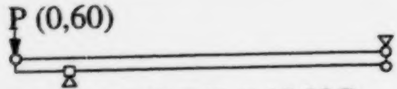	W310x39	3P
26	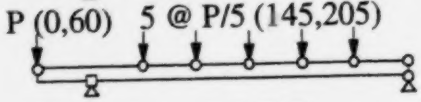 P (0,60) 5 @ P/5 (145,205)	W310x39	3P
27	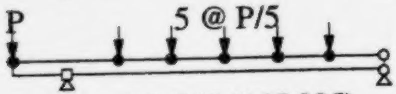	W310x39	3P
28	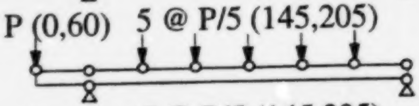 P (0,60) 5 @ P/5 (145,205)	W360x39	3H
29	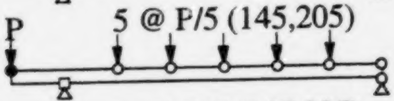 P 5 @ P/5 (145,205)	W360x39	3H
30	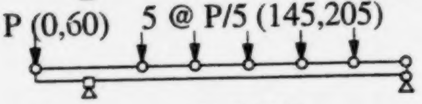 P (0,60) 5 @ P/5 (145,205)	W360x39	3H
31	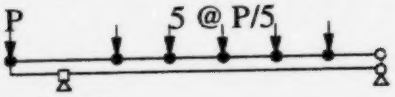	W310x39	3M
32	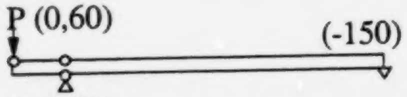	W360x39	3D
33	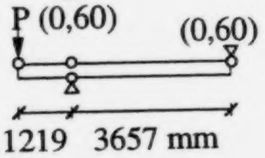 P (0,60) (0,60) 1219 3657 mm	W360x39	3D

○ Lateral restraint

□ Torsional restraint

‖ Web stiffener

△,▽ Reaction

(a,b) Height of load application and height of lateral restraint above top flange, mm, if applicable

● Lateral and torsional restraint

Fig. 4.6.c Loading and restraint configurations for tests 25 through 33

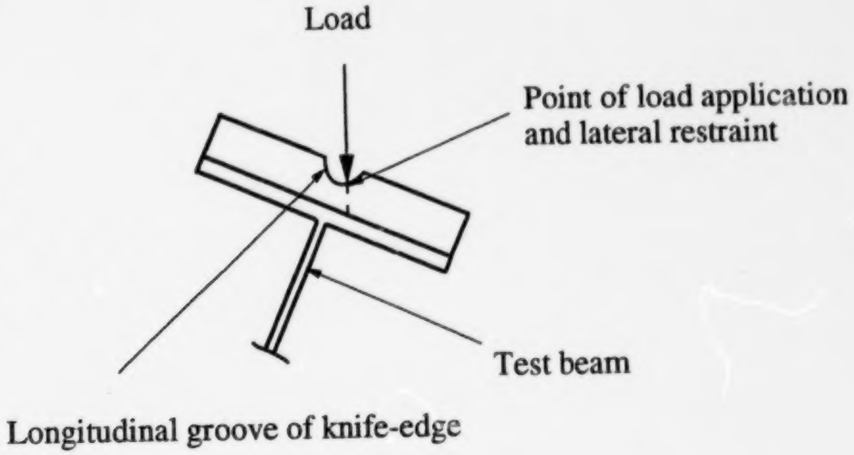
Load
Point of load application
and lateral restraint
Test beam
Longitudinal groove of knife-edge

(a)

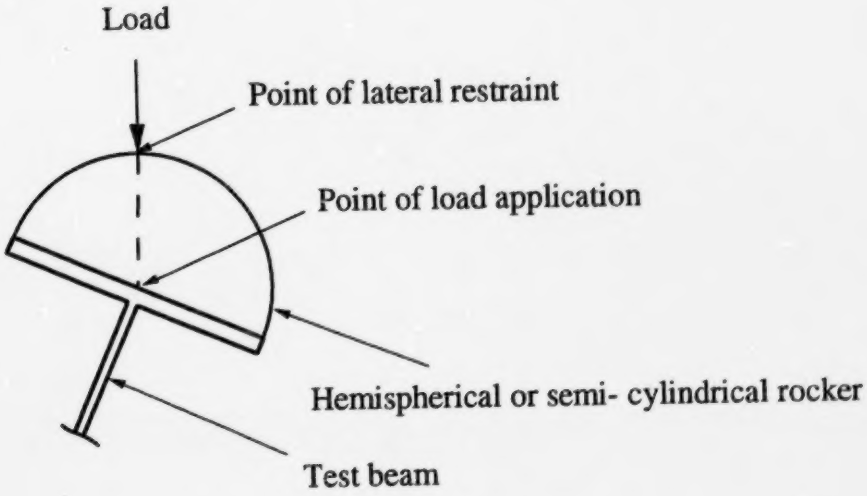
Load
Point of lateral restraint
Point of load application
Hemispherical or semi- cylindrical rocker
Test beam

(b)

Fig. 4.7 Determination of the height of load application and the height of lateral restraint

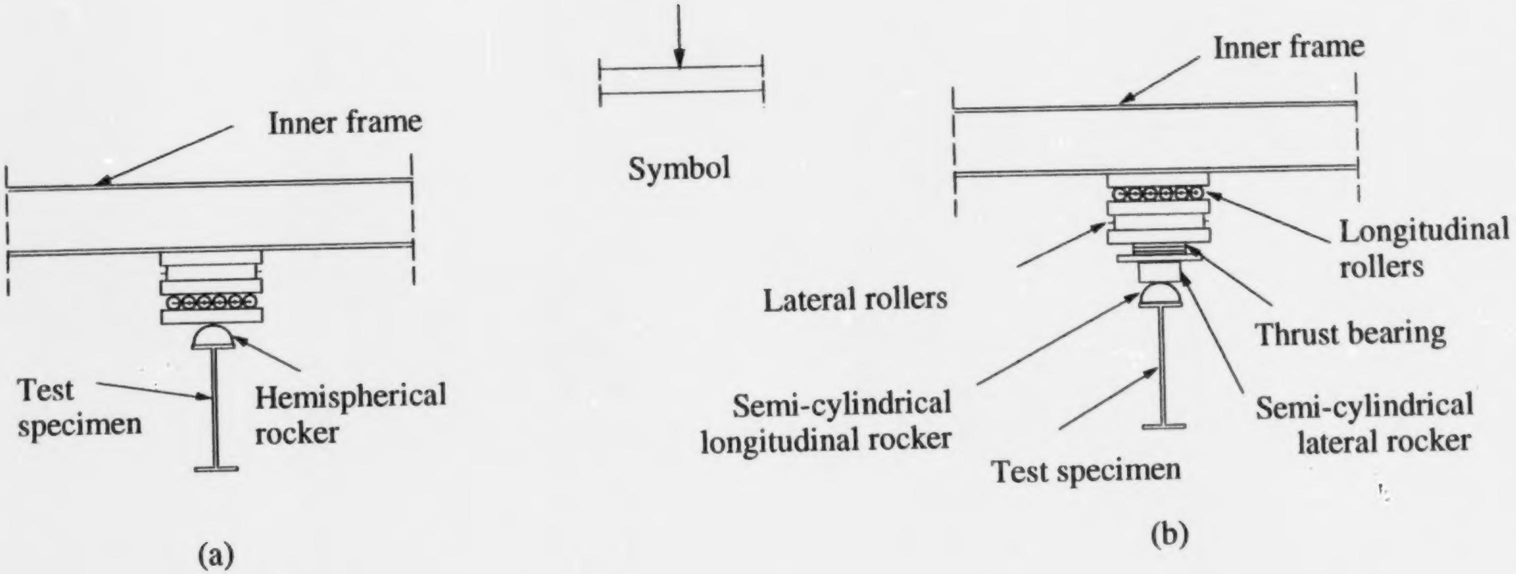
Inner frame
Test
specimen
Hemispherical
rocker
(a)
Symbol
Inner frame
Longitudinal
rollers
Lateral rollers
Thrust bearing
Semi-cylindrical
longitudinal rocker
Semi-cylindrical
lateral rocker
Test specimen
(b)

Fig. 4.8 Details of two different arrangements for a free top flange at a loading point

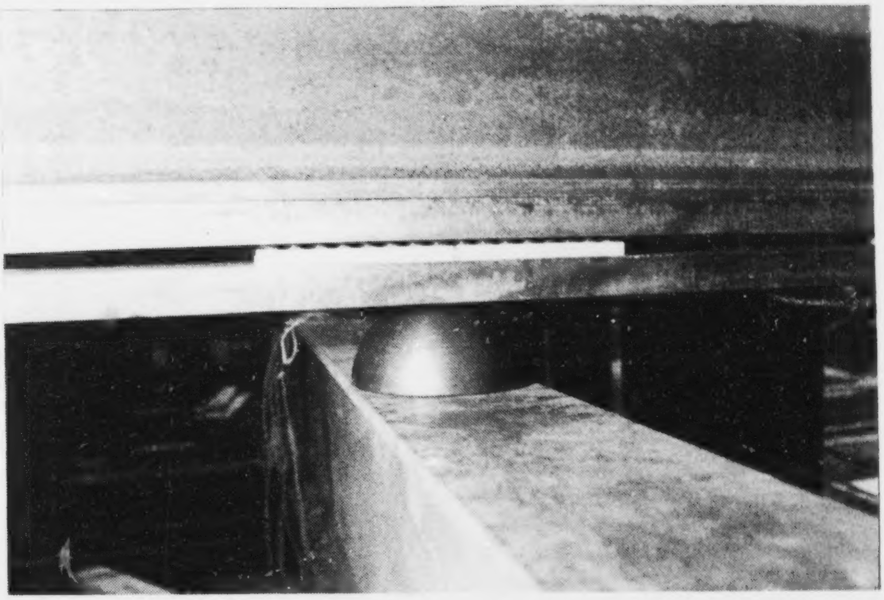

Fig. 4.9 Top flange loaded freely using ball bearings

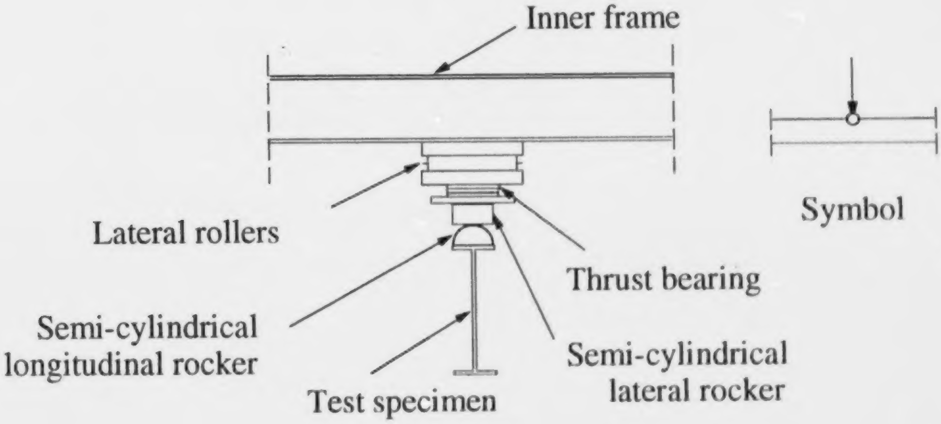
Inner frame
Symbol
Lateral rollers
Thrust bearing
Semi-cylindrical longitudinal rocker
Semi-cylindrical lateral rocker
Test specimen

Fig. 4.10 Details of lateral restraint condition of top flange

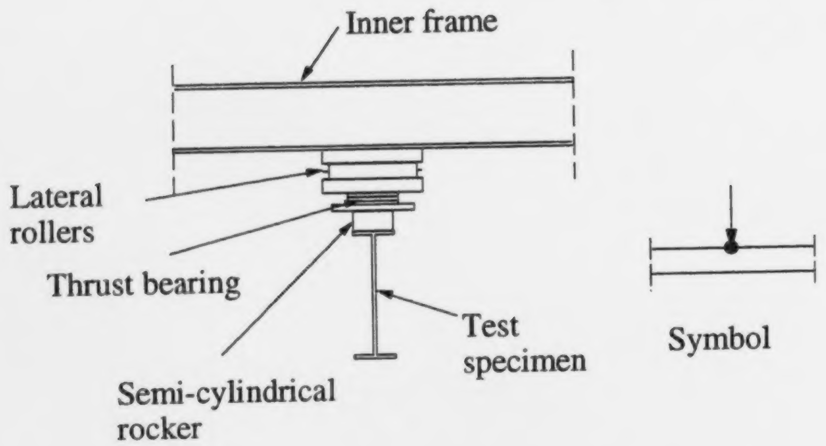
Inner frame
Lateral rollers
Thrust bearing
Semi-cylindrical rocker
Test specimen
Symbol

Fig. 4.11 Details of lateral and torsional restraint for top flange

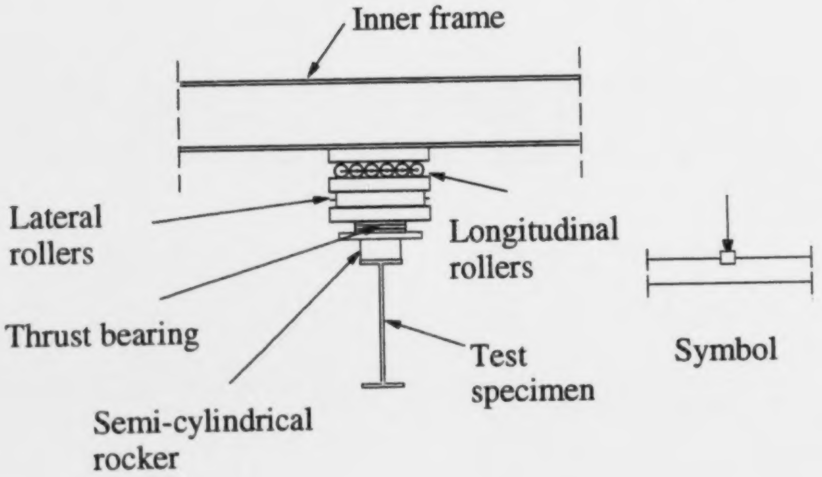
Inner frame
Lateral rollers
Longitudinal rollers
Thrust bearing
Semi-cylindrical rocker
Test specimen
Symbol

Fig. 4.12 Details of torsional restraint for top flange

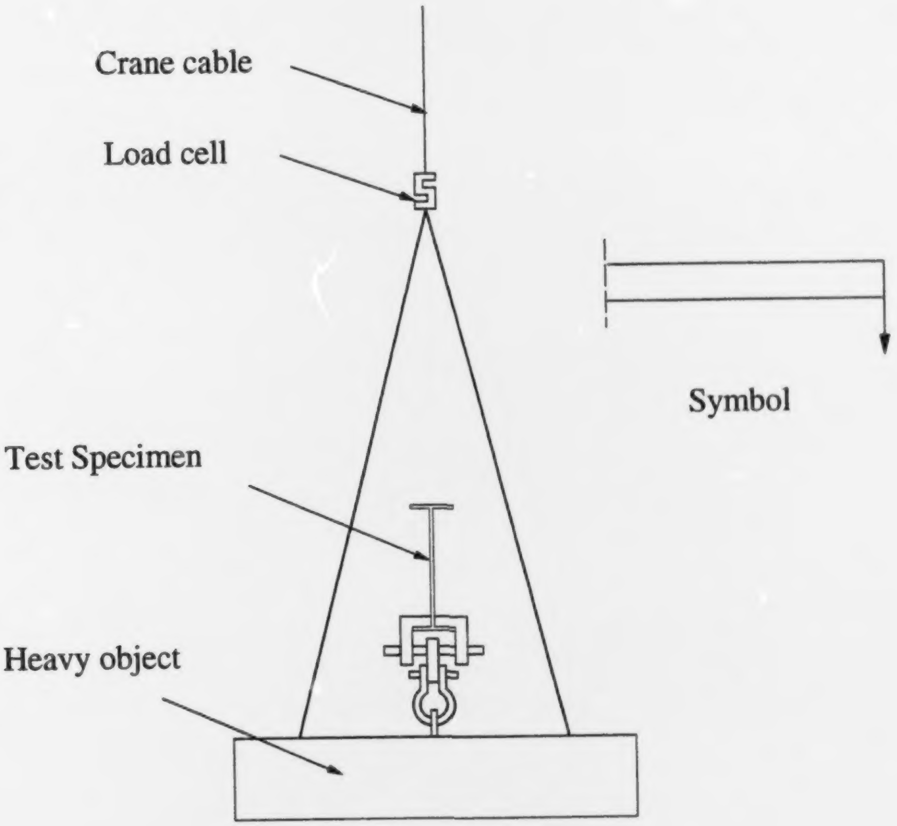
Crane cable
Load cell
Symbol
Test Specimen
Heavy object

Fig. 4.13 Details of bottom flange loaded with no restraint

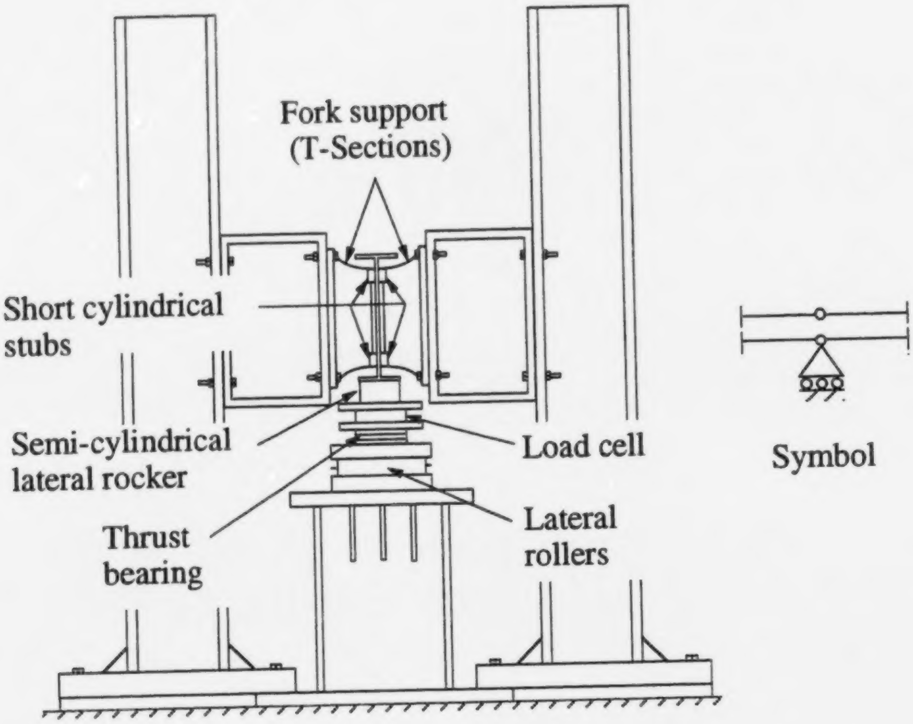
Fork support
(T-Sections)
Short cylindrical stubs
Semi-cylindrical lateral rocker
Load cell
Thrust bearing
Lateral rollers
Symbol

Fig. 4.14 Fork support at column location equivalent to joist connection with bottom chord extension

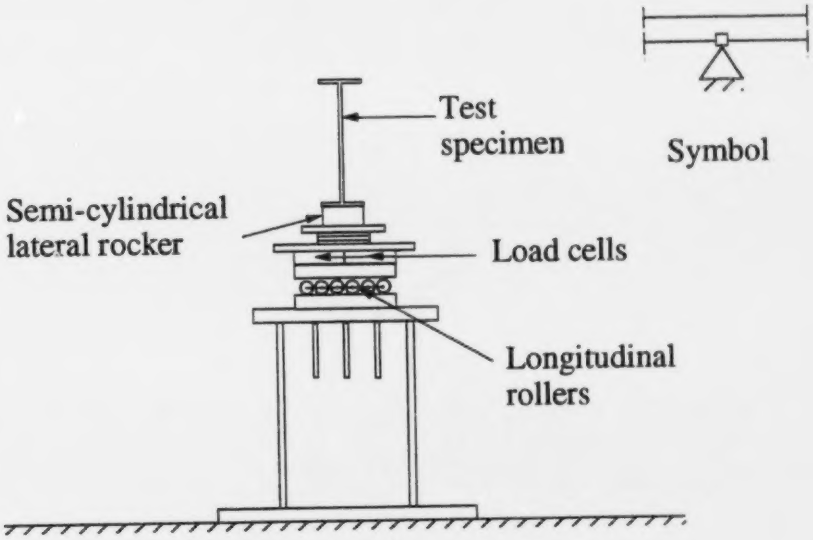
Test
specimen
Semi-cylindrical
lateral rocker
Load cells
Longitudinal
rollers

Symbol

Fig. 4.15 Details of torsional restraint for bottom flange at column location.

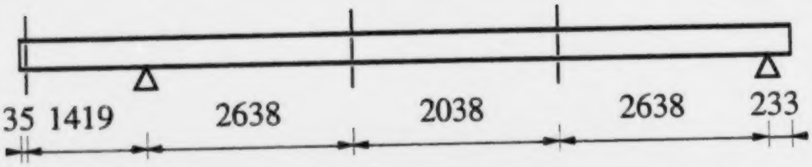
35
1419
2638
2038
2638
233

Fig. 4.16 Stations for measuring displacements

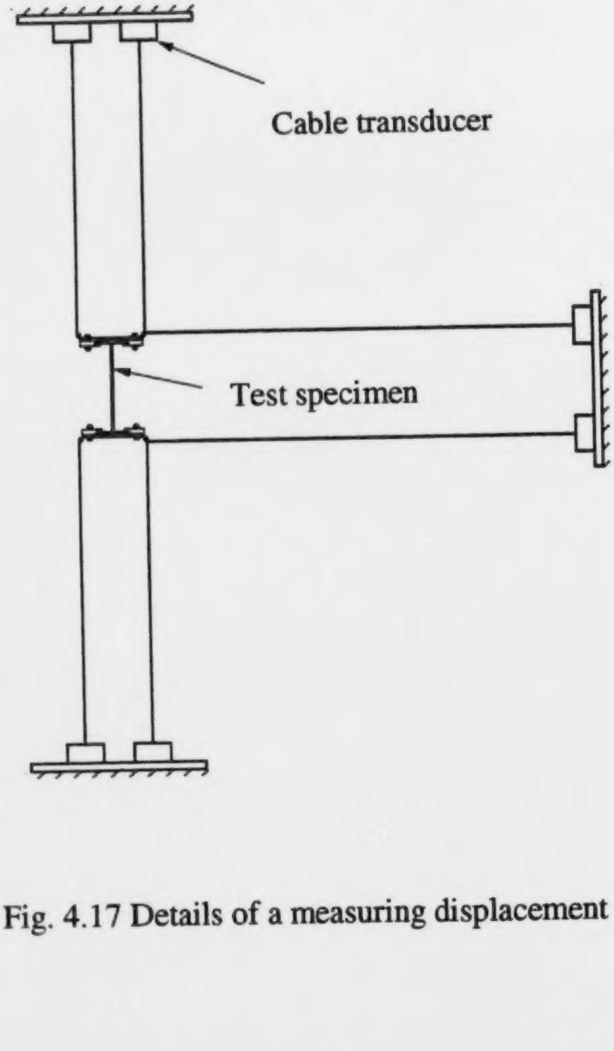
Cable transducer
Test specimen

Fig. 4.17 Details of a measuring displacement station

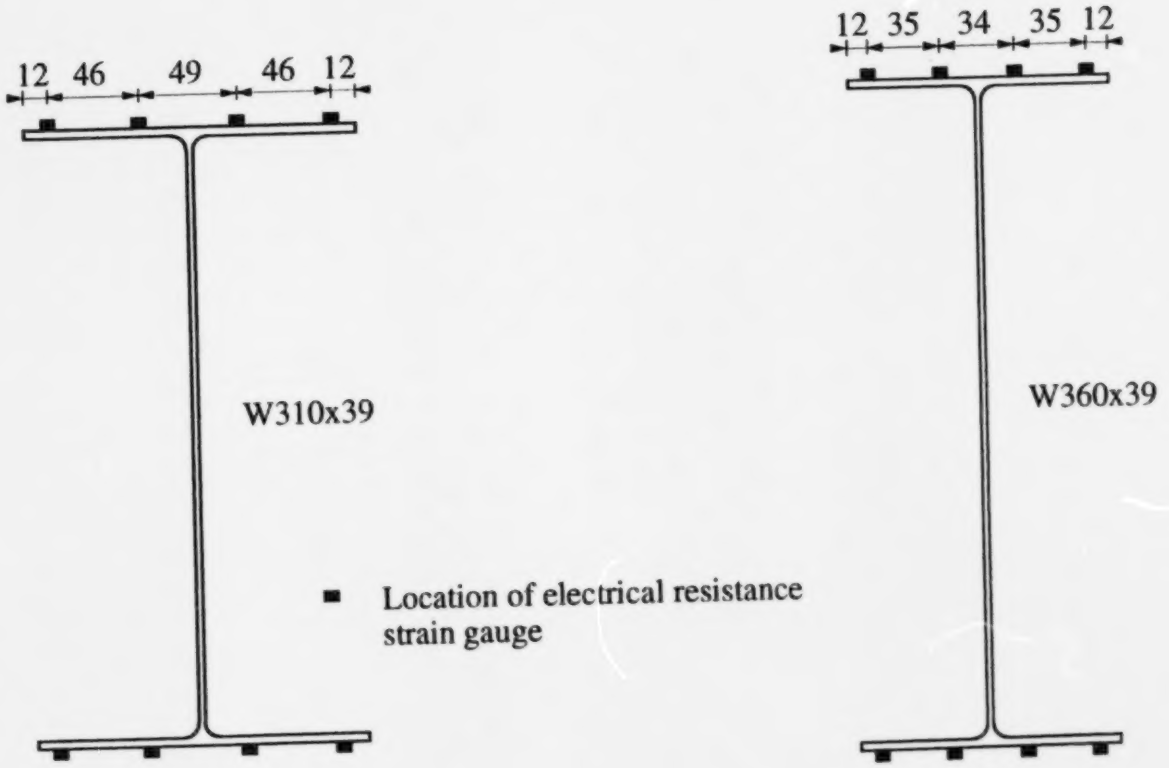
12
46
49
46
12
W310x39
12
35
34
35
12
W360x39
■ Location of electrical resistance strain gauge

Fig. 4.18 Locations of strain gauges on the cross section at a typical station

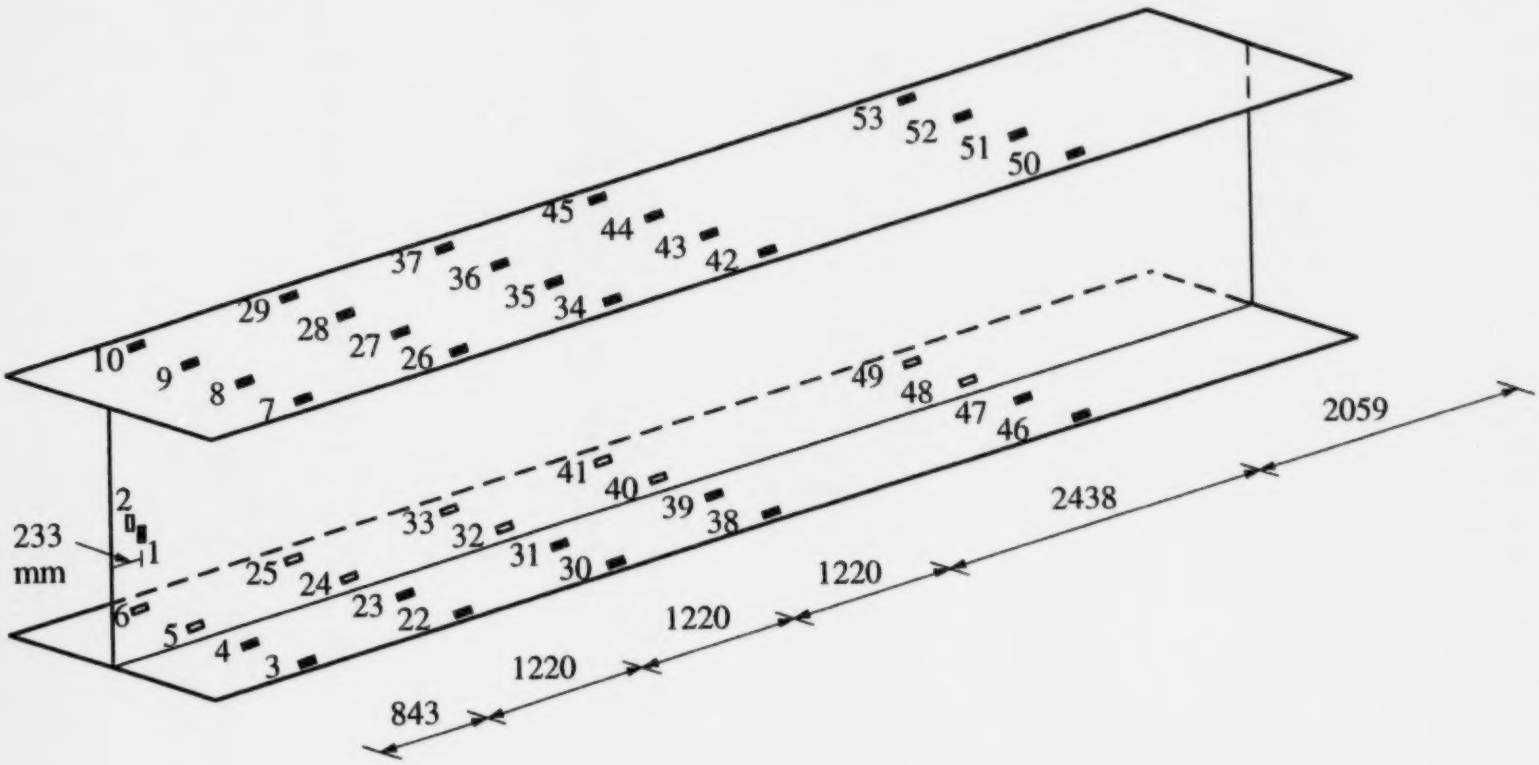
10
9
8
7
29
28
27
26
37
36
35
34
45
44
43
42
53
52
51
50
2
1
233 mm
6
5
4
3
25
24
23
22
33
32
31
30
41
40
39
38
49
48
47
46
843
1220
1220
1220
2438
2059

Fig. 4.19 Strain gauge identification numbers and locations along a beam specimen

Chapter 5

DISTORTIONAL BUCKLING TESTS OF STEEL BEAMS

5.1 Introduction

The results of the full-scale beam tests are presented and analyzed in this chapter, as are the results obtained from the finite element analysis used to predict the behaviour of these tests. Thirty three tests were conducted on a total of 11 beam specimens, composed of seven W360x39 sections and four W310x39 sections. By testing a given beam in a sequence of generally increasing restraints, the beam could be used repeatedly because in the earlier tests it buckled elastically and returned to its original shape upon unloading. A specimen was replaced after undergoing inelastic buckling that resulted in noticeable inelastic deformations, as discussed subsequently. The 33 tests were performed under different loading and restraint conditions except for a few tests which were duplicated in order to rectify some experimental errors.

In cantilever-suspended span construction encountered in practice, the reaction from a suspended span is usually transferred to the tips of the cantilever beam through a shear connection between the webs and near the shear centre of the beam. In these tests, the cantilever tip loads, as were considered in the finite element analysis, were applied at or above the top flange. It is recognized that this test situation represents a more severe loading condition because of the destabilizing effect of the load applied above the shear centre.

5.2 Results of experimental and finite element analyses

The experimental and predicted buckling loads applied at the cantilever tip and the test-to-predicted ratio of the cantilever tip loads of the tests are given in Tables 5.1.a, b and c. The second line in both the test and predicted load columns (as in test 6) gives the magnitude of the additional loads, applied between supports. The loading and restraint diagrams and other data for each test have been given in Figs. 4.6.a, b and c. The test loads include the dead weight of 3 kN of each of the loading frames and thus, the ratios of interior loads to the cantilever load may not coincide exactly with the nominal ratios shown in those figures (e.g. P/5) which refer to the applied jack loads only.

Figs. 5.1 and 5.2 show the finite element meshes used to predict the buckling loads for tests 1 through 32 and 33, respectively. The mesh was refined in the vicinity of the column support next the cantilever span where the bending moment is a maximum and yielding sometimes occurs. A mesh refinement was also required at the cantilever tip to model cross-sectional distortions when torsional restraint is involved. The self-weight of the beam was neglected in the analysis of all tests except for test 32 where it proved to be significant because of the special boundary conditions involved. The finite element analyses are based on the ratio of the loads applied on the cantilever and back spans observed at failure (assuming that this ratio remained constant up to the occurrence of buckling), the measured material properties, residual stresses and cross-sectional dimensions.

5.3 General observations

5.3.1 Test-to-predicted ratios

A measure of the accuracy of both the experimental work and the analytical method is afforded by computing the test-to-predicted ratio for each test and the mean value for all the tests. In such a comparison, experimental errors contribute to deviations from a value of 1.0 and increase the variation. The results of tests 6 and 8 were considered unreliable, as discussed subsequently, because unwanted frictional restraints caused higher energy buckling modes. These tests were repeated in tests 7 and 28. Excluding tests 6 and 8 (indicated by asterisks in Table 5.1), the mean test/predicted ratio obtained for the remaining 31 tests is 0.99 with a standard deviation of 0.063. This mean value, for a wide range of boundary conditions, indicates that the analytical model has good predictive capacity. The coefficient of variation of 0.064 related both to experimental errors and model simplifications is relatively small. For comparison, Yura et al. (1978) reported a coefficient of variation of 0.11 for the uncomplicated tests of determining the fully plastic moment capacity of steel beams. The variation is considered to be due to variations in residual stress patterns, yield strengths and moduli of elasticity of the beam from the measured values, experimental errors in load measurements and unwanted friction in the reactive devices as well as model simplifications. Mirza and MacGregor (1982) suggested a coefficient of variation of 0.040 to account solely for errors in measurement when assessing the strength of reinforced and prestressed concrete beams. If this were applied, the resulting coefficient of variation would reduce to 0.050.

5.3.2 Effects of residual stresses

The residual stress distributions of the W360x39 and W310x39 cross sections, discussed previously (see Fig. 3.8), are characterized by significant tensile stresses at the flange-web junctions and approach zero at the flange tips, ranging from small tensile stresses for the W360x39 to small compressive stresses for the somewhat stockier W310x39. A significant portion of both webs is in residual compression. These findings agree with Bjorhovde (1980), who expected that the residual stresses of the relatively light beam-type sections are not as adverse, i.e. not as great in compression at the flange tips, as those of column shapes, they would be expected therefore to affect the lateral stability less and in fact, the tensile residual stresses proved to be beneficial, as discussed subsequently, in delaying the onset of loss of stiffness.

Based on the mean level of maximum tensile residual stresses given in Fig. 3.8 of 198 MPa and 74 MPa for the W360x39 and W310x39 sections, respectively, tensile yielding of the cross section would be predicted to occur at 0.31 and $0.79M_y$ or 0.27 and $0.71M_p$, respectively, where M_y is the yield moment and M_p is the plastic moment. For compressive yielding at the flange tips, the mean level of compressive residual stresses of -0.02 (tensile) and $0.06F_y$ for the

W360x39 and W310x39 sections, respectively, would result in values of 1.02 and $0.94M_y$ or 0.89 and $0.84M_p$ at the onset of cross-sectional yielding or degradation in lateral stiffness. Nethercot (1974) suggested that lateral-torsional buckling can be classified as inelastic only when the level of applied bending stresses equals or exceeds the level required to initiate yielding at the compression flange tips. Even though significant yielding may already have occurred at the tension flange-web junction, this has little effect on the effective moment of inertia about the weak axis. Accepting Nethercot's hypothesis, all tests except for tests 5, 14, 15, 19, 21, 27, 28 and 31, can be classified as elastic.

To investigate the effects of residual stresses on the stability of steel beams, two finite element model predictions were obtained for each test, by considering and neglecting the effects of yielding and residual stresses. These predictions are called inelastic and elastic, respectively. Tables 5.2.a, b and c give the critical buckling moment, occurring at the root of the cantilever for the two predictions as a fraction of the plastic moment and, as well, the ratio of the two predictions. In the tests performed on the W360x39 cross section, where the whole flange is under tensile residual stresses with a peak value at the flange-web junction of $0.69F_y$, a significant beneficial effect is evident in the Nethercot "elastic" tests, with the ratio of the two predictions varying from 1.04 to 1.36. This is because the tensile residual stresses tend to reduce the compressive stresses of the compression flange, to increase the geometric stiffness of the flanges and therefore to delay the onset of lateral instability of the overall beam. On the other hand, early yielding at the tension flange-web junction has comparatively little effect. The tension flange deflects only slightly during buckling and makes only a small contribution to the buckling resistance (Trahair 1983b). This phenomenon was also observed by Kitipornchai and Trahair (1975).

The beneficial effect of residual stresses in the elastic range is less noticeable for the W310x39 tests than for the W360x39 tests because the peak tensile residual stress at the flange-web junction of the W310x39 is only about $0.21F_y$ and moreover, the compressive residual stresses at the flange tips, although relatively small, have a detrimental effect. As can be observed in Tables 5.2.b and c, the beneficial effect of residual stresses is significantly reduced for tests 23, 24, 25, 26, 29 and 30, even though elastic buckling occurred. Here, the distortional buckling mode is characterized by a significant web distortion over a considerable length of the beam near the interior support location. This in turn results in less participation of the flange in the overall behaviour and consequently a less stabilizing effect of residual stresses.

For the inelastic tests, again using Nethercot's definition, the beneficial effect of residual stresses is reduced significantly because of yielding at the compression flange tips. In real cantilever-suspended span construction, it is expected that the depth/width ratio for the range of beams used would be larger than 1.8, that is the beam flanges are relatively narrow. Therefore, the residual stress patterns (Ballio and Mazzolani 1983) would be similar to those obtained for the W360x39 and W310x39 cross sections with depth to width ratios of 2.76 and 1.88, respectively, for which the residual stresses are beneficial in the elastic range. With these residual stress patterns, a wide range of beams used in real structures would still buckle elastically even though the critical buckling moment is just slightly less than the yield moment.

5.3.3 Double cantilever beams

Tests 32 and 33 (see Fig. 4.6.c) were tested in a double cantilever configuration to examine the stabilizing effect of a load applied below the shear centre (test 32) and the effect of span length (test 33). A single fork support was provided at the common root of the two cantilevers of unequal span. In test 32, The load at the end of the long cantilever span was applied 150 mm below the unrestrained bottom flange to model the loading on a monorail beam. In test 33, the top flange was laterally restrained at both cantilever tips. The test/predicted load ratios of 1.02 and 1.05 for the two tests indicate excellent agreement between test and prediction. An end view of the buckled cross section at the tip of the long span cantilever in test 33 is given in Fig. 5.3. This shows that the whole cross section exhibited a significant twisting about the enforced axis of twist above the top flange, with little evidence of cross-sectional distortion.

5.3.4 Buckled shapes

The main characteristics of the buckled shape in a distortional buckling mode are the different lateral deflections and twists of top and bottom flanges due to web distortion. The finite element model predicts not only the buckling load but also the buckled shape contained in the eigenvector resulting from the solution of the governing equation. Because the analytical model is based on the bifurcation theory, the governing equation does not give the magnitude of the displacements but a normalized shape only.

The arrangement of twelve cable transducers installed at three stations along the test specimen (see Figs. 4.16 and 4.17) enabled the main features of the buckled shape to be discerned. More information about the displacements was obtained from the restraint conditions at the supports. When fork supports are provided, no lateral displacements or twists occur at these locations. In the case when lateral bracing of the column is omitted at the cantilever root, lateral deflections of both flanges were monitored throughout the test and the twisting angle of the top flange was measured at failure.

The measured lateral displacements and twists of both flanges as well as the vertical displacements of the top flange, at the maximum test load level, are given in Figs. 5.4 through 5.8 for tests 3, 4, 7, 27 and 28, respectively. The corresponding buckled shapes, as predicted by the finite element analyses, are given in Figs. 5.9 through 5.13. These shapes show the normalized lateral displacements of the top flange, the middle of the web and the bottom flange. These figures show that the measured and predicted buckled shapes agreed favourably, as can be seen for example in Fig. 5.14 for test 3. The only exception is in test 7, where the top flange within the cantilever span moved slightly while it was predicted not to move. Distortion of the web can be deduced from the diagrams giving the angles of the two flanges in Figs. 5.4 to 5.8. When no distortion occurs, the twist angles of the top and bottom flanges are the same at any point along the length of the beam. Web distortions can also be inferred from the normalized displacements of the buckled shapes of Figs. 5.9 to 5.13 by noting that uneven spacing between the lines representing the top flange, neutral axis and bottom flange lateral displacements.

In tests 3, 7 and 28, no torsional restraint was involved and the twist angle of the two flanges in Figs. 5.4, 5.6 and 5.8 are about the same at any point along the beam. In the corresponding Figs. 5.9, 5.11 and 5.13, the three displacement lines are evenly spaced.

In test 4 (see Fig. 4.6.a) lateral and torsional restraints were provided to the top flange of the cantilever tip. From Fig. 5.5, the top flange displaced the least laterally and there was a significant difference in the angle of twist of the two flanges at the flange tips. This is also evident in the uneven spacing of the lateral displacement lines of Fig. 5.10.

In test 27 (see Fig. 4.6.c) torsional restraint was applied to the top flange at all 6 load points and as well to the bottom flange at the reaction support. Fig. 5.7 shows significant difference in the twist angles of the flanges and Fig. 5.12 shows uneven spacing of the three lateral displacement lines.

A plan view of a portion of the longitudinal buckled shape in test 5 is given in Fig. 5.15. The figure shows the main span with the fork support close to the cantilever located near the bottom of the photograph. The bottom flange, the top surface of which is painted white, has undergone a much greater lateral deflection than the top flange, with the maximum rotation occurring near the middle of the main span, towards the top of the photograph.

5.3.5 Effect of lateral and torsional restraints

In those cases where the only applied load is at the cantilever tip, and the top flange is laterally restrained at the load point, as in tests 2 and 16, (see Figs. 4.6.a and 4.6.b) the buckling capacities are little increased by the lateral restraint as compared to the cases where the cantilever tip is free as in tests 3 and 17 (Figs. 4.6.a and 4.6.b). The test loads are, respectively, 78.9 and 84.0 for tests 2 and 16 as compared to 77.1 and 77.6 for tests 3 and 17. This is explained by the different behaviour of cantilever beam with an unrestrained back span as compared to a cantilever with warping restrained at its root. In the latter case, the top flange deflects more than the bottom flange but the opposite is observed, as seen in the buckled shape of test 3 in Fig. 5.4 for an overhanging beam, where the bottom flange has the greater lateral deflection at the cantilever tip. Thus, when only the top flange is restrained laterally, little benefit is gained. The situation is changed when the back span is restrained laterally at locations of interior loads.

Test 7 was conducted with five loads, each about one-fifth of the cantilever load, applied on the back span. This loading configuration models the limit of the unbalanced condition in which the suspended span is loaded to the full intensity of a uniformly distributed load and the main span is loaded to one half the intensity. However, no lateral support was provided at any of the load points with lateral restraint occurring solely from the fork supports. A shorter length of the bottom flange is in compression in test 7 as compared to test 3, where the entire bottom flange in compression. Unlike test 3, the buckled shape of test 7 (Fig. 5.6) showed little bottom flange movement while the top flange displayed significant lateral displacements at the interior load points, where it is in compression. Notwithstanding this, the predicted buckling load for test 3 of 78.4 kN is greater than that for test 7 of 65.6 kN.

The addition of lateral restraint, 205 mm above the top flange, at all load points in test 28 (Fig. 4.6.c), increased the predicted buckling strength from 65.6 kN for test 7 to 136.7 kN and greatly altered the buckled shape, as seen by comparing Figs. 5.6 and 5.8. This is attributed to the enhancement of strength of the back span by reason of the fact that most of the top flange within the back span is under compression and laterally restrained. Test 21, carryed out on a W310x39, gave similar performance and behaviour to test 28.

Now consider tests 3, 7 and 9, all unrestrained except for the fork supports provided at support locations. The cantilever tip loads in tests 3 and 7 were applied at the same height of 40 mm above the top flange, while in test 9 the height was 95 mm. All of the bottom flange of the back span in test 3 is in compression while in test 7 only about 0.29 of the bottom flange of the back span is in compression. However, the predicted buckling load in terms of the cantilever tip load reduced from 78.4 kN to 65.6 kN because of the destabilizing effect of the loads acting on top flange of the back span in test 7. In test 9, the predicted buckling load was further reduced to 36.6 kN because both the cantilever tip load and the interior load were applied higher above the shear centre and also because of the shape of bending moment diagram is more critical than in test 7 with the compression flange in the back span more heavily stressed.

Compare tests 4 and 14, both laterally and torsionally restrained at the cantilever tip but with lateral restraint also provided to the top flange at the middle of the back span in test 14. The significant increase in the predicted buckling load of test 14 to that of 4 (137.1 kN versus 112.6 kN), is due to the change in the shape of the bending moment diagram and the additional lateral restraint provided.

In spite of the beneficial effects of the lateral restraints and the shape of bending moment diagram in tests 24 and 26 on W360x39 and W310x39, respectively, as compared to tests 23 and 25 respectively, the predicted buckling strength actually reduced to 43.9 kN from 49.8 kN and to 45.4 kN from 54.1 kN because the back span loads were applied higher above the top flange.

In tests 9 through 15, loads were applied at the cantilever tip and at mid-point of the back span of a W360x39, using various ratios of the two loads and various restraint conditions. Although the height of the cantilever tip load and the bending moment diagram are more severe in test 10 than in test 9, both tending to decrease the failure load, the test and predicted loads actually increased because of the lateral restraint provided at the mid-point load in test 10. The increase in the cantilever test loads was from 35.5 to 41.1 kN and in the predicted loads from 36.6 to 40.8 kN. Test 13 showed a slight increase in predicted strength from 50.4 kN to 52.9 kN compared to test 12, other things being equal, because of the added torsional restraint at mid-span in test 13.

One method to investigate the behaviour of an overhanging beam (Essa and Kennedy 1992) is to consider it as an interaction buckling problem between the cantilever and back spans, both free to warp at the common end. Considering all the tests with fork supports at column locations, the cantilever span is the critical span while the back span is the restraining one. Restraining the critical cantilever span is, in fact, more effective in enhancing the overall buckling strength than providing restraint to the restraining back span as is evident from an examination of tests 13 and 14. In these tests, loads were applied at the cantilever tip and at the mid-point of the back span. Even though the back span loading condition of test 13 is considered to be less severe than that of test 14 with a shorter length of unsupported compression flange, providing lateral and torsional restraints of top flange at the cantilever tip in test 14 is much more effective in increasing the buckling strength than providing the same restraint to the top flange of the back span as in test 13. The predicted buckling loads are 137.1 kN and 52.9 kN with the test loads in about the same proportion.

Consider tests 16, 17, 18 and 22 as a set with a load applied only at the cantilever tip of a W310x39. The tests, in order of increasing restraint at the point of load application are: 17, no restraint, 16, lateral restraint only, 18, torsional restraint only and 22, lateral and torsional restraints. Both the test and predicted loads show an orderly increase in loads through this progression: 77.6, 84.0, 118.9 and 133.3 kN for the test loads and 78.0, 83.9, 111.5 and 129.6 for the predicted or theoretical loads. Test 18 was the only test in which torsional restraint alone was provided without lateral restraint of the top flange and resulted in a greater strength, in this case, than in test 16 which was provided only with lateral restraint. When both lateral and torsional restraints were provided as in test 22, there was a slight improvement in the strength as compared with providing torsional restraint only. This sequence of tests therefore clearly demonstrates theoretically and experimentally that torsional restraint is much more effective than lateral restraint in enhancing the strength of the beam.

5.3.6 Web distortion and effect of stiffeners

The buckling modes observed in these tests were characterized in general by changes in the cross-sectional shape, arising from web distortions. The webs of I-shaped beam cross sections are relatively thin. Web distortion permits the flanges at a cross section to undergo different angles of twist about the longitudinal axis. This greater flexibility tends to reduce the buckling strength of the beam as compared to that if the web remains rigid. Test observations show that web distortion is noticeable and critical where: 1) lateral bracing at column locations is omitted, 2) torsional restraint is provided to one flange only and 3) load is applied relatively high above the top flange.

When lateral bracing at a column is omitted, it is normal practice to provide torsional restraint to the bottom flange by means of a rigid connection between the beam and the column. Under practical loading conditions, as in test 26, the bottom flange is in considerable compression at the column location. Lateral restraint is provided by the open-web steel joists to the top flange at the cantilever tip as well as at the back span loading points, and because of the lateral stiffness of the top flange to some extent, to the top flange at the column location. Under such conditions, for the bottom flange to deflect laterally at column location, significant web distortion must occur. Fig. 5.16 illustrates the web distortion, observed in test 26, at the main column and at the cantilever tip. Web distortion can be reduced at column supports by providing either lateral bracing or web stiffeners at the supports. The latter are effective only when they are connected to the beam flanges and there is a moment connection between the column and the beam.

The increase in the buckling strength due to torsional restraint applied to the tension flange is reduced due to web distortions. In cantilever-suspended span construction, lateral and torsional restraints are provided at discrete locations by means of the open-web steel joists attached to the top flange. Under practical loading conditions, web distortion becomes noticeable within the cantilever span where the top flange is in tension. In Fig. 5.17 for test 4, the top flange at the cantilever tip has not twisted because of the torsional restraint, while the twisting of the bottom flange has resulted in significant web distortion. Although, because of the introduction of lateral and torsional restraints in test 4, the test buckling load of that test (104.9 kN) showed a significant increase as compared to the unrestrained case of test 3 (77.1 kN), the beneficial effect of the torsional restraint is not obtained in full because of web distortion.

Web stiffeners can be used to minimize the distortion occurring in the web and further enhance the buckling capacity. In tests 5 and 19, a web stiffener was used at the load point which was also laterally and torsionally restrained at the top flange. A significant improvement in the test buckling loads was obtained in test 5 (125.8 kN) as compared to test 4 (104.9 kN) on the W360x39 and in test 19 (152.6 kN) as compared to test 22 (133.3 kN) on the W310x39. These four tests indicate, based on the relative values of buckling loads, that the reduction of buckling capacity due to web distortion increases with the depth of the cross section.

The elevated point of application of the cantilever load in tests 11 through 13 showed a destabilizing effect which tended to increase twisting in the top flange and induce a noticeable distortion in the web. In test 11, the cantilever tip load was applied 275 mm above the top flange. A view of the cross-sectional deformations is given in Fig. 5.18, where the top flange has undergone a much greater twist than the bottom flange and the web is significantly distorted. Another example of significant web distortion at the cantilever tip is seen in Fig. 5.19 for test 20, which was conducted using a W310x39 cross section with the load was applied at 200 mm above the top flange.

5.3.7 Effect of lack of lateral restraint at column locations

When lateral restraint is omitted at a column location and only torsional restraint is provided to the bottom flange through a rigid moment connection, the web is forced into a distortional buckling mode. This situation was simulated at the main support in tests 23 through 27 and 29 through 31. In test 23, a W360x39 beam was loaded and laterally restrained at the cantilever tip. A test load of 45.9 kN was obtained as compared to 78.9 kN in test 2 in which fork supports (top and bottom bracing) were provided at both columns. These results clearly indicate that torsional restraint alone at the column as may be supplied by a rigid connection between the beam and the column does not compensate for the omission of bracing or alternatively of web stiffeners.

In test 24 on a W360x39, lateral restraint was provided at all six load points and the bottom flange of the beam was provided with torsional restraint at the main support but was free to translate there. The test load at the cantilever tip was only 40.7 kN as compared to 128.8 kN obtained in test 28, in which lateral bracing was supplied at the column but was otherwise identical. A comparison of parallel tests 23 and 2 on a W360x39 with lateral restraint at the cantilever tip where the only load was applied but with only torsional restraint at the column in test 23 and forked supports in test 2 give test loads of 45.9 kN and 78.9 kN, respectively.

The same phenomenon was demonstrated in the companion tests on W310x39 beams, test 26 similar to test 24 with torsional restraint at the column only had a test load of 46.7 kN while test 21 with forked supports has a test load of 154.5 kN. In the W310x39 beams with loads at the cantilever tip only (tests 25 and 16), the respective loads are 55.9 kN and 84.0 kN.

Three conclusions can be drawn from these comparisons. First as stated previously, torsional restraint of the bottom flange at a column is not nearly as effective as lateral restraint to both flanges. Second, the reduction in buckling load for such restraint conditions is greater when loads are applied to the back span as well as the cantilever tip because of the destabilizing effect of the back span loads applied above the top flange (the relative load ratios are 40.7/128.8 = 0.32 and 45.9/78.9 = 0.58 for the W360x39 and 46.7/154.5 = 0.30 and 55.9/84.0 = 0.65 for the W310x39). Third, the reduction of buckling capacity due to web distortion, as discussed in section 5.3.6, increases with the depth of the cross section. For tests with a cantilever tip load only, test 23, on a W360x39, with torsional restraint only at the column support has only 0.58 of the strength of test 2 with fork supports while for the parallel tests (tests 25 and 16) on a W310x39, the ratio is 0.67.

Providing torsional restraint to the top flange in addition to lateral restraint has a significant effect in enhancing the buckling strength of the beam. Essentially identical tests 27 and 31 with lateral and torsional restraints at all load points have a test load of about 128 kN at the cantilever tip while test 26 with only lateral restraint at load points but otherwise identical reached a failure load of only 46.7 kN, only 37% of the former. Again, the only difference between tests 24 and 29 is that test 29 had lateral and torsional restraints at the cantilever tip while 24 had lateral restraint only. At all other load points only lateral restraint was provided. Test 24 had a failure load of 40.7 kN, only 53% of the 76.3 kN of test 29. Torsional restraint mobilizes the distortional strength of the web whenever it is provided and thus enhances the resistance of the beam.

The distortional buckling mode at the cantilever tip in test 31 is seen in Fig. 5.20. The top flange, restrained intentionally by the loading system, has remained horizontal while the bottom flange has rotated and translated laterally, with considerable distortion in the web. When joist shoes are properly welded to the top flange of the beam, the joists provide torsional restraint to the beam flange and enhance the stability of the beam. While in the tests, essentially complete torsional restraint was obtained, the actual degree of fixity in practice is proportional to the flexural stiffness of the joists.

5.3.8 Effect of shape of bending moment diagram

To investigate the effect of the shape of the bending moment diagram on the critical buckling resistance, the finite element predictions were made for the several restraint and loading conditions given in Fig. 5.21, for a W360x39 beam. Fig. 5.21a shows two different restraint conditions: condition A with only fork supports at the column locations and condition B with fork support at the right end, complete torsional restraint only applied to the bottom flange at the intermediate support location and complete lateral and torsional restraints applied to the top flange at the cantilever tip. As indicated in Fig. 5.21b, four different loading configurations are considered with all the loads being applied at either the shear centre or the top flange. The corresponding bending moment diagrams are also given in Fig. 5.21b.

Finite element predictions were obtained for each loading and restraint condition with the residual stresses being either neglected or considered. The predicted ratios of M_{cr}/M_p are given in Table 5.3. For the cases of shear centre loading, the results of both restraint conditions indicate that the shape of bending moment diagram has an orderly effect on the buckling resistance increasing in the following order: case IV, where the maximum moment occurs at the centre of the back span, case III, where the maximum moment occurs at the interior support, case II, where positive moment with a maximum value of 0.4M covers a significant length of the back span, and case I, where most of the back span is under a positive moment with a maximum value of 0.25M. When all the loads are applied at the top flange the same order of severity of bending moment diagrams persists except that cases II and III are switched because the destabilizing effect of the loads applied to the back span is more pronounced than the effect of the shape of bending moment diagram. Again, the beneficial effect of residual stresses in restraint condition B is less noticeable than in restraint condition A. This is attributed to the web distortion which reduces the flange participation in the overall behaviour of the beam.

5.3.9 Load-strain behaviour and strain distributions

The measured flange strains reflect the effects of bending about both the strong and weak axes and of warping associated with the deformations due to lateral-torsional buckling. The measured vertical web strains reflect the effects of bending due to web distortion as well as the effects of vertical loads. To investigate all of these effects, four strain gauges were mounted longitudinally on each flange at every strain gauge station and, as well, a strain gauge was mounted vertically on each side of the web at the cantilever tip, as shown and identified in Fig. 4.19.

In Figs. 5.22, 5.23 and 5.24, for test 4 are plotted the test load versus flange strains of the outer (3 and 6) and inner (4 and 5) strain gauge pairs on the bottom flange and of outer pair of gauges (7 and 10) on the top flange, respectively, of the station located at 843 mm from the cantilever tip, about half way between the cantilever tip load and the main support. The general behaviour of these curves is the same. At relatively small loads, strains due to the strong axis bending dominate. The inner and outer bottom flange strains increase linearly with load and are about the same in compression and of opposite sign to the top flange strains in tension. As the beam begins to buckle laterally, the strains on the same flange but on opposite sides of the webs begin to diverge as lateral bending and warping take place. Readings of the two strain gauges mounted on the same side of the bottom flange, gauges 6 and 5, tend to develop tensile strains. In all cases, the load versus strain relationship reaches a horizontal asymptote at the maximum load, indicating that buckling is imminent. Strain gauge 6 on the bottom flange and strain gauge 10 on the top flange are on the same side of the web. As buckling was approached, both showed tensile straining, indicating that the lateral bending effect, in this case, was more pronounced than warping.

The load versus mid-height web strains obtained from gauges 1 and 2 in the vertical direction, 233 mm from the cantilever tip and therefore directly under the load point, for test 4 are given in Fig. 5.25. The diverging strain readings with one gauge in tension and the other in compression indicates that out of plane bending of the web or web distortion begins almost immediately on loading.

Fig. 5.26 shows the distributions of normal strains due to major axis bending, minor axis bending and warping of a cross section located at 4267 mm from the end support (gauges 38 through 45) for test 3 at the buckling load. As indicated in this figure, the strains due to lateral bending exceed that due to major axis bending. The total strain distribution in bottom flange was obtained using the best-fit line of the strain readings of the gauges mounted on bottom flange. For the top flange, the slope of the best-fit line for the strain readings as well as the strain determined at the bottom flange-web junction (448 $\mu\varepsilon$) were used to be consistent. Knowing the general shape of the strain distributions for lateral bending, warping and major axis bending, the strain values of these distributions at the flange tips could be determined from the total strain distribution. As a check, the maximum major axis bending strain was computed based on the buckling load, the self-weight, cross-sectional dimensions and material properties, and a value of 444 $\mu\varepsilon$ was obtained as compared to 448 $\mu\varepsilon$ given by the strain distributions.

Figs. 5.27 and 5.28 show the cantilever tip load versus the strains of the outer pair of gauges mounted on the bottom and top flanges (gauges 38 and 41 and 42 and 45, respectively, as shown) for test 21 at a station located about 1/2 way along the back span. The strains all increase at zero load when the self-weight of the inner frames is applied at the five interior load points. The figures show that the warping had more effect than lateral bending from the beginning until buckling load was approached. At any intermediate load level, the tensile straining of gauge 38 on the bottom flange increases more rapidly than that of gauge 41 on the opposite side of the web while the compression straining of gauge 42 on the top flange and on the side of the web as 38 increases more rapidly than that of gauge 45 on the opposite side of the web. This is consistent with warping. At the buckling load, the lateral bending effects dominated and significant tensile strain increments occurred on the side of gauges 38 and 42.

5.3.10 Load-deflection behaviour

By monitoring the load-deflection behaviour during the test, deformation control could be invoked as the buckling load was approached. Buckling was considered to occur when the load-deflection curve reached a horizontal asymptote. In those tests where the beam behaved elastically and was intended to be used again, the beam was unloaded shortly after the buckling was observed in order to eliminate or minimize any permanent deformations which would magnify initial imperfections. For inelastic tests, on the other hand, the investigation of the post buckling behaviour was only restricted by the deformation limit of the loading or reaction devices such as rockers or knife-edges.

The load-lateral deflection curve for both the loading and unloading stages of the bottom flange about 1/3 of the back span from the main support for test 17 is shown in Fig. 5.29. The lateral deflection increases first slowly and then more rapidly as the ultimate load is approached. The deformations before buckling were relatively small, as would be expected from the small measured initial geometrical imperfections. The unloading curve shows a nonlinear behaviour which is almost identical to the loading curve and resulted, at zero load, in a negligible permanent deformation. Thus, the specimen, which unloaded in a nonlinear elastic manner, could be used in another test.

The load-lateral deflection curves for tests 5 and 19 in Figs. 5.30 and 5.31, are examples of tests that showed a significant inelastic behaviour. These curves are plotted for the same location as test 17, i.e. about 1/3 of the back span from the main support. In test 5, a relatively little lateral deflection was observed up to the ultimate load where the load decreased with increasing deformations. When the load was removed, the lateral deformations decreased rapidly but a significant amount of permanent lateral deformation of about 70 mm remained at this location. Comparing Fig. 5.31 for test 19 with Fig. 5.30 for test 5, it is seen that the effect of initial imperfections is more pronounced in the early stage of loading in test 19 than in test 5. This is attributed to the fact that the specimen used in test 19, beam 3V, had already been used in three previous tests and although care was exercised to minimize any inelastic action in these tests, they probably contributed to an increase of initial imperfections. The specimen in test 5, beam 3C, was used only in that test. Notwithstanding this, the test/predicted ratio in test 19 was still 0.95. In test 19, the post buckling behaviour was characterized by the development of large deformations accompanied by a slight drop in the loading capacity. The beam was only deflected laterally about 65 mm as compared to 200 mm in test 5 and upon unloading, most of the lateral deflection was recovered.

Fig. 5.32 shows an example of the load-vertical deflection curve for the cantilever tip of test 5. As would be expected, the vertical deflection, including the effect of shear deflection, is in a good agreement with the calculated values based on the linear elastic theory. Beyond a load of 40 kN where yielding commenced at the tension flange-web junction due to the presence of residual stresses, the vertical deflections increase more rapidly than the elastic theory predicts.

5.3.11 Experimental errors

In full-scale distortional buckling tests of steel beams, several factors may contribute to experimental errors. For these tests, the factors include: (i) errors in calibration of load cells, (ii) incorrect measurements of the geometry of both the cross section and the overall specimen, (iii) incorrect assessment of the material properties of the specimen, (iv) unintentional eccentricity in loading, (v) reaction and load devices that either do not function properly over the entire test loading range or introduce unwanted restraint or friction and (vi) reaction devices that do not provide the restraint anticipated.

To minimize errors in the calibration of load cells, all load cells were calibrated and, by measuring each and every reaction and load point, statics provides an overall check on the calibration. In an initial test this check revealed an error in the calibration of a load cell which otherwise would have resulted in a greater scatter of the test/predicted ratio. Furthermore, as the reactions were measured directly beneath the beams and the loads were measured only at the jacks, any frictional losses in the loading apparatus as the inner loading frame rolls inside the outer loading frame is at once detected.

Errors due to the second two factors listed are minimized or eliminated by taking sufficient measurements to have samples of sufficient statistical size. The measures taken to eliminate errors in factors (ii) and (iii), as related to the beams themselves, are more fully discussed in Chapter 3. The cross-sectional properties of each beam were determined, as discussed, by taking measurements of the depth, flange width and thickness and web thickness. Initial sweep and camber were also determined. The overall geometry of each test setup was checked to eliminate blunders. Special attention was paid to the determination of the height at which loads were applied as this is a critical parameter in determining the buckling loads. The material properties of the various cross sections tested were established as given in Chapter 3, using redundant measurements. As in the case of residual stress measurements, the equations of statics can be used to detect errors.

Errors in factors (i), (ii) and (iii) are as likely to have a positive effect as a negative effect and are minimized by careful measurement using statistically significant samples. Unintentional load eccentricities will reduce the buckling strength and again can only be minimized by careful experimentation.

Reaction or load devices that do not function properly for the full range of the test by introducing unwanted restraints or friction increase the test load. Elimination of these unwanted restraints is the most difficult challenge for the experimentalist and requires increased vigilance. Discussion of some of the difficulties encountered and steps taken to overcome them follow.

Test 1 was performed under the same loading and restraint conditions of test 2 except that the cantilever tip load was applied 95 mm above the top flange in test 1 and only 40 mm above in test 2. Test 1, was therefore predicted to have a lesser capacity but actually carried a slightly greater load than in test 2. This is attributed to the use of a longitudinal knife-edge at the cantilever tip, which was intended to provide the freedom of rotation about the longitudinal axis but developed a small torsional restraint due to friction. Fig. 5.33 shows the relationship between the load and the lateral displacement of the bottom flange at the cantilever tip for tests 1 and 2. Because the top flange was laterally restrained, the lateral displacement of the bottom flange is an indirect measure of the cross-sectional twisting at the cantilever tip. In test 1, very little twist occurred before the maximum load was reached when the bottom flange abruptly deflected about 45 mm as the load decreased from 84.4 kN to 75.1 kN. This indicates that the torsional restraint developed due to friction in the knife-edge was overcome and the load decreased to about the buckling load consistent with rotational freedom. Taking this second load as the true value gives a test/predicted ratio for test 1 of 1.05. On the other hand, test 2 displayed a completely different behaviour. The displacement increased considerably more as the load approached the buckling value. This indicates that even though the same type of longitudinal knife-edge was used in both tests, only that in test 2 functioned properly. It is essential that knife-edges be examined carefully to ensure that no burrs or scratches exist that will restrain movement even minutely and that movement is not restrained by the geometry of the knife-edge and its matching groove.

This problem was encountered again in test 8, when the same longitudinal knife-edge as used in test 1 was apparently inadvertently used again at the cantilever tip. This test was repeated as test 28 where the longitudinal knife-edge at the cantilever tip was replaced by a semi-cylindrical rocker and resulted in a test/ predicted ratio of 0.94 instead of 1.33. Fig. 5.33 shows the cantilever tip load versus the lateral deflection of bottom flange at the cantilever tip for tests 8 and 28. In test 8, the lateral deflection was about 5 mm at the buckling load, while in test 28 it exceeded 40 mm. Thus, the specimen in test 8 rotated less than one degree about the longitudinal axis at the cantilever tip as compared to about 6 degrees in test 28. Furthermore in test 8, the fact that the initial tendency of the specimen to deflect laterally to the left was reversed indicates that torsional restraint was active. The test/predicted ratios of 0.94 in test 28, which is one of the lower values in all the tests in this series, is likely partly attributable to an unintentional eccentricity. Fig. 5.34 shows that on the first increment of load, the bottom flange lurched almost 2 mm sideways. This has the opposite effect of unwanted restraints and tends to reduce the buckling load.

Once again improper functioning of the longitudinal knife-edge was discovered in test 17, but here when the applied load exceeded the anticipated buckling capacity and the beam showed no sign of buckling, the load was removed and the test was repeated with a semi-cylindrical rocker replacing the longitudinal knife-edge. Fig. 5.35 shows the results of the two loadings of test 17. The excellent results of the second loading are indicated by a test/predicted ratio of 0.99 (Table 5.1.b) and as well the lateral deflection at buckling increased asymptotically. The major difference in behaviour between the first and second loadings is that lateral displacement of the bottom flange did not occur in the first loading. Because buckling was not observed in the first loading, the result is not reported in Table 5.1.

In test 6, arrays of 13 mm diameter ball bearings were used at the interior load points in an attempt to provide lateral, longitudinal and rotational freedom about the vertical axis. Fig. 5.36 shows the load versus lateral displacement of the top flange near the middle of the back span for tests 6 and 7. For test 6, almost no displacement was observed up to the maximum load when a small lateral disturbing force estimated at 0.6 kN was applied by hand to the top flange near the middle of the interior span. The load then suddenly dropped from 94.5 kN to about 71 kN when a significant lateral displacement and twist was observed. This indicates that a relatively small amount of friction between the ball bearings and the bearing plates was enough to restrain the top flange laterally, forcing the beam into a higher energy buckling mode. Test 7 was a duplicate of test 6 with the same loading and restraint conditions. However, in test 7 a small lateral disturbing force of about 0.6 kN was applied after every load step to overcome friction. Buckling occurred with considerable lateral deflection of the top flange, as indicated by the load-deflection curve of Fig. 5.36 and in Fig. 5.6. The test/predicted ratio decreased from 1.47 in test 6 to 1.16 in test 7. It is apparent, however, that the lateral disturbing force of 0.6 kN was not enough to eliminate the effect of friction completely, as the test/predicted ratio of 1.16 in test 7 is still too high. The ball bearings were not used subsequently. A corollary to the fact that a small amount of unwanted lateral restraint increases the test buckling load substantially means that in practice a small amount of unaccounted for lateral restraint may improve the load carrying capacity of a structural member considerably.

Test 11 was a duplicate of test 10 because an unintentional eccentricity of about 2 mm of the cantilever tip load was observed after buckling occurred in test 10. The buckling load in test 11 was 44.1 kN compared to 41.1 kN in test 10.

Another source of errors in the test series is the incomplete torsional restraint at column location where lateral restraint is not provided. In tests 23 and 24, it was attempted to provide torsional restraint to the bottom flange, while allowing lateral translation to take place, as shown in Fig. 4.15, by sitting the beam on a relatively wide plate supported by two load cells to provide a stable base with the entire assembly free to move laterally on a nest of rollers. For this system to be effective in providing torsional restraint, the beam flange must not lift off the supporting plate. The narrow flange width of 127 mm of the W360x39 was insufficient to completely prevent the rotation about the longitudinal axis and a slight separation between the edge of the flange and the supporting assembly was observed at failure in these two tests. This explains the relatively low test/predicted ratio obtained in tests 23 and 24 of 0.92 and 0.93, respectively.

Test number	Buckling loads		Test/Predicted
	Test (kN)	Predicted (kN)	
1	75.1	71.7	1.05
2	78.9	79.0	1.00
3	77.1	78.4	0.98
4	104.9	112.6	0.93
5	125.8	136.6	0.92
6	94.5 21.4	64.5 14.6	1.47*
7	76.1 17.1	65.6 14.7	1.16
8	164.9 35.9	124.1 27.0	1.33*
9	35.5 35.0	36.6 36.1	0.97
10	41.1 22.5	40.8 22.3	1.01
11	44.1 23.8	40.3 21.7	1.09
12	46.4 24.7	50.4 26.8	0.92

Table 5.1.a Test and predicted buckling loads for tests 1 through 12

Test number	Buckling loads		Test/Predicted
	Test (kN)	Predicted (kN)	
13	48.2 25.9	52.9 28.4	0.91
14	132.4 46.8	137.1 48.5	0.97
15	136.8 48.5	143.0 50.7	0.96
16	84.0	83.9	1.00
17	77.6	78.0	0.99
18	118.9	111.5	1.07
19	152.6	160.7	0.95
20	52.7 27.9	50.6 26.8	1.04
21	154.5 33.1	155.4 33.3	0.99
22	133.3	129.6	1.03
23	45.9	49.8	0.92
24	40.7 9.6	43.9 10.4	0.93

Table 5.1.b Test and predicted buckling loads for tests 13 through 24

Test number	Buckling loads		Test/Predicted
	Test (kN)	Predicted (kN)	
25	55.9	54.1	1.03
26	46.7 11.2	45.4 10.9	1.03
27	127.5 26.7	142.8 29.9	0.89
28	128.8 28.2	136.7 29.9	0.94
29	76.3 17.5	72.4 16.6	1.05
30	42.2 10.7	43.0 10.9	0.98
31	127.8 27.2	143.9 30.6	0.89
32	72.3	70.9	1.02
33	73.4	70.0	1.05

$\mu = 0.99$
$\sigma = 0.063$
$V = 0.064$

Table 5.1.c Test and predicted buckling loads for tests 25 through 33

Test number	Beam depth	Range	Predicted M_σ/M_p		Ratio M_σ/M_p
			Residual stresses		$\frac{\sigma_r \text{ considered}}{\sigma_r \text{ neglected}}$
			Neglected	Considered	
1	353	elastic	0.362	0.468	1.226
2	353	elastic	0.388	0.516	1.248
3	353	elastic	0.387	0.512	1.244
4	353	elastic	0.614	0.735	1.165
5	353	inelastic	0.852	0.892	1.045
6	353	elastic	0.325	0.421	1.228
7	353	elastic	0.328	0.428	1.234
8	353	elastic	0.628	0.810	1.225
9	353	elastic	0.184	0.239	1.230
10	353	elastic	0.218	0.267	1.184
11	353	elastic	0.217	0.263	1.175
12	353	elastic	0.265	0.329	1.195

Table 5.2.a Theoretical predictions demonstrating the beneficial effects of residual stresses on tests 1 through 12

Test number	Beam depth	Range	Predicted M_{cr}/M_p		Ratio M_{cr}/M_p
			Residual stresses		
			Neglected	Considered	$\frac{\sigma_r \text{ considered}}{\sigma_r \text{ neglected}}$
13	353	elastic	0.286	0.346	1.173
14	353	inelastic	0.779	0.894	1.129
15	353	inelastic	0.838	0.934	1.103
16	310	elastic	0.450	0.493	1.087
17	310	elastic	0.407	0.458	1.111
18	310	elastic	0.629	0.655	1.040
19	310	inelastic	1.126	0.944	0.838
20	310	elastic	0.272	0.297	1.084
21	310	inelastic	0.909	0.913	1.004
22	310	elastic	0.702	0.761	1.078
23	353	elastic	0.308	0.325	1.052
24	353	elastic	0.272	0.287	1.052

Table 5.2.b Theoretical predictions demonstrating the beneficial effects of residual stresses on tests 13 through 24

Test number	Beam depth	Range	Predicted M_{cr}/M_p		Ratio M_{cr}/M_p
			Residual stresses		$\frac{\sigma_r \text{ considered}}{\sigma_r \text{ neglected}}$
			Neglected	Considered	
25	310	elastic	0.307	0.318	1.035
26	310	elastic	0.261	0.267	1.022
27	310	inelastic	0.842	0.839	0.996
28	353	inelastic	0.728	0.893	1.185
29	353	elastic	0.454	0.473	1.040
30	353	elastic	0.268	0.281	1.046
31	310	inelastic	1.840	0.845	1.006
32	353	elastic	0.372	0.466	1.202
33	353	elastic	0.296	0.459	1.355

Table 5.2.c Theoretical predictions demonstrating the beneficial effects of residual stresses on tests 25 through 33

Restraint condition	Loading case	Load position	M_{cr}/M_p residual stresses Neglected	M_{cr}/M_p residual stresses Considered
A	I	Shear centre	1.05	1.000
A	II	Shear centre	0.575	0.731
A	III	Shear centre	0.482	0.599
A	IV	Shear centre	0.386	0.448
B	I	Shear centre	0.544	0.578
B	II	Shear centre	0.535	0.566
B	III	Shear centre	0.386	0.438
B	IV	Shear centre	0.351	0.397
A	I	Top Flange	0.467	0.641
A	II	Top flange	0.395	0.513
A	III	Top flange	0.415	0.538
A	IV	Top flange	0.232	0.291
B	I	Top flange	0.425	0.468
B	II	Top flange	0.364	0.428
B	III	Top flange	0.385	0.434
B	IV	Top flange	0.220	0.267

Table 5.3 Finite element predictions, effect of shape of bending moment diagram

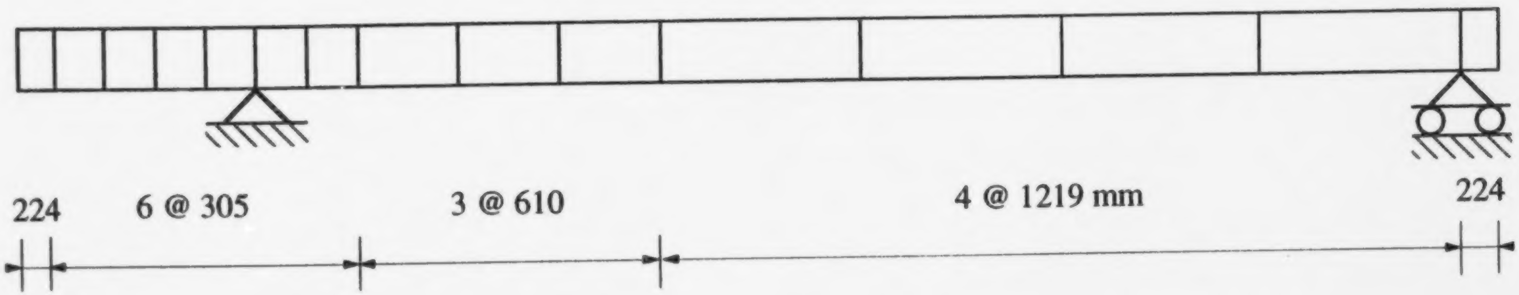
224
6 @ 305
3 @ 610
4 @ 1219 mm
224

Fig. 5.1 Finite element mesh used to predict buckling loads for tests 1 through 32

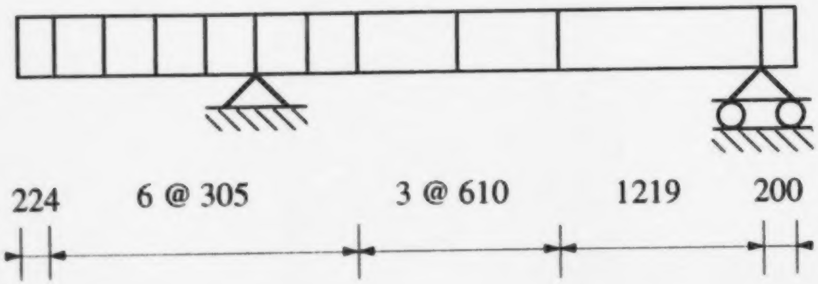
224
6 @ 305
3 @ 610
1219
200

Fig. 5.2 Finite element mesh used to predict buckling load for test 33

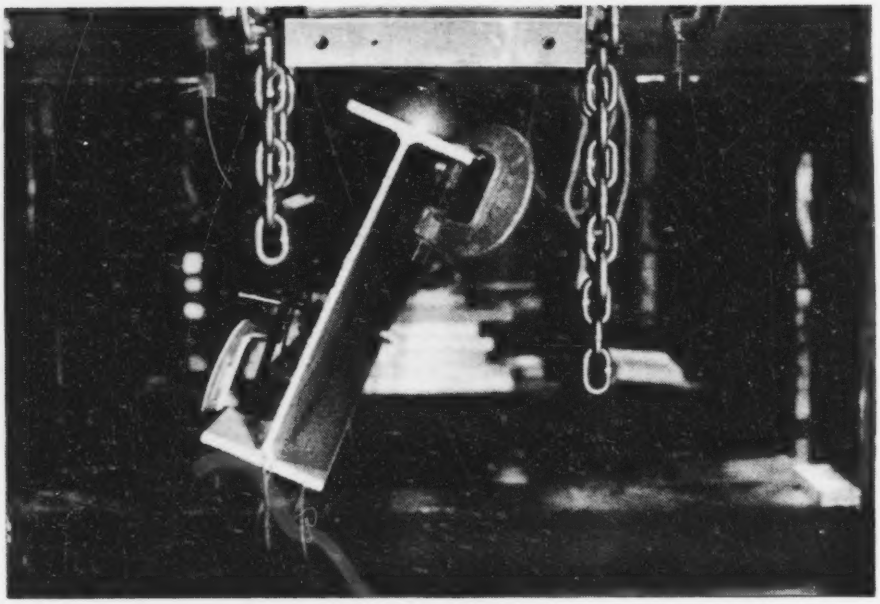

Fig. 5.3 End view of buckled specimen in test 33

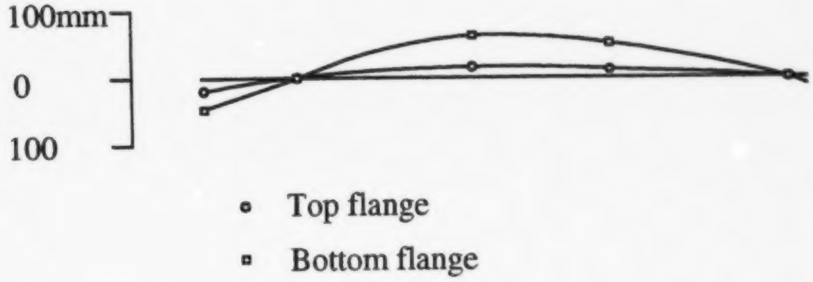

a) Lateral displacements

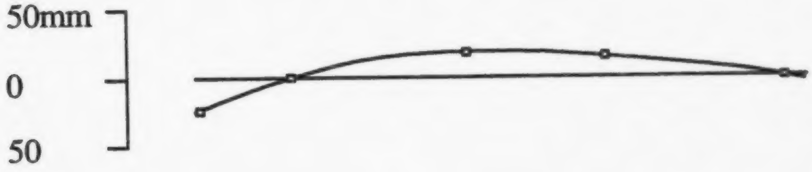

b) Vertical displacements of top flange

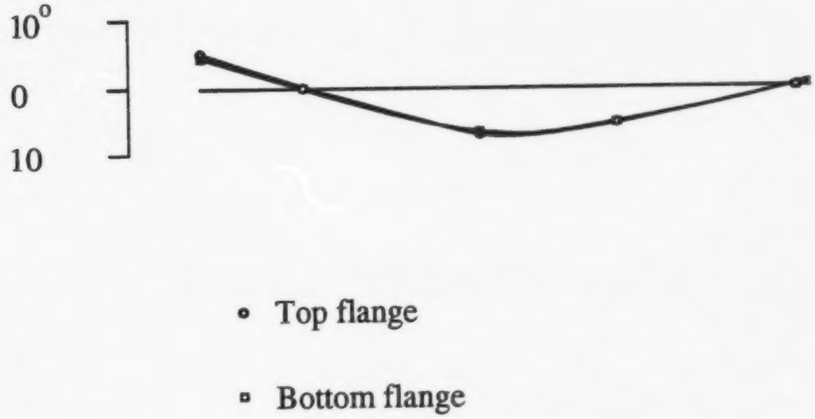

c) Twist angles

Fig. 5.4 Buckling displacements of test 3

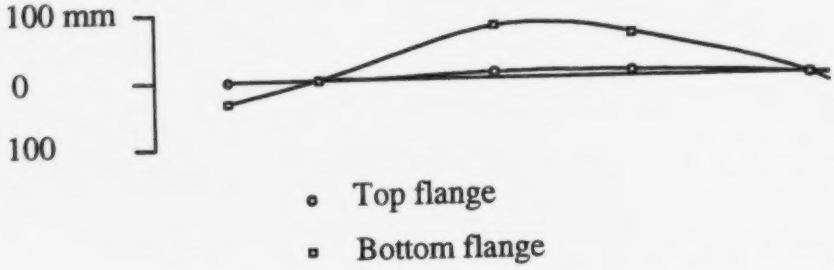

a) Lateral displacements

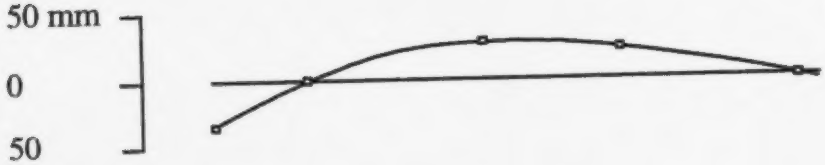

b) Vertical displacements of top flange

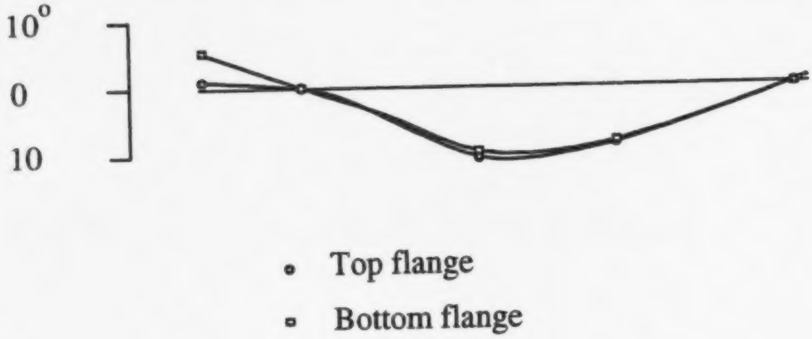

c) Twist angles

Fig. 5.5 Buckling displacements of test 4

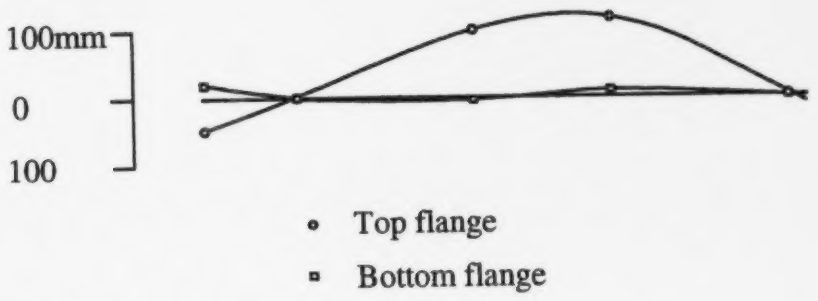

a) Lateral displacements

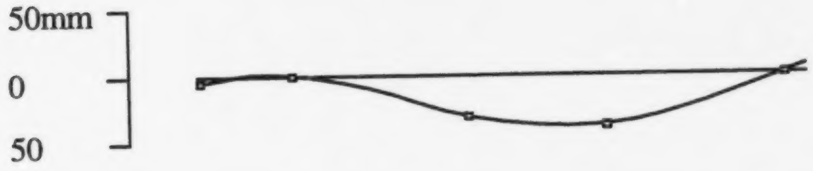

b) Vertical displacements

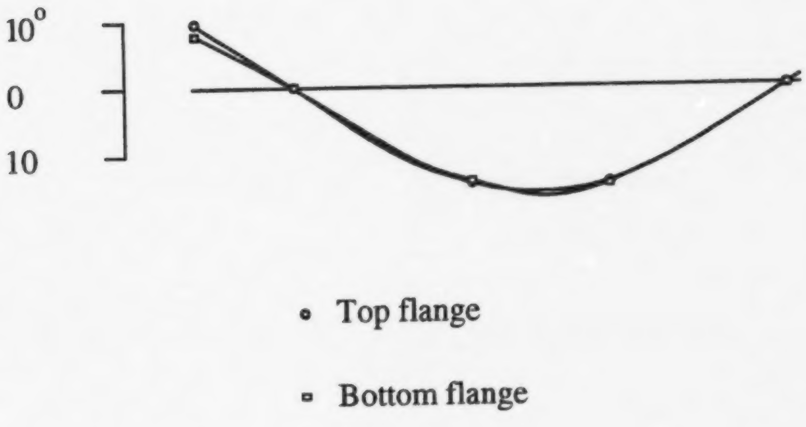

c) Twist angles

Fig. 5.6 Buckling displacements of test 7

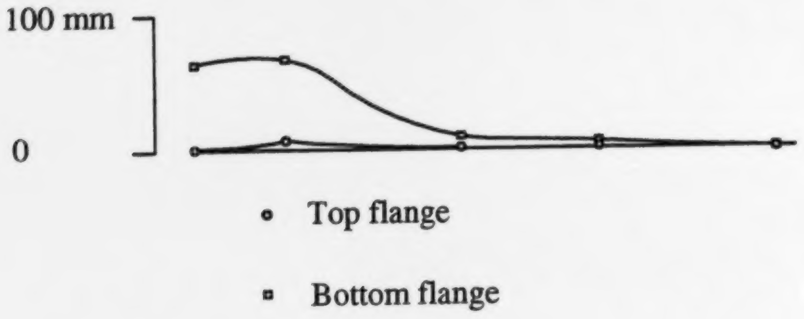

a) Lateral displacements

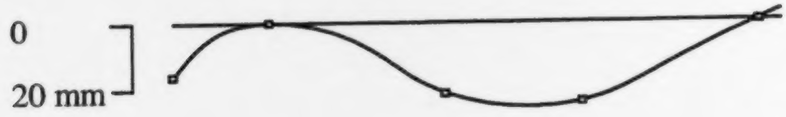

b) Vertical displacements of top flange

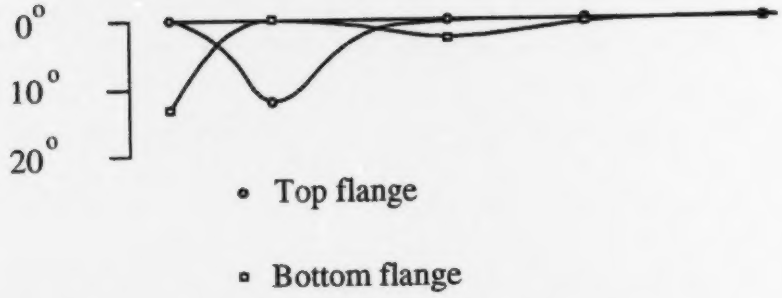

c) Twist angles

Fig. 5.7 Buckling displacements of test 27

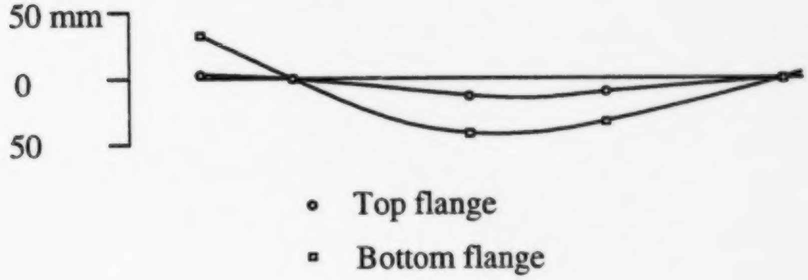

a) Lateral displacements

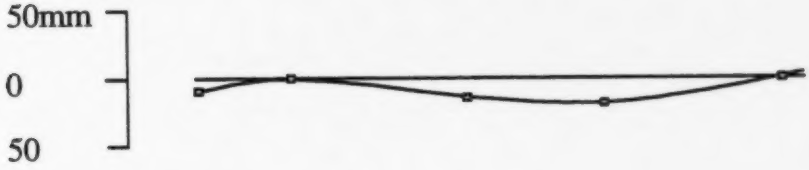

b) Vertical displacements of top flange

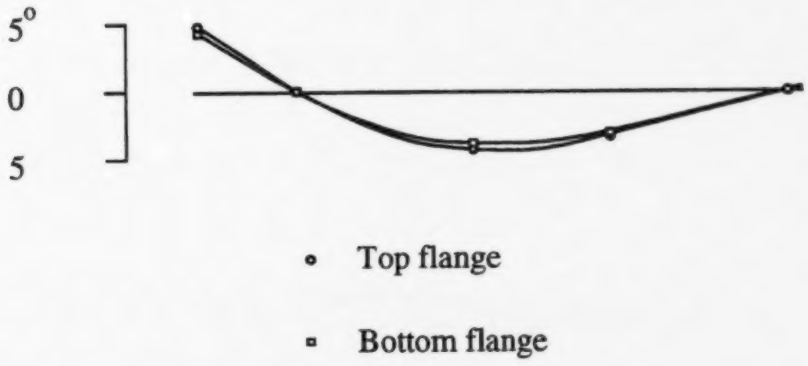

c) Twist angles

Fig. 5.8 Buckling Displacements of test 28

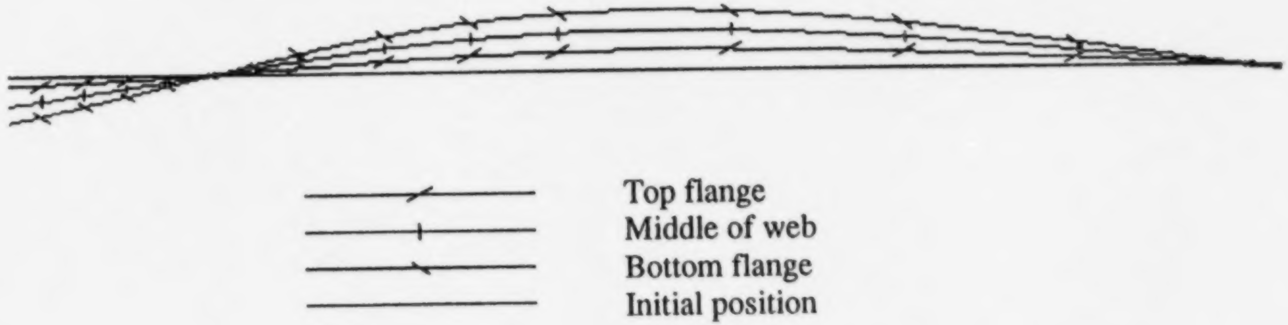

Fig. 5.9 Predicted normalized buckled shape, test 3

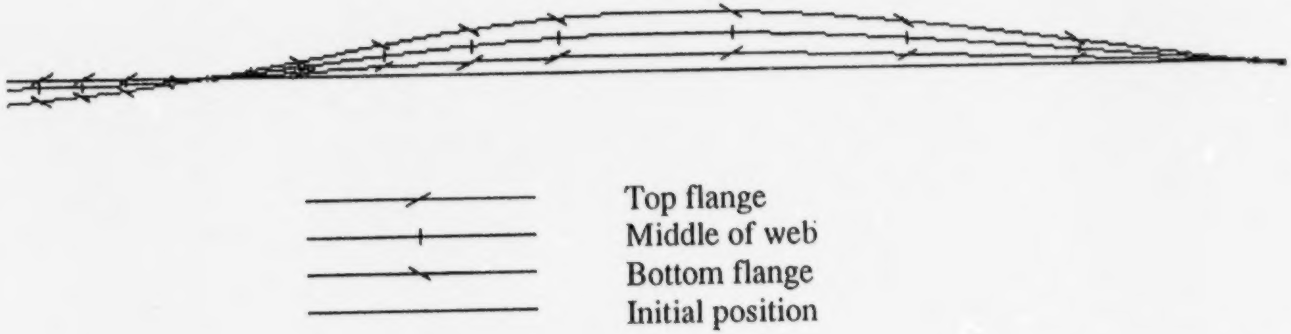

Fig. 5.10 Predicted normalized buckled shape, test 4

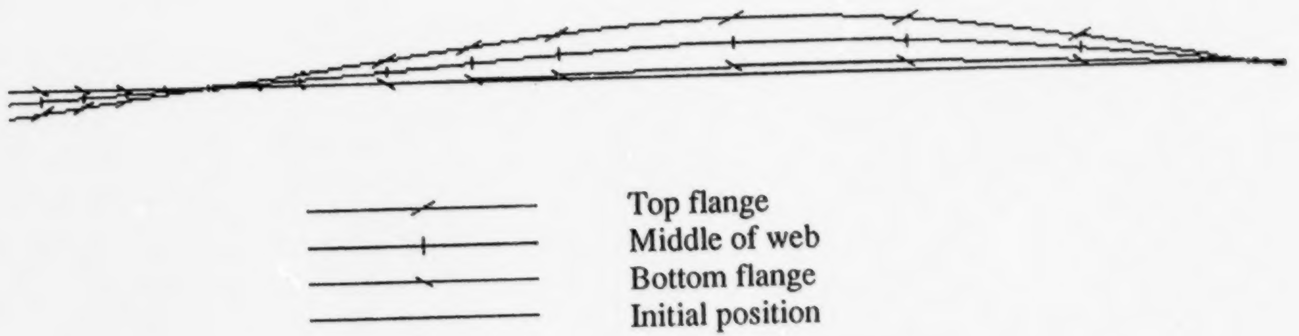

Fig. 5.11 Predicted normalized buckled shape, test 7

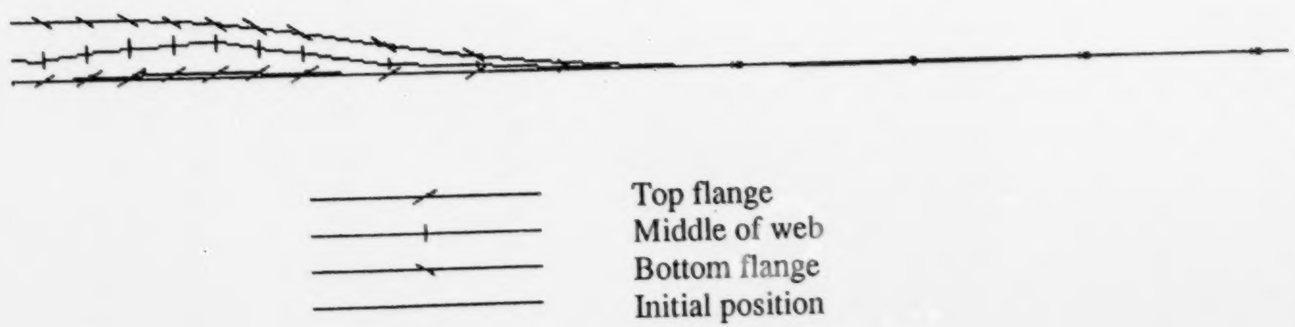

Fig. 5.12 Predicted normalized buckled shape, test 27

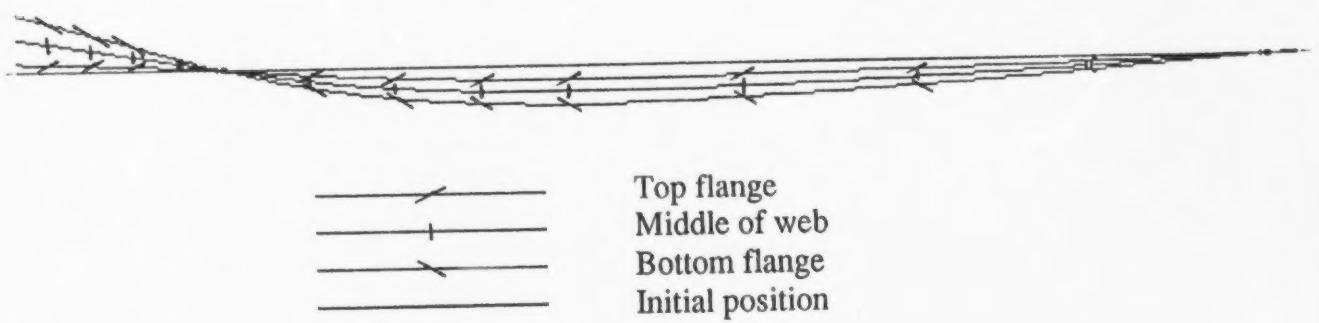

Fig. 5.13 Predicted normalized buckled shape, test 28

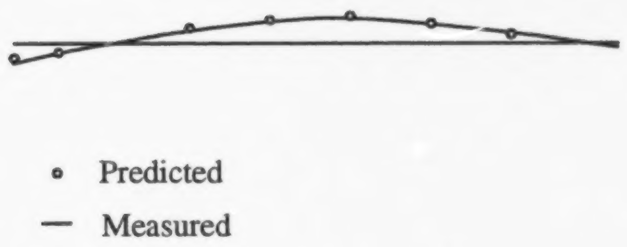

a) Lateral displacement of top flange

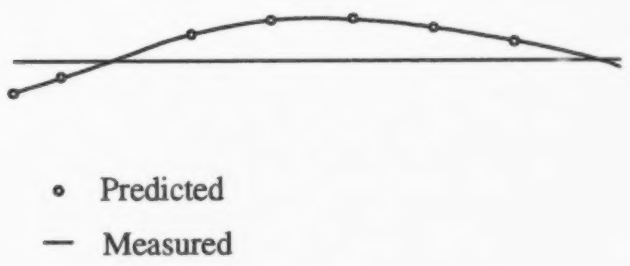

b) Lateral displacement of bottom flange

Fig. 5.14 Measured and predicted buckled shapes, test 3

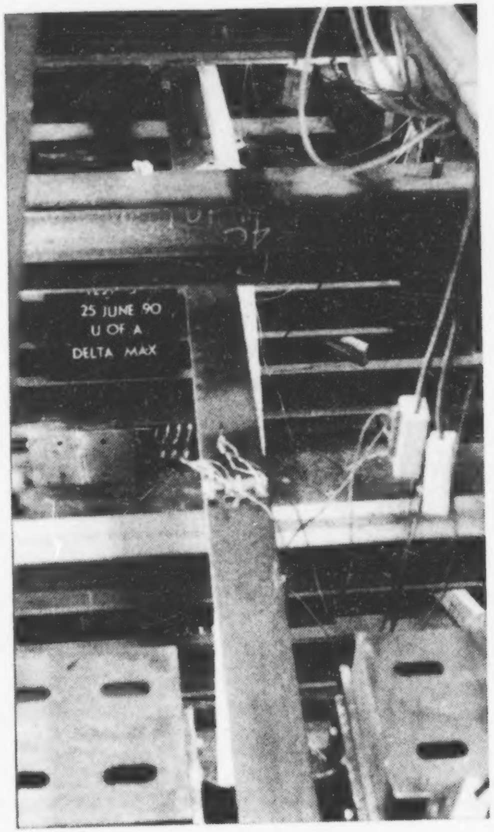
25 JUNE 90
U OF A
DELTA MAX

Fig. 5.15 Plan view of longitudinal buckled shape in test 5

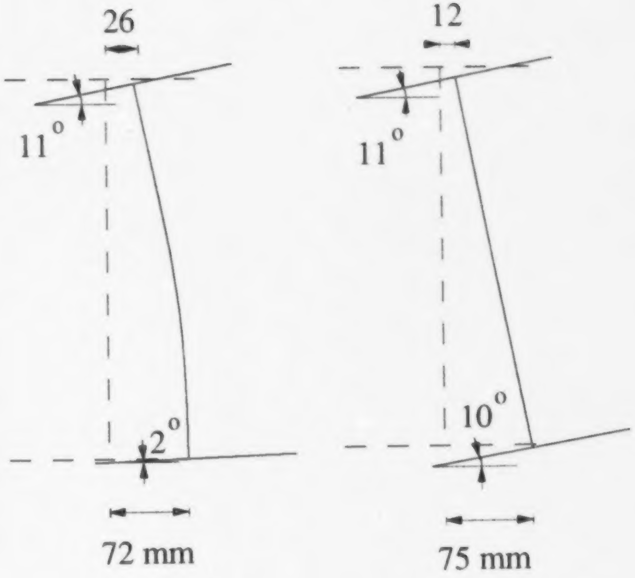
26
11°
2°
72 mm
12
11°
10°
75 mm

a) at interior support b) at cantilever tip

Fig. 5.16 Deflected shape of the cross section at the interior support and the cantilever tip in test 26

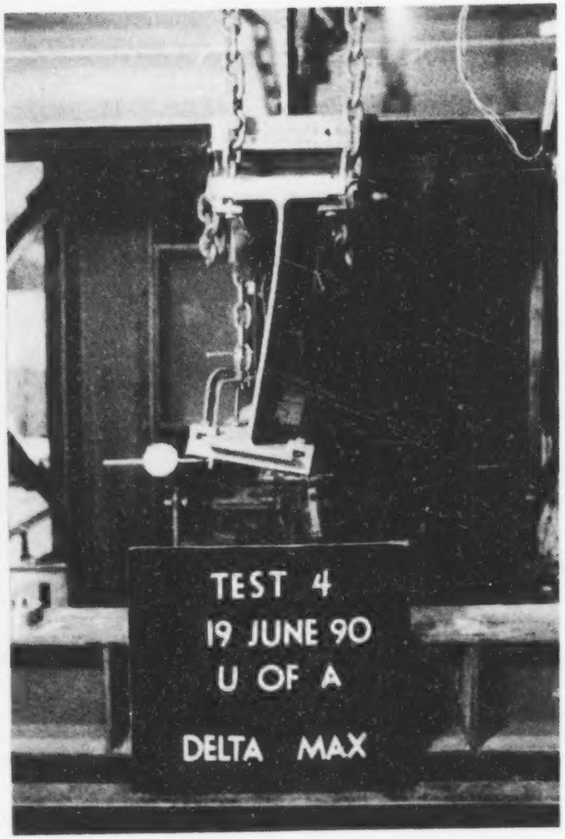
TEST 4
19 JUNE 90
U OF A
DELTA MAX

Fig. 5.17 End view of distorted cross section at the cantilever tip, test 4

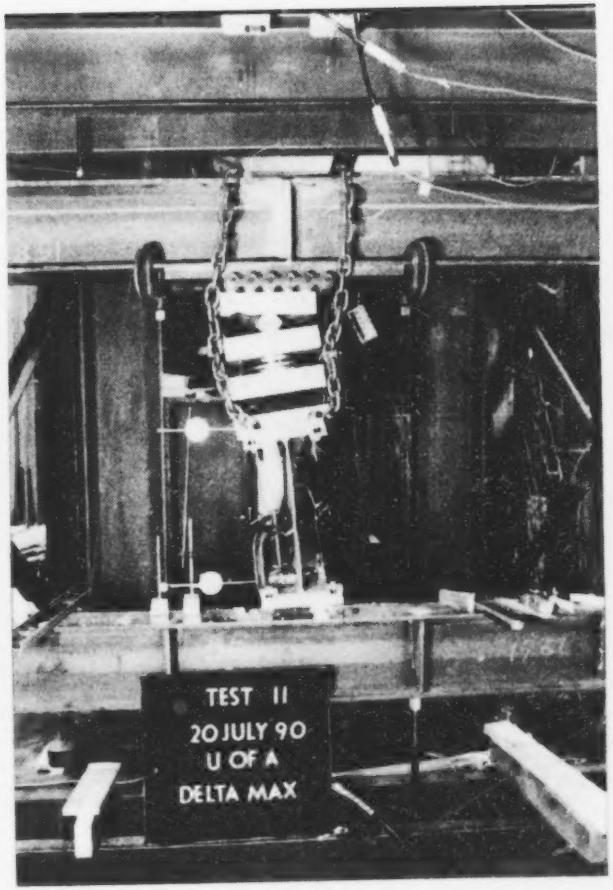
TEST 11
20 JULY 90
U OF A
DELTA MAX

Fig. 5.18 End view of distorted cross section at the cantilever tip, test 11

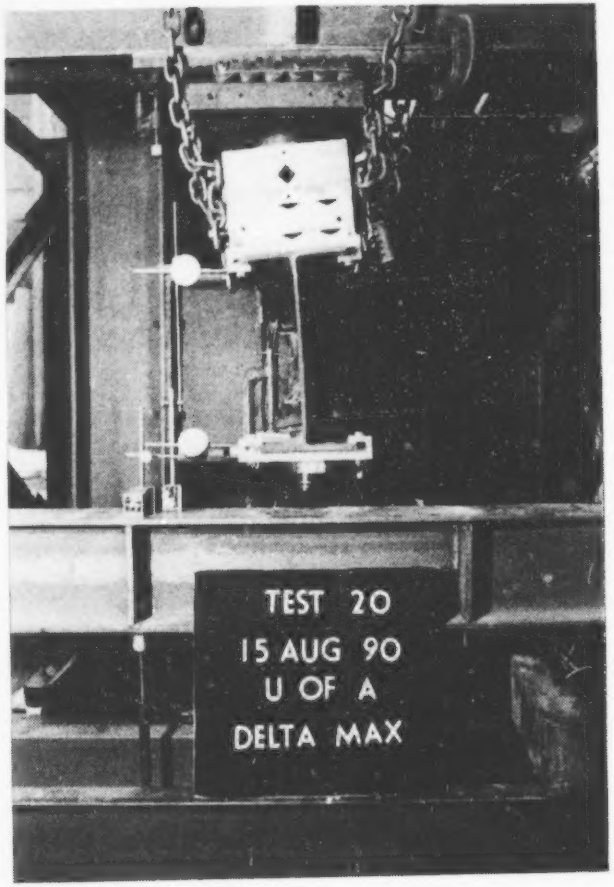
TEST 20
15 AUG 90
U OF A
DELTA MAX

Fig. 5.19 End view of distorted cross section at the cantilever tip, test 20

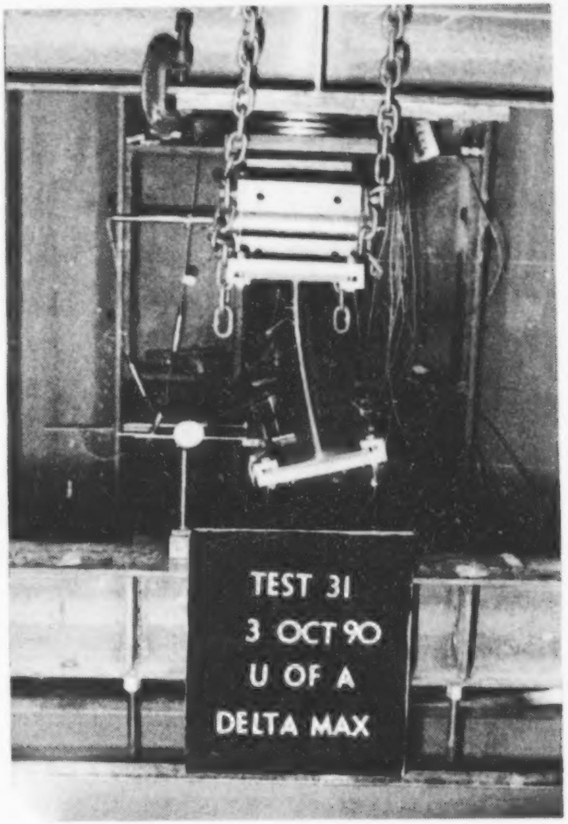
TEST 31
3 OCT 90
U OF A
DELTA MAX

Fig. 5.20 End view of distorted cross section at the cantilever tip, test 31

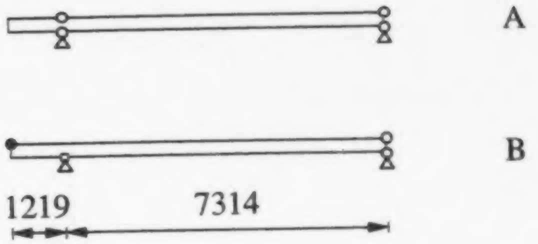
A
B
1219
7314

a) Restraint conditions

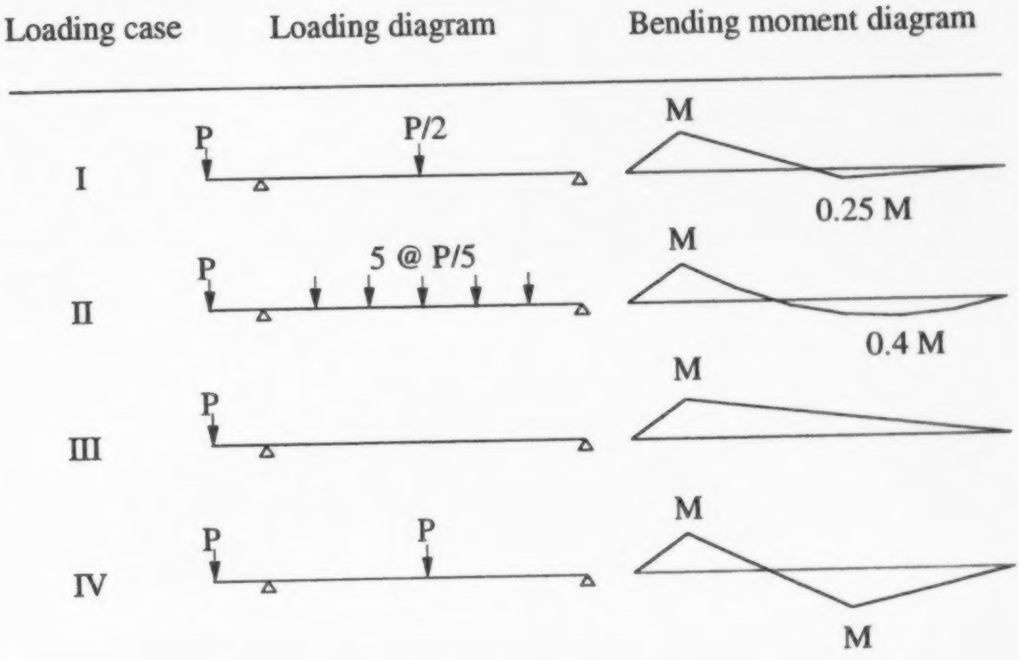
Loading case
Loading diagram
Bending moment diagram
I
P
P/2
M
0.25 M
II
P
5 @ P/5
M
0.4 M
III
P
M
IV
P
P
M
M

b) Loading conditions

Fig. 5.21 Restraint and loading conditions used to investigate the effect of bending moment diagrams

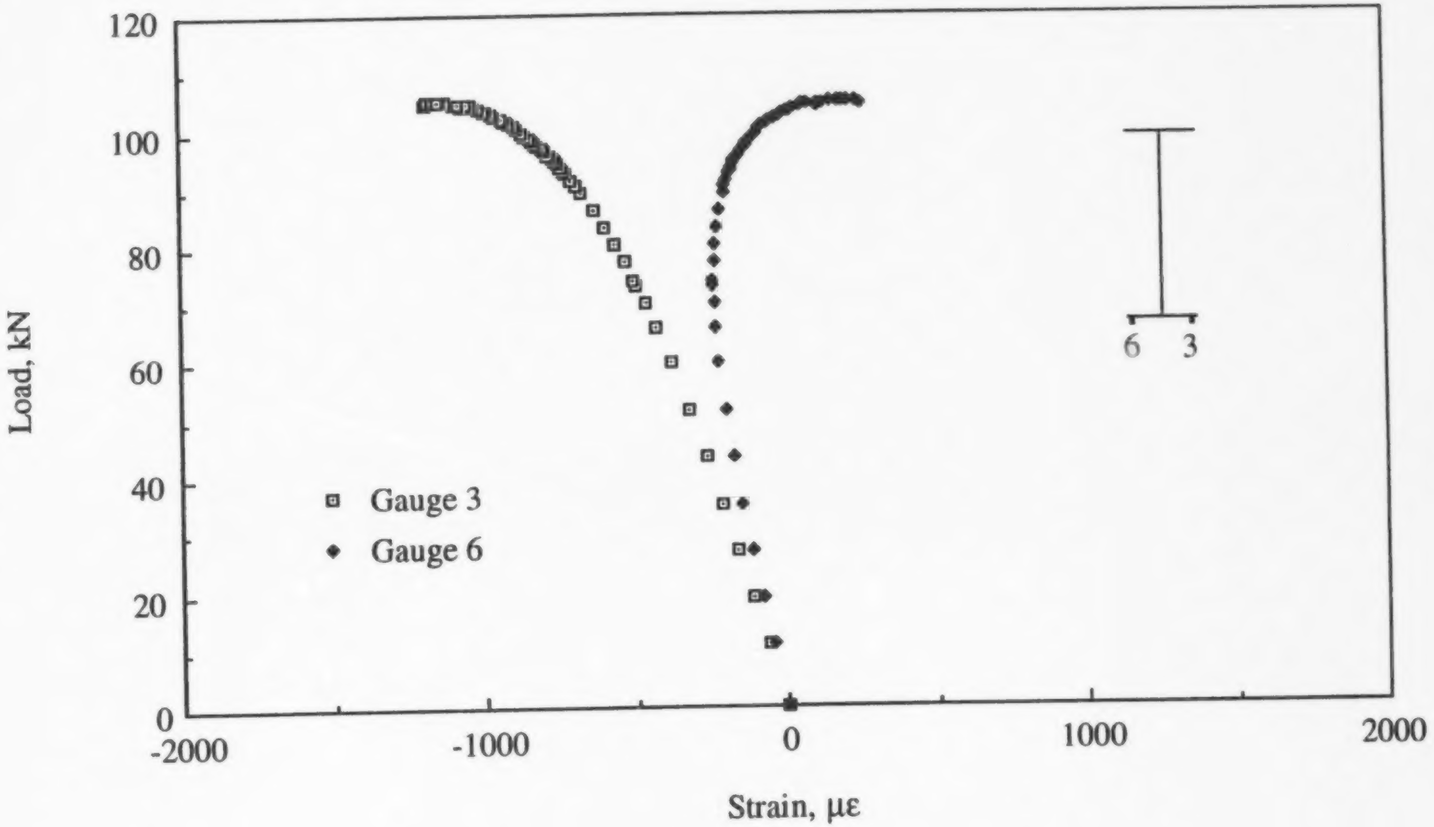

Fig. 5.22 Load versus longitudinal flange strains, strain gauges 3 and 6, test 4

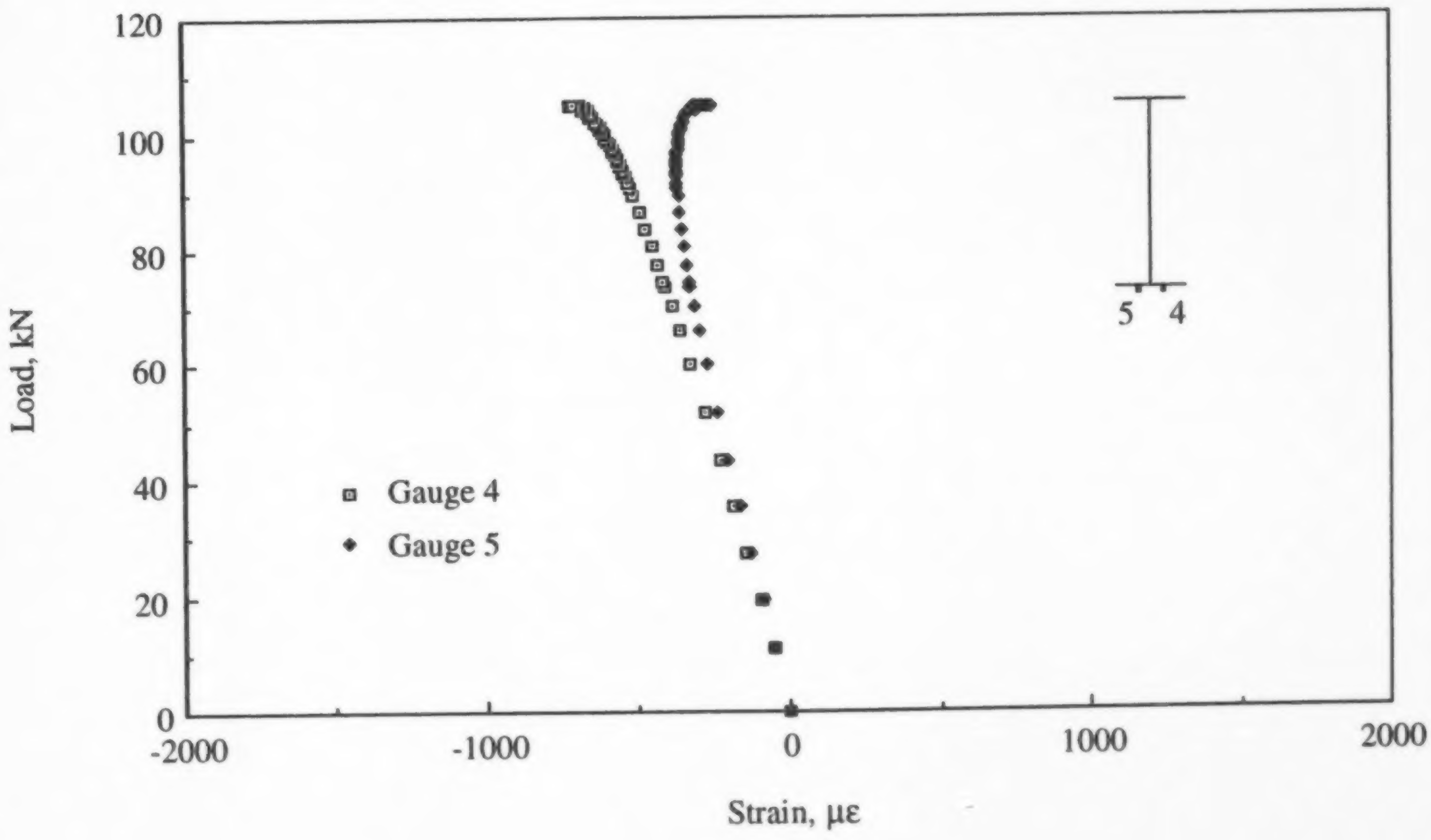

Fig. 5.23 Load versus longitudinal flange strains, strain gauges 4 and 5, test 4

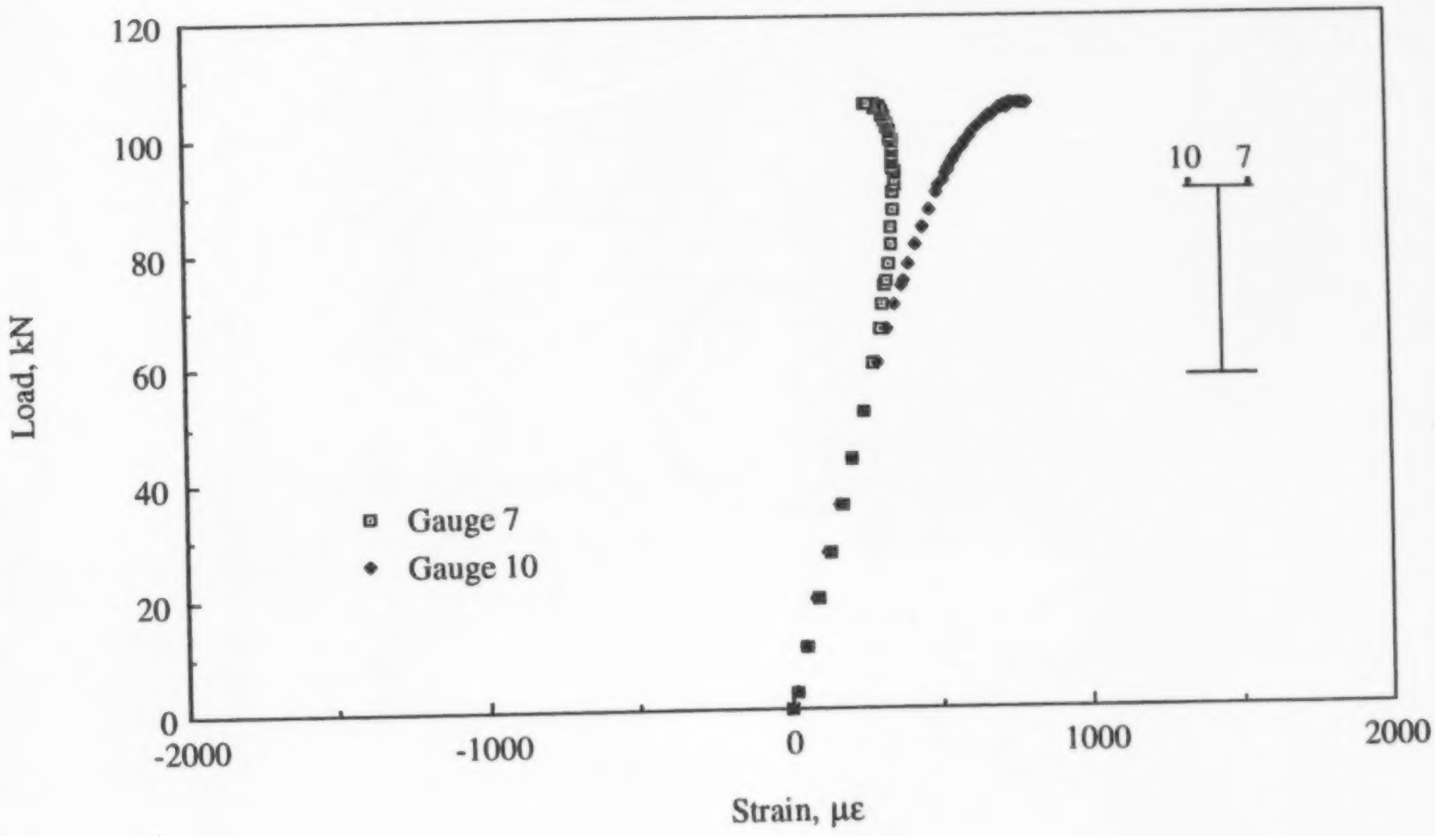

Fig. 5.24 Load versus longitudinal flange strains, strain gauges 7 and 10, test 4

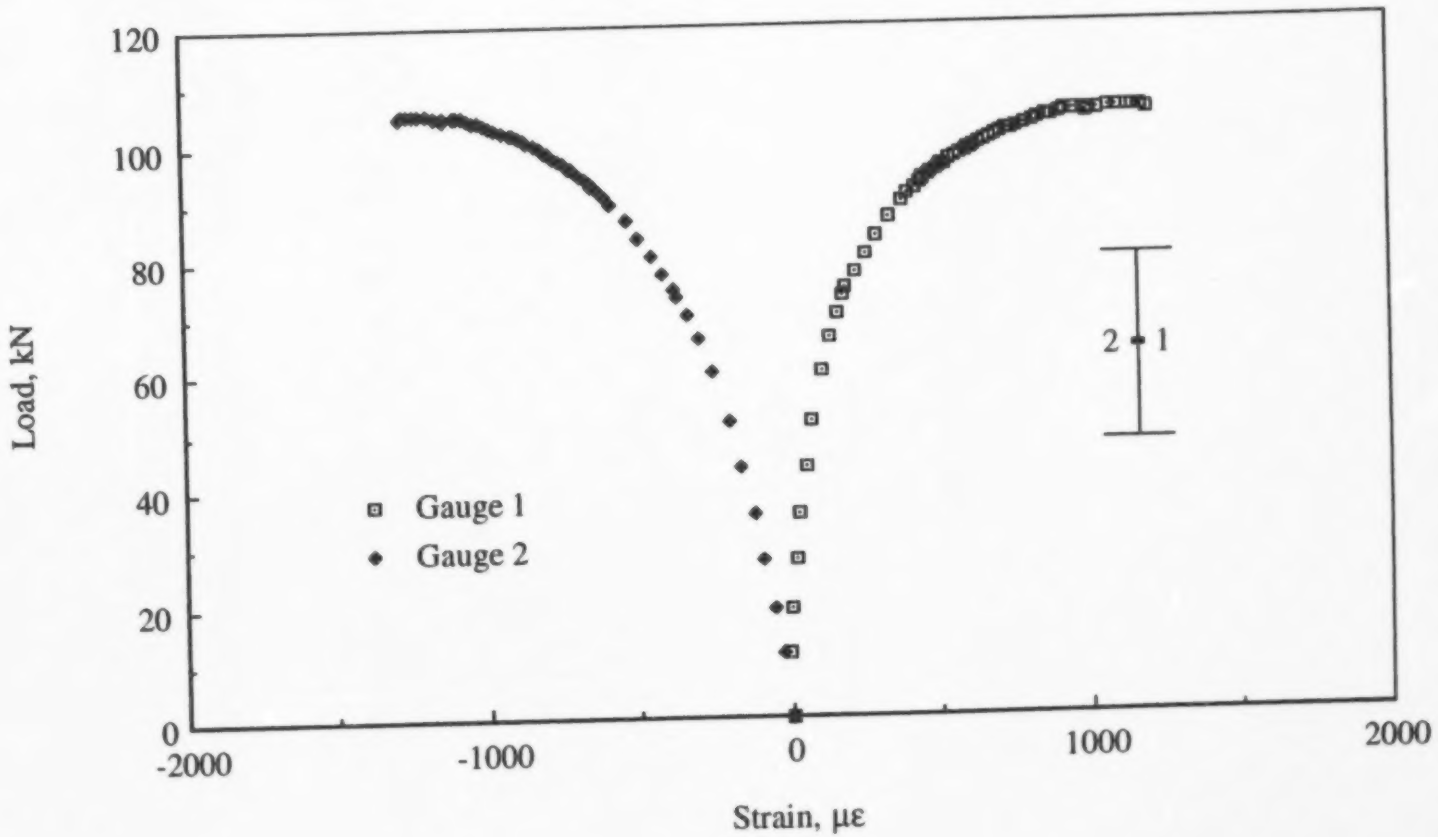

Fig. 5.25 Load versus vertical web strains, strain gauges 1 and 2, test 4

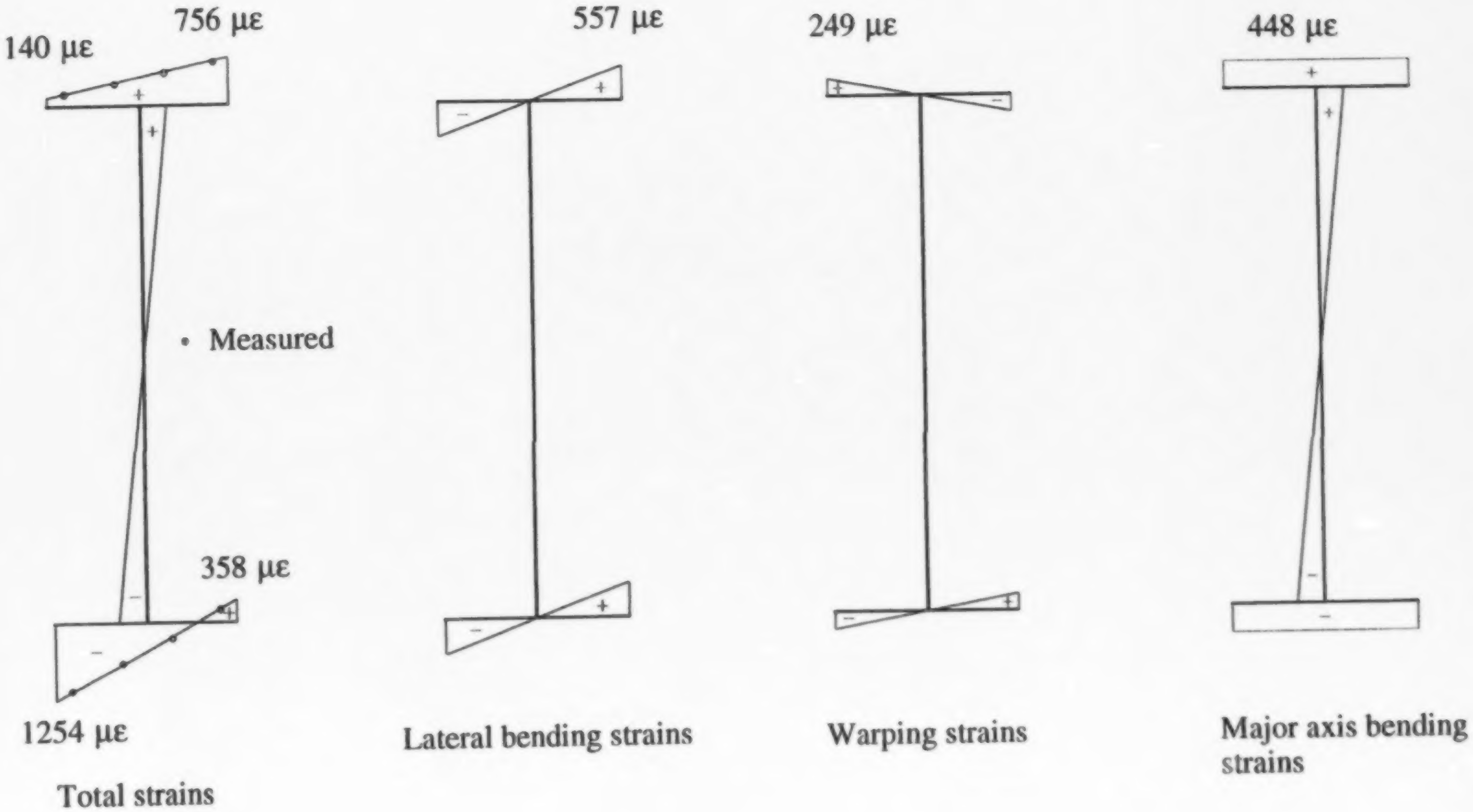
140 με
756 με
• Measured
358 με
1254 με
Total strains
557 με
Lateral bending strains
249 με
Warping strains
448 με
Major axis bending strains
+
−

Fig. 5.26 Strain distributions obtained from gauges 38 through 45 at buckling load of test 3

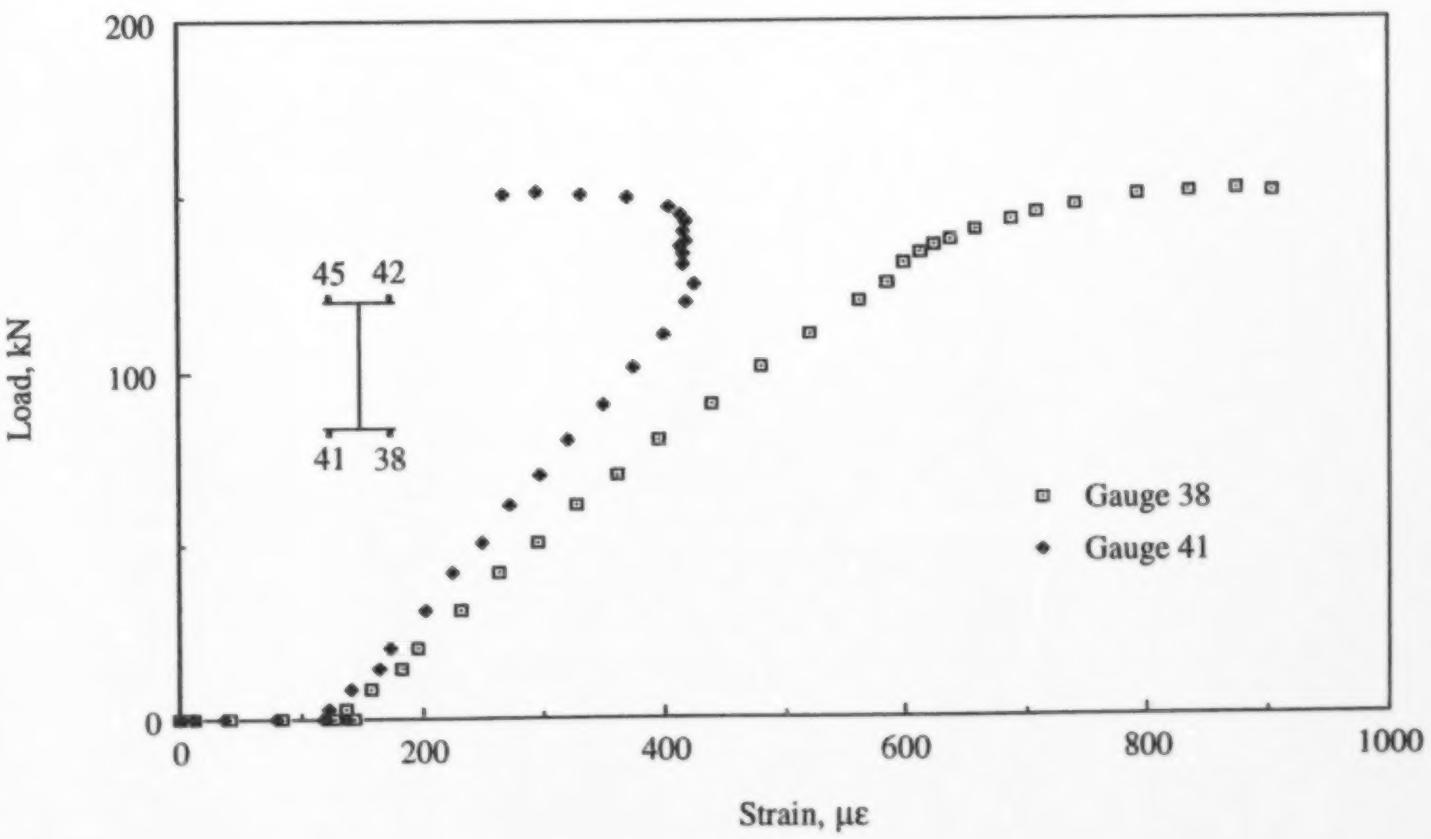

Fig. 5.27 Load versus strains, gauges 38 and 41, test 21

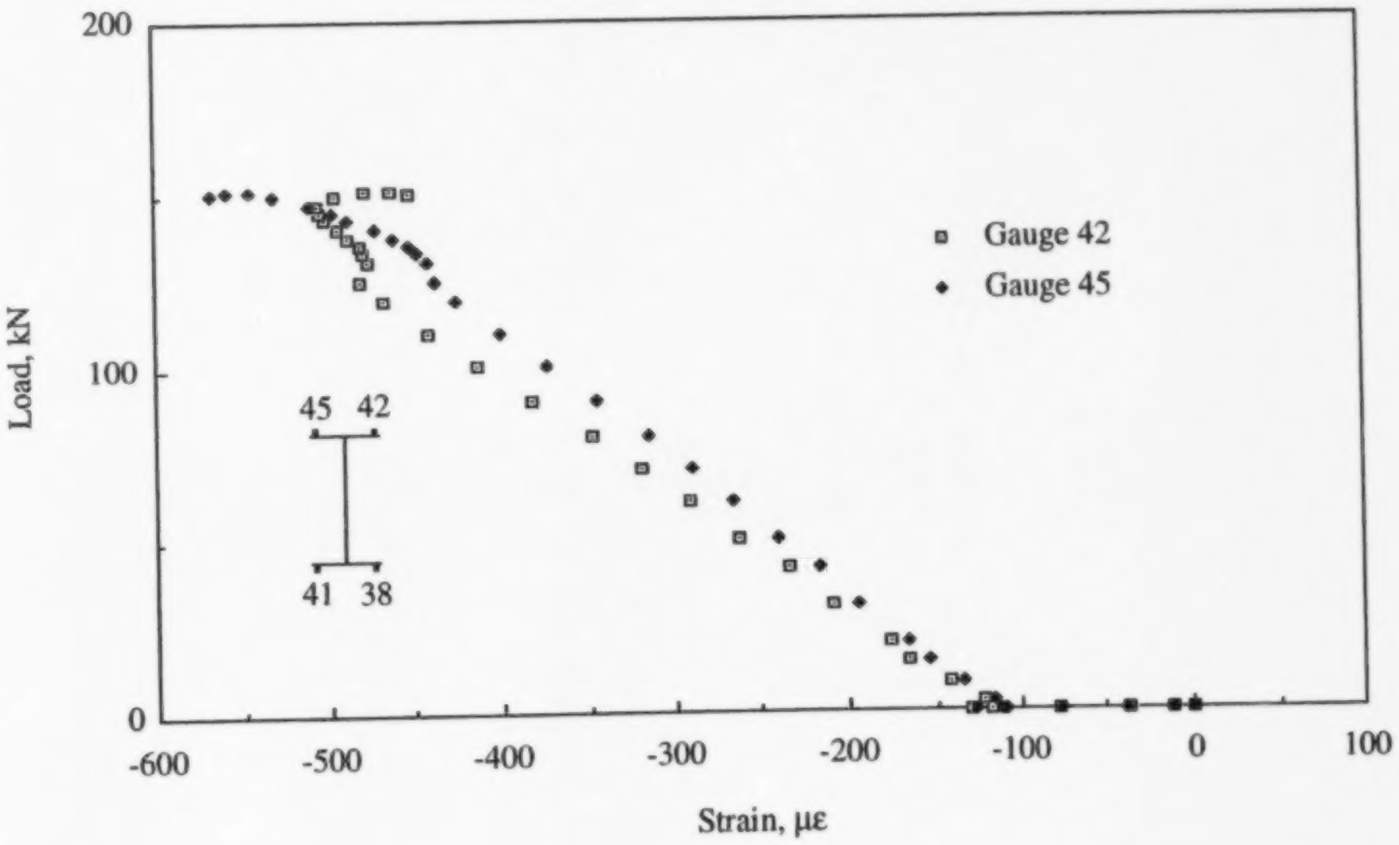

Fig. 5.28 Load versus strains, gauges 42 and 45, test 21

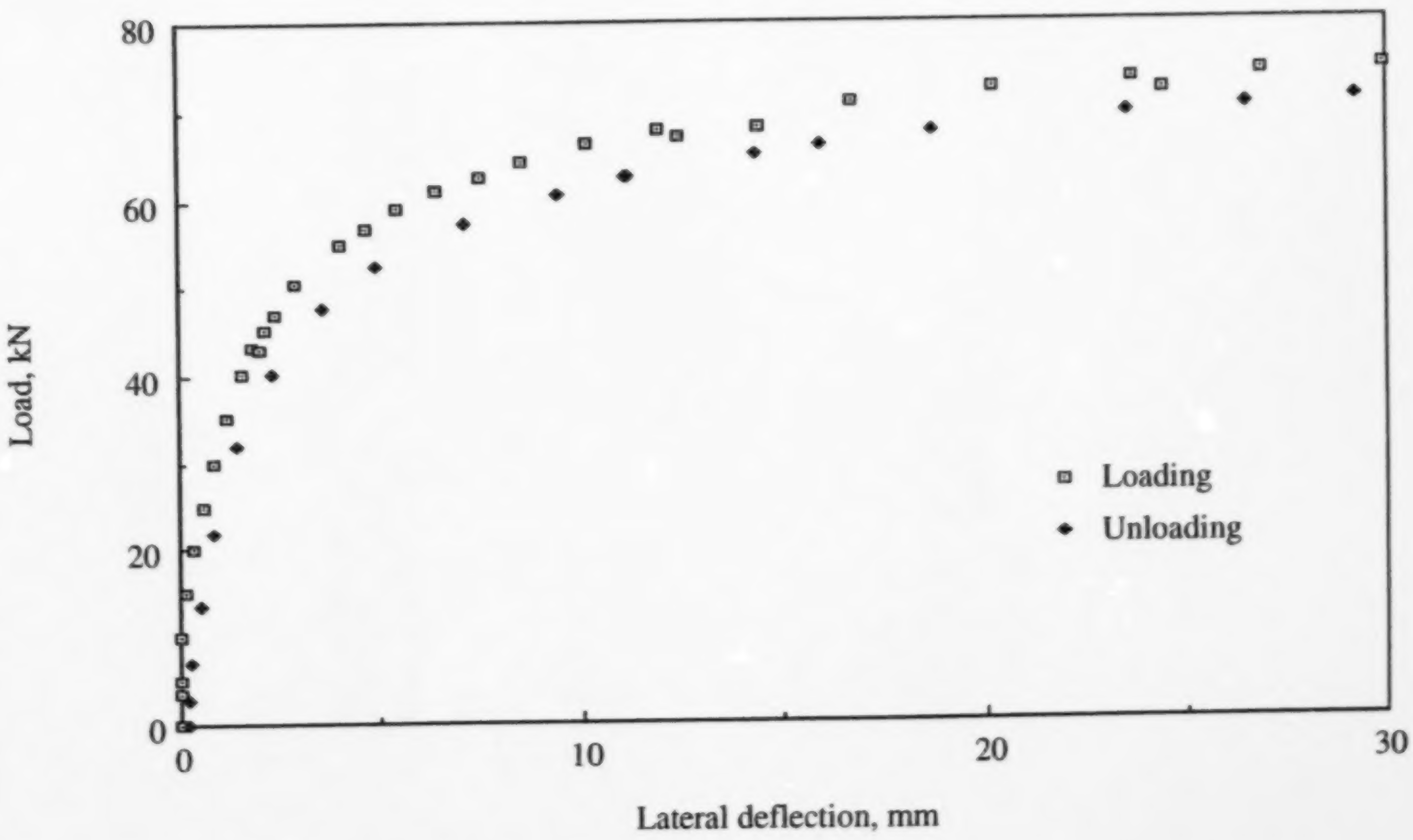

Fig. 5.29 Lateral deflection behaviour of bottom flange at one-third point of back span, test 17

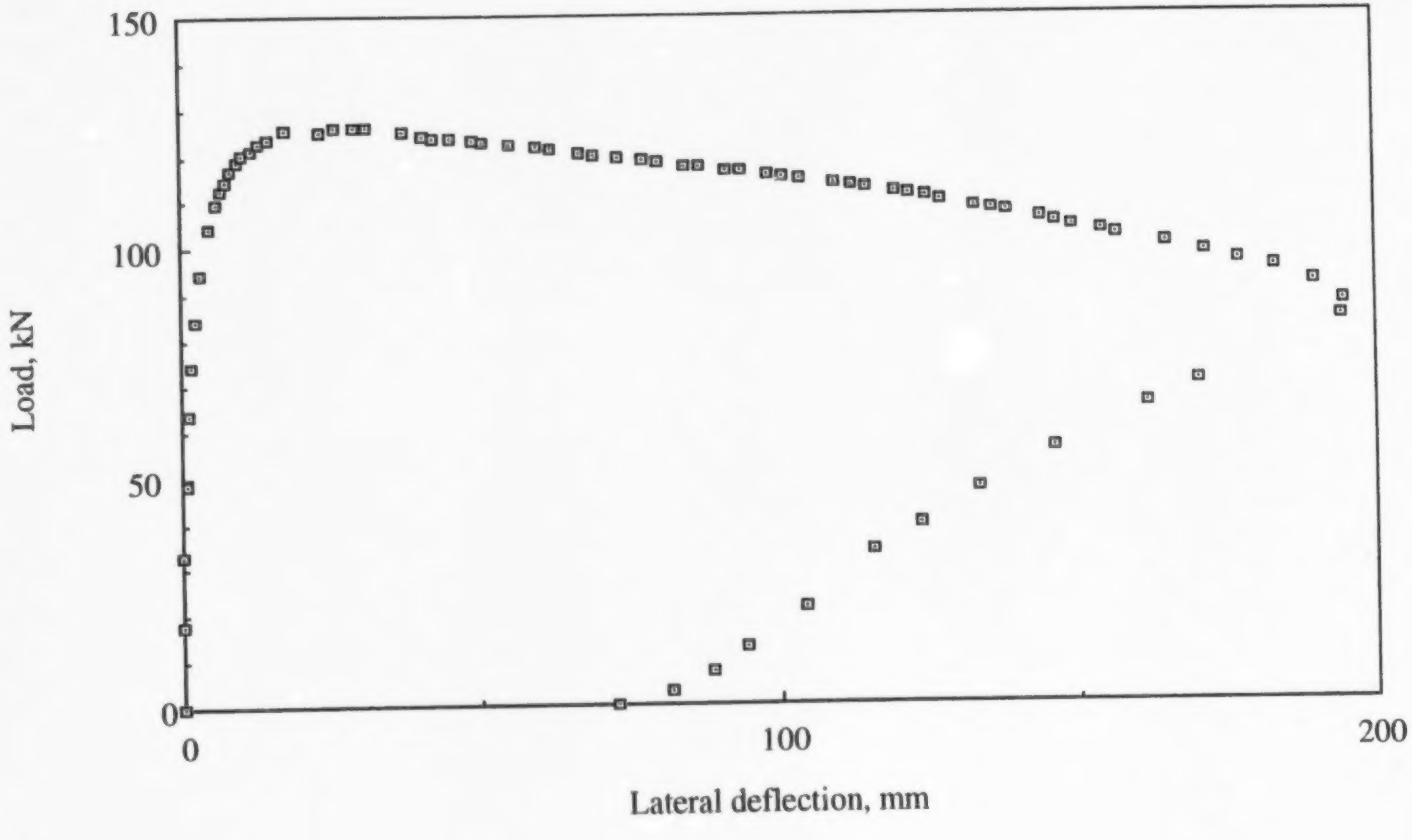

Fig. 5.30 Lateral deflection behaviour of bottom flange at one-third point of back span, test 5

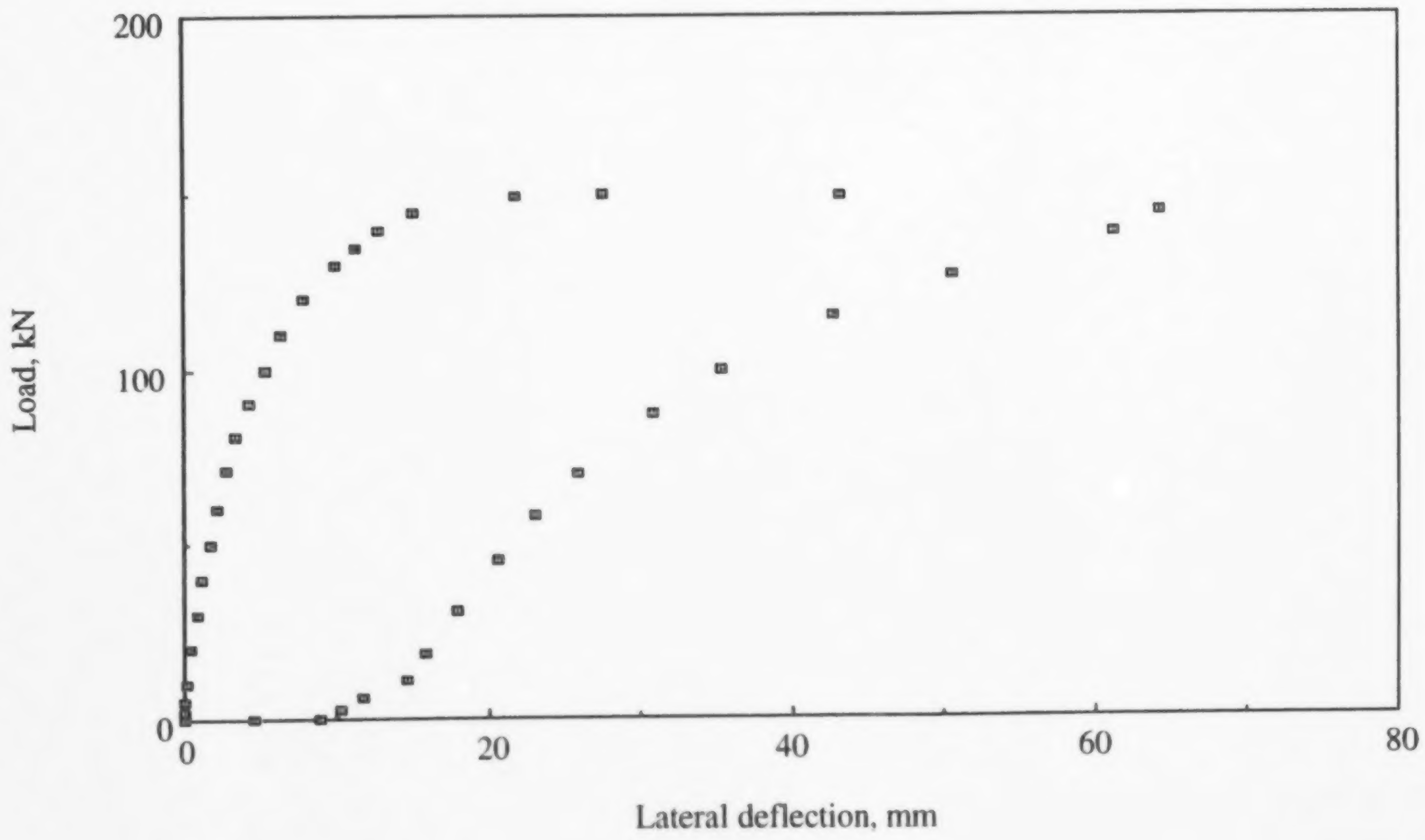

Fig. 5.31 Lateral deflection behaviour of bottom flange at one-third point of back span, test 19

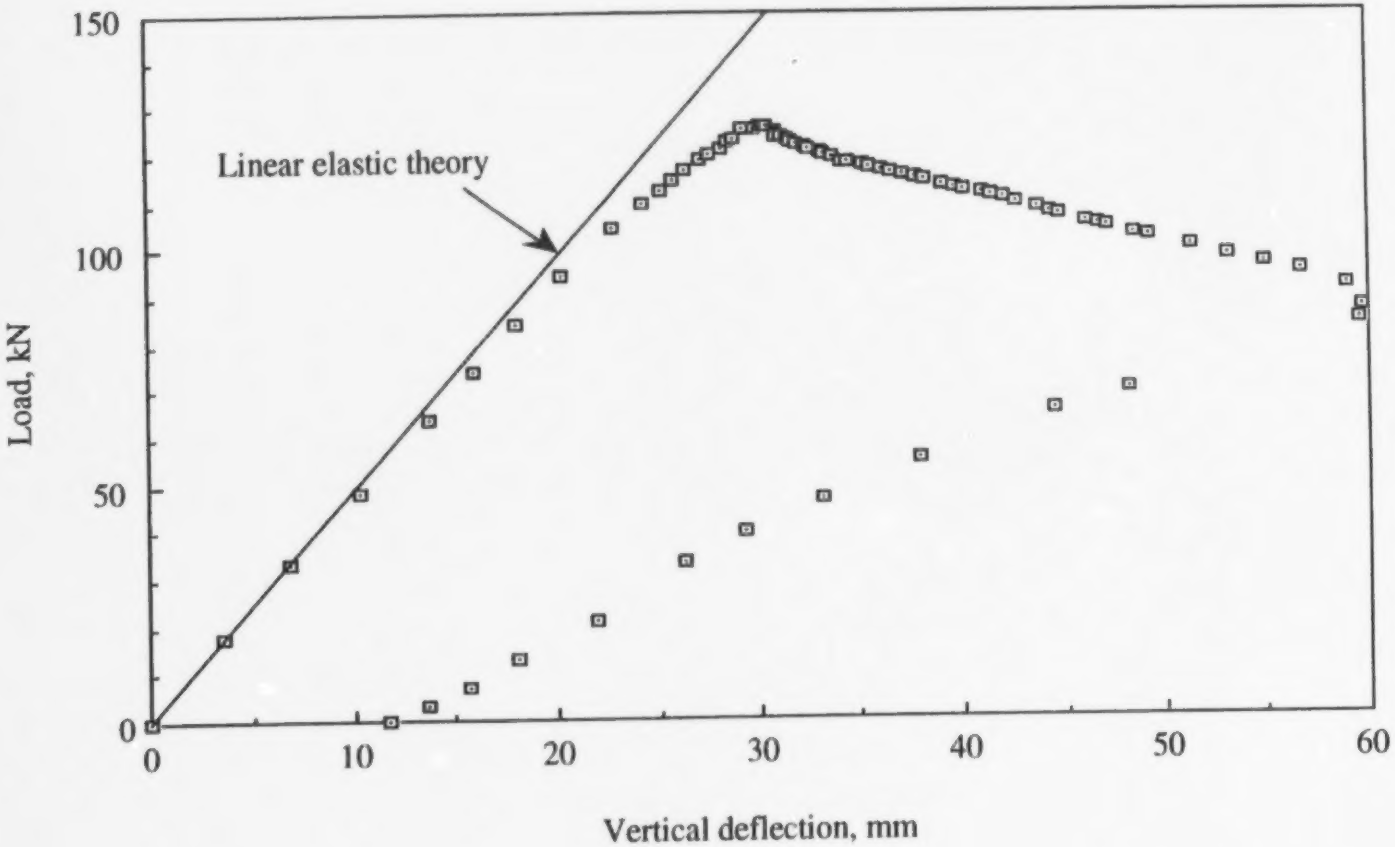

Fig. 5.32 Load-vertical deflection curve of the cantilever tip, test 5

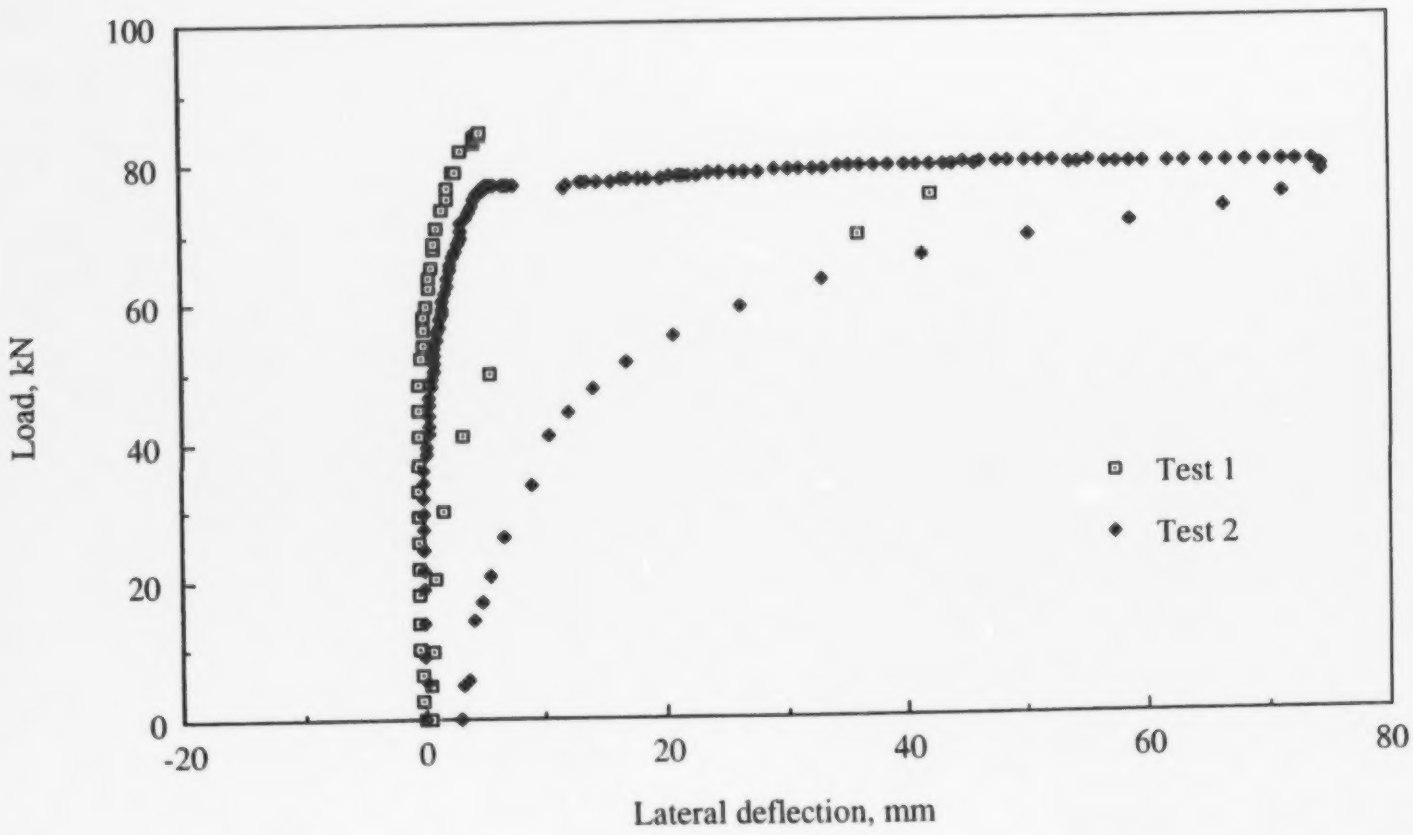

Fig. 5.33 Lateral deflection of bottom flange at cantilever tip, tests 1 and 2

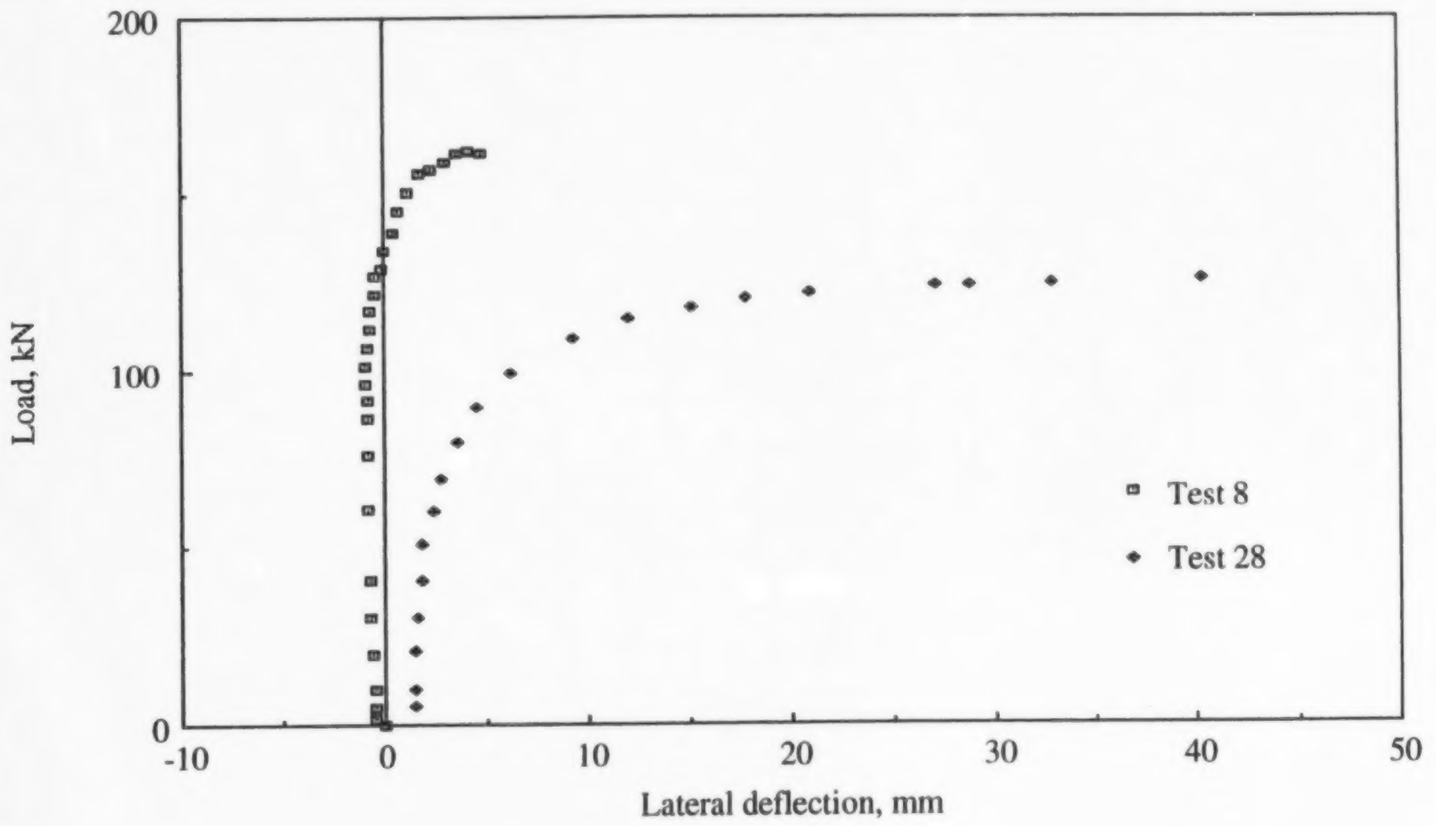

Fig. 5.34 Lateral deflection of bottom flange at cantilever tip, tests 8 and 28

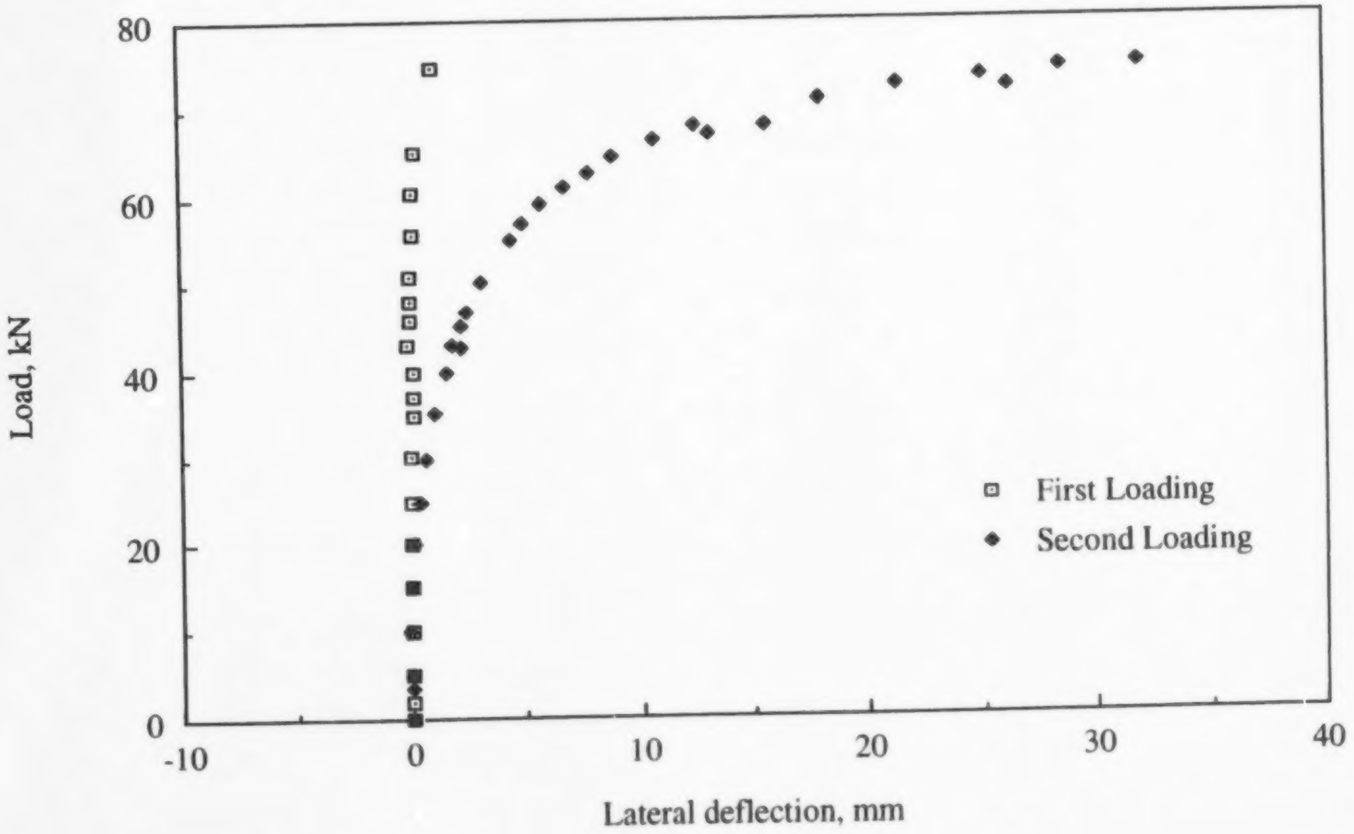

Fig. 5.35 Lateral deflection of bottom flange at cantilever tip, first and second loadings of test 17

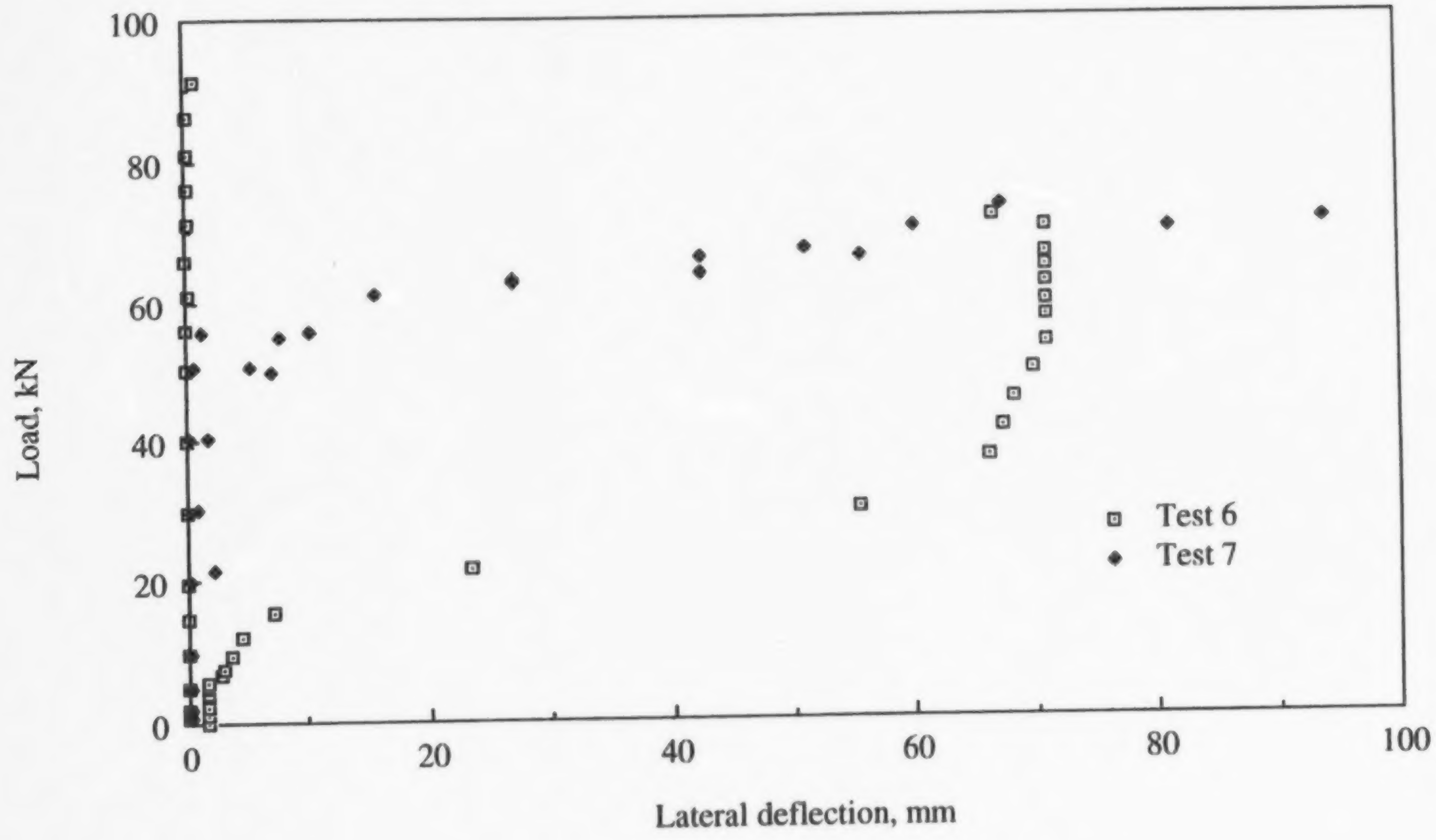

Fig. 5.36 Lateral deflection of top flange at one-third point of back span, tests 6 and 7

Chapter 6

FINITE ELEMENT ANALYSIS

6.1 General

A significant feature of lateral-torsional buckling of cantilever-suspended span beams is the possibility of cross-sectional distortion. Local and lateral buckles combine to produce coupled buckling modes in which there is simultaneous distortion and deflection of the cross section. Such instability is called distortional buckling. Johnson and Will (1974) have suggested the use of two dimensional plate elements to model both flange and web elements to reflect the cross-sectional distortion. However, because the flanges of wide flange beam sections are relatively thick and narrow as compared to the web, the distortion of the flanges is not as significant as that of the web, and the model of Johnson and Will may be unnecessarily complicated introducing more degrees of freedom than really required and requiring too much computer time.

The finite element model adopted here (Albert et al. 1992) uses 4-node plate elements for the web and 2-node line elements for the flanges, as shown in Fig. 6.1. All nodes are located at the intersection of the middle surfaces of the flanges and web plates. At each node, there are three degrees of freedom associated with out of plane displacements : the lateral displacement, w, along the z-axis; rotation, θ_x, about the x-axis; and rotation, θ_y, about the y-axis. The right-hand rule is used as a sign convention for all rotations. Under a practical loading condition, three types of in-plane stresses are induced in the web: σ_x, σ_y, and τ_{xy} as indicated in Fig. 6.1. This model has been implemented on a micro-computer to predict lateral-torsional buckling on the basis of bifurcation theory. It computes the tangent modulus buckling load based on the extent of yielding just prior to buckling (Galambos 1968).

The finite element approach presented herein differs from that adopted by Bradford (1986) in the following three ways:

(1) The solution technique used herein (inverse iteration with shift) converges faster than the determinant search method used by Bradford.

(2) Bradford used the consistent approach in which both the structural and geometric stiffnesses are based on the same displacement assumptions (cubic displacement shape functions for the flanges and the web). The present model uses cubic shape functions for deriving the structural stiffnesses and lower order polynomials (linear displacement shape functions for the flanges and bilinear displacement shape functions for the web) to derive the geometric stiffnesses. The later approach has been shown to yield sufficient accuracy (Clough and Felippa 1968) for plate buckling. Also, it requires less computational effort and simplifies the formulation.

(3) In order to account for the destabilizing effect of vertical loads, Bradford assumed that the slope of the line joining the shear centre and the point of load application is equal to the angle of twist of the

top flange. This underestimates the destabilizing effect. The procedure adopted by the present approach is given in section 6.5.2.

6.2 Basic assumptions

The present finite element approach uses the following assumptions

(1) The material model is elastic-perfectly plastic and strain hardening is neglected. Strain hardening only occurs where there is significant yielding in the cross section. In practice, the critical bending moment is high. Therefore, if there is a significant yielding at that location, strain hardening is confined to a short length of the beam and most of the beam remains elastic. The inclusion of strain hardening may be useful when the bending moment is nearly constant over a significant length. However, when the case of a nearly uniform bending moment is the critical loading condition, it is likely, for the practical range of beam geometries, that the buckling load will be elastic and therefore strain hardening is not an issue.

(2) The yield stress is assumed to be the same within the whole cross section and is taken as that of the flanges. Normally, the yield stress of the web is higher than that of the flanges. However, since the effect of web yielding on the loss of lateral stability (governed mostly by I_y) is small in most cases, it is adequate to adopt a uniform yield stress over the cross section.

(3) Because the contribution of the fillets to the lateral stability is small, it is reasonable to exclude the fillets from the geometry of the cross section.

(4) It is assumed that no distortion occurs in the flanges. This is justified because the flanges are relatively thick and, therefore, the distortion of the flanges is not as significant as that of the web. This assumption has been adopted by Bradford (1986), Bradford and Trahair (1981, 1982) and Akay et al. (1977). For this reason, local buckling cannot be predicted using the present model, and must be computed independently.

(5) The problem of lateral-torsional buckling is treated as a bifurcation problem, neglecting the effect of initial imperfections. As given by Galambos (1963), small initial imperfections do not affect the buckling strength.

(6) Shifting of the shear centre due to different yielding patterns of the top and bottom flanges is neglected. The significance of this assumption is related to the fact that the shear centre is the centre of rotation of the cross section. With a beneficial residual stress distribution, characterized by predominantly tensile stresses in the flanges, the tension flange yields before the compression flange. In positive sagging moment regions, the shear centre shifts upwards (i.e towards the compression flange), and tends to decrease the destabilizing effect of the loads applied above the shear centre. In cantilever-suspended span construction, yielding likely starts in the negative moment region of the beam above the column support. The

effect of shifting of the shear centre downward towards the reaction is again favourable, but becomes insignificant when cross-sectional twisting is prevented at that location.

6.3 Material properties

Because the finite element model deals with inelastic lateral-torsional buckling, in which the effects of both yielding and residual stresses are considered, material properties such as the stress-strain relationship and residual stress distribution, substantially affect the critical loads.

The elastic-perfectly plastic stress-strain relationship, given in Fig. 6.2, was used for the analysis. The effect of strain hardening was neglected as discussed previously.

The shear modulus, G, is assumed to be equal to the elastic shear modulus in both the elastic and inelastic ranges. As given by Horne and Ajmani (1973), the retention of an elastic value for G is justified by two considerations. First, the shear stress is usually small when inelastic action starts. Secondly, since the beam is torsionally flexible, large shear stresses cannot be induced in the practical range of deformations. The relationship between the shear modulus and the modulus of elasticity is given as

$$[6.1] \qquad G = \frac{E}{2(1+\nu)}$$

where ν is Poisson's ratio which is taken as 0.3 for steel.

The residual stress model must be flexible enough to enable the analytical model to represent any possible residual stress distribution which may be encountered in hot rolled steel cross sections. As indicated in Fig. 6.3, residual stresses are specified at discrete points spaced at b/8 and h'/8 where b is flange width and h' is the distance between the middle surfaces of the flanges. Because of cross-sectional symmetry, only ten values are specified. There are two requirements which must be satisfied by the residual stress distribution: at the web-flange junction, the tensile residual stresses in both the flange and web must be the same; and the residual stress distribution must be in equilibrium ($\Sigma\ \sigma_r\, dA = \Sigma\ \sigma_r\, ydA = \Sigma\ \sigma_r\, zdA = 0$).

6.4 Structural element stiffnesses

6.4.1 Flanges

Flanges are modelled by one dimensional line elements. Each element consists of two nodes and a total of six degrees of freedom. A cubic shape function is used, Akay et al. 1977, to express the lateral deflection of a flange element as follows

$$[6.2] \qquad w(\xi) = A_1\xi^3 + A_2\xi^2 + A_3\xi + A_4$$

in which $\xi = [2(x - x_i)/L_f] - 1$ (ranging from -1 to 1) and the coefficients A_1, A_2, A_3 and A_4 are determined in terms of the nodal displacements by applying the boundary conditions. The resulting expression for lateral displacement is given as

[6.3] $$w(\xi) = w_i\, f_1(\xi) + \theta_{yi}\, f_2(\xi) + w_j\, f_3(\xi) + \theta_{yj}\, f_4(\xi)$$

in which

[6.4] $$\begin{aligned} f_1(\xi) &= \xi^3/4 - 3\xi/4 + 1/2 \\ f_2(\xi) &= -L(\xi^3 - \xi^2 - \xi + 1)/8 \\ f_3(\xi) &= -\xi^3/4 + 3\xi/4 + 1/2 \\ f_4(\xi) &= -L(\xi^3 + \xi^2 - \xi - 1)/8 \end{aligned}$$

A linear shape function is assumed for the twisting displacement across the flange element. After applying the boundary conditions, the resulting expression is given as

[6.5] $$\theta_x(\xi) = \theta_{xi}(1 - \xi)/2 + \theta_{xj}(1 + \xi)/2$$

The strain energy of a flange element is given by

[6.6] $$U_f = \frac{1}{2}\int_{L_f} (E\, I_{yf}\, w''^2 + G\, J_f\, \theta_x'^2)\, dx$$

A linear variation of lateral bending rigidity, EI_{yf}, over the element length is assumed as follows

[6.7] $$EI_{yf}(\xi) = (EI_{yf})_i\, (1 - \xi)/2 + (EI_{yf})_j\, (1 + \xi)/2$$

where $(EI_{yf})_i$ and $(EI_{yf})_j$ are lateral bending rigidities of the flange section at nodes i and j, respectively, taking into account the extent of yielding. Under combined bending and residual stresses, yielding begins at the tips of a compression flange and in the middle of a tension flange. Numerical integration is used with nine integration points across the flange width and two integration points over the length of the element. Because the modulus of rigidity, G, is assumed to be the same in both the elastic and inelastic ranges, the torsional rigidity, GJ_f, at any flange cross section is not affected by yielding and given as

$$[6.8] \qquad GJ_f(\xi) = b\, t^3\, G/3$$

Where b is the flange width and t is the flange thickness. Using Castigliano's first theorem, the strain energy expression in [6.6] and numerical integration, the structural stiffness of a flange element is obtained as shown in Fig. 6.4.

6.4.2 Web

The web is modelled using nonconforming rectangular four node plate bending elements. Unlike the model adopted by Akay et al. (1977), the plate element used here has only one division over the depth of the web. With this modelling, the effect of two dimensional state of stress in the web is included and the vertical stresses, σ_y, which may give rise to local buckling of the web and contribute to the occurrence of lateral buckling are considered.

As shown in Fig. 6.5 there are twelve degrees of freedom per plate element. Thus the nodal displacement vector is defined as

$$[6.9] \qquad \{r\}^t = [\ [r_i]\quad [r_j]\quad [r_k]\quad [r_l]\ ]$$

in which $[r_i] = [\ w_i \ \ \theta_{xi} \ \ \theta_{yi}\ ]$ and $[r_j]$, $[r_k]$ and $[r_l]$ are defined similarly. However, from plate theory, Equation [6.9] can be rewritten as

[6.10] $$\{r\}^t = [\ [R_i] \ \ [R_j] \ \ [R_k] \ \ [R_l]\ ]$$

in which

[6.11] $$[R_i] = [\ w_i \ \ -\left(\frac{\partial w}{\partial y}\right)_i \ \ -\left(\frac{\partial w}{\partial x}\right)_i\ ]$$

and $[R_j]$, $[R_k]$ and $[R_l]$ are defined similarly.

The two dimensional cubic shape function for the lateral displacement, w, (Zienkiewicz 1977) can be written as

[6.12] $$[n] = [\ [n_i] \ \ [n_j] \ \ [n_k] \ \ [n_l]\ ]$$

in which

[6.13] $$[n_i] = [\ (\xi_o + 1)(\eta_o + 1)(2 + \xi_o + \eta_o - \xi^2 - \eta^2)/8$$

$$b\eta_i(\xi_o + 1)(\eta_o + 1)^2(\eta_o - 1)/8 \qquad - a\xi_i(\xi_o + 1)^2(\xi_o - 1)(\eta_o + 1)/8\ ]$$

where $\xi = (x - x_c)/a_1$, $\eta = (y - y_c)/b_1$, $\xi_o = \xi\,\xi_i$ and $\eta_o = \eta\,\eta_i$. The shape functions $[n_j]$, $[n_k]$ and $[n_l]$ are defined similarly. It is now possible to write the expression for the out of plane displacement, w, within the element as

[6.14] $$w(\xi, \eta) = [n]\ \{r\}$$

From elastic plate theory, applying equilibrium gives (Brown 1984)

[6.15] $$\begin{Bmatrix} M_x \\ M_y \\ M_{xy} \end{Bmatrix} = \frac{E\, t_w^3}{12(1-\nu^2)} \begin{bmatrix} 1 & \nu & 0 \\ \nu & 1 & 0 \\ 0 & 0 & (1-\nu)/2 \end{bmatrix} \begin{Bmatrix} -\dfrac{\partial^2 w}{\partial x^2} \\ -\dfrac{\partial^2 w}{\partial y^2} \\ 2\dfrac{\partial^2 w}{\partial x \partial y} \end{Bmatrix}$$

or {M} = [D] {C} where {C} is the curvature vector for element dxdy; M_x, M_y and M_{xy} are moments/unit length as shown in Fig. 6.6; t_w is the web thickness; and [D] is the elastic constitutive matrix. Within the inelastic range, the constitutive matrix becomes

[6.16] $$[D]_{in} = \begin{bmatrix} 0 & 0 & 0 \\ 0 & 0 & 0 \\ 0 & 0 & G t_w^3/12 \end{bmatrix}$$

The strain energy of an element dxdy can be expressed as

[6.17] $$U_p = \frac{1}{2}\{-M_x dy(\frac{\partial^2 w}{\partial x^2})dx - M_y dx(\frac{\partial^2 w}{\partial y^2})dy + 2M_{xy}(\frac{\partial^2 w}{\partial x \partial y})dxdy\}$$

Using [6.15], equation [6.17] can be rewritten as

[6.18] $$U_p = \{C\}^t \{M\}\, dxdy/2 = \{C\}^t [D] \{C\}\, dxdy/2$$

However from [6.14], the curvatures can be found such that

$$[6.19] \qquad \{C\} = \begin{Bmatrix} -\dfrac{\partial^2 w}{\partial x^2} \\ -\dfrac{\partial^2 w}{\partial y^2} \\ 2\dfrac{\partial^2 w}{\partial x \partial y} \end{Bmatrix} = [B]\,\{r\}$$

where [B] is given as

$$[6.20] \qquad [B] = \begin{bmatrix} -\dfrac{\partial^2 [n_i]}{\partial x^2} & -\dfrac{\partial^2 [n_j]}{\partial x^2} & -\dfrac{\partial^2 [n_k]}{\partial x^2} & -\dfrac{\partial^2 [n_l]}{\partial x^2} \\ -\dfrac{\partial^2 [n_i]}{\partial y^2} & -\dfrac{\partial^2 [n_j]}{\partial y^2} & -\dfrac{\partial^2 [n_k]}{\partial y^2} & -\dfrac{\partial^2 [n_l]}{\partial y^2} \\ 2\dfrac{\partial^2 [n_i]}{\partial x \partial y} & 2\dfrac{\partial^2 [n_j]}{\partial x \partial y} & 2\dfrac{\partial^2 [n_k]}{\partial x \partial y} & 2\dfrac{\partial^2 [n_l]}{\partial x \partial y} \end{bmatrix}$$

The structural stiffness matrix of the web element can be obtained using [6.18] and [6.19] in the form

$$[6.21] \qquad [k]_w = \int_{A_w} [B]^t\,[D]\,[B]\,d\,A_w$$

where A_w is the web area. Because the resulting form of integrand in [6.21] cannot be integrated in a closed form, recourse is made to numerical integration. For elastic solutions, a 3x3 pattern of Gaussian integration is used. Inelastic solutions use a refined pattern, featuring 3 points across the length and 9 points across the depth in order to represent the extent of yielding in the web. The Gaussian integration points used for inelastic solutions do not coincide with the points used in defining the residual stress distribution. In this model, residual stresses at Gaussian points are obtained by linear interpolation between the equally spaced points used to define the residual stress pattern. As expected, the resulting element stiffness matrix of the web involves all three degrees of freedom per node.

6.4.3 Stiffeners

Web stiffeners, if present, are modelled as line elements. Each element consists of two nodes with a total of six degrees of freedom. It is assumed that the stiffeners extend over the full depth of the web and are symmetrically arranged on both sides of the web. It is also assumed that stiffeners are not affected by yielding. The element stiffness matrix of stiffeners as obtained from Segerlind (1984) is given in Fig. 6.7.

6.5 Geometric element stiffnesses

6.5.1 Flanges

The geometric stiffness matrix is constructed by differentiating, with respect to nodal displacements, the work done by in-plane stresses as component plates shorten during buckling. For a flange element, the geometric stiffness involves only the longitudinal stresses σ_x . Integrating the work done by an elemental force $\sigma_x dA_f$ through a displacement dr, the work done by longitudinal stresses in a flange element is given by:

[6.22] $$W_f = \int_{L_f}\int_{A_f} \sigma_x dA_f dr$$

where L_f and A_f are the element length and cross-sectional area, respectively. The displacement dr can be obtained by expanding the arc length, ds, as follows (Galambos 1968):

[6.23] $$dr = ds - dx = \sqrt{1 + (v')^2 + (w')^2}\, dx - dx$$

$$\approx [1 + \frac{1}{2}(v')^2 + \frac{1}{2}(w')^2]\, dx - dx$$

$$\approx \frac{1}{2}\, [(v')^2 + (w')^2]\, dx$$

where v' and w' are derivatives with respect to x of the displacements along the y and z axes, respectively. Substituting the relationship $v=-\theta_x z$ into [6.23] and differentiating [6.22] with respect to nodal displacements, w and θ_x, we obtain:

[6.24] $$\left[k_g^w\right]_f = \int_V \{\psi\}_{,x}\, \sigma_x\, \{\psi\}_{,x}^t\, dV$$

[6.25] $$\left[k_g^{\theta_x}\right]_f = \int_V \{\psi\}_{,x}\, z^2 \sigma_x\, \{\psi\}_{,x}^t\, dV$$

where $dV = dA_f dx$, $\left[k_g^w\right]_f$ and $\left[k_g^{\theta_x}\right]_f$ are the geometric stiffness matrices of a flange element associated with lateral displacements and rotations about the longitudinal axis, respectively. Commas denote differentiation with respect to x. The expression $\{\psi\}$ is a vector of linear shape functions for interpolating the displacements, w or θ_x, between the two nodes of a flange element, which has the same form as the one used in [6.5]. In evaluating [6.24] and [6.25], it is assumed that the integral of the stress terms σ_x and $z^2\sigma_x$ over the cross-sectional area vary linearly over the length of a flange element.

Following the above procedure, the geometric stiffness matrix of a flange element is obtained as given in Fig. 6.8, in which:

[6.26] $\overline{N} = (N_i + N_j)/2 \ , \ \overline{\beta} = (\beta_i + \beta_j)/2$ where

[6.27] $$N = \int_b \sigma_x t \, dz \ , \quad \beta = \int_b z^2 \sigma_x t \, dz$$

where b is the flange width. The subscripts i and j given in [6.26] denote the end node of the element at which the indicated function (N or β) is evaluated. The integrals in [6.27] are computed numerically.

6.5.2 Web

The geometric stiffness of a web element due to longitudinal and shear stresses is given by Johnson and Will (1974) as:

[6.28] $$\left[k_g^1 \right]_w = \int_V \left[\{\phi\}_{,x} \quad \{\phi\}_{,y} \right] \begin{bmatrix} \sigma_x & \tau_{xy} \\ \tau_{xy} & 0 \end{bmatrix} \begin{bmatrix} \{\phi\}^t_{,x} \\ \{\phi\}^t_{,y} \end{bmatrix} dV$$

where $\{\Phi\}$ is a vector of bilinear shape functions for interpolating the lateral displacement w between the four nodes of a web element:

[6.29] $\{\Phi\}^t = [\Phi_i \quad \Phi_j \quad \Phi_k \quad \Phi_l]$ in which

[6.30] $\Phi_i = (\xi_o + 1)(\eta_o + 1)/4$

where $\xi_o = \xi\,\xi_i$ and $\eta_o = \eta\,\eta_i$. The values of Φ_j, Φ_k and Φ_l are defined similarly. The commas in [6.28] denote differentiation with respect to the indicated coordinate (x or y). Rotational displacements, θ_x and θ_y, are not included in the formulation. Taking advantage of a statically determinate beam system, the longitudinal and shear stresses can be determined easily from the bending moment and shear diagrams through ordinary theory of flexure. The distribution of shear stresses is assumed to be constant over the web depth. Once the stresses, σ_x and τ_{xy}, are thus obtained, they can be substituted in [6.28]. The same Gauss-Legendre numerical integration scheme used for obtaining the structural stiffness of web element is also used herein. To determine the longitudinal stress due to bending at a sampling point, a linear variation of the longitudinal stress is assumed over the length of a web element, while the shear stress is virtually the same at all sampling points since loads are applied at longitudinal points which form the right and left sides of a web element.

The geometric stiffness due to vertical stress, σ_y, which results from vertical loads and reactions, follows from the work done by vertical forces applied above or below the shear centre as the point of application of the forces moves vertically during lateral-torsional buckling. A simple expression for this work is given by:

$$[6.31] \qquad W_p = P\,\Delta$$

where Δ is the vertical displacement of the load point during twisting of the cross section due to buckling, as shown in Fig. 6.9.a. For loads applied above the shear centre but between the flanges, the angle of twisting rotation, θ_x, is expressed in terms of the nodal lateral displacements, w_t and w_b, of the top and bottom flanges respectively and the vertical displacement, Δ, is approximated by the first term of its polynomial expansion:

$$[6.32] \qquad \Delta = a\,(1 - \cos\theta_x) = a\,\frac{\theta_x^2}{2} = \frac{a}{2}\left(\frac{w_t - w_b}{h'}\right)^2$$

where h' is the distance between the middle surfaces of the flanges and a is the height of load application with respect to the shear centre. Using the principle of minimum potential energy, the geometric stiffness matrix, $[k_g^2]_w$, due to σ_y for this case is obtained as given in Fig. 6.10. Web distortion is ignored in [6.32] since its effect is less significant for loads applied between the flanges.

For loads applied at distance a_2 above the top flange, as shown in Fig. 6.9.b, an additional vertical displacement occurs due to the effect of web distortion and can be expressed in terms of the nodal rotation of the top flange about the longitudinal axis, θ_{xt}. The resulting expression for the vertical displacement is given as:

[6.33] $$\Delta \approx \frac{1}{2}\frac{h'}{2}\left(\frac{w_t - w_b}{h'}\right)^2 + \frac{1}{2} a_2 \theta_{x\,t}^{\;2}$$

For this case, the geometric stiffness, $[k_g^3]_w$, due to vertical stresses, σ_y, is given in Fig. 6.11.

When loads or reactions are applied at a distance a below the shear centre but above the bottom flange, as shown in Fig. 6.9.c, the vertical displacement, Δ, is approximated as follows (neglecting web distortion):

[6.34] $$\Delta \approx -\frac{a}{2}\left(\frac{w_t - w_b}{h'}\right)^2$$

Fig. 6.12 gives the geometric stiffness, $[k_g^4]_w$, due to vertical stresses for this case.

For loads applied at a distance a_2 below the bottom flange, as shown in Fig. 6.9.d, the effect of web distortion is significant and must be taken into account. The expression for total vertical displacement of the load point is given as:

[6.35] $$\Delta \approx -\frac{1}{2}\frac{h'}{2}\left(\frac{w_t - w_b}{h'}\right)^2 - \frac{1}{2} a_2 \theta_{x\,b}^{\;2}$$

where $\theta_{x\,b}$ is the nodal rotation of the bottom flange about longitudinal axis. The geometric stiffness, $[k_g^5]_w$, due to vertical stresses for this case is given in Fig. 6.13.

In obtaining the geometric stiffnesses of a web element due to vertical stresses for all the above four cases, it is assumed that the shear centre is not displaced due to inelastic behaviour. When the buckling load falls between the yield and plastic capacities of the beam, the location of shear centre can vary drastically. Shifting of shear centre is not considered because it leads to instability in the numerical solution of inelastic beams. The shear centre is therefore assumed to be located at mid-depth of the doubly symmetric cross section up to the theoretical plastic moment, if could be reached.

6.6 Restraints

Because the finite element model is designed to simulate the boundary conditions of beams in cantilever-suspended span construction, restraints provided either by the columns to the bottom flange of the beam through a rigid moment connection or by properly welded open-web steel joists to the top flange of the beam, must be considered. Generally, a displacement corresponding to a degree of freedom, r_i, is prevented by adding an arbitrarily large number on the main diagonal of the global structural stiffness matrix at the address corresponding to r_i. A value of 10^{15} is used to avoid overflow errors. An elastic restraint of a given stiffness can be specified by adding the stiffness directly to the global structural stiffness matrix. This procedure is followed when the restraint is applied directly to either the top or bottom flange (nodal points).

When lateral restraint is applied at a point other than the top or bottom flange, as shown in Fig. 6.14, a fictitious 2-node element i-j is used with a bending stiffness EI. In order to avoid ill-conditioning problems due to the use of a too large value of I, it has been found that a value as large as the weak axis moment of inertia of the flange is appropriate. The force-displacement relationship for this element involving forces and displacements at node j is given as

$$[6.36] \qquad \begin{Bmatrix} F_j \\ M_j \end{Bmatrix} = \frac{3EI}{a_3^3} \begin{bmatrix} 1 & a_3 \\ a_3 & a_3^2 \end{bmatrix} \begin{Bmatrix} w_j \\ \theta_{xj} \end{Bmatrix}$$

where w_j is the displacement of node j in the Z direction, θ_{xj} is the rotation of the node j about the longitudinal axis of the beam, a_3 is the distance between the middle surface of top flange and the enforced axis of twist while F_j and M_j are nodal forces as indicated in Fig. 6.12. The coefficients given in [6.36] are added to the global structural stiffness matrix as shown in Fig. 6.15. A similar procedure can be used to simulate the restraint provided by the column to the bottom flange of the beam.

6.7 Solution technique

The finite element inelastic distortional buckling analysis of a complete beam can be represented in matrix form by:

$$[6.37] \qquad ([K] + [K_g])\{r\} = \{R\} = \{0\}$$

where [K] and $[K_g]$ are the global structural and geometric stiffness matrices, respectively, which are functions of the load factor λ; {r} is the vector of out of plane nodal displacements; and {R} is the vector of (zero) global out of plane forces.

When the effects of yielding and residual stresses are not considered (elastic analysis), the geometric stiffness, $[K_g]$ is a linear function of the loading intensity and [6.37] reduces to

[6.38] $$([K] + \lambda [K_g]_p)\{r\} = \{0\}$$

where λ is a load factor and $[K_g]_p$ is the global geometric stiffness matrix computed at a loading intensity corresponding to a maximum in-plane bending moment along the beam equals to the plastic moment.

The global matrices, $[K]$ and $[K_g]$, can be assembled from the individual element structural and geometric stiffness matrices, respectively. The values of λ which yield a nontrivial solution for $\{r\}$ in [6.37] are the eigenvalues, while the corresponding values of $\{r\}$ are the eigenvectors. In general, [6.37] is only solved for the smallest λ since it corresponds to the smallest buckling load. Buckling is assumed to take place from the initial geometry. Both $[K]$ and $[K_g]$ are referenced from the initial geometry as well as the stresses that are used to form $[K_g]$. Since [6.37] is homogeneous, the buckled mode shape may be determined while the actual magnitude of displacements remains undefined.

The eigenvalue problem is solved using a routine for inverse iteration with shifts (Bathe 1982 and Humar 1990), in which a loading intensity is assumed and iterations are performed until the computed intensity agrees with the assumed value. By choosing a shift point close to the anticipated eigenvalue, a more accurate estimate of such eigenvalue as well as of the corresponding eigenvector can be obtained after a relatively small number of iterations. As indicated in Fig. 6.16, if the shift point is located between the eigenvalues λ_n and λ_{n+1}, and $\mu - \lambda_n$ is smaller than $\lambda_{n+1} - \mu$, iteration will converge to λ_n and the rate of convergence will depend on $(\mu - \lambda_n)/(\lambda_{n+1} - \mu)$; the smaller this ratio, the faster the convergence. On the other hand, if $\lambda_{n+1} - \mu$ is smaller than $\mu - \lambda_n$, iteration will converge to λ_{n+1} and the rate of convergence will depend on the ratio $(\lambda_{n+1} - \mu)/(\mu - \lambda_n)$. Obviously, rapid convergence can be achieved if the shift, μ, is located close to the desired eigenvalue.

In the case where an approximate value for the desired eigenvalue is not known, it is recommended to use the following scheme:

1. Select a relatively small positive value for the shift, μ, as indicated in Fig. 6.17.

2. If the solution converges to the negative eigenvalue, λ_{-1}, try again with a shift slightly more than $2\mu - \lambda_{-1}$. A positive eigenvalue is anticipated, which would be the right solution.

3. If the solution converges to a positive eigenvalue, try again with a slightly reduced shift. A negative eigenvalue is anticipated to confirm that the obtained positive eigenvalue is the right solution.

6.8 Computer program

6.8.1 Introduction

A complete list for the distortional buckling finite element program (FEM) is given in Appendix A. The computer program is written in BASIC and designed to be implemented on a micro-computer. The major operations for the main program are given in Fig. 6.18, which frequently uses the main routine shown in Fig. 6.19. As indicated in Fig. 6.18, the program allows the user to select an elastic or an inelastic solution. The elastic solution, which is much faster, neglects the effects of residual stresses and yielding. In an inelastic solution, the extent of yielding in the beam is determined at each cross section iterating on the curvature and neutral axis with the bisection method. The global structural and geometric stiffness matrices in an inelastic solution are non-linear functions of the loading intensity due to the presence of residual stresses and partial yielding, which are not linearly proportional to the loading intensity. This renders the problem highly non-linear. The solution is obtained using the bisection method by specifying an upper and lower limits for the loading intensity, between which the solution is anticipated, in the input data. For convenience, all the units used throughout the program are expressed in terms of Newtons and millimetres.

6.8.2 Mesh characteristics

The first step in solving a specific problem, using the FEM program, is to select the mesh characteristics. In order to enable the finite element model to accurately simulate a beam with two overhangs which is used typically in cantilever-suspended span construction, the finite element mesh must be refined in the vicinity of column supports where the bending moment is a maximum and yielding is more likely to occur. A mesh refinement is also necessary at the cantilever tips to model web distortion in the case when torsional restraint is provided for only the top flange at this location. Points where loads, reactions, restraints and stiffeners act must be included in the longitudinal points.

As indicated in Fig. 6.20, the beam is divided into a number of main divisions. Each main division contains a group of equally spaced subdivisions. Each longitudinal point should be numbered in a left-right order. There are two nodes at each longitudinal point located at mid-surfaces of top and bottom flanges. The nodes should be numbered in a left-right and bottom-top order.

6.8.3 Input data

The FEM program first reads all the user input data, which are listed immediately after the main program. All the units are in Newtons and millimetres. The necessary input data required for the program are as follows:

1. Select the type of solution: 0 for elastic and 1 for inelastic.

2. Cross-sectional dimensions:

    1. Depth, breadth, flange thickness and web thickness.

3. Mesh characteristics:

1. Number of main divisions.

2. For each subdivision, with a left-right order along the beam, write the number of subdivisions and their regular spacing.

4. Material properties:

1. Elastic modulus, yield stress and Poisson's ratio.

5. Residual stresses. Positive for tension and negative for compression (refer to Fig. 6.3). Required only for inelastic solution, otherwise the zero values should be used to keep the order of data:

1. Flanges: $(\sigma_{rf})_1$, $(\sigma_{rf})_2$, $(\sigma_{rf})_3$, $(\sigma_{rf})_4$ and $(\sigma_{rf})_5$.

2. Web: $(\sigma_{rw})_1$, $(\sigma_{rw})_2$, $(\sigma_{rw})_3$, $(\sigma_{rw})_4$ and $(\sigma_{rw})_5$.

6. Loads and reactions:

1. Number of loads and reactions.

2. For each load and reaction, write the longitudinal point number at which it acts, its magnitude (positive if acts upwards and vice versa) and height of application (measured upwards from the shear centre).

7. Bending moment at a selected longitudinal point:

1. Selected longitudinal point number and magnitude of bending moment at that point (positive if causing tension at the bottom surface of the beam and vice versa).

8. Shift, lower bound and upper bound, for the ratios of anticipated maximum (critical) moment to the plastic moment of the cross section (lower and upper bounds are used only for inelastic solution, otherwise they may be taken as zeroes to keep the order of the data).

9. Nodal restraints (where the restraints are applied directly to the nodal points):

1. Number of restrained nodes.

2. For each restrained node, enter the node number, stiffness in N/mm for lateral restraint, stiffness in Nmm/rad for rotational restraint against twisting about the longitudinal axis and stiffness in Nmm/rad for restraint against rotation about the vertical axis. For infinite values of stiffnesses, use -1.

10. General restraints (where the restraint is applied at a distance above the top flange).

In this case, any torsional restraint acting above the top flange can be assumed to be applied directly to the top flange and, therefore, can be considered in the last data section. Only lateral restraints above the top flange are taken into account at this stage.

1. Number of points which are laterally restrained above the top flange.

2. For each point, enter the node number nearest to the point and the height of lateral restraint above the middle surface of top flange.

11. Initial displacement vector

Inverse iteration solution requires a non-zero initial vector to start vector iteration. The ideal initial vector will closely resemble the displacements of the expected buckled shape, ensuring shift convergence. However, very simple displacement vectors including the normalized value (usually taken equal to 1) of a single displacement or rotation at a selected node will also work. It is important to realize that this initial vector does not represent initial imperfections.

1. Number of nodes at which displacements are specified.

2. For each node, enter the node number, the specified values for lateral displacement, rotation about the longitudinal axis, and rotation about the weak axis.

12. Stiffeners

1. Number of stiffeners.

2. For each stiffener, enter the longitudinal point number at which the stiffener is located, its width, and its thickness.

6.8.4 Solution methodology

In any practical problem, an approximate value for buckling load is difficult to estimate because many variables are involved such as the geometrical properties of the cross section, the material properties including residual stresses, loading and restraint conditions. Since an inelastic solution takes a considerable amount of computer time unless the values of shift, upper and lower bounds are sufficiently close to the expected buckling load, it is instructive to start with a quick elastic computer run with relatively small shift (usually takes about one minute on a 486 personal computer) to get a rough estimate for that load. Then, an inelastic run is performed using that estimate. A worked example is given in Appendix B.

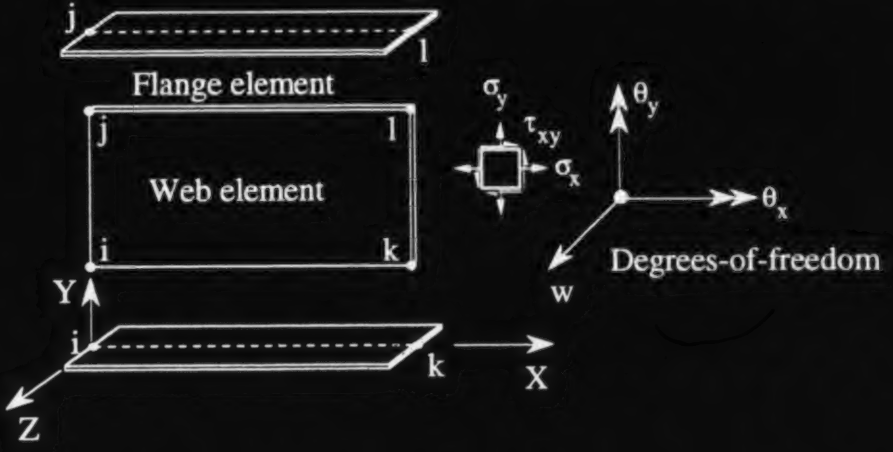
j
l
Flange element
j
l
Web element
i
k
Y
i
k
X
Z
σ_y
τ_{xy}
σ_x
θ_y
θ_x
w
Degrees-of-freedom

Fig. 6.1 Coordinate system and finite element model

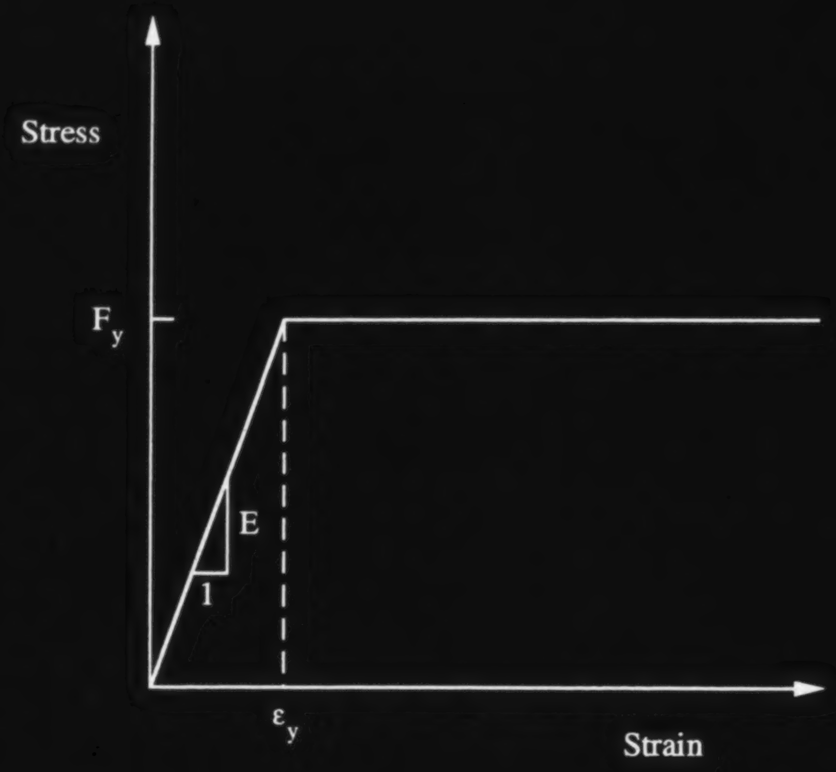
Stress
F_y
E
1
ε_y
Strain

Fig. 6.2 Idealised stress-strain relationship

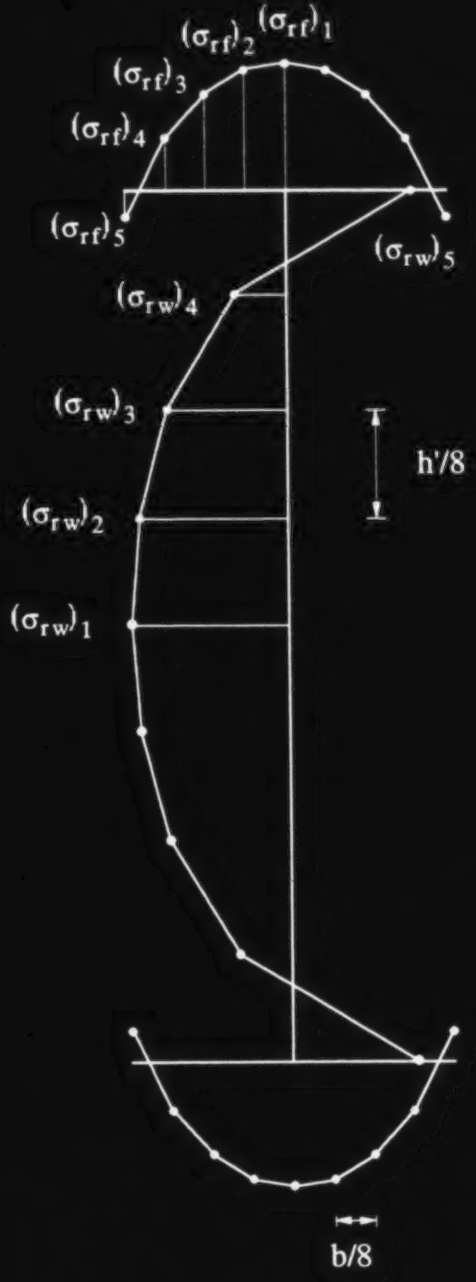
$(\sigma_{rf})_1$
$(\sigma_{rf})_2$
$(\sigma_{rf})_3$
$(\sigma_{rf})_4$
$(\sigma_{rf})_5$
$(\sigma_{rw})_5$
$(\sigma_{rw})_4$
$(\sigma_{rw})_3$
h'/8
$(\sigma_{rw})_2$
$(\sigma_{rw})_1$
b/8

Fig. 6.3 Residual Stress model

$$
\left[k \right]_f = \begin{array}{cccccc|c}
w_i & \theta_{x_i} & \theta_{y_i} & w_j & \theta_{x_j} & \theta_{y_j} & \\
\hline
\frac{1}{L_f^3}(6\bar{I}_i + 6\bar{I}_j) & 0 & \frac{1}{L_f^2}(-4\bar{I}_i - 2\bar{I}_j) & \frac{1}{L_f^3}(-6\bar{I}_i - 6\bar{I}_j) & 0 & \frac{1}{L_f^2}(-2\bar{I}_i - 4\bar{I}_j) & w_i \\
 & \frac{\bar{J}}{L_f} & 0 & 0 & -\frac{\bar{J}}{L_f} & 0 & \theta_{x_i} \\
 & & \frac{1}{L_f}(3\bar{I}_i + \bar{I}_j) & \frac{1}{L_f^2}(4\bar{I}_i + 2\bar{I}_j) & 0 & \frac{1}{L_f}(\bar{I}_i + \bar{I}_j) & \theta_{y_i} \\
 & & & \frac{1}{L_f^3}(6\bar{I}_i + 6\bar{I}_j) & 0 & \frac{1}{L_f^2}(2\bar{I}_i + 4\bar{I}_j) & w_j \\
 & \text{Symmetric} & & & \frac{\bar{J}}{L_f} & 0 & \theta_{x_j} \\
 & & & & & \frac{1}{L_f}(\bar{I}_i + 3\bar{I}_j) & \theta_{y_j}
\end{array}
$$

$\bar{I}_i = (E\,I_{yf})_i$, $\bar{I}_j = (E\,I_{yf})_j$ and $\bar{J} = G\,J_f$

Fig. 6.4 Structural stiffness matrix of flange element

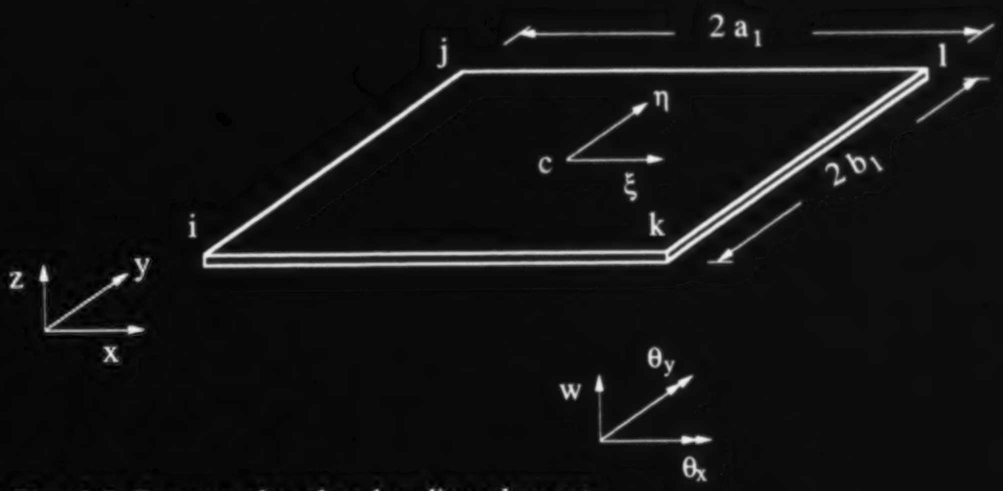
2 a1
j
l
η
c
ξ
2 b1
i
k
z
y
x
w
θy
θx

Fig. 6.5 Rectangular plate bending element

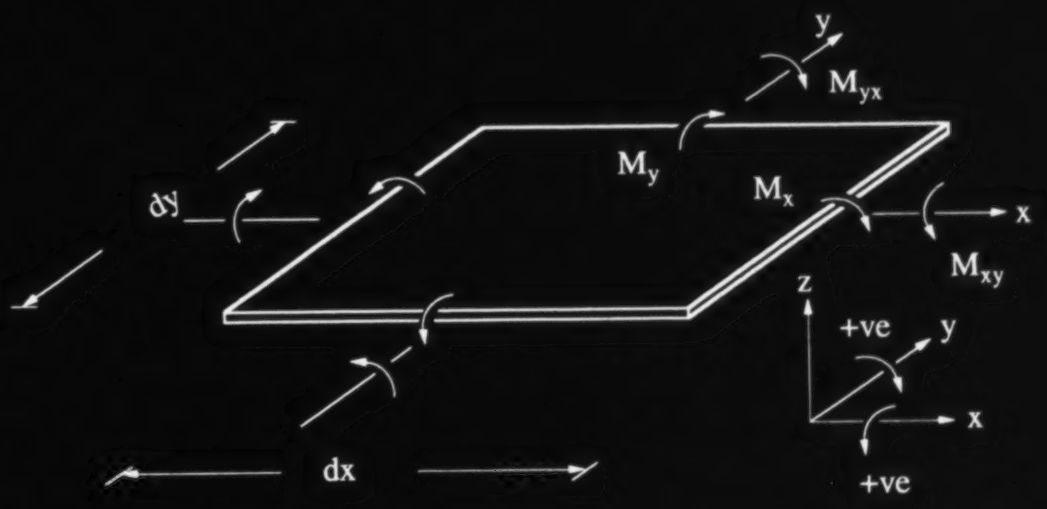
y
Myx
My
Mx
x
Mxy
dy
z
+ve
y
x
+ve
dx

Fig. 6.6 Stress resultants in a sub-element of plate bending

$$
\left[k \right]_s =
\begin{array}{cccccc|c}
w_i & \theta_{x_i} & \theta_{y_i} & w_j & \theta_{x_j} & \theta_{y_j} & \\
\hline
\frac{12EI_s}{h^{'3}} & \frac{6\,EI_s}{h^{'2}} & 0 & \frac{-12EI_s}{h^{'3}} & \frac{6\,EI_s}{h^{'2}} & 0 & w_i \\
 & \frac{4\,EI_s}{h^{'}} & 0 & \frac{-6\,EI_s}{h^{'2}} & \frac{2\,EI_s}{h^{'}} & 0 & \theta_{x_i} \\
 & & \frac{GJ_s}{h^{'}} & 0 & 0 & \frac{-\,GJ_s}{h^{'}} & \theta_{y_i} \\
 & & & \frac{12EI_s}{h^{'3}} & \frac{-6\,EI_s}{h^{'2}} & 0 & w_j \\
 & \text{Symmetric} & & & \frac{4\,EI_s}{h^{'}} & 0 & \theta_{x_j} \\
 & & & & & \frac{GJ_s}{h^{'}} & \theta_{y_j}
\end{array}
$$

Fig. 6.7 Structural stiffness matrix of stiffener element

$$\left[k_g\right]_f = \begin{array}{cccccc|c} w_i & \theta_{x_i} & \theta_{y_i} & w_j & \theta_{x_j} & \theta_{y_j} & \\ \hline \frac{\bar{N}}{L_f} & 0 & 0 & \frac{-\bar{N}}{L_f} & 0 & 0 & w_i \\ & \frac{\bar{\beta}}{L_f} & 0 & 0 & \frac{-\bar{\beta}}{L_f} & 0 & \theta_{x_i} \\ & & 0 & 0 & 0 & 0 & \theta_{y_i} \\ & & & \frac{\bar{N}}{L_f} & 0 & 0 & w_j \\ & \text{Symmetric} & & & \frac{\bar{\beta}}{L_f} & 0 & \theta_{x_j} \\ & & & & & 0 & \theta_{y_j} \end{array}$$

Fig. 6.8 Geometric stiffness matrix of flange element

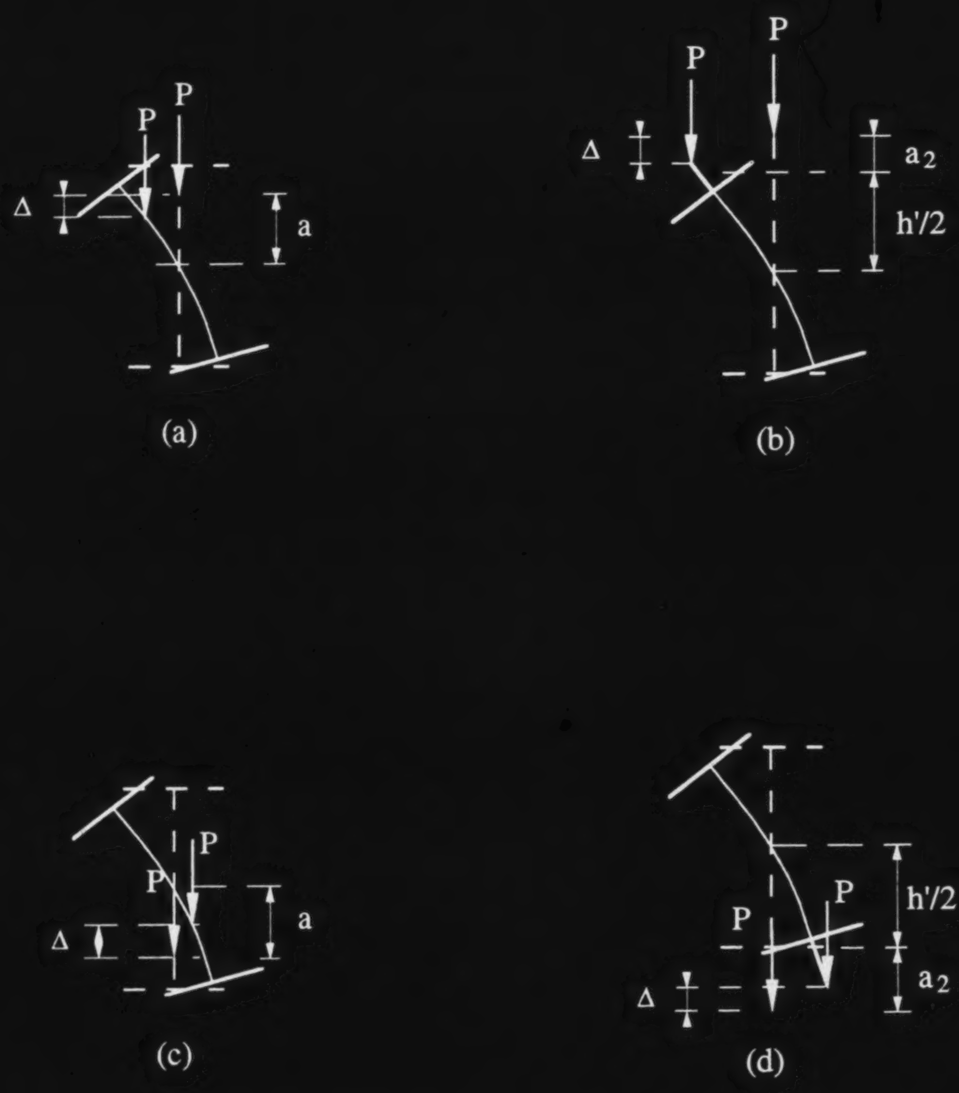
P
P
Δ
a
(a)
P
P
Δ
a2
h'/2
(b)
P
P
Δ
a
(c)
h'/2
P
P
Δ
a2
(d)

Fig. 6.9 Vertical displacements used to obtain the work done by verical loads, applied at different positions

$$\left[k_g^2\right]_w = \frac{P}{(h')^2} \begin{array}{c} \\ \\ \end{array} \begin{array}{cccccc|c} w_b & \theta_{x_b} & \theta_{y_b} & w_t & \theta_{x_t} & \theta_{y_t} & \\ \hline a & 0 & 0 & -a & 0 & 0 & w_b \\ & 0 & 0 & 0 & 0 & 0 & \theta_{x_b} \\ & & 0 & 0 & 0 & 0 & \theta_{y_b} \\ & & & a & 0 & 0 & w_t \\ & \text{Symmetric} & & & 0 & 0 & \theta_{x_t} \\ & & & & & 0 & \theta_{y_t} \end{array}$$

Fig. 6.10 Geometric stiffness matrix of web element due to vertical stresses caused by a load P applied at a distance a above the shear centre but between flanges

$$\left[k_g^3\right]_w = \frac{P}{(h')^2} \begin{array}{cccccc|c} w_b & \theta_{x_b} & \theta_{y_b} & w_t & \theta_{x_t} & \theta_{y_t} & \\ \hline \frac{h'}{2} & 0 & 0 & -\frac{h'}{2} & 0 & 0 & w_b \\ & h'^2 a_2 & 0 & 0 & 0 & 0 & \theta_{x_b} \\ & & 0 & 0 & 0 & 0 & \theta_{y_b} \\ & & & \frac{h'}{2} & 0 & 0 & w_t \\ & \text{Symmetric} & & & 0 & 0 & \theta_{x_t} \\ & & & & & 0 & \theta_{y_t} \end{array}$$

Fig. 6.11 Geometric stiffness matrix of web element due to vertical stresses caused by a load P applied at a distance a_2 above the top flange

$$\left[k_g^4\right]_w = \frac{P}{(h')^2}\begin{array}{c|cccccc|c} & w_b & \theta_{x_b} & \theta_{y_b} & w_t & \theta_{x_t} & \theta_{y_t} & \\ \hline & -a & 0 & 0 & a & 0 & 0 & w_b \\ & & 0 & 0 & 0 & 0 & 0 & \theta_{x_b} \\ & & & 0 & 0 & 0 & 0 & \theta_{y_b} \\ & & & & -a & 0 & 0 & w_t \\ & \text{Symmetric} & & & & 0 & 0 & \theta_{x_t} \\ & & & & & & 0 & \theta_{y_t} \end{array}$$

Fig. 6.12 Geometric stiffness matrix of web element due to vertical stresses caused by a load P applied at a distance a below the shear centre but between flanges

$$\left[k_g^5\right]_w = \frac{P}{(h')^2}\begin{array}{c|c} \begin{array}{cccccc} w_b & \theta_{x_b} & \theta_{y_b} & w_t & \theta_{x_t} & \theta_{y_t} \end{array} & \\ \begin{bmatrix} -\frac{h'}{2} & 0 & 0 & \frac{h'}{2} & 0 & 0 \\ & 0 & 0 & 0 & 0 & 0 \\ & & 0 & 0 & 0 & 0 \\ & & & -\frac{h'}{2} & 0 & 0 \\ & \text{Symmetric} & & & -h'^2 a_2 & 0 \\ & & & & & 0 \end{bmatrix} & \begin{array}{c} w_b \\ \theta_{x_b} \\ \theta_{y_b} \\ w_t \\ \theta_{x_t} \\ \theta_{y_t} \end{array} \end{array}$$

Fig. 6.13 Geometric stiffness matrix of web element due to vertical stresses caused by a load P applied at a distance a_2 below the bottom flange

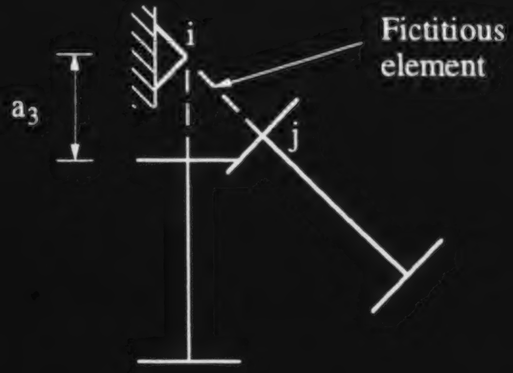
i
Fictitious element
a_3
j

Fig. 6.14 Simulation of lateral restraint applied at a point other than nodal points

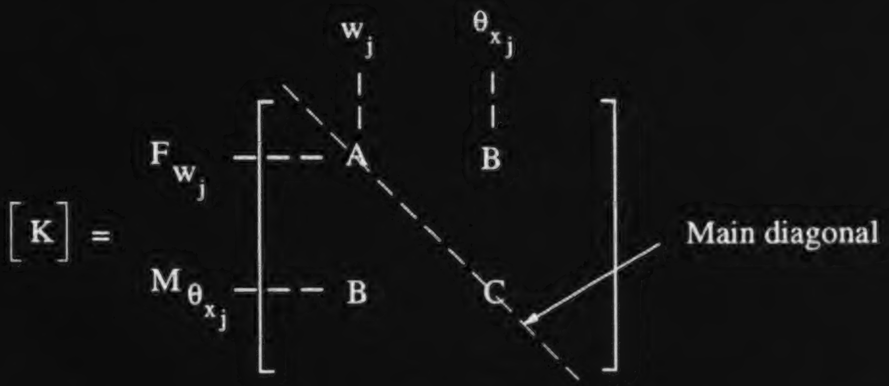
$[K] =$
w_j
θ_{x_j}
F_{w_j}
$M_{\theta_{x_j}}$
A
B
B
C
Main diagonal

where $A = \dfrac{3EI}{a_3^3}$ $B = \dfrac{3EI}{a_3^2}$ $C = \dfrac{3EI}{a_3}$

Fig. 6.15 Addition of restraint conditions to the global structural stiffness matrix when lateral restraint is applied at a point other than nodal points

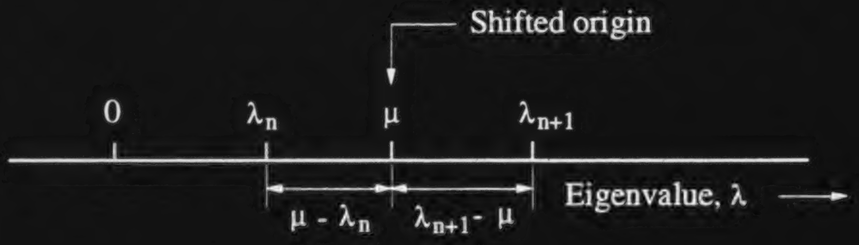
Shifted origin
0
λ_n
μ
λ_{n+1}
$\mu - \lambda_n$
$\lambda_{n+1} - \mu$
Eigenvalue, λ

Fig. 6.16 Measurement of eigenvalues from a shifted origin

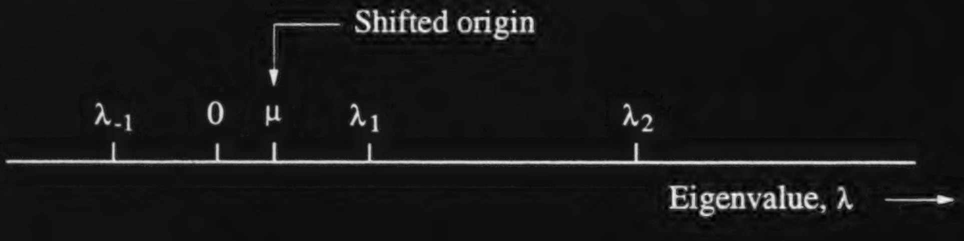
Shifted origin
λ_{-1}
0
μ
λ_1
λ_2
Eigenvalue, λ

Fig. 6.17 Optimum location for eigenvalue shift

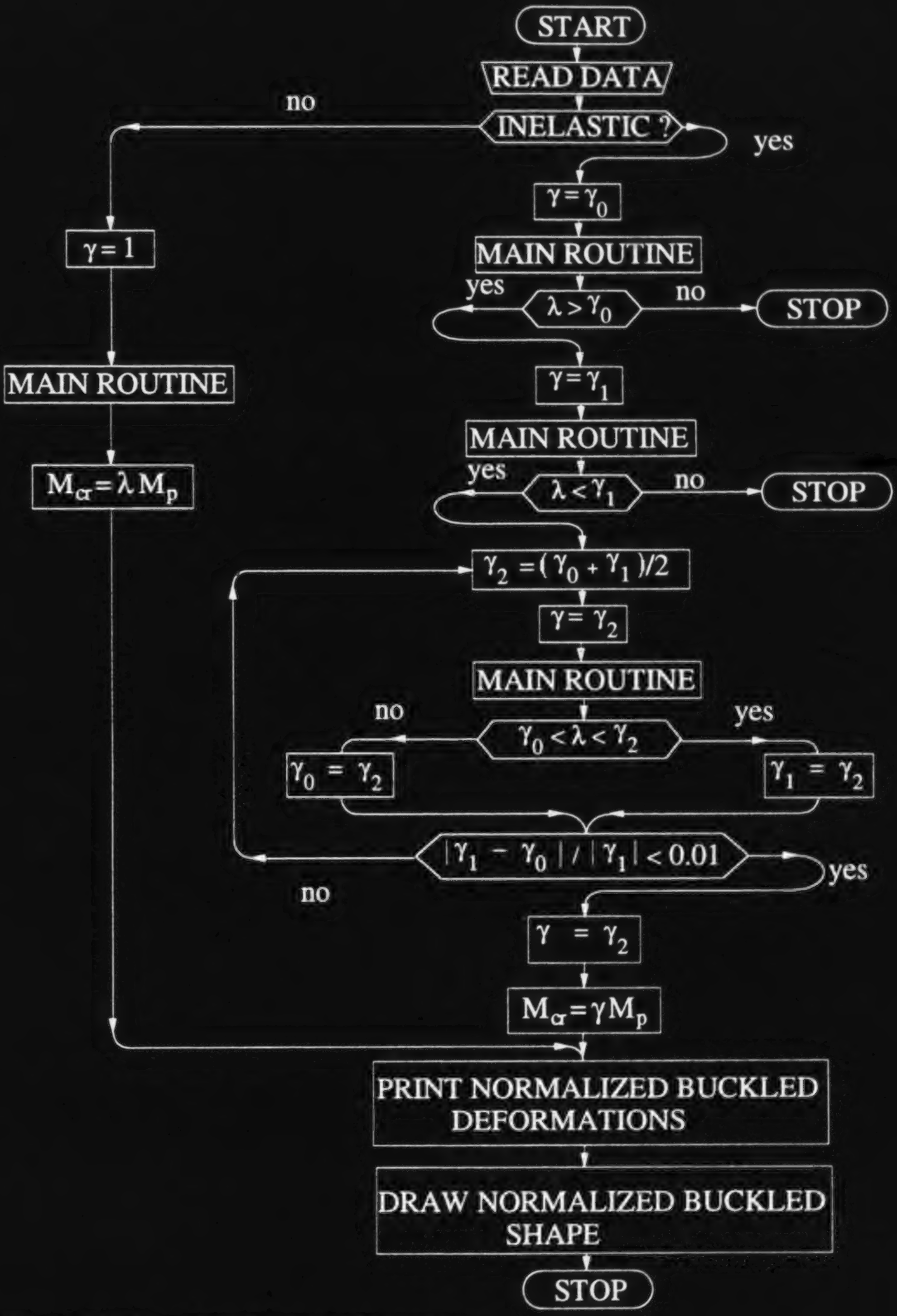
START
READ DATA
INELASTIC ?
no
yes
$\gamma = \gamma_0$
$\gamma = 1$
MAIN ROUTINE
yes
$\lambda > \gamma_0$
no
STOP
MAIN ROUTINE
$\gamma = \gamma_1$
MAIN ROUTINE
$M_{cr} = \lambda M_p$
yes
$\lambda < \gamma_1$
no
STOP
$\gamma_2 = (\gamma_0 + \gamma_1)/2$
$\gamma = \gamma_2$
MAIN ROUTINE
no
yes
$\gamma_0 < \lambda < \gamma_2$
$\gamma_0 = \gamma_2$
$\gamma_1 = \gamma_2$
$|\gamma_1 - \gamma_0| / |\gamma_1| < 0.01$
no
yes
$\gamma = \gamma_2$
$M_{cr} = \gamma M_p$
PRINT NORMALIZED BUCKLED DEFORMATIONS
DRAW NORMALIZED BUCKLED SHAPE
STOP

Fig. 6.18 Flow chart for main program

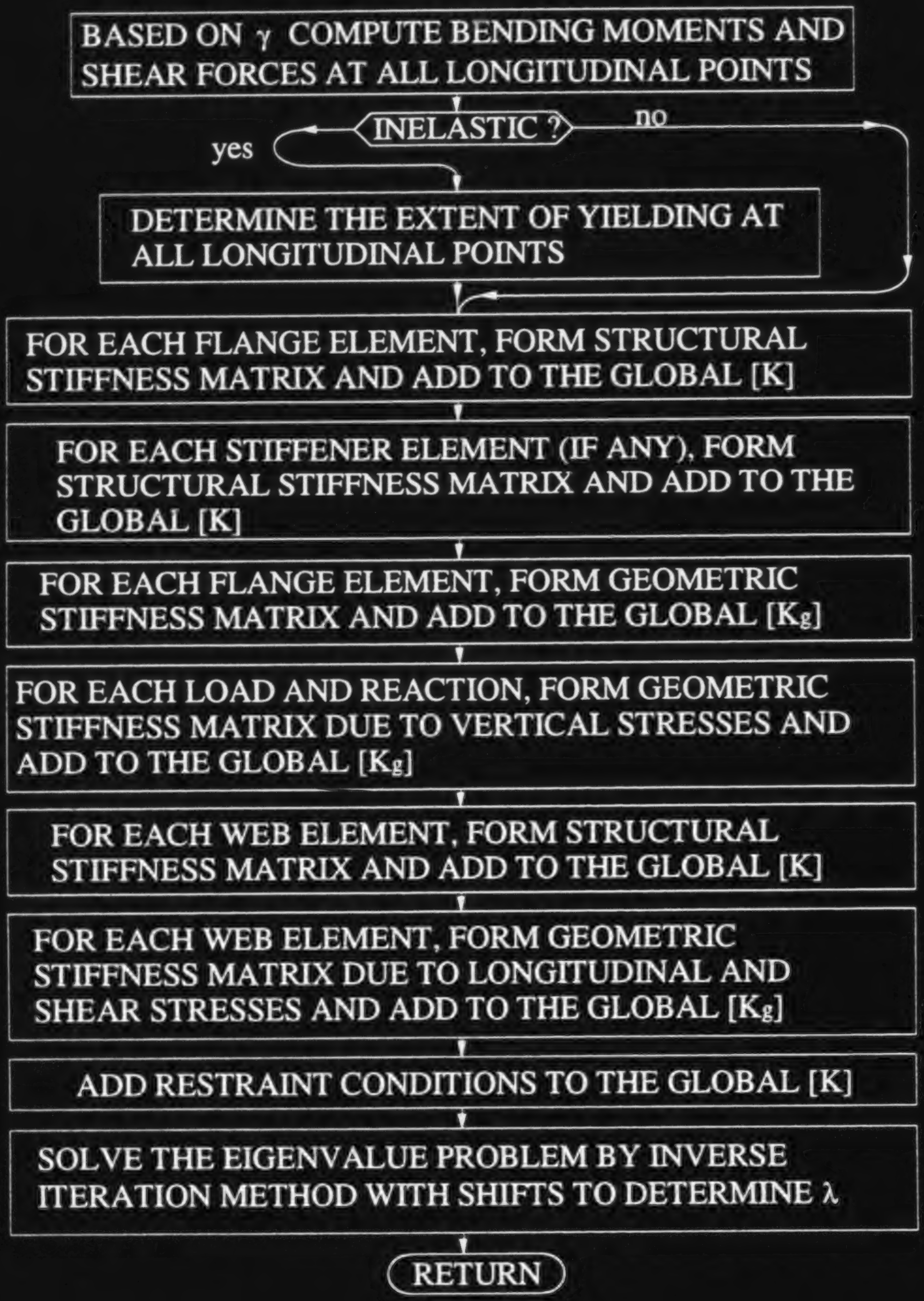
BASED ON γ COMPUTE BENDING MOMENTS AND SHEAR FORCES AT ALL LONGITUDINAL POINTS
INELASTIC ?
no
yes
DETERMINE THE EXTENT OF YIELDING AT ALL LONGITUDINAL POINTS
FOR EACH FLANGE ELEMENT, FORM STRUCTURAL STIFFNESS MATRIX AND ADD TO THE GLOBAL [K]
FOR EACH STIFFENER ELEMENT (IF ANY), FORM STRUCTURAL STIFFNESS MATRIX AND ADD TO THE GLOBAL [K]
FOR EACH FLANGE ELEMENT, FORM GEOMETRIC STIFFNESS MATRIX AND ADD TO THE GLOBAL [K_g]
FOR EACH LOAD AND REACTION, FORM GEOMETRIC STIFFNESS MATRIX DUE TO VERTICAL STRESSES AND ADD TO THE GLOBAL [K_g]
FOR EACH WEB ELEMENT, FORM STRUCTURAL STIFFNESS MATRIX AND ADD TO THE GLOBAL [K]
FOR EACH WEB ELEMENT, FORM GEOMETRIC STIFFNESS MATRIX DUE TO LONGITUDINAL AND SHEAR STRESSES AND ADD TO THE GLOBAL [K_g]
ADD RESTRAINT CONDITIONS TO THE GLOBAL [K]
SOLVE THE EIGENVALUE PROBLEM BY INVERSE ITERATION METHOD WITH SHIFTS TO DETERMINE λ
RETURN

Fig. 6.19 Flow chart for main routine

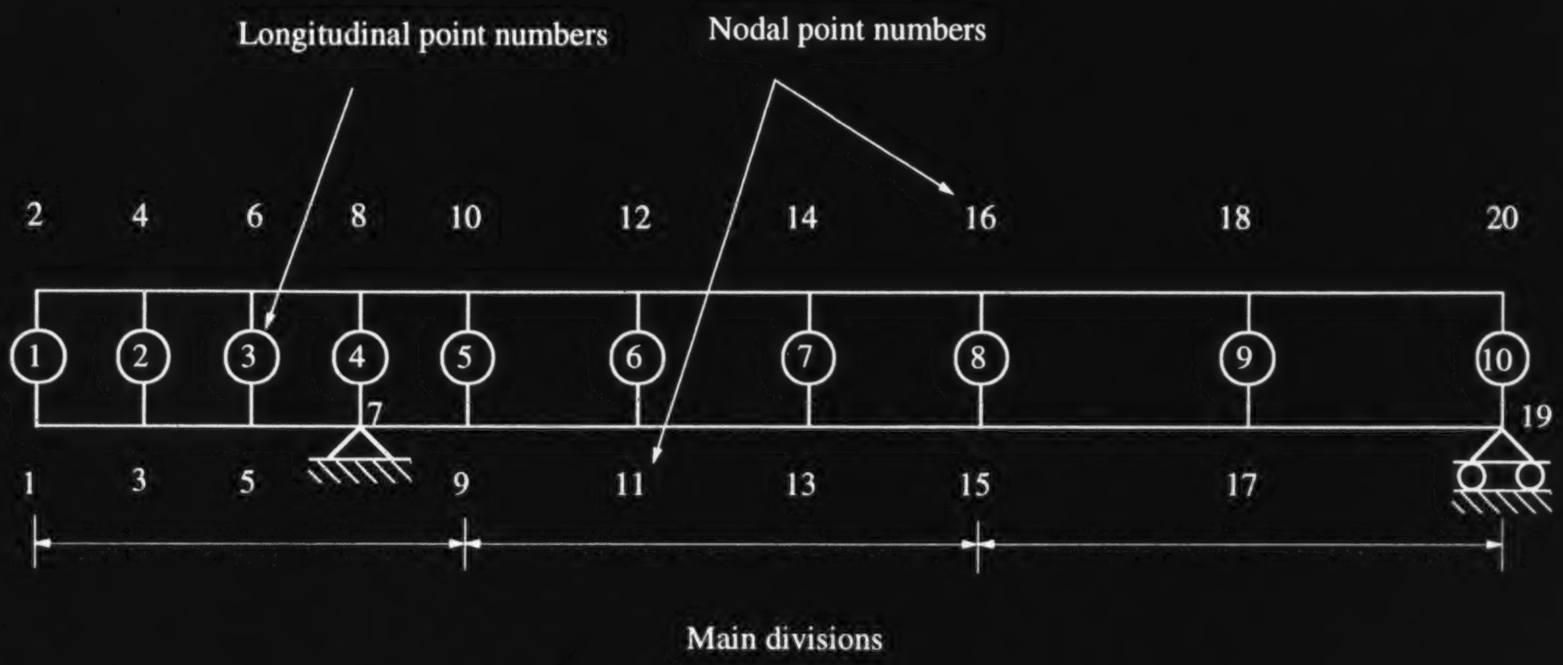
Longitudinal point numbers
Nodal point numbers
2
4
6
8
10
12
14
16
18
20
①
②
③
④
⑤
⑥
⑦
⑧
⑨
⑩
7
19
1
3
5
9
11
13
15
17
Main divisions

Fig. 6.20 Mesh characteristics

Chapter 7

DESIGN PROCEDURES FOR LATERALLY UNSUPPORTED BEAMS

7.1 Introduction

Several simplified procedures are presented in this chapter for designing laterally unsupported doubly symmetric I-shaped beams against lateral-torsional buckling, under different types of support, loading and restraint conditions. Included is a refined approach for the design of cantilever beams which avoids the defects of solutions currently available. Approaches are also proposed for the design of overhanging beams, suspended beams acted upon by their self-weight, simply supported beams which are restrained laterally and torsionally along one flange at discrete locations and cantilever-suspended span beams. In all cases, the suggested solutions were checked numerically against analysis made using the distortional buckling finite element program.

7.2 Built-in cantilever beams

A built-in cantilever is defined as a beam completely fixed at the root. Three restraint conditions at the cantilever tip are considered: (i) completely free, (ii) laterally restrained at the top flange and (iii) laterally restrained at both the top and bottom flanges. A point load, applied to either the top flange or the shear centre at the tip, is considered. This represents practical cases and is more severe than a distributed loading case. The elastic lateral-torsional buckling resistance is taken as

$$[7.1] \qquad M_{cr} = \frac{\pi}{k_b L}\sqrt{EI_y GJ}\sqrt{1+\left(\frac{X}{k_b}\right)^2}$$

$$= \frac{\pi}{k_b L}\sqrt{EI_y GJ + \frac{\pi^2 E^2 I_y C_w}{(k_b L)^2}}$$

where X is the beam torsional parameter, defined by [2.9], L is the span, E is the modulus of elasticity, I_y is the moment of inertia about the minor axis, G is the modulus of rigidity, J is the Saint Venant torsional constant and C_w is the warping constant. The effective length factor, k_b in [7.1] which models the effects of the type of loading, the level of load application and the type of end restraint is given in Table 7.1 as a function of the beam torsional parameter X. The effective length factors have been obtained by curve fitting to the results of the finite element program.

7.2.1 Cantilevers with free tips

Figs. 7.1 and 7.2 show comparisons for a W410x39 cross section of the finite element method, the proposed method and that given in the SSRC Guide for top flange and shear centre loadings, respectively. The upper values of cantilever lengths shown are recognized as being impractical. Although the SSRC solution is conservative for shear centre loading condition (Fig. 7.2), it becomes extremely unconservative for top flange loading with relatively short spans (Fig. 7.1). The problem arises with the SSRC solution because the limitation of [2.10] has not been applied.

Nethercot (1973) chose the range given by [2.10] based on a study embracing all beam and column sections in the British Steel Handbook to limit buckling to the elastic range. Subsequently, Nethercot (1983) stated that the solutions were applicable to the practical range of beam torsional parameter, X. Equation [2.10] limits the cantilever span to more than four metres for the W410x39 cross section. Therefore the SSRC solution is not applicable to a wide range of spans. From Figs. 7.1 and 7.2, it is observed that the proposed expressions for effective length factors give results which are in good agreement with the finite element solution.

7.2.2 Lateral restraint at top flange

Comparisons of the different solutions for top flange and shear centre loadings are given in Figs. 7.3 and 7.4, respectively, for the case when lateral restraint provided to the top flange at the cantilever tip. It is clear that SSRC solutions are conservative by a factor of up to 1.8. The reason is apparent from Fig. 2.2. While Nethercot (1973) obtained the solutions for lateral restraint of the shear centre at the cantilever tip, he (1983) recommended conservatively the same solution when lateral restraint of the top flange is provided.

7.2.3 Lateral restraint of top and bottom flanges

In this case, the cross section at the cantilever tip is, in effect, laterally and torsionally restrained, and the height of load application at this location is immaterial. Fig. 7.5 show a comparison of the different solutions. Again, the SSRC solution is very conservative as can be seen as well from Fig. 2.2. Torsional restraint applied at the shear centre does not prevent lateral movement of the beam at the cantilever tip. Lateral restraint of both top and bottom flanges prevents both lateral movement and twisting.

7.2.4 Effect of load position

As can be seen in Fig. 2.1, the SSRC Guide gives only two load positions: top flange loading and "all other cases". As the "all other cases" was originally based on shear centre loading, it can lead to unconservative results when the load position is located somewhere between the top flange and the shear centre.

In practice, a cantilever tip load can be applied at any level by means of a shear connection. When this level is located at a distance, h, above the shear centre, the effective length factor, k_b, can be interpolated between the factors of the two extreme cases of top flange loading, k_t, and the shear centre loading, k_s, both obtained from Table 7.1, as follows

[7.2] $$k_b = rk_t + (1 - r)k_s$$

where

[7.3] $$r = \frac{h}{d}(1.5 + \frac{h}{d}), \text{ and}$$

d = depth of the cross section

For the case when two loads are applied at the cantilever tip, say one at the top flange and the other at any level between the shear centre and the top flange, the effective length factor can be interpolated between the effective length factors corresponding to the applied load levels in proportion to the loads.

7.3 Overhanging beams

In practice, a cantilever beam may exist as the cantilever projection of a simply supported beam over an end support, as depicted in Fig. 7.6. Predicting the buckling resistance for this type of beams is much more complicated than for a single built-in cantilever because many variables, such as the ratio of cantilever span to back span and the loading and restraint conditions of both the cantilever and back spans, must be taken into account. In this study, the restraint conditions considered at the tips of the cantilever spans are: free; lateral restraint at the top flange or lateral restraint at both the top and bottom flanges. Also, the back span is assumed to be free except at the supports.

Without interaction, the buckling resistances of both cantilever and central segments are based on the free to warp conditions, in which lateral deflection and twist about a longitudinal axis are prevented at support locations. However, interaction will occur between adjacent segments during buckling and the less critically loaded segment will elastically restrain the more critically loaded segment. When the back span segment is more critical, Trahair (1983) has shown that the effects of warping restraints provided by the overhanging segments are not significant, and the buckling resistance of the back span segment can be taken as the overall buckling resistance of the overhanging beam. When the overhanging segments are more critical, the buckling resistance of the overall overhanging beam can be determined as

[7.4] $$M_{cr} = M_c + F(M_b - M_c)$$

where M_c is the elastic critical moment of the cantilever segment which is free to warp at the root, M_b is the elastic critical moment of the back span which is free to warp at both ends and F is the interaction factor which is a function of the ratio of the back span to the cantilever span.

When two overhanging cantilevers with either different spans or different loading conditions are encountered, a conservative approach is to use the lesser value of M_c in [7.4]. The buckling resistance of a cantilever which is free to warp at its root with either a free of laterally restrained top flange at the tip for top flange loading and shear centre loading was found, using the finite element program for a variety of cross sections, to be closely approximated by

[7.5] $$M_c = 1.5\ GJ/d$$

and

[7.6] $$M_c = \frac{4}{L_c}\sqrt{EI_y GJ}$$

where L_c = cantilever span, respectively. The equations for free tip cantilevers are also in good agreement with the results given by Trahair (1983).

For shear centre loading, the elastic critical moment of the back span is given by

$$[7.7] \qquad M_b = \frac{\omega_2 \pi}{L} \sqrt{EI_y GJ + \frac{\pi^2 E^2 I_y C_w}{L^2}}$$

where L is the back span and ω_2 accounts for nonuniform moments. For the cases when the back span loads are applied at the top flange level, the finite element program must be used to obtain the elastic critical moment of the back span.

For the case of overhanging beams with free tip cantilevers (see Fig. 7.6a), the value of the interaction factor, F, for a particular ratio of L/L_c for a single cantilever overhang configuration with a concentrated load at the flange tip and with top flange loading was found by establishing the elastic critical moment using the finite element program and back computing, knowing M_c and M_b, from [7.4]. By repeating this procedure for different ratios of L/L_c, other values of F were found. A good approximation for F by curve fitting is

$$[7.8] \qquad F = -0.08 + 0.18\ L/L_c - 0.009(L/L_c)^2$$

In the case where lateral deflections and longitudinal twisting are prevented at the support locations and lateral restraint is provided for the top flange at the cantilever tips (see Fig. 7.6b), equations [7.5] and [7.6] are still valid to obtain M_c but the interaction factor F to be used in [7.4] is approximated as

[7.9] $$F = 0.064 + 0.162\ L/L_c - 0.009(L/L_c)^2$$

The case where lateral deflection and twist are prevented at both support and cantilever tip locations (see Fig. 7.6c), can be treated easily using procedures for interaction buckling of laterally continuous segments as given in the SSRC Guide or by Schmitke and Kennedy (1985).

7.4 Stability of suspended and spreader beams

7.4.1 Suspended beams under self-weight

During the construction process, the need often arises to lift into place a slender beam acted upon by its self-weight. After placing the beam, bracing or connection to other members stabilizes the beam under the imposition of further loading. Therefore, the lifting process represents one of the most critical stages at which the beam could buckle under its self-weight. Due to the unusual boundary conditions involved, the classical buckling formulae (Galambos 1988) are not applicable in assessing the lateral-torsional buckling strength of the beam while being lifted.

Dux and Kitipornchai (1989) established a basis for the stability of suspended beams. They used the finite integral method to obtain buckling capacity charts in a non-dimensional format to be used for checking the stability of I-beams when lifted under self-weight for different cable angles and attachment positions. Their solutions are verified herein using the finite element technique and some simplifications are suggested for the case when the lifting cables are vertical. This situation occurs when a spreader beam is used. Because the only restraints are the lateral restraints of the top flange applied at the loading points, rigid body twisting modes at zero load represent a potential problem during investigation. This problem is overcome by using the inverse iteration with shift technique to solve the eigenvalue problem involved in the finite element analysis. While both symmetric and anti-symmetric buckling modes are possible, because the problem is symmetric with regard to loading, restraint and geometry, it has been observed throughout this study that the symmetric mode is the critical one. This observation was also reported by Dux and Kitipornchai (1989).

Consider the flexural member shown in Fig. 7.7, which is lifted symmetrically by vertical cables and acted upon by its self-weight, w, applied along the shear centre. As suggested by Dux and Kitipornchai (1988 and 1989), the critical buckling load can be approximated as

$$[7.10] \qquad w_{cr} = \gamma \sqrt{E I_y GJ} / L^3$$

in which γ is the non-dimensional elastic buckling load parameter and L is the length of the member.

The value of the elastic buckling load parameter, γ, proved to be dependent on the location of cables along the lifted member and the beam torsional parameter, X, defined in [2.9]. Using the finite element approach, the curves giving the elastic buckling load parameter versus different symmetrical arrangements of vertical cables (Z_a/L, where Z_a is the distance of cable attachment from the mid-span as indicated in Fig. 7.7) are given in Fig. 7.8 for X = 0.2, 0.4, 0.6 and 0.8. These results were obtained using a W360x39 cross section for the case where the cables are attached directly to the top flange but subsequently checked against a wide range of other cross sections and the difference was found to be in all cases less than 5%. The results of these curves are in good agreement with those obtained by Dux and Kitipornchai (1989) and indicate that buckling resistance is greatest when the cables are placed near the quarter points. In the vicinity of that optimum location, the buckling capacity is extremely sensitive to the cable attachment position. This indicates that extra care should be given to insure the right position of the cables while operating in this region. As the cable attachment positions move from the optimum location towards either the middle or the ends, the buckling strength decreases.

For the case where the cable attachment positions are located between the midspan and the quarter points, the relationship between γ/X and Z_a/L reduces to a unique curve as indicated in Fig. 7.9. By curve fitting the available data, the value of the elastic buckling load parameter, γ, can be approximated as

$$[7.11] \qquad \gamma = \frac{1000\,X}{9.91 - 5.47\frac{Z_a}{L} - 324.61\left(\frac{Z_a}{L}\right)^2 + 794\left(\frac{Z_a}{L}\right)^3}$$

Further simplification for the right hand branch of the curves given in Fig. 7.8 (where $0.3 < Z_a/L < 0.5$) proved to be difficult to obtain. Therefore, it is recommended, for this range, to find the value of by γ by interpolating between the curves as suggested by Dux and Kitipornchai (1989). The elastic buckling load parameter curves for Z_a/L in the range 0.3 to 0.5 are presented separately with expanded scale in Fig. 7.10.

In checking the stability of beams under self-weight lifting the overall safety factor, F_s, can be defined as:

$$[7.12] \qquad F_s = w_{cr} / w_{sw}$$

where w_{sw} is the self-weight of the beam. Dux and Kitipornchai suggested that a value of 2 for the overall safety factor should be used because elastic buckling results in a catastrophic sudden failure and to account for dynamic effects and initial imperfections. Engineers may wish to decide on an appropriate overall safety factor based on the circumstances at hand.

7.4.2 Spreader beams

In case when the spreader beam is picked up by inclined crane cables attached at its ends, the spreader beam is designed as a beam-column. When a spreader beam, as shown in Fig. 7.11, is lifted at midspan, the lateral-torsional stability must be checked. Neglecting the self-weight of the beam and assuming elastic behaviour, Dux and Kitipornchai (1988) suggested that the critical buckling load, W_{cr}, be obtained in the form

$$W_{cr} = \gamma \sqrt{E I_y G J} / L^2 \qquad [7.13]$$

where γ is a function of the beam torsional parameter, X. Using the finite element program and a W360x39 cross section, the values of γ were obtained for different values of X. As given in Fig. 7.12, this curve is almost a straight line and can be approximated as

$$\gamma = 1 + 12X \qquad [7.14]$$

7.5 Stability of restrained beams

A design procedure is given here for the lateral-torsional stability of doubly symmetric I-shaped beams laterally and torsionally restrained by purlins fastened to one flange only. While the restraint provided by purlins may significantly increase the moment resistance of the beam, it also increases the difficulty of the solution. Current standards consider bracing of this type to be effective only when it is attached to the critical flange, that is the compression flange except for the case of cantilevers. However, in cantilever-suspended span construction, only the top flange is laterally and torsionally braced at discrete locations and the compression bottom flange, except at column location, is unrestrained. Under such circumstances, the restraint provided to the tension flange may be sufficient to preclude lateral-torsional buckling.

The proposed solutions presented here are applicable to beam members, in which axial loads are small and can be neglected. This situation commonly arises in low rise industrial buildings. It is assumed that lateral displacements and twists are prevented at each end and the ends are free to warp. When the beam ends are not simply supported, warping interaction occurs between the beam under consideration and the other members, and the solutions tend to give either the upper or the lower bound prediction of the buckling resistance, depending on whether the beam in question is the restraining or the restrained member, respectively.

7.5.1 Simply supported beam under uniform moment

Consider the simply supported beam, shown in Fig. 7.13, subjected to uniform moment and with discrete braces attached at equally spaced intervals to the tension flange. The braces exert complete (infinite) lateral restraint and incomplete (finite) torsional restraint. Milner (1975) used the energy method to obtain the following expression for the critical buckling moment

$$[7.15] \qquad M_{cr} = \frac{GJ}{d} + \frac{2 n^2 \pi^2 E C_w}{d L^2} + \frac{K_e L^2}{n^2 \pi^2 d}$$

where most terms are as defined previously in chapter 2, n is the number of half waves of the buckled compression flange, which is selected so as to minimize the critical moment as follows

[7.16] $$n = \sqrt[4]{\frac{K_e L^4}{2\pi^4 E C_w}}$$

The effective continuous torsional restraint stiffness, K_e in [7.15] and [7.16] is defined as the the equivalent continuous stiffness of the torsional restraint which is effectively applied to the compression flange. Because the actual torsional restraint is applied to the tension flange at discrete locations, it is transmitted to the compression flange through the beam-purlin connection as well as the web. The value of K_e depends on: (1) the bending stiffness of the purlins, (2) the moment-rotation characteristics of the beam-purlin connection, (3) local web distortion and (4) twisting of the braced flange between braces. A useful model to account for the effects of all the above variables is that suggested by Milner (1975). The effective continuous torsional restraint stiffness, K_e, is estimated as

[7.17] $$\frac{1}{K_e} = \frac{1}{K_b} + \frac{1}{K_w} + \frac{1}{K_j} + \frac{1}{K_f}$$

where K_b is the bending stiffness of the purlins divided by the purlins spacing, K_w is the web stiffness, K_j is the stiffness of the beam-purlin connection divided by the purlins spacing and K_f is the effective torsional stiffness of the flange.

The web stiffness, K_w ,which accounts for the web distortion is given as

$$[7.18] \qquad K_w = \frac{Et_w^3}{4(1-v^2)d} = \frac{Et_w^3}{4\ d}$$

where t_w is the web thickness, v is Poisson's ratio and s is the spacing between purlins. The equivalent continuous stiffness of the beam-purlin connection, K_j, depends on the moment-rotation characteristic of the connection. Milner (1977a) recommended an infinite value for K_j in cases of welded and friction grip bolted joints. Milner and Rao (1978) presented some recommendations for estimating K_j for bolted joints based on experimental tests.

Because the bracing is provided only at discrete locations along the tension flange, the flange between the braces tends to twist, causing a reduction in the effectiveness of the torsional restraint of the overall system. This effect can be taken into account by considering the torsional stiffness of the portion of the braced flange between bracing points. The equivalent continuous torsional stiffness of the flange can be taken as

$$[7.19] \qquad K_f = \frac{C\,G\,b\,t^3}{s^2}$$

where b is the flange width, t is the flange thickness and C is a constant which is determined so that the results of the present design model would agree with the finite element solution. Using this procedure, a value of 7.29 is obtained for C.

In practice, the bending moment distribution along the beam is nonuniform. However, Milner (1977a) recommended that the present design approach could be applied conservatively to check the stability of a beam element extracted from a complete structure where the boundary conditions of the basic analysis are reasonably satisfied, and assuming that a uniform moment equals the maximum moment.

7.5.2 Simply supported beam under nonuniform moment

The conservative assumption of a uniform moment in the application of [7.15] may lead to a considerable underestimation of the buckling resistances. Consider the beam shown in Fig. 7.14, which is braced laterally and torsionally at discrete locations along the top flange and is acted upon by end moments as well as a uniform top flange loading. The beam ends are assumed to be laterally restrained and free to warp. When the beam is continuous over supports, warping interaction occurs between the beam under consideration and the adjacent ones, and the following procedure tends to give either the upper or the lower bound predictions of the buckling resistance, depending on whether the beam is the restraining or the restrained member, respectively. For the purpose of generalization, assume β to be the ratio of the end moments and R to be the ratio between the maximum static moment due to the loads and the maximum end moment. Lindner (1987) suggested that the critical buckling moment can be estimated as

[7.20] $$M_{cr} = \frac{k}{L}\sqrt{EI_yGJ^*}$$

where k is the effective buckling coefficient, obtained from the finite element analysis, and J^* is a modified Saint Venant torsional constant, given as

[7.21] $$J^* = J + \frac{K_e L^2}{\pi^2 G}$$

The design approach given by [7.20] and [7.21] was suggested by Lindner (1987) to handle the stabilization of I-section beams by corrugated sheeting. However, it can be used when the bracing system is as depicted in Fig. 7.14, provided that the effective continuous torsional restraint stiffness, K_e, is taken as given in [7.17]. Lindner (1987) showed that the effective buckling coefficient, k, is actually a function of the bending moment diagram as well as the beam torsional parameter X. In order to understand the correlation between the solutions given by [7.15] and [7.20], consider the simplified case of a beam under uniform moment and no torsional restraint. In this case, equation [7.15] reduces to

[7.22] $$M_{cr} = \frac{GJ}{d} + \frac{2\pi^2 E C_w}{dL^2}$$

Equating [7.20] and [7.22] gives

[7.23] $$k = \frac{\pi}{2X}(1 + 2X^2)$$

As indicated in Fig. 7.15, the effective buckling coefficient, k, varies considerably with the beam torsional parameter. The minimum value of k is 4.44, which corresponds to a value of the beam torsional parameter, X, 0.71. Lindner (1987) showed that for a wide range of variation in the bending moment distribution, the minimum values of k occur within the range $0.31 < X < 0.71$. It is important at this stage to define the range of practical values of the beam torsional parameter. Kirby and Nethercot (1979) presented graphically the relationship between X^2 and L/d for relatively narrow cross sections and for relatively wide cross sections (column sections). Using these curves and assuming L/d to be within the range of 15 to 25, it can be shown that the corresponding range of variation in the beam torsional parameter is 0.35 to 1, with an average of 0.68.

As suggested by Lindner (1987), the minimum values of k, corresponding to different bending moment distributions, can be used directly for design. This is justified by its simplicity, which is a major requirement in any design approach, and the fact that the practical range of the beam torsional parameter is close enough to the range within which the minimum values of k are located for a wide range of bending moment distributions. Fig. 7.16 gives the minimum values of the effective buckling coefficient, k, for a range of end moment ratios, β, between 0 and 1 and a range of R values between 0 and 2. It should be noted that the critical buckling resistance given by [7.20] corresponds to the critical value of the maximum end moment, even though the absolute value of the maximum positive moment may be larger.

The above procedure tends to overestimate the elastic lateral-torsional buckling resistances. This occurs because it is assumed that the increase in Saint Venant torsional constant due to torsional restraint given by [7.21] is independent of the bending moment distribution. However, it has been found that [7.21] is only valid for the case when the whole braced flange is under tension. When the bending moment distribution is such that a part of the braced flange is under compression, the unbraced flange does not tend to buckle within the part under tension, and the effect of torsional restraint within that region is reduced. Therefore, [7.21] tends to overestimate the modified Saint Venant torsional constant under these circumstances. However, under such bending moment distributions and the applied lateral and torsional restraints, the beam buckling is highly inelastic. Using the empirical inelastic buckling formula given by CSA Standard CAN/CSA-S16.1-M89 (CSA 1989), the differences between the inelastic buckling resistance corresponding to the elastic solution given by [7.20] and that corresponding to the elastic solution given by the finite element, tend to be only within 2%.

7.7 Design of beams in cantilever-suspended span construction

Lindner (1972) has shown that the critical buckling moment for a back span with a single overhang cantilever, restrained laterally at top flange, can be estimated using the same formula for the back span that is free to warp (equation [7.20] in which J^* is replaced by the Saint Venant torsional constant), provided that the span ratios and loading conditions are to be taken into account for determining the value of the effective buckling coefficient, k. This concept is used here, together with [7.20] to obtain a design procedure for steel beams in cantilever-suspended span construction.

Consider the double overhanging beam shown in Fig 7.17, which is restrained laterally and torsionally at the level of top flange at joist locations. The boundary conditions at the column supports, as well as at the cantilever tips are dependent on whether or not joists with or without bottom chord extension exist at these locations. The elastic critical buckling moment at the support location is assumed to be given by [7.20], where L is the length of the back span. The value of the effective buckling coefficient, k, is dependent on the loading, geometry and boundary conditions. Because insufficient information is available about the residual stress patterns in relatively narrow flange beams, it is recommended that the inelastic reduction formula given in the CSA Standard CAN/CSA-S16.1-M89 (CSA 1989) be used when the elastic buckling moment exceeds 0.67 M_p, i.e.,

[7.24] $$M_i = 1.15\ M_p(1 - 0.28\ M_p/M_{cr})$$

where M_i is the unfactored inelastic buckling moment resistance.

In order to estimate the modified Saint Venant torsional constant, J^*, using [7.21], the effective continuous torsional restraint stiffness, K_e can be obtained from

$$[7.25] \qquad \frac{1}{K_e} = \frac{1}{K_b} + \frac{1}{K_w} + \frac{1}{K_f}$$

where K_w and K_f are given by [7.18] and [7.19], respectively. Equation [7.25] is basically the same as [7.17] except that the K_j is considered to assume an infinite value for welded connection (Milner 1977a). The value of K_b is determined as the in-plane bending stiffness of the brace, K_B, divided by the brace spacing. A simplified expression for the in-plane bending stiffness of the open-web steel joists is given in Appendix C. Hence, the value of K_b can be obtained as

$$[7.26] \qquad K_b = \frac{K_B}{s} = \frac{E\,I_2}{L_p\,s}$$

where K_B is the in-plane bending stiffness of the joist, I_2 is the moment of inertia of the top chord of the joist about the centroidal horizontal axis, L_p is the length of the end panel and s is the joists spacing. Based on a study embracing the practical range of joists, it is recommended that a minimum value of 3×10^7 Nmm/rad. be used for K_B in cases where no data are available. In the case of interior beams with joists on both sides, the value of K_b can be obtained by adding the contribution of the joists on each side. In the case where the joist acts compositely a with concrete slab, a significant enhancement of the torsional stiffness is achieved and the moment of inertia of the composite section of the concrete and the top chord acting together is used instead to compute I_2 in [7.26]. However, the composite action is effective for the joists on only one side of the beam because when the beam tends to rotate, the joists are bent in opposite directions and the concrete would be in tension on one side.

7.7.1 Basic assumptions

Because the loading, geometry and boundary conditions of the beams in cantilever-suspended span construction may vary considerably, it is reasonable to make the following assumptions

1. Symmetric geometry and loading conditions. As indicated in Fig. 7.17, the overhanging cantilever spans are assumed to have the same length and loading configuration.

2. The ratio of the back span to the cantilever span is assumed to be within the range of 4 to 6.

3. The load transmitted from the suspended span to the cantilever tip is assumed to act at a maximum distance of 0.15 the depth of the beam above the shear centre.

4. The joist loads within the back span are applied at the level of top flange of the beam.

5. All the joists have the same in-plane bending stiffness.

6. The value of beam torsional parameter, X, based on the back span length is assumed to be within the range of 0.4 to 1.2. This is based on Kirby and Nethercot (1978) and was checked using the W-shaped cross sections given by the Canadian standard for practical range of beam spans.

7. The columns are spaced uniformly.

8. All the joist seats are welded to the top flange of the beam.

7.7.2 Critical bending moment diagrams

Two distinct systems may be encountered in cantilever-suspended span construction, depending on whether or not fork supports (lateral restraint of both the top and bottom flanges of the beam at column locations) exist. A fork support, which is the main feature of the "forked system", is provided by an open-web steel joist with its top chord welded to the top flange and its bottom chord extended to either the beam or the top of the column to provide lateral restraint. The "unforked system" is encountered when no open-web steel joists exist at either column location.

Consider the forked and unforked systems, with symmetrical loading and restraint conditions, given in Fig. 7.18. The beam is a W360x39 cross section having geometrical and material properties as determined in the test program. For the case when only lateral restraint is applied to the top flange at loading points and for a given value of R, the finite element program may be used to determine the buckling capacity when the effect of residual stresses is taken into account and when it is neglected. For the forked support system, the values of M_{cr}/M_p for a range of R values between 0 and 2 are given in Fig. 7.19.

In the forked system, as the value of R increases, either the compressive stresses decrease or the tensile stresses increase within a considerable portion of the unrestrained bottom flange within the back span and, therefore, the critical buckling moment increases. The critical loading condition for a combination of dead and live loads, as given in Fig. 7.20, can be obtained by maximizing the negative moments above the supports and minimizing the static moment caused by the back span loads.

The critical loading condition in the unforked system is not as obvious as that in the forked system because, in this case, the critical buckling moment increases as R increases up to a certain limit, then decreases up to R=2 and then increases again as shown in Fig. 7.21. For values of R less than 2, the negative moment over the supports is the critical moment and for values of R greater than 2, the positive moment at the middle of the back span is the critical moment. For small values of R, the beneficial effect of the shape of the bending moment diagram causes the buckling capacity to increase. Beyond these values of R up to 2, the buckling capacity is significantly reduced because the destabilizing effects of both the loads applied at top flange level of the back span and the reactions are more pronounced than the beneficial effect of the shape of the bending moment diagram. The buckling resistance increases for values of R greater than 2 because the midspan moment, which is larger than the negative moment, becomes the critical moment.

It can be observed from Fig. 7.19, for the forked system, for values of R between 0 and 2, that the beneficial effect of residual stresses (with the flanges predominantly in tension) is noticeable throughout the range of R. On the other hand, in the unforked system as seen from Fig. 7.21, the effect of residual stresses diminishes as the value of R increases because the increased web distortion due to the destabilizing effect of the reactions dominates and flange participation in the overall behaviour is of secondary importance.

Consider the unforked system given in Fig. 7.18b. Neglecting the effects of residual stresses, the values of M_{cr}/M_p obtained from the finite element program for a range of R values between 0 and 2 are given in Fig. 7.22 for the case when only lateral restraints and the case when lateral and torsional restraints with $K_B = 3x10^7$ Nmm/rad. are provided. It is apparent that the apex of the curve is shifted to the left when torsional restraint is applied. This corresponds to the practical restraint condition.

Generally, roofs of structures can be classified as either standard roofs or, simply, roofs in which the only loads considered are the dead and snow (with rain) loads, or parking roofs, in which the dead, parking or snow loads are considered. As given in Table 7.2, the ratio of maximum to minimum factored loads for a range of roof structures with specified loads in accordance with the National Building Code of Canada (1990) is within the range of 1.08 to 2.2. Using these results together with the critical loading condition described in Fig. 7.20 for beam with fork supports, the value of R (ratio of static moment to the moment at the column location) was found to be within the range of 0.6 to 1.6.

For beams without fork supports, the two loading conditions of full and partial loading shown in Fig. 7.21 need to be investigated.

Following the same procedure as for the forked system, the corresponding range of R for the unforked system was found to be 1.3 to 4.

7.7.3 Design of beams with fork supports

This type of beam is encountered in a regular grid system, in which an open-web steel joist with bottom chord extension exists at both column locations. Under symmetrical geometry, loading and boundary conditions, three distinct cases arise. As given in Fig. 7.24, these cases are: case 1, in which an open-web steel joist with bottom chord extension exists at each cantilever tip; case 2, in which an open-web steel joist without bottom chord extension exists at each cantilever tip; and case 3, in which no open-web steel joist exists within the cantilever spans. For these cases, the critical loading condition is that given in Fig. 7.20, where the negative moments at the column locations are maximized and the sagging moment at the middle of the back span is minimized.

a) Case 1

In this case (Fig. 7.24a), the beam cross section at the cantilever tips is in effect laterally and torsionally restrained and the height of load application at that location is immaterial. Because the value of the effective buckling coefficient, k, is dependent on many parameters such as the ratio of the cantilever span to the back span, the moment ratio, R, and the beam torsional parameter, X, the procedure given in section 7.5.2 which uses the minimum values of k within the practical range of the beam torsional parameter (0.4 to 1.2) is followed.

Using the finite element program, the minimum values of k were obtained for a practical range of loading conditions (0.6 < R < 1.6) and practical ratios of cantilever span to the back span (1/6, 1/5 and 1/4) for a W610x82 beam and are given in Fig. 7.25.

To check the general applicability of these design curves, critical moments were computed using the finite element program and using the design curves for a broad range of parameters as given in Table D.1.

The design procedure to determine the factored moment resistance is as follows

(i) Establish the geometric and material properties of the assumed beam section,

(ii) From the given loading condition, establish the value of R,

(iii) Determine the web stiffness as

$$K_w = \frac{E t_w^3}{4(1-v^2)d} \approx \frac{E t_w^3}{4\,d} \tag{7.18}$$

(iv) Determine the effective torsional stiffness of the flange as

$$K_f = \frac{7.29\, G\, b\, t^3}{s^2} \tag{7.19}$$

(v) Determine the in-plane bending stiffness, K_B, of the joists attached to the beam as given in Appendix C. A value of 3×10^7 Nmm/rad. can be used if no data are available. The value of K_b is determined as

[7.26] $$K_b = \frac{K_B}{s}$$

where s is the joists spacing,

(vi) Determine the effective continuous torsional restraint stiffness, K_e, from

[7.25] $$\frac{1}{K_e} = \frac{1}{K_b} + \frac{1}{K_w} + \frac{1}{K_f}$$

(vii) Determine the modified Saint Venant torsional constant as

[7.21] $$J^* = J + \frac{K_e L^2}{\pi^2 G}$$

(viii) From Fig. 7.25 establish the value k, interpolating between the curves of L_c/L as necessary,

(ix) Determine the value of the elastic critical moment from

[7.20] $$M_{cr} = \frac{k}{L} \sqrt{E I_y G J^*}$$

(x) To determine the factored moment resistance based on the procedures of the CSA Standard CAN/CSA-S16.1-M89 (CSA 1989), it is first necessary to establish an appropriate value of the resistance factor as discussed subsequently.

Table D.1 shows that there is excellent agreement between the factored moment resistance obtained using the finite element program and that obtained using Fig. 7.25 with a mean ratio of the predicted/design moment (without resistance factors) of 1.002 with a coefficient of variation of 0.010.

b) Case 2

This case (Fig. 7.24b) corresponds to the existence of open-web steel joists without bottom chord extensions at the cantilever tip locations. In this case, the effective buckling coefficient has been found to be virtually independent of the ratio of the cantilever span to the back span. For the practical range of torsional restraint stiffnesses provided by the joists, the effective buckling coefficient, k, has also been found to be independent of the torsional restraint stiffness. For practical geometrical conditions in cantilever-suspended span construction, the ratio of the load transferred from the suspended span to that applied directly by the joist is within the range of 0.5 to 1.5. However, this ratio has been found to affect the critical buckling moment by not more than 5%. The significant parameters affecting the effective buckling coefficient are the shape of bending moment diagram and the value of the beam torsional parameter, X, of the back span. Fig. 7.26 gives the values of k as a function of these two parameters for this case.

The general applicability of the design curves of Fig. 7.26 is confirmed by Table D.2, which gives a ratio of the mean value of the predicted/design moment of 1.012 with a coefficient of variation of 0.020.

The design procedure to determine the factored moment resistance is basically the same as in case 1, except for step (viii), which is as follows:

(viii) Determine the value of the beam torsional parameter as

$$X = \sqrt{\frac{\pi^2 E C_w}{G J L^2}} \qquad [2.9]$$

and hence from Fig. 7.26, the value of k interpolating between the curves of R values as necessary.

c) Case 3

In this case (Fig. 7.24c), no open-web steel joist exists at the cantilever tips and the only loads acting at these locations are provided by the shear connections near the shear centre. The significant parameters affecting the values of k are the shape of the bending moment diagram, the beam torsional parameter, X, of the back span and the ratio of the back span to the cantilever span. Figs. 7.27, 7.28 and 7.29 give the values of k for ratios of the cantilever span to the back span of 0.25, 0.20 and 0.167, respectively.

As indicated by Figs. 7.27, 7.28 and 7.29, the value of critical buckling coefficient, k, decreases as the ratio of the cantilever span to the back span increases. Table D.3 shows for this case that the design curves of these figures are generally applicable. A conservative simplified approach for design purposes would be to use the values of k given by Fig. 7.27 and neglect the effect of the ratio of the cantilever span to the back span. However, this approach results in as much as 23% conservatism in predicting the elastic critical buckling moment.

The design procedure followed is the same as for case 2.

d) Resistance factors

It is necessary to develop resistance factors which can be used with the design procedures given for cases 1, 2 and 3.

Generally, the value of the modulus of elasticity, E, is significant for elastic buckling, whereas the value of the yield stress, F_y, is significant for inelastic buckling. Kennedy and Baker (1984) give the statistics of these material properties for rolled sections as

[7.28] $$\rho_E = 1.020,\ V_E = 0.012,\ \rho_{F_y} = 1.060,\ V_{F_y} = 0.051$$

where ρ is the ratio of the mean value to the nominal value and V is the coefficient of variation. The statistical properties of the material (ρ_M and V_M) are taken as those of either E or F_y. The significant geometric property in beam buckling is taken as the plastic modulus.

The statistics of this geometric property of rolled sections is also given in Kennedy and Baker (1984) as

[7.29] $\rho_G = 0.99, V_G = 0.038$

The value of ρ, corresponding to the test/design ratio is obtained as the product

[7.30] $\rho_P = \rho_{P1} \times \rho_{P2}$

where ρ_{P1} is the mean value of the test/predicted, and ρ_{P2} is the mean value of the predicted/design. The corresponding value of V is given as

[7.31] $V_P = \sqrt{V_{P1}^2 + V_{P2}^2}$

As obtained from the test series, the value of ρ for the test/predicted ratio is 0.99 with a coefficient of variation of 0.064. In Appendix D, the finite element predictions and the design predictions (given by the proposed design procedure) for different beam sections, restraint and loading conditions are given in Tables D.1, D.2 and D.3 for cases 1, 2 and 3, respectively. Also given in these tables are the mean values and coefficients of variations for the predicted/design ratios.

The value of ρ corresponding to the resistance of the member is given as

[7.32] $\rho_R = \rho_G \times \rho_M \times \rho_{P1} \times \rho_{P2}$

and the corresponding value of V is given as

[7.33] $$V_R = \sqrt{V_G^2 + V_M^2 + V_{P1}^2 + V_{P2}^2}$$

The resistance factor, ϕ, is taken as

[7.34] $$\phi = \rho_R \exp(-\beta\, \alpha_R V_R)$$

where β is the reliability index, taken as 3.0, and α_R is the coefficient of separation, taken as 0.55.

A resistance factor of 0.90 was found to be appropriate for all the three cases of a beam with fork supports. This procedure assumes, in the inelastic range, that the inelastic curves of S16.1 do not introduce any additional variability, as the residual stresses are more favourable than assumed in S16.1. However any error is expected be relatively small.

7.7.4 Design of beams without fork supports

Fig. 7.30 gives the geometry of a beam with symmetric geometry and boundary conditions, with no joists on the column lines. The joists are evenly spaced with a joist on each cantilever span, and with the columns located halfway between two neighbouring joists. When the top of the column is unbraced, the bottom flange of the beam can move laterally at the columns but torsional restraint is provided to the bottom flange due to the rigid connection of the beam to the column. The support is unforked.

As discussed previously, two loading conditions need to be investigated for a beam under such boundary conditions (see Fig.

7.23). As a result of the significant web distortion of the beam near the columns, a substantial degradation of the critical buckling capacity is expected in the unforked system as compared to that of the forked system. For this reason, this system is not recommended. Using the finite element program, the values of k were obtained as given in Fig. 7.31. Table D.4 shows that the design curves of Fig. 7.31 result in factored moment resistances in good agreement with the finite element predictions. It should be noted that the critical buckling resistance given by [7.20] together with Fig. 7.31 corresponds to the critical value of the maximum negative moment over the column support, even though the absolute value of the maximum positive moment may be larger. The design procedure followed is basically the same as for cases 2 and 3, except that the inelastic buckling moment resistance is determined based on the maximum absolute elastic buckling moment along the beam, which is the negative moment over the support for $R < 2$ and is the positive moment at midspan for $R > 2$. The elastic critical midspan moment resistance can be estimated from the corresponding value of the negative moment over the support and the value of R.

Using the procedure described in [7.28] through [7.34], together with the statistical properties of the predicted/design ratio, given in Table D.4, a resistance factor of 0.85 is obtained.

Restraint conditions		Effective length factor, k_b	
At root	At tip	Top flange loading	Shear centre loading
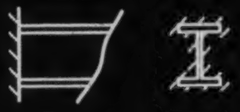	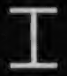	$0.57 + 0.71X - 0.1X^2$	0.75
	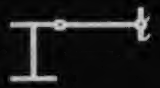	$1.2 - \frac{0.161}{X} - \frac{0.184}{X^2}$ $\not< 0.85$	0.5
	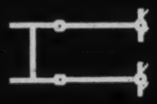	0.44	0.44

Table 7.1 Effective length factors for built-in cantilevers

Type of structure	Dead loads, psf	Live loads, psf	Range of $\frac{\text{Maximum factored load}}{\text{Minimum factored load}}$
Standard roof	15-30	21-135	1.27-1.84
Parking roof, with parking loads	50-150	50	1.40-2.20
Parking roof, with snow loads	50-150	21-135	1.08-2.20

Table 7.2 Ratios of maximum to minimum factored loads

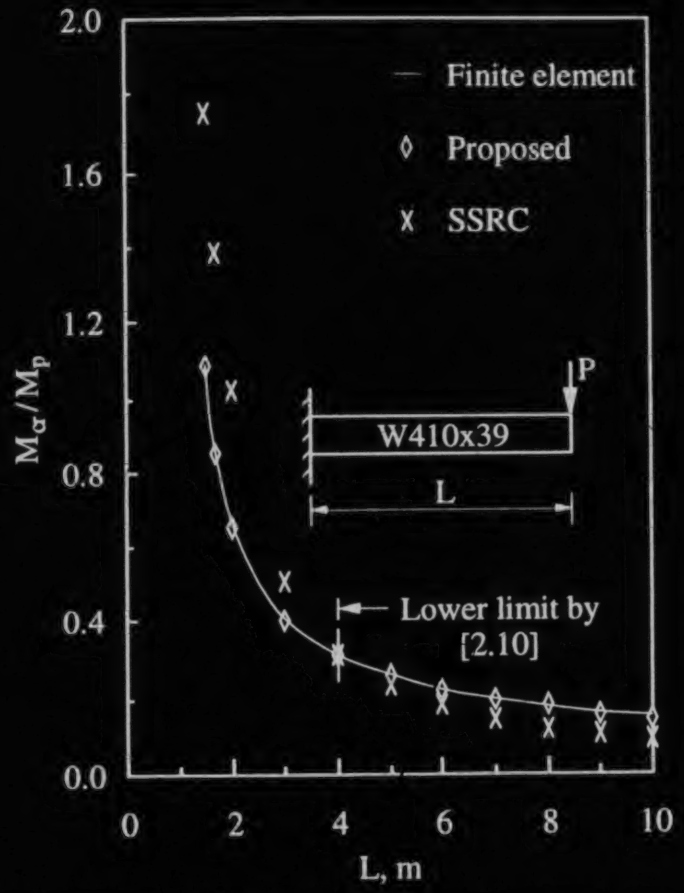

Fig. 7.1 Comparison of design rules with finite element solution for unrestrained tip, top flange loading

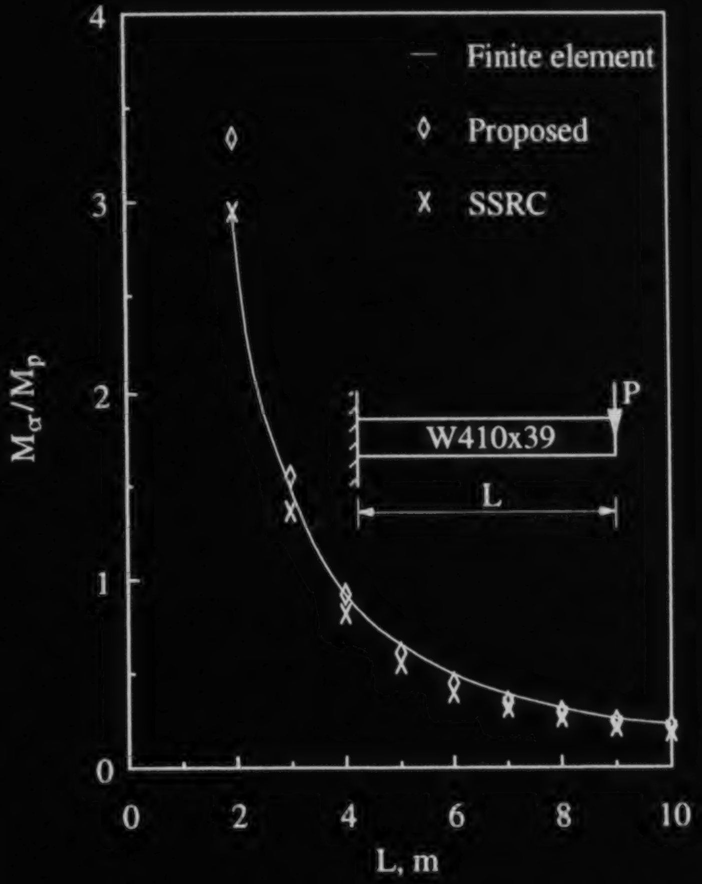

Fig. 7.2 Comparison of design rules with finite element solution for unrestrained tip, shear centre loading

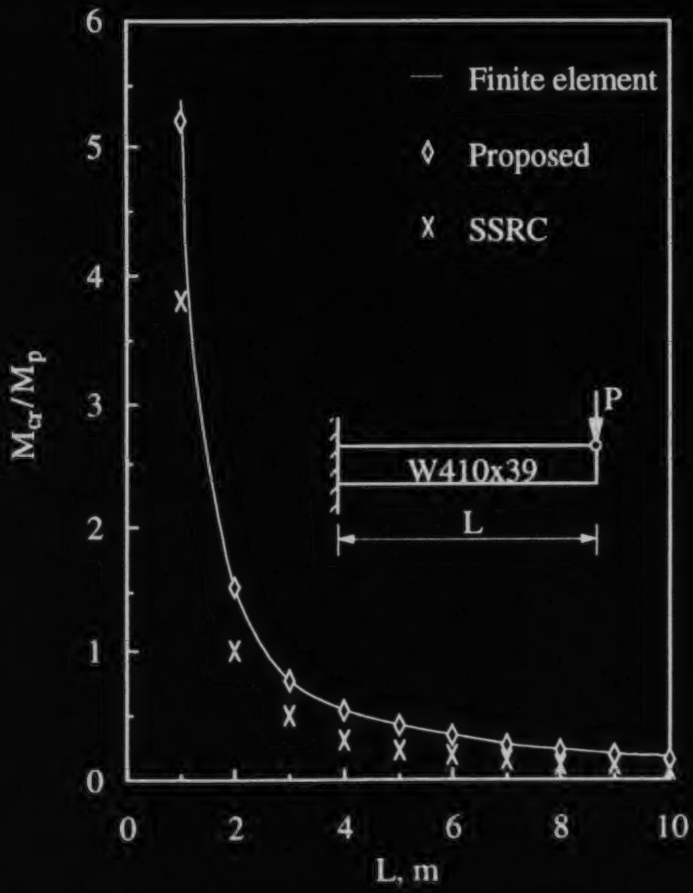

Fig. 7.3 Comparison of design rules with finite element solution for laterally restrained top flange at tip, top flange loading

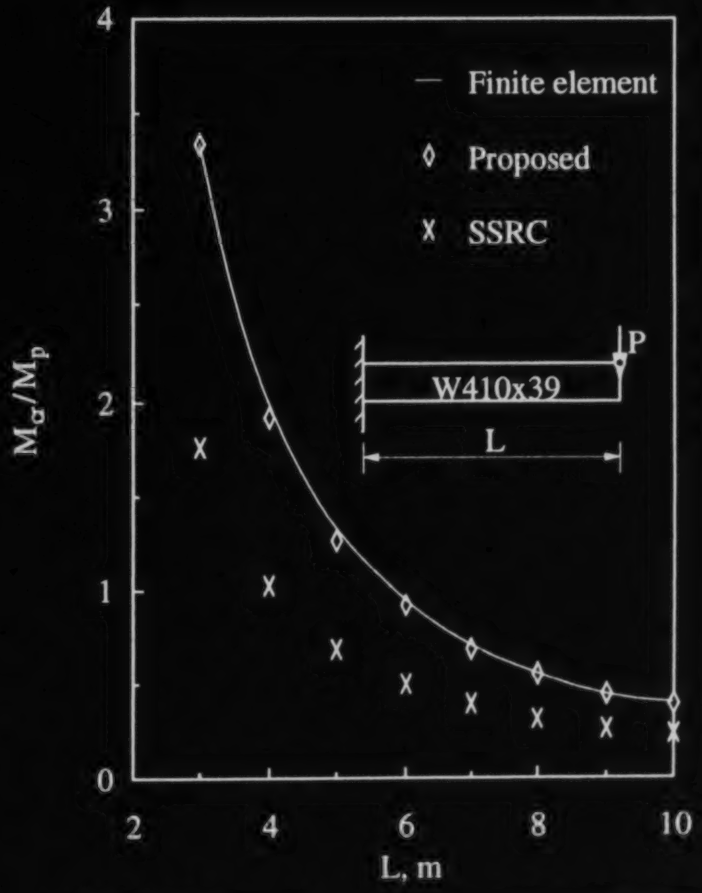

Fig. 7.4 Comparison of design rules with finite element solution for laterally restrained top flange at tip, shear centre loading

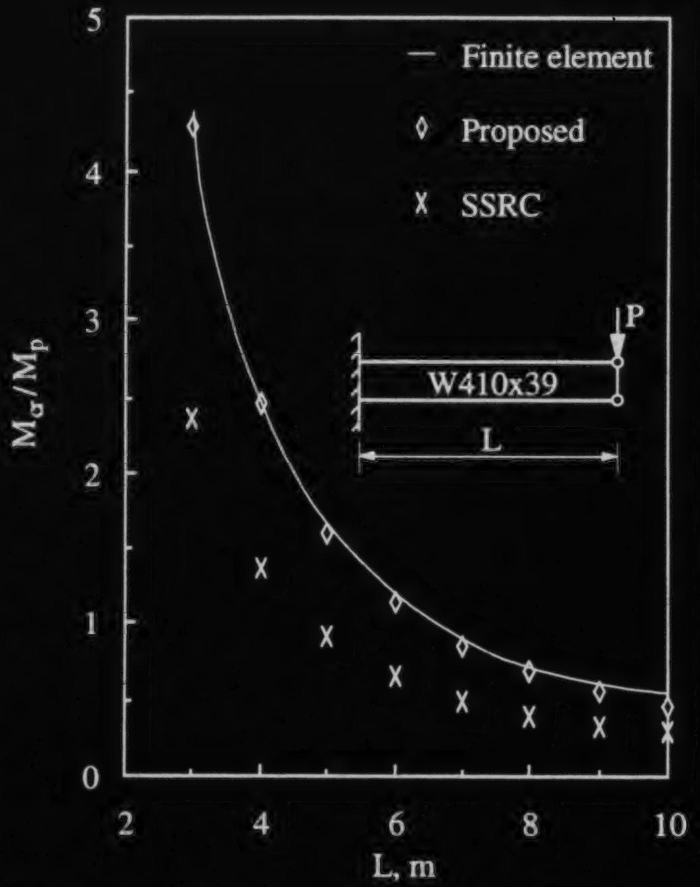

Fig. 7.5 Comparison of design rules with finite element solution for laterally restrained top and bottom flanges at tip

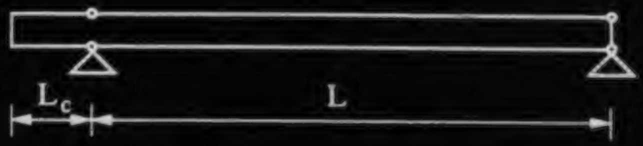

a) Free

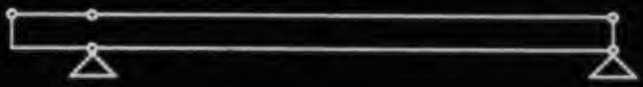

b) Laterally restrained top flange

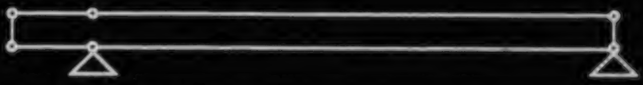

c) Laterally restrained top and bottom flanges

Fig. 7.6 Restraint conditions at the cantilever tip of overhanging beams

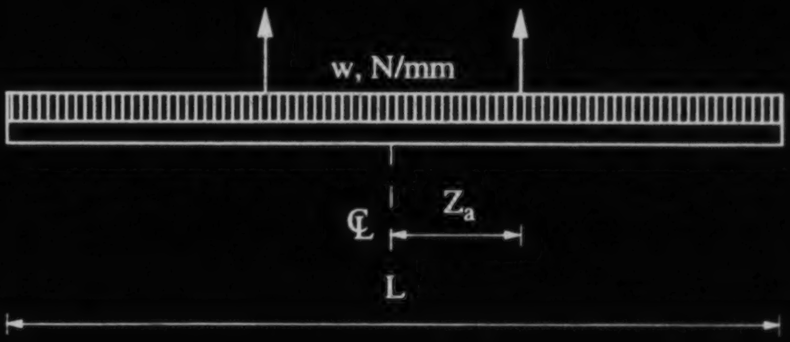

Fig. 7.7 Loading and geometry of suspended flexural member

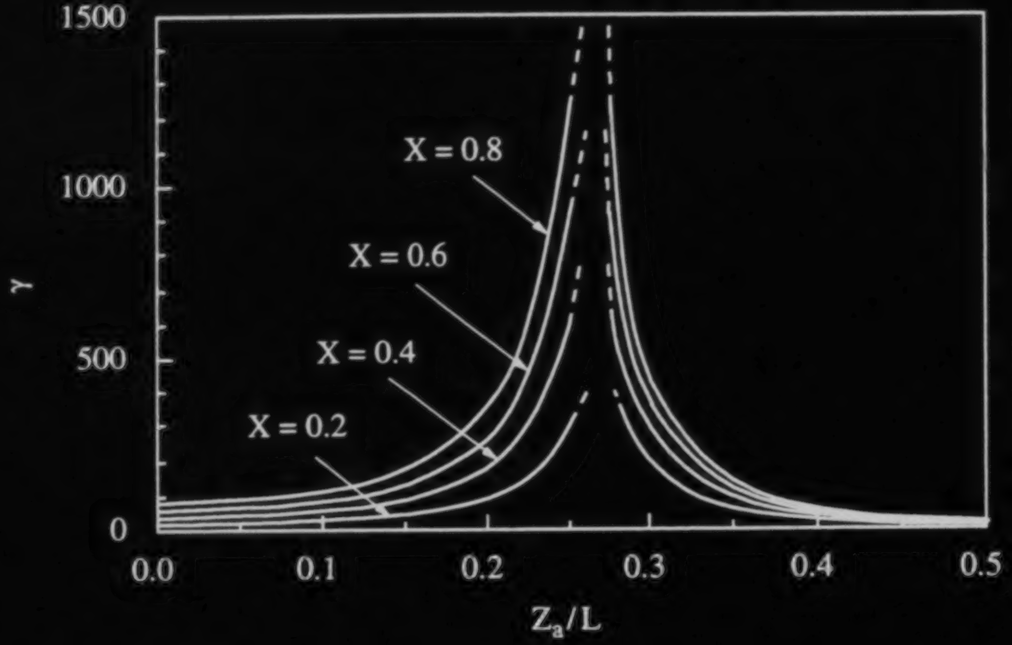

Fig. 7.8 Buckling load parameter for different lift points

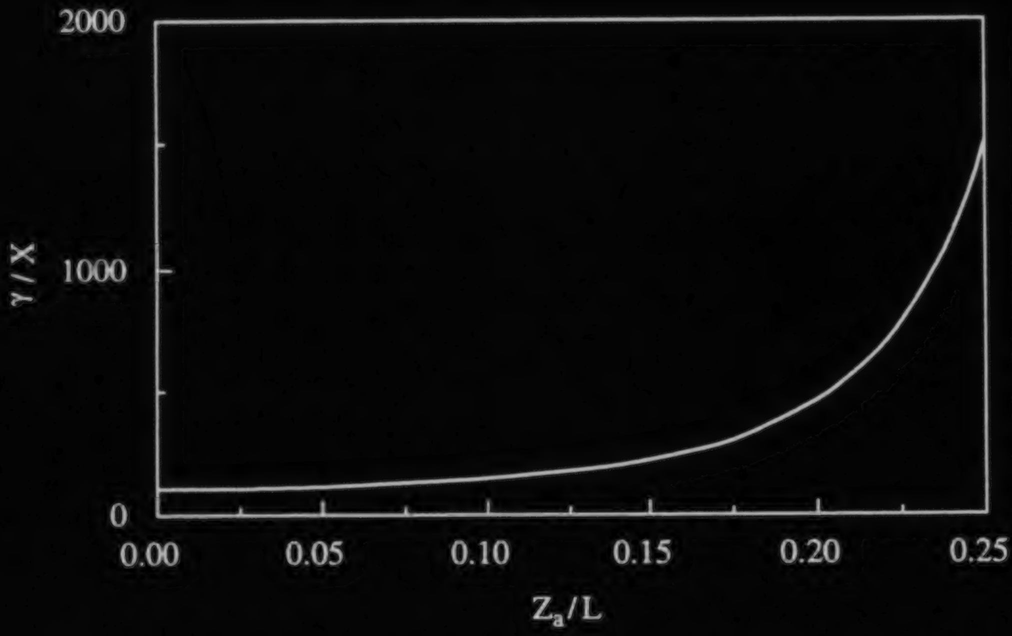

Fig. 7.9 Unique curve of buckling load parameter for members lifted near midspan

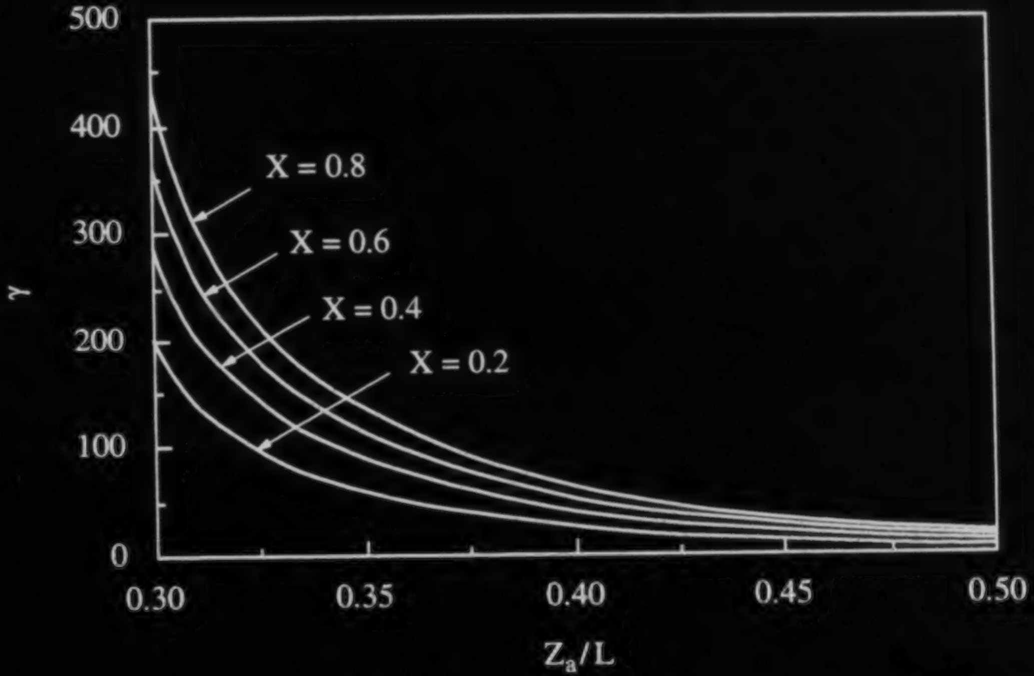

Fig. 7.10 Buckling load parameter for members lifted near ends

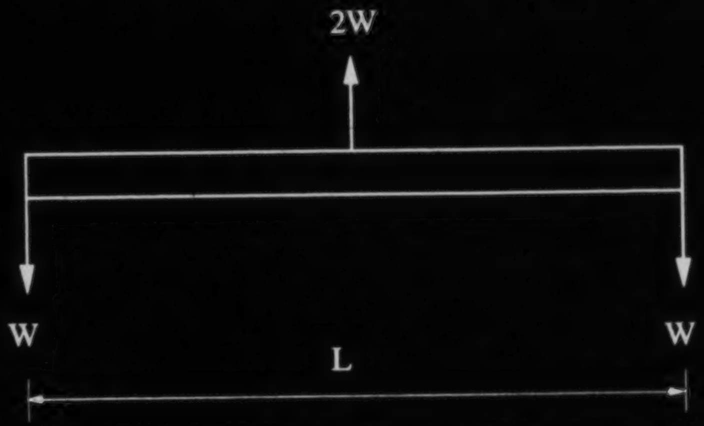

Fig. 7.11 Spreader beam lifted at midspan

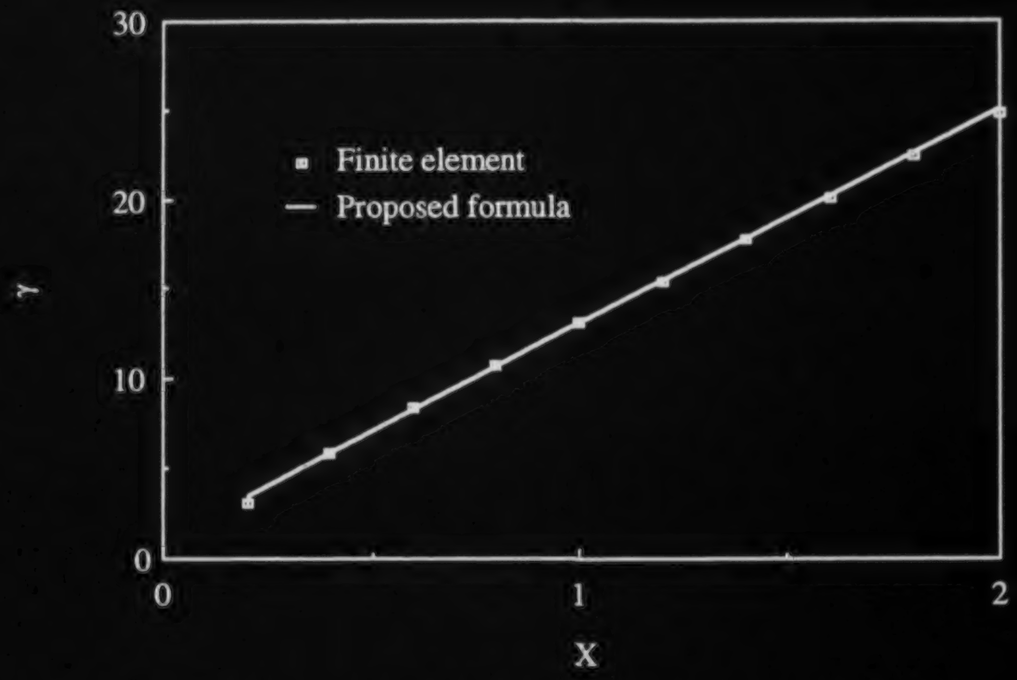

Fig. 7.12 Buckling load parameter for spreader beam lifted at midspan

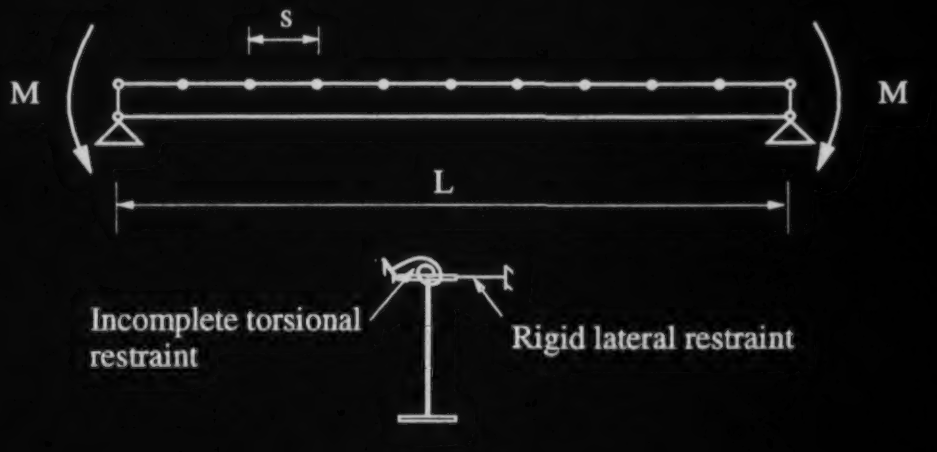
s
M
M
L
Incomplete torsional restraint
Rigid lateral restraint

Fig. 7.13 Simply supported restrained beam under uniform moment

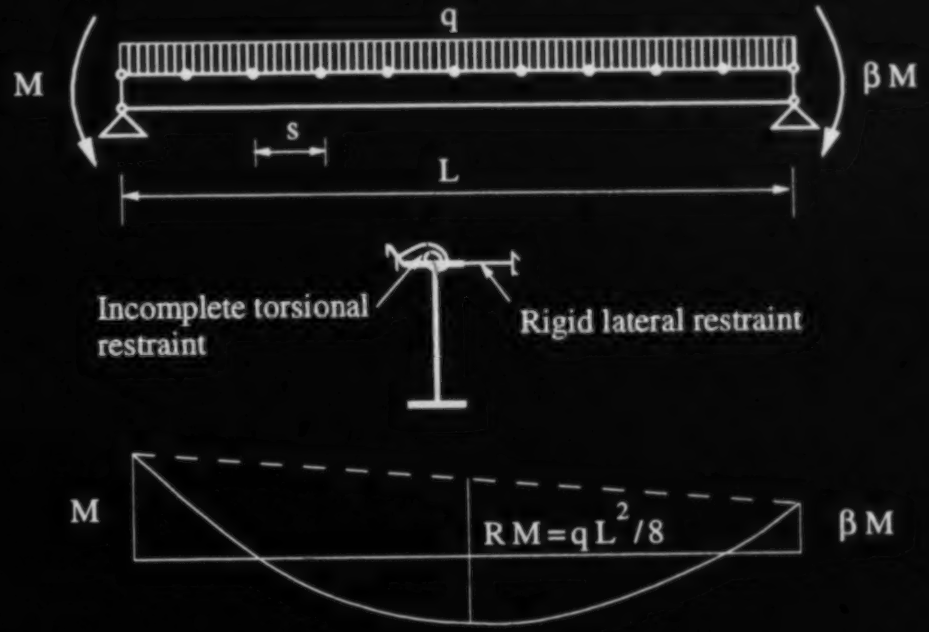
q
M
βM
s
L
Incomplete torsional restraint
Rigid lateral restraint
M
RM=qL²/8
βM

Fig. 7.14 Simply supported restrained beam under nonuniform moment

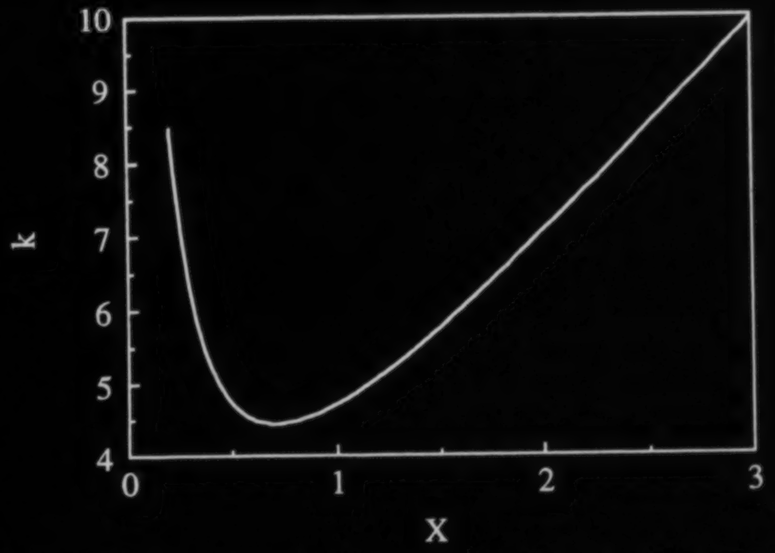

Fig. 7.15 Effective buckling coefficient for beams under uniform moment

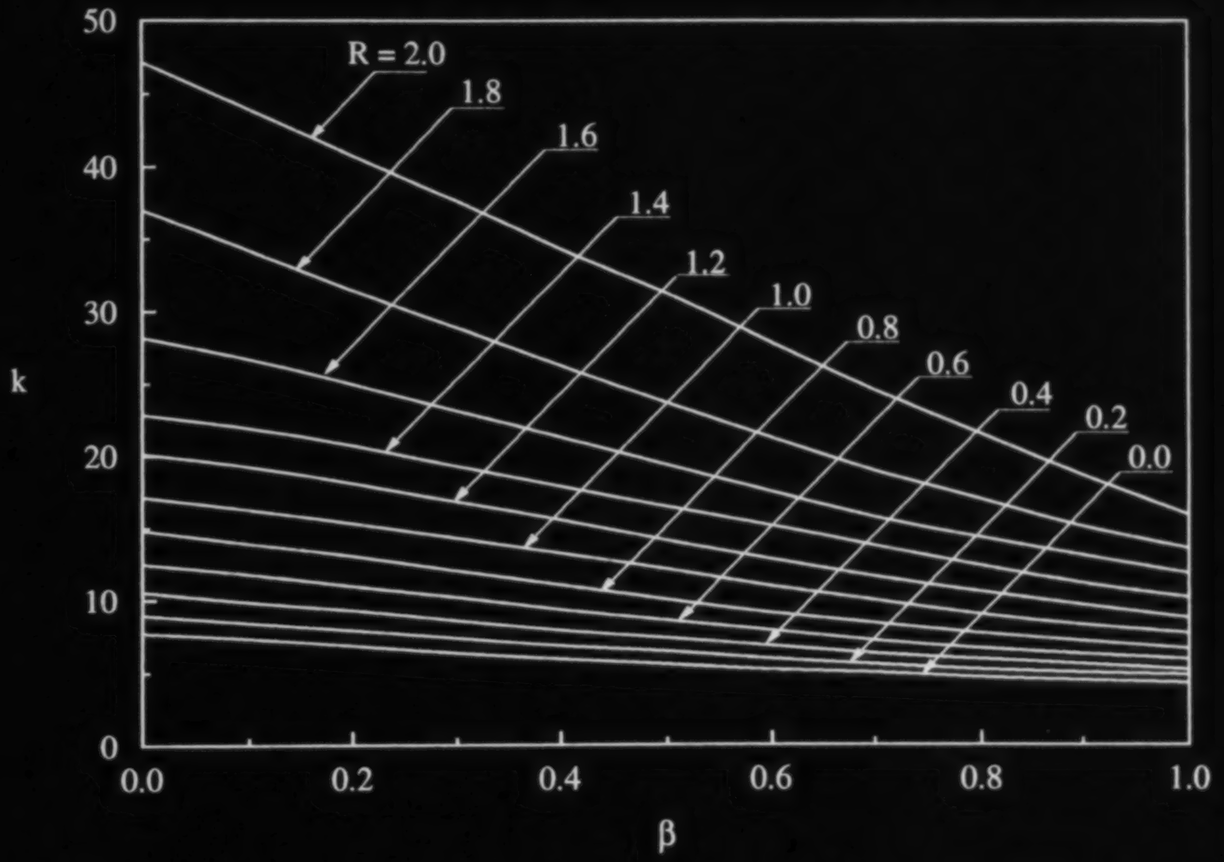

Fig. 7.16 Effective buckling coefficients for free-to-warp back span

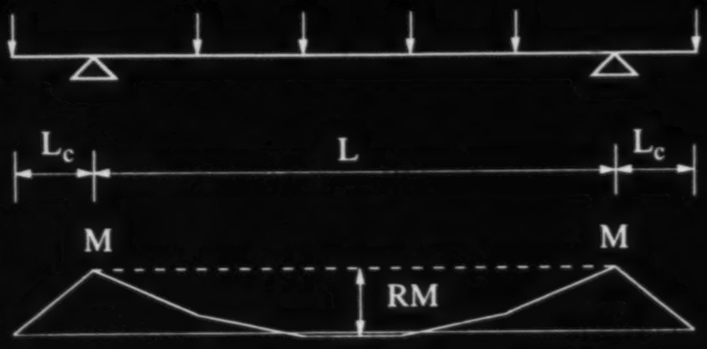

Fig. 7.17 Double overhanging beam with symmetrical geometry, loading and restraint conditions

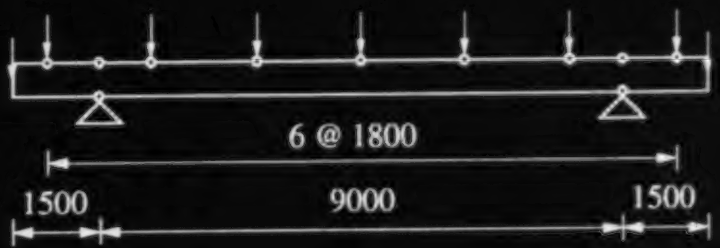
6 @ 1800
1500
9000
1500

a) Forked system

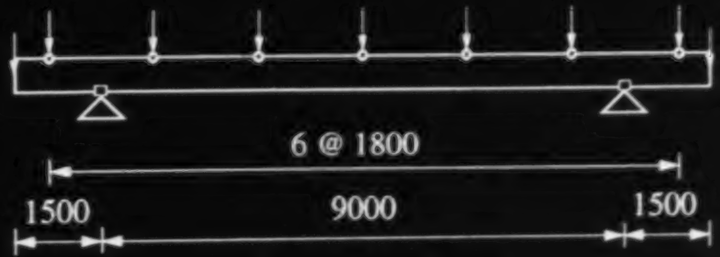
6 @ 1800
1500
9000
1500

b) Unforked system

Fig. 7.18 Case studies, effect of shape of bending moment diagram

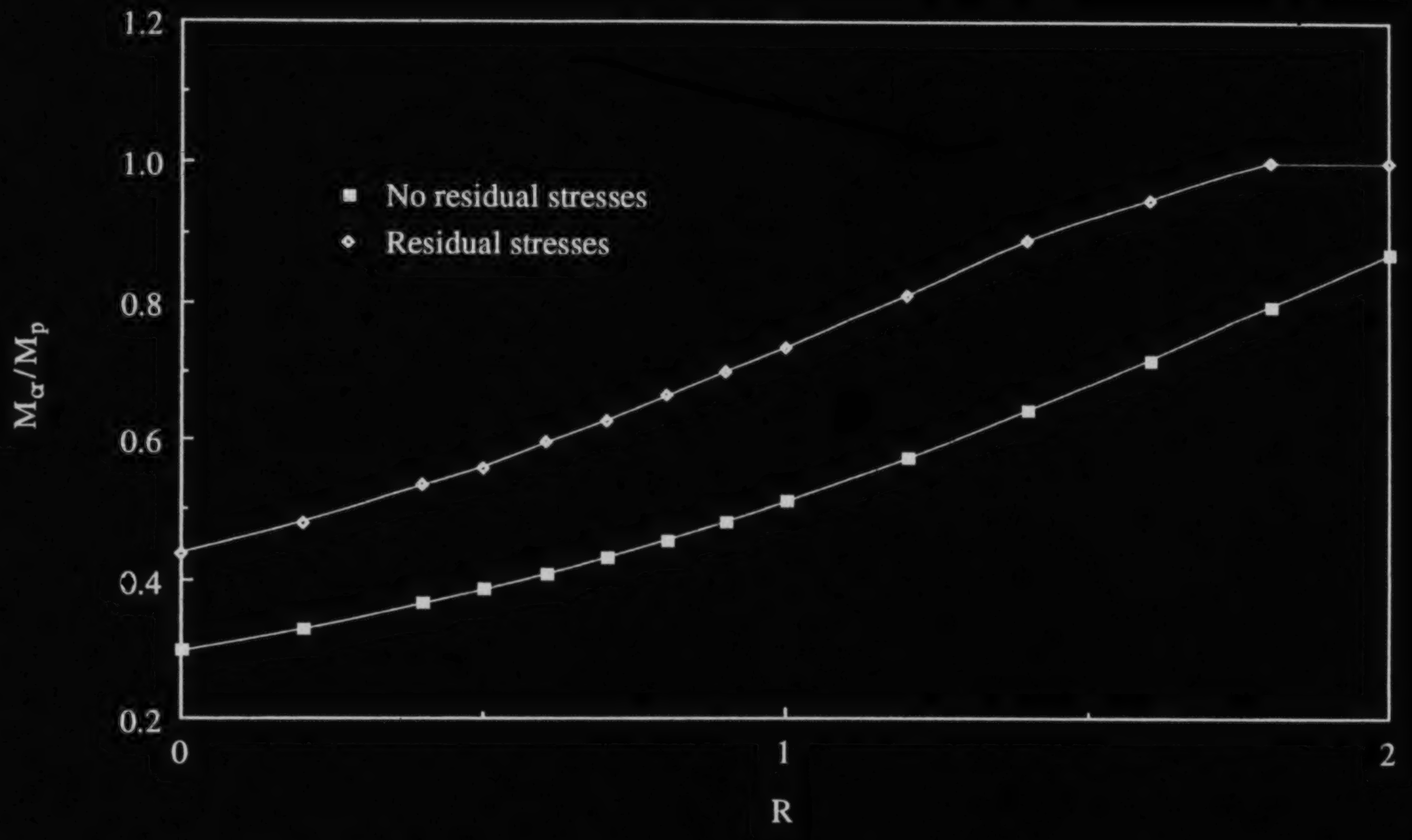

Fig. 7.19 Effect of shape of bending moment on the buckling capacity of forked system

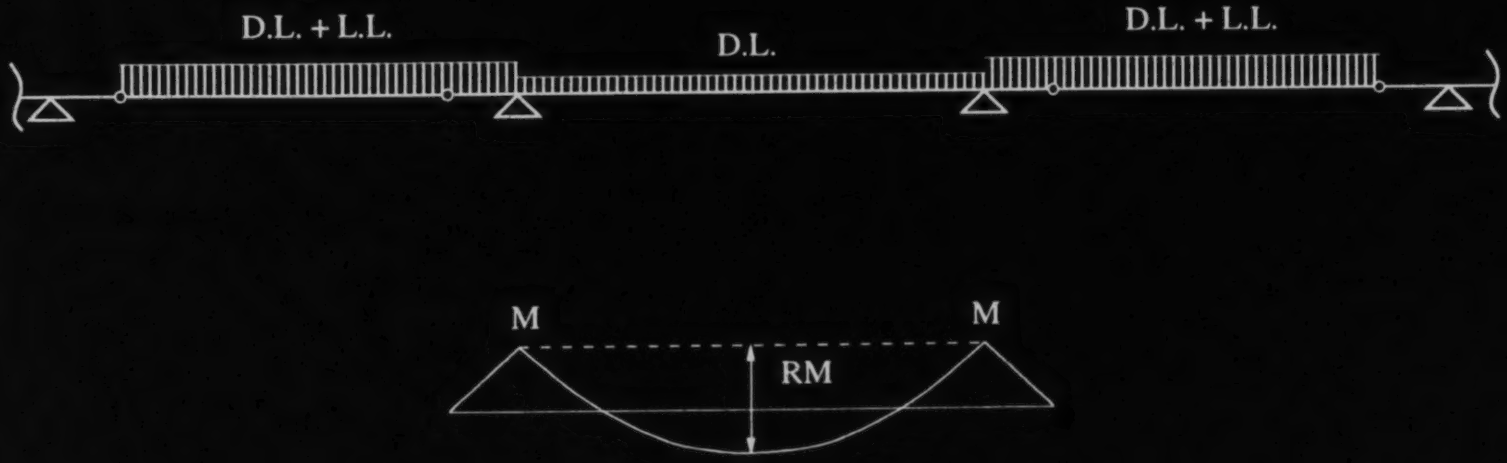
D.L. + L.L.
D.L.
D.L. + L.L.
M
M
RM

Fig. 7.20 Critical loading condition for beams with fork supports

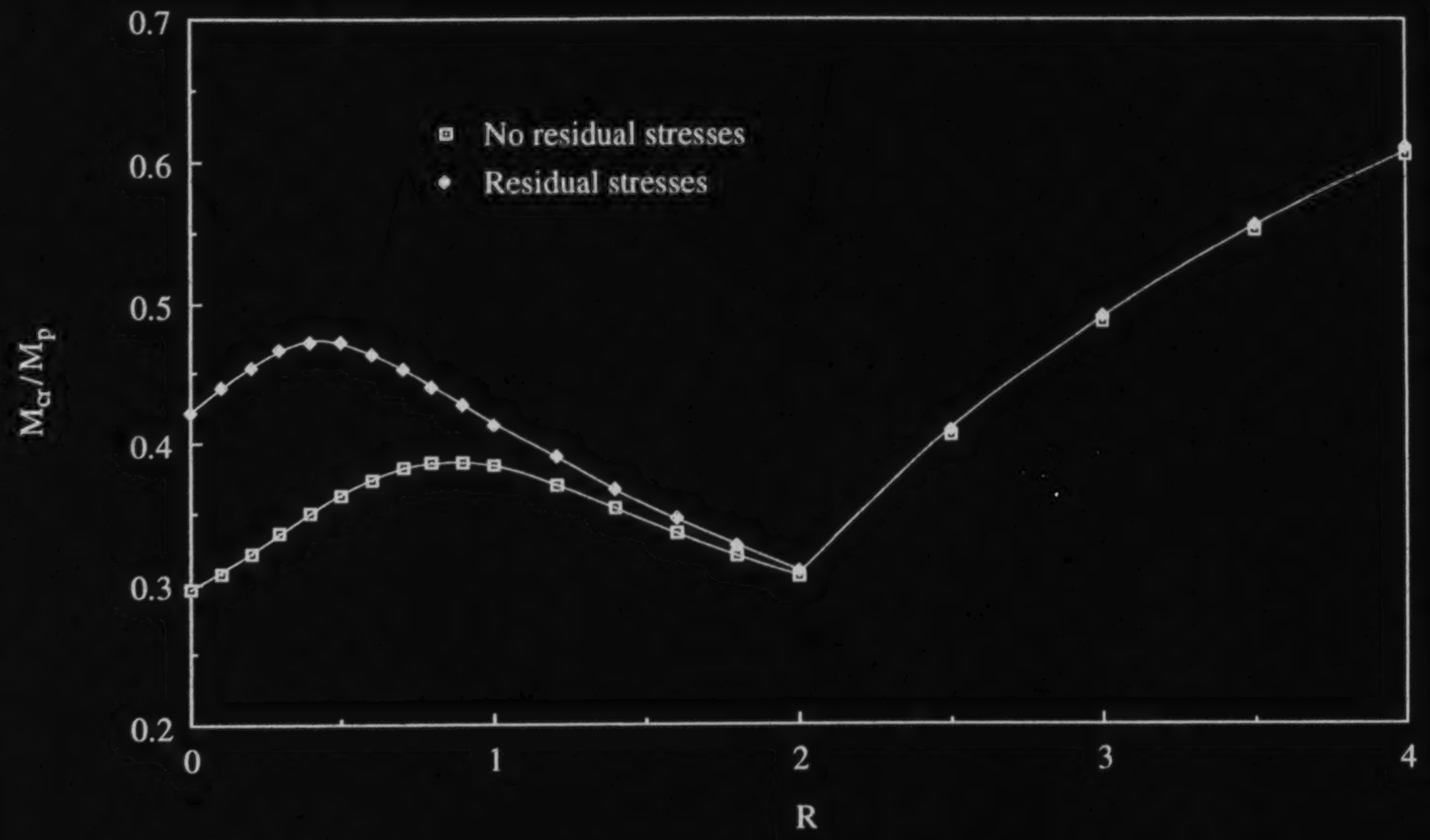

Fig. 7.21 Effect of shape of bending moment on the buckling capacity of unforked system

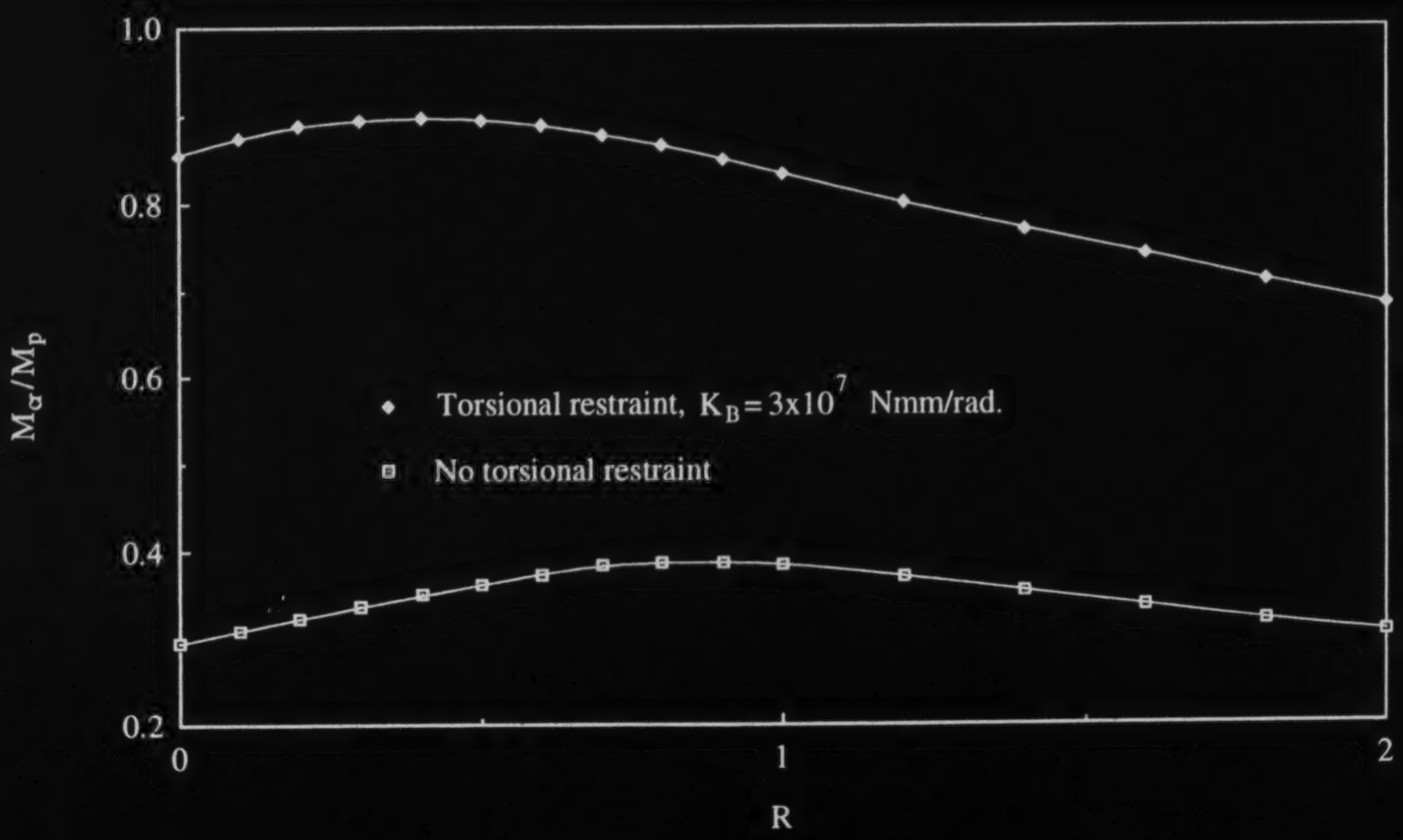

Fig. 7.22 Effects of shape of bending moment and torsional restraint on the buckling capacity of unforked system

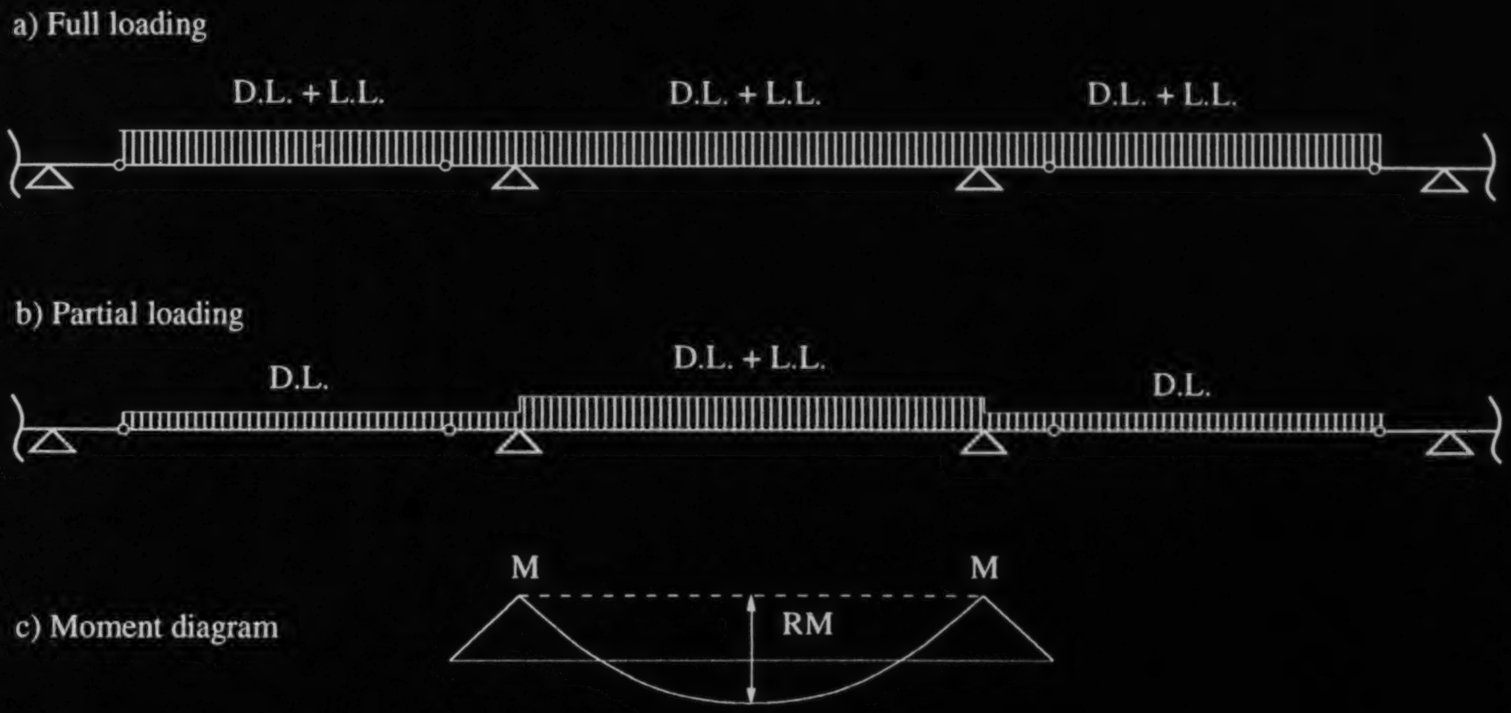
a) Full loading
D.L. + L.L.
D.L. + L.L.
D.L. + L.L.
b) Partial loading
D.L.
D.L. + L.L.
D.L.
c) Moment diagram
M
M
RM

Fig. 7.23 Loading conditions for beams without fork supports

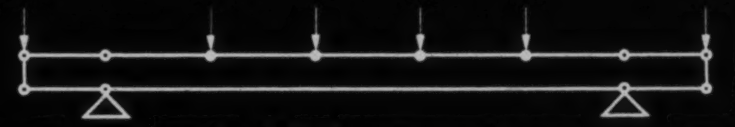

a) Case 1

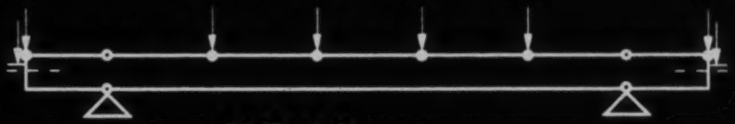

b) Case 2

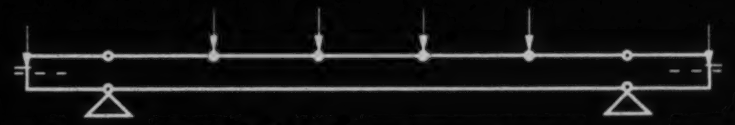

c) Case 3

Fig. 7.24 Design cases for beams with fork supports

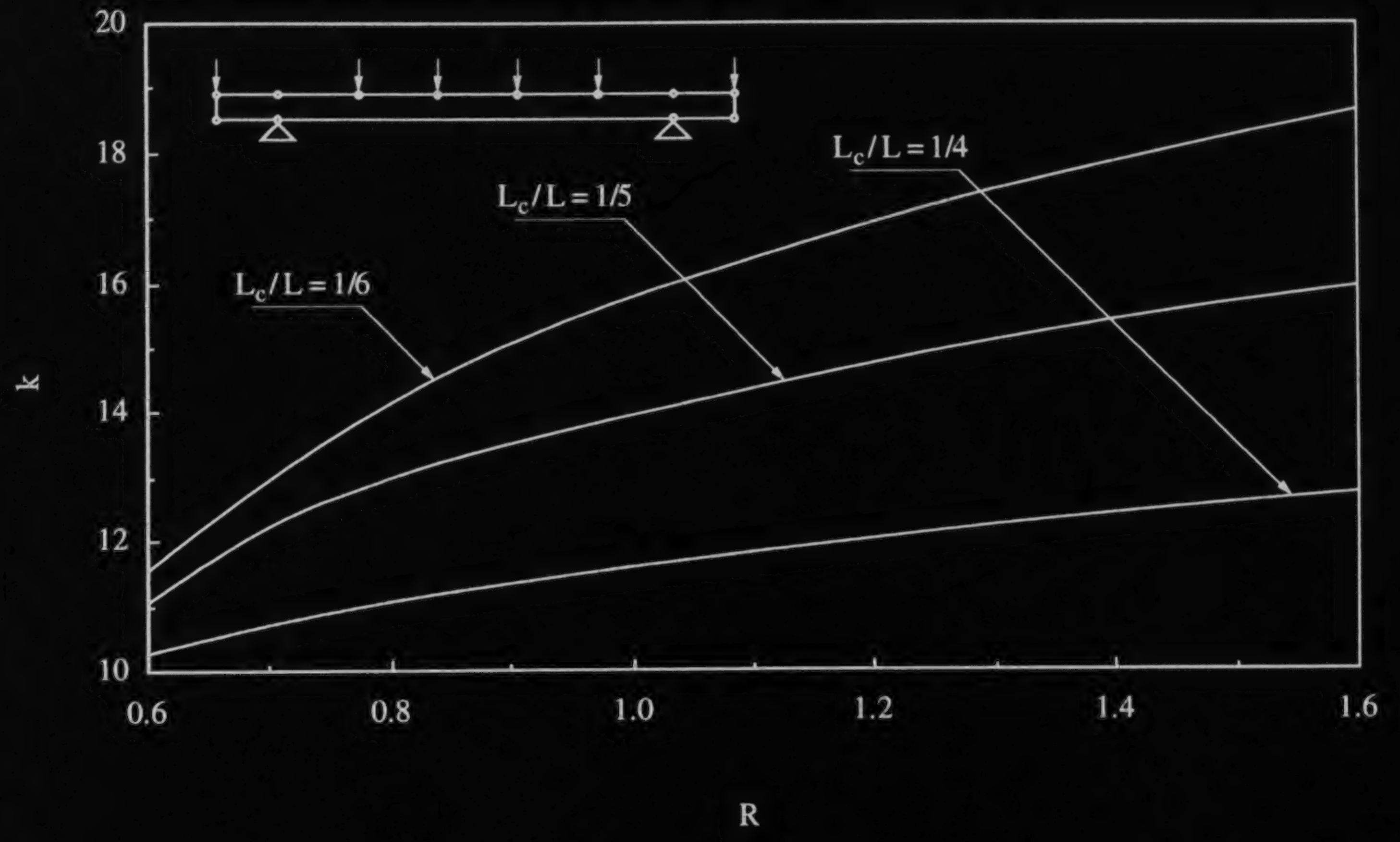

Fig. 7.25 Design curves for beams with fork supports, case 1

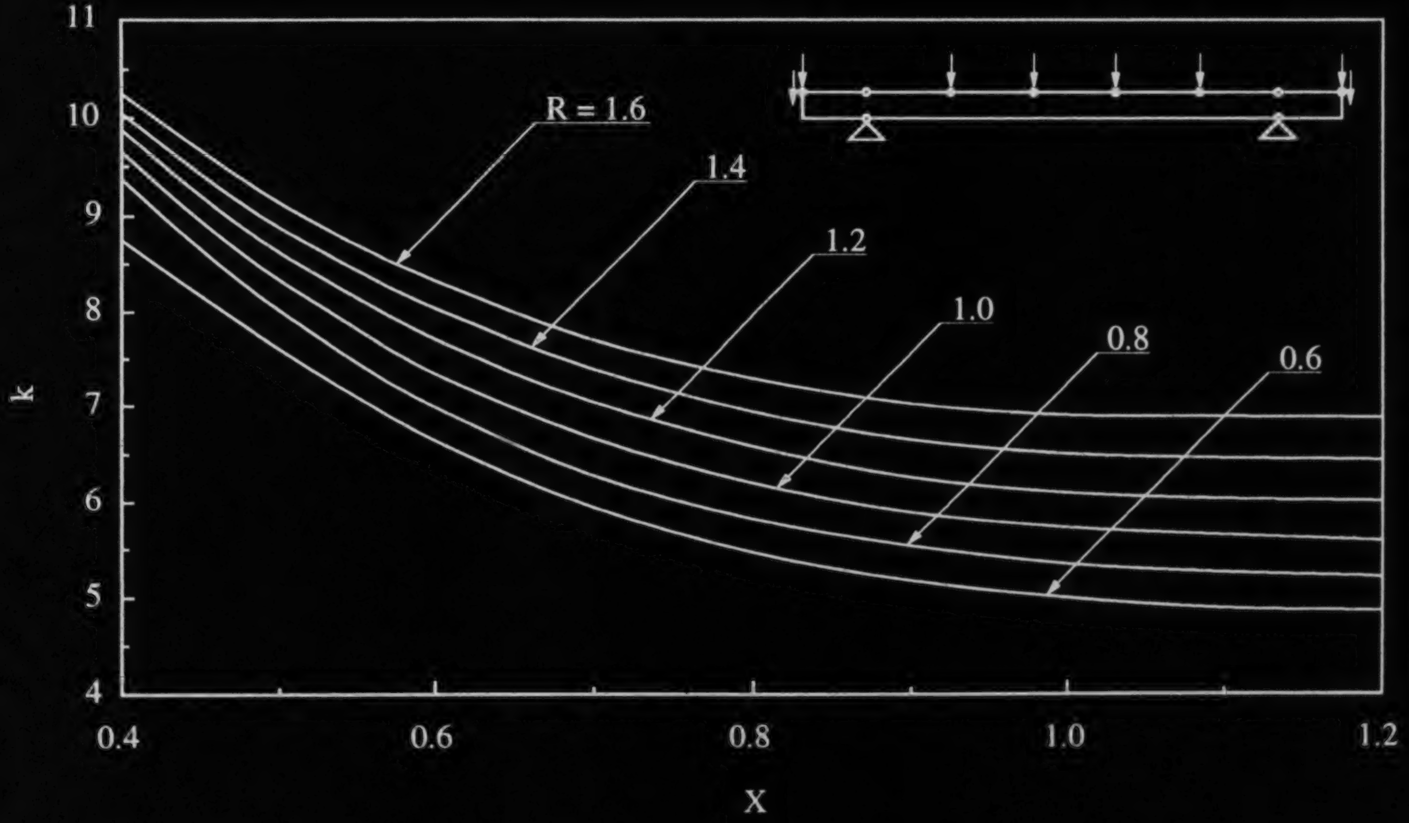

Fig. 7.26 Design curves for beams with fork supports, case 2

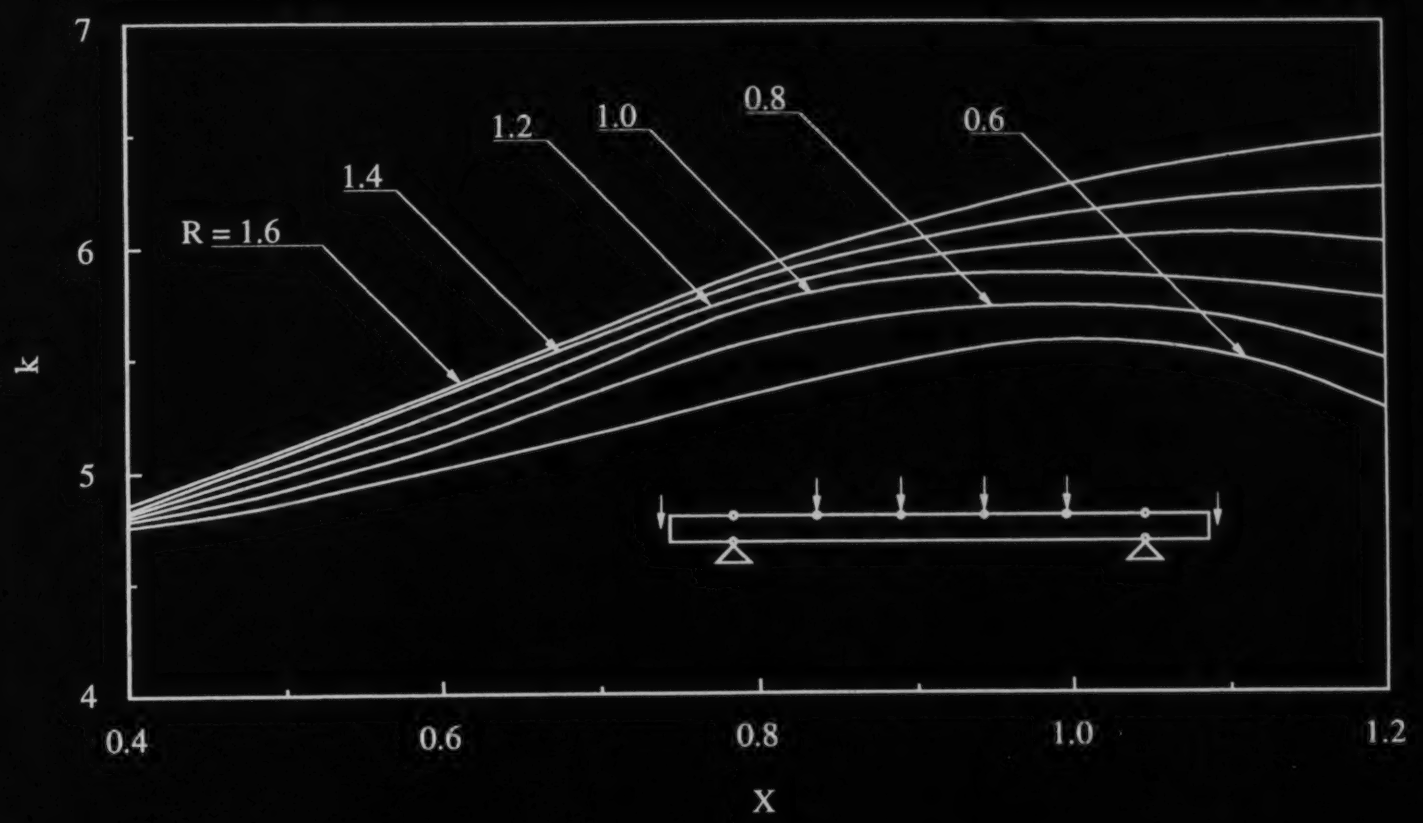

Fig. 7.27 Design curves for beams with fork supports, case 3 with $L_c / L = 0.25$

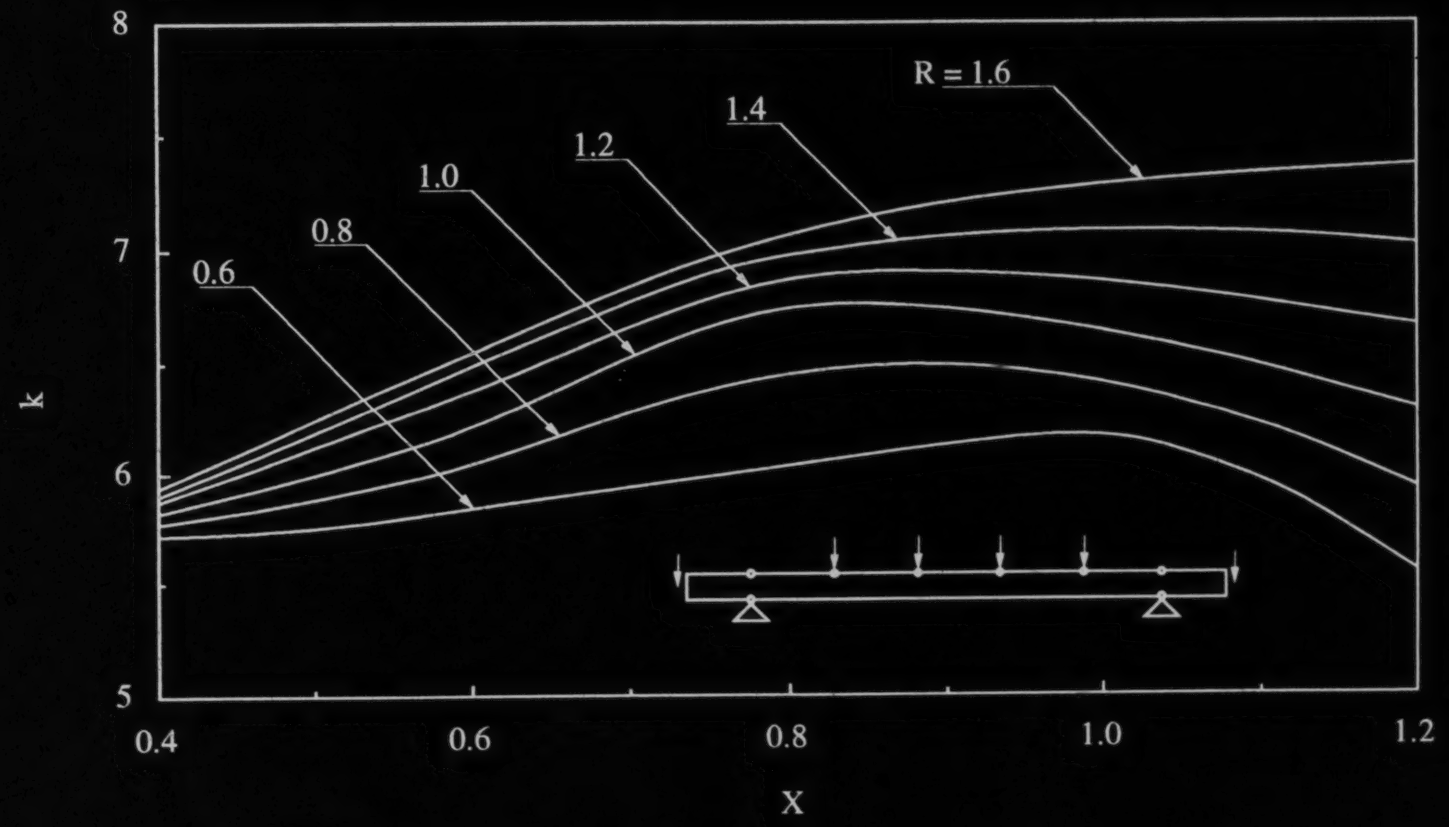

Fig. 7.28 Design curves for beams with fork supports, case 3 with $L_c / L = 0.20$

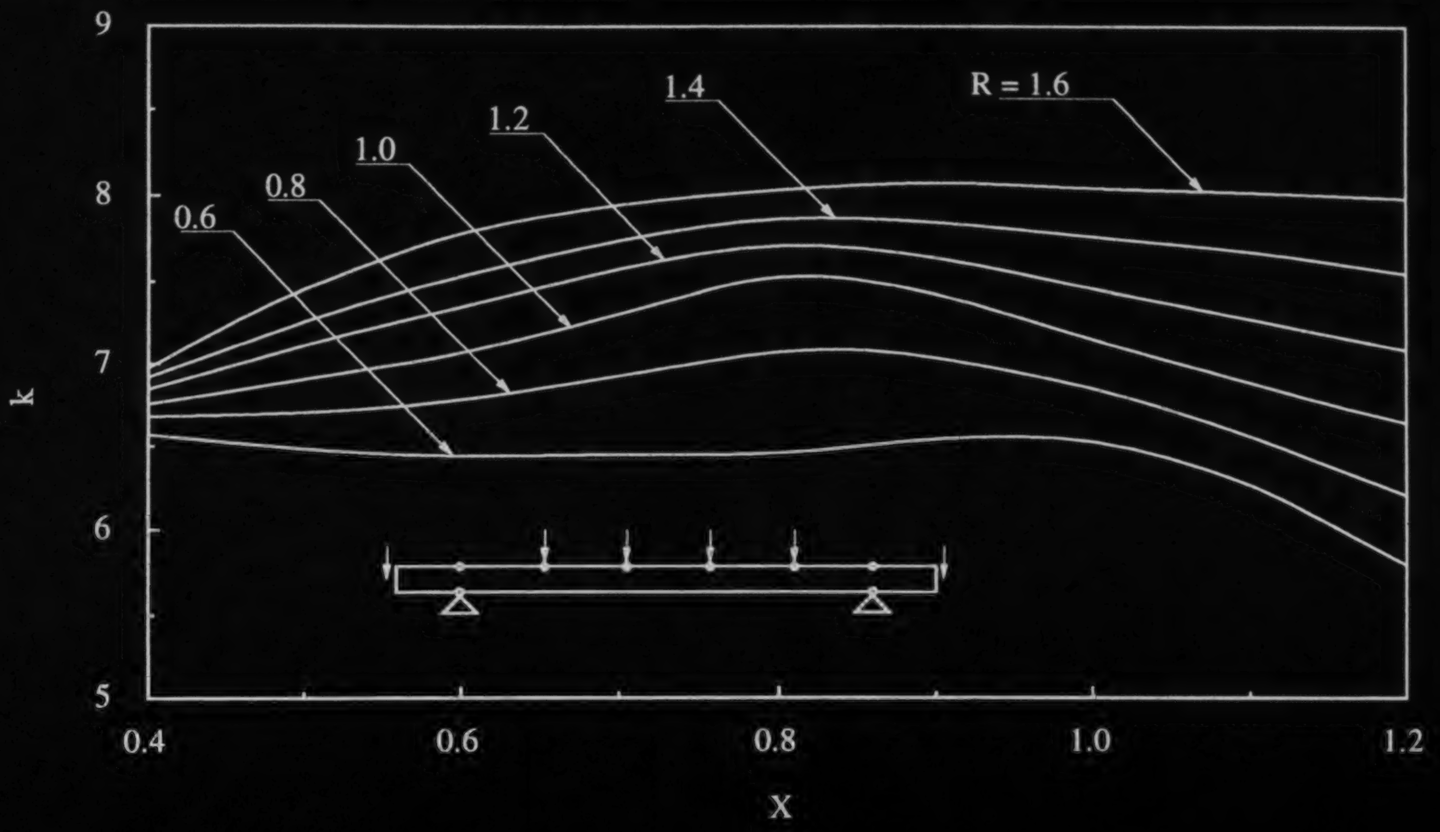

Fig. 7.29 Design curves for beams with fork supports, case 3 with $L_c / L = 0.167$

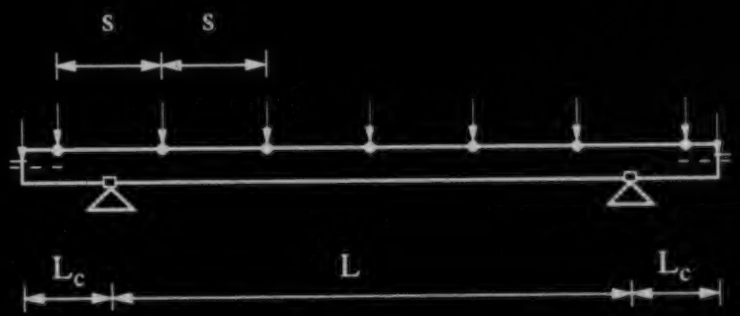

Fig. 7.30 Geometry of beam without fork supports

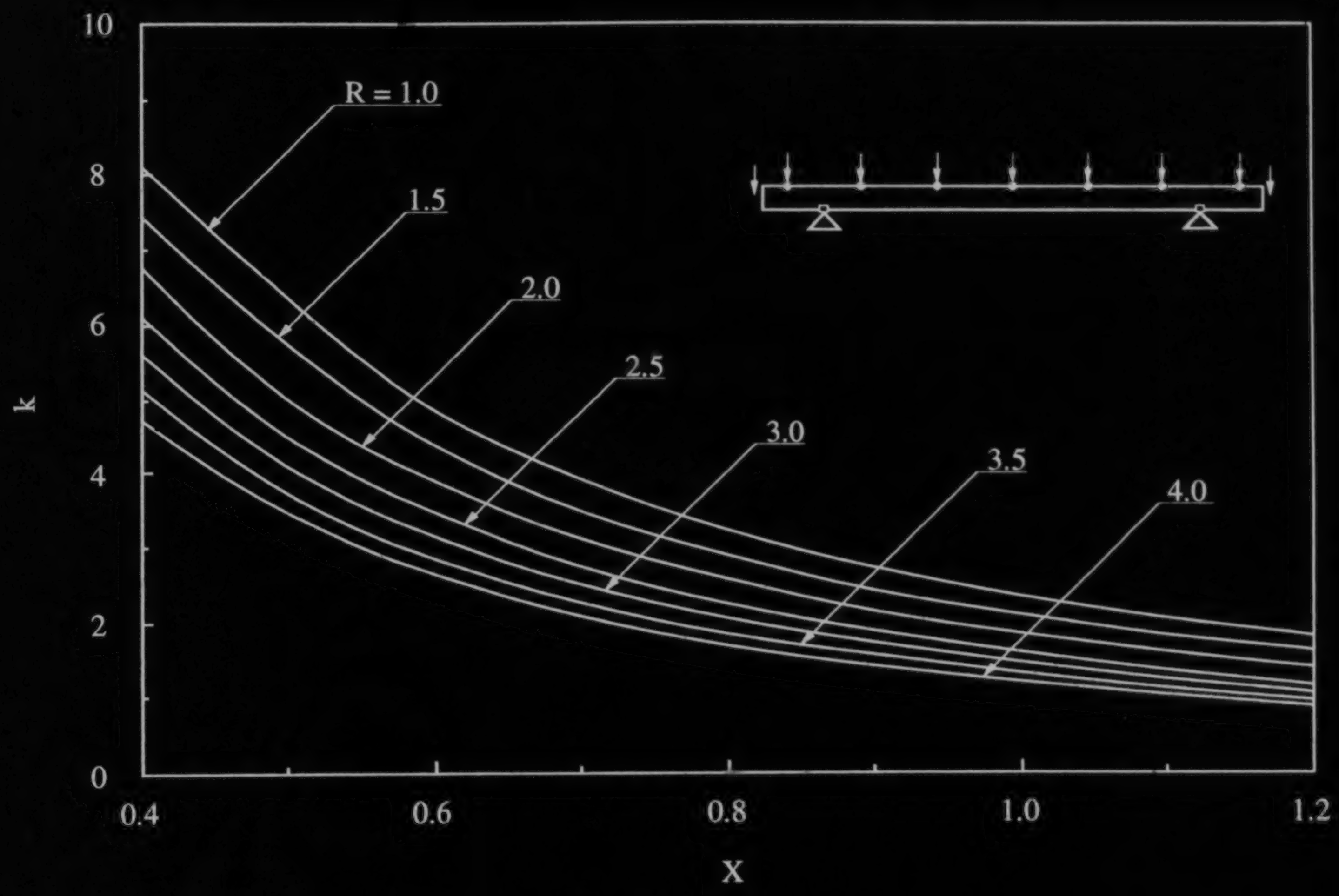

Fig. 7.31 Design curves for beams without fork supports

Chapter 8

CONCLUSIONS

8.1 Observations and conclusions

1. Residual stresses were determined using a sectioning technique in which the gauge length was established between hardened steel balls pressed into the steel surface. The measuring procedure gives good repeatable readings and consequently very reliable results.

2. Based on the determined residual stress patterns of two different W-shaped beam cross sections, it is expected that a wide range of beams used in real structures would buckle elastically even though the critical buckling moment may be just slightly less than the yield moment. This arises because residual stresses patterns in hot-rolled W-shaped beam sections with relatively narrow flanges are significantly different from those in column sections. Most of the flange is in tension and at the flange tips the residual stresses are either tensile or of small compressive value. Most of the web is under compression, with high tensile stresses at the web-flange junction. Because of the favourable tensile stresses in the flanges, there is a stabilizing effect increasing the range of elastic behaviour. The geometric stiffness of the flanges is increased over inelastic values and the onset of lateral instability is delayed.

3. The analytical method modelling web distortion, residual stresses, and inelastic behaviour is reliable in predicting the

distortional buckling capacity of steel beams under a variety of loading and restraint conditions, as confirmed by a test/predicted ratio of 0.99 with a coefficient of variation 0.066 for 31 tests.

4. The experimental results are very sensitive to unforeseen restraints. Even a minimal amount of friction will force the beam into a higher energy buckling mode. In test 6, for example, it was observed that a relatively small amount of friction between the ball bearings and the bearing plates was sufficient to restrain the top flange laterally, forcing the beam into a higher energy buckling mode. The corollary is that the lateral bracing force required to restrain a real beam is quite small.

5. Because the bifurcation model predicted the test results closely, the influence of initial imperfections on the buckling strength does not appear to be significant so long as the imperfections are within rolling and fabrication tolerances.

6. The effects of web distortion are particularly significant for beams with relatively deep cross sections and thin webs, and especially when the beam is braced torsionally along one flange or when the load is applied relatively high above the shear centre. When a web stiffener is introduced at a section where one flange is torsionally restrained, the overall stability is enhanced by eliminating web distortion and preventing twisting of the cross section about its longitudinal axis.

7. When open-web steel joists are properly welded to supporting

beams, they provide both lateral restraint to the top flange and torsional restraint through their flexural action. The provision of torsional restraint to the top flange further improves the buckling strength by forcing the beam into a distortional buckling mode. The in-plane bending stiffness of open-web steel joists is relatively large, particularly when the joist acts compositely with a concrete slab. The torsional restraint provided to the beam enhances its stability dramatically, even though it acts at discrete locations only and twisting of the braced flange between bracing points tends to localize the effect of torsional bracing. This bracing is considered reliable in enhancing the beam stability.

8. Both the experimental and theoretical results show that the restraint conditions dominate the behaviour of steel beams in cantilever-suspended span construction. At the same time the shape of the moment diagram, that is to say, which flange and how much of it is in compression, is significant.

9. When lateral restraint is not supplied to the column at the cantilever root, otherwise identically loaded and restrained beams have failure loads reduced to as low as 30% of those when such restraint is provided.

10. Lateral restraint of the top flange is particularly effective in increasing the buckling strength when it is provided where that flange is in compression.

11. For beams with fork supports in cantilever-suspended span

construction, the additional conditions that most enhance the beam stability are joists with bottom chord extensions to provide lateral support to the bottom flange of the beam at each cantilever tip.

12. While the critical loading condition for a beam with fork supports is obtained by maximizing the negative moment at the supports and minimizing the positive moment within the back span, two loading conditions need to be investigated for a beam without fork supports that can translate at the column supports. Web distortion predominates in the latter case.

13. The effective length factors for cantilever beams given by the SSRC Guide (Galambos 1988) tend to give unreliable results because the original limitation on the beam parameter was overlooked and the original restraint assumptions in deriving these factors are overly conservative.

14. The effective length factors for overhanging beams given by the SSRC Guide do not take into account the restraint and loading conditions of the back span and the ratio of the cantilever to the back span. This results in inaccurate, and, in some cases, unconservative designs.

15. Although the general design procedure for beams in cantilever-suspended span construction given by the Canadian Institute of Steel Construction (1989) neglects the beneficial effect of torsional restraint, unconservatism may result due to the destabilizing effect of loads applied above the shear centre.

16. When a beam is braced laterally and torsionally along one flange, the effective length concept is not accurate in predicting its lateral-torsional buckling resistance.

17. The design procedures proposed here to predict the lateral-torsional buckling resistances of cantilever beams are in good agreement with the finite element results.

18. The buckling resistance of a beam lifted under self-weight, is greatest when the cables are placed near the quarter points. In the vicinity of that optimum location, the buckling resistance is extremely sensitive to the cable attachment position. The design procedure to predict the lateral-torsional buckling resistance of such beams given here is in good agreement with finite element analyses.

19. Design procedures are developed for cantilever-suspended span beams under a variety of loading and restraint conditions based on the distortional buckling model that is in excellent agreement with the finite element model, itself corroborated by tests. Resistance factors proposed for these design procedures range from 0.85 for the case when the column supports are not restrained laterally to 0.90 for the case when fork supports are provided.

8.2 Areas of further research

Areas that need further research are:

1. Studies are needed to evaluate the residual stress distributions in a wide range of beam sections with relatively narrow flanges. Based on these studies, more accurate predictions for the inelastic lateral-torsional buckling can be developed, taking into account the expected beneficial effect of residual stresses in extending the elastic range.

2. The development of design formulas for single overhanging cantilever beams in cantilever-suspended span construction.

3. It is expected that loading conditions which involve wind suction loads, are not critical because they are countered by the dead loads and because they act upwards at the level of top flange, giving a significant stabilizing effect. However, it is recommended that design formulas be developed for such loading conditions of cantilever-suspended span beams.

4. The design approach suggested here, accounting for the effect of torsional restraint offered by the joists with welded seats should be extended to joists with bolted seats provided that moment-rotation characteristics of such connections are established.

REFERENCES

Akay, H.U., Johnson, C.P. and Will, K.M. 1977. Lateral and local buckling of beams and frames. Journal of the Structural Division, American Society of Civil Engineers, Vol. 103, No. ST9, pp. 1821-1832.

Albert, C., Essa, H.S. and Kennedy, D.J.L. 1992. Distortional buckling of steel beams in cantilever-suspended span construction. Canadian Journal of Civil Engineering. Vol. 19, No. 5, pp. 767-780.

Ballio, G. and Mazzolani, F.M. 1983. Theory and design of steel structures. Chapman and Hall, London, England.

Bartels, D. and Bos, C.A.M. 1973. Investigation of the effect of the boundary conditions on the lateral buckling phenomenon, taking account of cross-sectional deformations. Heron. Vol. 19, No. 1, pp. 3-26.

Bathe, K.-J. 1982. Finite element procedures in engineering analysis, Prentice-Hall, Englewood Cliffs, N.J.

Bjorhovde, R. 1980. Research needs in stability of metal structures. Journal of the Structural Division, American Society of Civil Engineers, Vol. 106, No. ST12, pp. 2425-2442.

Bose, B. 1982. The influence of torsional restraint stiffness at supports on the buckling strength of beams. The Structural Engineer, Vol. 60B, No. 4, pp. 69-75.

Bradford, M.A., 1986. Inelastic distortional buckling of I-beams. Computers and Structures, Vol. 24, No. 6, pp. 923-933.

Bradford, M.A. 1988. Buckling of elastically restrained beams with web distortions. Thin-Walled Structures, Vol. 6, pp. 287-304.

Bradford, M.A. 1989. Buckling of beams supported on seats. The Structural Engineer, Vol 67, No. 23, pp. 411-414.

Bradford, M.A. and Trahair, N.S. 1981. Distortional buckling of I-beams. Journal of the Structural Division, American Society of Civil Engineers, Vol. 107, No. ST2, pp. 355-370.

Bradford, M.A. and Trahair, N.S. 1982. Distortional buckling of thin-web beam-columns. Engineering Structures, Vol. 4, No. 1, pp. 2-10.

Bradford, M.A. and Trahair, N.S. 1983. Lateral stability of beams on seats. Journal of Structural Engineering, American Society of Civil Engineers, Vol. 109, No. 9, pp. 2212-2215.

Brown, D.K. 1984. An introduction to the finite element method using basic programs. Surrey University Press, London, England.

Canadian Institute of Steel Construction. 1989. Roof framing with cantilever (Gerber) girders & open web steel joists. Willowdale, Ontario.

Canadian Standard Association (CSA). 1989. Limit states design of steel structures. National Standard of Canada CAN/CSA-S16.1-M89, Canadian Standard Association, Rexdale, Ontario.

Clough, R.W. and Felippa, C.A. 1968. A refined quadrilateral element for analysis of plate bending. Procedures, Second conference on matrix methods in structural mechanics, Air Force Institute of Technology, Wright-Patterson Air Force Base, Ohio.

Dux, P.F. and Kitipornchai, S. 1981. Inelastic beam buckling experiments. Research Report No. CE24, Department of Civil Engineering, University of Queensland, St. Lucia, Australia.

Dux, P.F. and Kitipornchai, S. 1988. Buckling of suspended I-beams. Research Report No. CE99, Department of Civil Engineering, University of Queensland, St. Lucia, Australia.

Dux, P.F. and Kitipornchai, S. 1989. Stability of I-beams under self-weight lifting. Steel Construction, Australian Institute of Steel Construction, Vol. 23, No. 2, pp. 2-11.

Essa, H.S. and Kennedy, D.J.L. 1992. Design of cantilever beams against lateral-torsional buckling. Proceedings of the 1992 Candian Society for Civil Engineering Conference. Quebec City, Quebec, Vol. IV, pp. 135-144.

Galambos, T.V. 1963. Structural members and frames. Prentice-Hall, Englewood Cliffs, N.J.

Galambos, T.V. (Editor). 1988. Guide to stability design criteria for metal structures. Structural Stability Research Council. 4th Edition, John Wiley and Sons, New York.

Goldberg, J.E., Bogdanoff, J.L. and Glauz, W.D. 1964. Lateral and torsional buckling of thin walled beams. Publications, International Association of Bridge and Structural Engineering, Vol. 24, pp. 92-100.

Goltermann, P and Svensson, S.E. 1987. Lateral distortional buckling: predicting elastic critical stress. Journal of Structural Engineering, American Society of Civil Engineers, Vol. 114, No. 7, pp. 1606-1625.

Goodier, J.N. and Barton, M.V. 1944. Effect of web deformation on the torsion of I-beams. Transactions, American Society of Mechanical Engineers, Vol. 66, pp. 35-40.

Hancock, G.L. 1978. Local, distortional and lateral buckling of I-beams. Journal of the Structural Division, American Society of Civil Engineers, Vol 104, No. ST7, pp. 1557-1571.

Hancock, G.L., Bradford, M.A. and Trahair, N.S. 1980. Web distortion and flexural-torsional buckling. Journal of the Strucural Division, American Society of Civil Engineers, Vol. 106, No. 7, pp. 1557-1571.

Horne, M.R. and Ajmani, J.L. 1969. Stability of columns supported laterally by side-rails. International Journal of Mechanical Sciences, Vol. 11, pp. 159-174.

Horne, M.R. and Ajmani, J.L. 1971. Design of column restrained by side-rails. The Structural Engineer, Vol. 49, No. 8, pp. 339-345.

Horne, M.R. and Ajmani, J.L. 1973. *Reply to discussion of* Failure of columns laterally supported on one flange. The Structural Engineer, Vol. 51, No. 7, pp. 251-260.

Humar, J.L. 1990. Dynamics of Structures. Prentice-Hall, Englewood Cliffs, N.J.

Johnson, C.P. and Will, K.M. 1974. Beam buckling by finite element procedure. Journal of the Structural Division, American Society of Civil Engineers, Vol. 100, No. ST3, pp. 669-685.

Johnson, R.P. and Bradford, M.A. 1983. Distortional lateral buckling of unstiffened composite bridge girders. Proceedings ot the international conference on instability and plastic collapse of steel structures (ed. L.J. Morris), Manchester, Sept., 20-22. Granada Publishing, London.

Kennedy, D.J.L. and Baker, K.A. 1984. Resistance factors for steel highway bridges. Canadian Journal of Civil Engineering. Vol. 11, No. 2, pp. 324-334.

Kirby, P.A. and Nethercot, D.A. 1979. Design for structural stability. Constrado Nomographs, Granada Publishing, London.

Kitipornchai, S. and Richter, N.J. 1978. Elastic lateral buckling of I-beams with discrete intermediate restraints. Civil Engineering Transactions, The Institution of Engineers, Australia. Vol. CE20, No. 2, pp. 105-111.

Kitipornchai, S. and Trahair, N.S. 1975. Inelastic buckling of simply supported steel I-beams. Journal of the Structural Division, American Society of Civil Engineers, Vol. 101, No. ST7, pp. 1333-1347.

Lee, G.C. 1960. A survey of the literature on the lateral instability of beams. Welding Research Council Bulletin, Vol 63, Aug, pp.

Lindner, J. 1972. Gebundene Kippung beim Einfeldtrager mit Kragarm. Der Stahlbau, Vol. 41, No. 7, pp. 216-218.

Lindner, J. 1987. Stabilisierung von Tragern durch Trapezbleche (Stabilization of supporting I-beams by corrugated sheeting). Der Stahlbau, Vol. 55, No. 1, pp. 9-15.

Mehta, P.B. 1981. A graphical method for design of cantilevered and suspended beams. Engineering Journal, American Institute of Steel Construction, Vol. 18, No. 2, pp. 54-57.

Michell, A.G.M. 1899. Elastic stability of long beams under transverse forces. Philosophical Magazine, Nov., Vol. 48.

Milner, H.R. 1975. The elastic buckling of equal flanged beams torsionally restrained by discrete braces. Proceedings of the 5th Australian Conference on the mechanics of structures and materials, Melbourne, Australia. pp. 405-420.

Milner, H.R. 1977a. The Design of simple supported beams braced against twisting on the tension flange. Civil Engineering Transactions, Institution of Engineers, Australia, Vol. CE19, No. 1, pp. 84-91.

Milner, H.R. 1977b. Tests on equal flanged beams braced against twisting on the tension flange. Civil Engineering Transactions, Institution of Engineers, Australia, Vol. CE19, No. 1, pp. 92-100.

Milner, H.R. and Rao, S.N. 1978. Strength and stiffness of moment resisting beam-purlin connections. Civil Engineering Transactions, Institution of Engineers, Australia, Vol. CE20, No. 1, pp. 37-42.

Milner, H.R. and Rao, S.N. 1983. The design of tension flange braced beams. Proceedings ot the international conference on instability and plastic collapse of steel structures (ed. L.J. Morris), Manchester, Sept., 20-22. Granada Publishing, London.

National Research Council of Canada. 1985. National building code of Canada. Ottawa.

Nethercot, D.A. 1973a. Buckling of laterally and torsionally restrained beams. Journal of the Engineering Mechanics Division, American Society of Civil Engineers, Vol. 99, No. EM4, pp. 773-791.

Nethercot, D.A. 1973b. The effective lengths of cantilevers as governed by lateral buckling. The Structural Engineer, Vol. 51, No. 5, pp. 161-168.

Nethercot, D.A. 1974. Residual stresses and their influence upon the lateral buckling of rolled steel beams. The Structural Engineer, Vol. 52, No. 3, pp. 89-96.

Nethercot, D.A. 1983. Elastic lateral buckling of beams, in Beams and Beam Columns - Stability and Strength (ed. R. Narayanan). Applied Science Publishers, Barking, Essex, England.

Nethercot, D.A. and Trahair, N.S. 1976. Lateral buckling approximations for elastic beams. The Structural Engineer, Vol. 54, No. 6, pp. 197-204.

Nethercot, D.A. and Trahair, N.S. 1984. Bracing requirements in thin walled structures. Developments in Thin-Walled Structures (ed. J. Rhodes and A.C. Walker), Vol. 2. Elsevier Applied Science Publishers, London. pp. 93-130.

Prandtl, L. 1899. Kipperscheinungen. Dissertation. Munich.

Rajasekaran, S. and Murray, D.W. 1973. Coupled local buckling in wide-flange beam-columns. Journal of the Structural Division, American Society of Civil Engineers, Vol. 99, No. ST6, pp. 1003-1023.

Roberts, T.M. and Jhita, P.S. 1983. Lateral, local and distortional buckling of I-beams. Thin-Walled Structures. Vol. 1, pp. 289-308.

Roeder, C.W. and Assadi, M. 1982. Lateral stability of I-beams with partial supports. Journal of the Structural Division, American Society of Civil Engineers, Vol. 108, No. ST8, pp. 1768-1780.

Schmitke, C.D. and Kennedy, D.J.L. 1984. Effective lengths of laterally unsupported steel beams. Structural Engineering Report 118. Department of Civil Engineering, University of Alberta, 177 pp.

Segerlind, L.J. 1984. Applied finite element analysis. 2nd. Edition. John Wiley and Sons, N.Y.

Suzuki, Y. and Okumura, T. 1968. Final Report, Eighth Congress, International Association of Bridge and Structural Engineering, pp. 321-331.

Svensson, S.E. 1985. Lateral buckling of beams analysed as elastically supported columns subject to a varying axial force. Journal of Contructional Steel Research, Vol. 5, pp. 179-193.

Timoshenko, S.P. and Gere, J.M. 1961. Theory of elastic stability. 2nd Edition, McGraw-Hill, N.Y.

Trahair, N.S. 1977. Lateral buckling of beams and beam-columns. Chapter 3 of Theory of Beam-Columns (ed. W.F. Chen and T. Atsuta), Vol. 2, McGraw-Hill, N.Y.

Trahair, N.S. 1983a. Lateral buckling of overhanging beams. Proceedings ot the international conference on instability and plastic collapse of steel structures (ed. L.J. Morris), Manchester, Sept., 20-22. Granada Publishing, London.

Trahair, N.S. 1983b. Inlastic lateral buckling of beams, in Beams and Beam Columns - Stability and Strength (ed. R. Narayanan). Applied Science Publishers, Barking, Essex, England.

Wakabayashi, M and Nakamura, T. 1983. Buckling of laterally braced beams. Engineering Structures, Vol. 5, No. 2, pp. 108-118.

White, R.N. and Salmon, C.G. 1987. Building structural design hadbook. John Wiley and Sons, New York.

Winter, G. 1941. Lateral stability of unsymmetrical I-beams and trusses in bending. Proceedings of the American Society of Civil Engineers. Vol. 61, pp. 1851-1864.

Wong-Chung, A.D. and Kitipornchai, S. 1987. Partially braced inelastic beam buckling experiments. Journal of Constructional Steel Research. Vol. 7, pp. 189-211.

Yura, J.A., Galambos, T.V. and Ravindra, M.K. 1978. The bending resistance of steel beams. Journal of the Structural Division, American Society of Civil Engineers. Vol. 104, No. ST9, pp. 1355-1370.

Zienkiewicz, O.C. 1977. The finite element method. McGraw-Hill Book Company, London, England.

Appendix A

COMPUTER PROGRAM

```
10 REM FINITE ELEMENT PROGRAM
20 CLS:PRINT"BEAM BUCKLING, FINITE ELEMENT SOLUTION":PRINT
25 DEFDBL A-Z:REM DOUBLE PRECISION
50 REM ****************************************************
60 REM SOLUTION; BUCKLING MOMENT IS GIVEN AS FRACTION OF Mp
70 REM DATA INPUT *****************************************
100 REM All UNITS; N, mm
110 REM SOLUTION TYPE; 0 FOR ELASTIC AND 1 FOR INELASTIC
122 READ SOLUT
130 REM CROSS-SECTIONAL DIMENSIONS
145 READ D,B,T,W
146 HP=D-T:H=D-2*T
147 REM NUMBER OF LONGITUDINAL MAIN DIVISIONS
148 READ NPART
149 DIM NAR(NPART,2)
150 FOR I=1 TO NPART
151 READ NAR(I,1),NAR(I,2)
152 NEXT I
153 NLONG=1
154 FOR I=1 TO NPART
155 NLONG=NLONG+NAR(I,1)
156 NEXT I
160 DIM XLONG(NLONG)
161 XLONG(1)=0
162 COLON=0
163 CCC=1
164 FOR I=1 TO NPART
165 CCC=CCC+COLON
166 COLON=NAR(I,1)
167 FOR J=1 TO COLON
168 XLONG(J+CCC)=XLONG(J+CCC-1)+NAR(I,2)
169 NEXT J
170 NEXT I
180 NUMNP=2*NLONG:REM NUMBER OF NODES
190 NEL=NLONG-1:REM NUMBER OF LONGITUSINAL ELEMENTS
200 NEQ=3*NUMNP:REM NUMBER OF EQUATIONS
210 HBW=12:REM HALF-BANDWIDTH OF GLOBAL STIFFNESS MATRICES
271 REM ELMOD=MODULUS OF ELASTICITY IN ELASTIC RANGE
273 REM FY=YIELD STRESS OF FLANGES
275 REM NU=POISSON'S RATIO
280 READ ELMOD,FY,NU
290 SHMOD=ELMOD/2/(1+NU)
300 REM SECTION PROPERTIES
310 REM COMPUTE MOMENT OF INERTIA ABOUT MAJOR AXIS
320 IBEAM=(B*T^3/12+B*T*(HP/2)^2)*2+H^3*W/12
340 SSX=IBEAM/(D/2):MOYI=SSX*FY
350 ZZX=(B*T*HP/2+H/2*W*H/4)*2
360 MOPL=ZZX*FY:REM PLASTIC MOMENT
```

```
370 EY=FY/ELMOD:REM YIELD STRAIN
380 REM RESIDUAL STRESSES
387 DIM RESIDF(5),RESIDW(5)
390 FOR I=1 TO 5:READ RESIDF(I):NEXT I
400 IF SOLUT=1 THEN 440
430 FOR I=1 TO 5:RESIDF(I)=0:NEXT I
440 FOR I=1 TO 5:READ RESIDW(I):NEXT I
442 IF SOLUT=1 THEN 445
444 FOR I=1 TO 5:RESIDW(I)=0:NEXT I
445 REM INTERPOLATE WEB STRESSES AT GAUSSIAN POINTS
446 DIM RESIDWW(9):IF SOLUT=0 THEN 470
447 RESIDWW(5)=RESIDW(1)
448 RESIDWW(6)=RESIDW(2)+.296*(RESIDW(3)-RESIDW(2))
449 RESIDWW(7)=RESIDW(3)+.452*(RESIDW(4)-RESIDW(3))
450 RESIDWW(8)=RESIDW(4)+.344*(RESIDW(5)-RESIDW(4))
451 RESIDWW(9)=RESIDW(4)+.872*(RESIDW(5)-RESIDW(4))
452 RESIDWW(1)=RESIDWW(9):RESIDWW(2)=RESIDWW(8)
453 RESIDWW(3)=RESIDWW(7):RESIDWW(4)=RESIDWW(6)
460 REM KV()=STORING VECTOR FOR GLOBAL STRUCT. STIFF. MAT.
465 REM KGV()=STORING VECTOR FOR GLOBAL GEOM. STIFF. MAT.
470 TOTA=HBW*(HBW+1)/2+(NEQ-HBW)*HBW
480 DIM KEF(6,6),KEW(12,12),KGEF(6,6),KGEW(12,12),KV(TOTA)
490 DIM KEFS(6,6),QKL(6),QKU(6),KBAR(TOTA),KINV(TOTA)
500 DIM C(12,24),B(3,12),D(3,3),E(12,3),KGV(TOTA)
510 DIM F(12,12),M(2,12),SIGM(2,2),MTS(12,2),MTSM(12,12)
520 DIM R(NEQ),Y(NEQ),Z(NEQ),VX(NEQ),KGD(6,6),R0(NEQ)
530 DIM SHEAR(NEL,2),SHDIA(NEL,2),BETAT(NLONG)
540 DIM BEND(NLONG),MOMDIA(NLONG),ENC(NLONG)
550 DIM ET(NLONG),EC(NLONG),BETAC(NLONG),ENT(NLONG)
562 DIM IFC(NLONG),JFC(NLONG),IFT(NLONG),JFT(NLONG)
578 REM LOAD DATA; INCLUDE ALL LOADS AND REACTIONS
620 READ NNLOAD:REM NUMBER OF LOADS AND REACTIONS
630 DIM NLOADV(NNLOAD,3),LOADV(NNLOAD)
640 REM NLOADV(I,1)=LONGIT. POINT NUMB. OF LOAD OR REACTION
650 REM NLOADV(I,2)=MAGNITUDE OF LOAD
660 REM NLOADV(I,3)=HEIGHT OF LOAD APPLIC. ABOVE SH. CENTRE
670 FOR I=1 TO NNLOAD
680 READ NLOADV(I,1),NLOADV(I,2),NLOADV(I,3)
690 NEXT I
692 READ MMOMLON, MMOMENT
693 REM CONSTRUCT SHEAR AND MOMENT DIAGRAMS FROM LOADS
740 FOR I=1 TO NEL
742 SUM=0
743 FOR J=1 TO NNLOAD
744 IF NLOADV(J,1)>I THEN 748
746 SUM=SUM-NLOADV(J,2)
748 NEXT J
750 SHDIA(I,1)=SUM:SHDIA(I,2)=SUM
760 NEXT I
780 FOR I=1 TO NLONG
782 SUM=0
```

```
784 FOR J=1 TO I-1
786 SUM=SUM-SHDIA(J,1)*(XLONG(J+1)-XLONG(J))
788 NEXT J
790 MOMDIA(I)=SUM
792 NEXT I
794 MMOOMM=MMOMENT-MOMDIA(MMOMLON)
800 FOR I=1 TO NLONG:MOMDIA(I)=MOMDIA(I)+MMOOMM:NEXT I
802 REM EIGENVALUE SHIFT
804 READ SHIFT
806 REM LOWER AND UPPER BOUNDS,INELASTIC SOLUTION
807 READ GAMMA0,GAMMA1
809 PLOTINC=2
810 REM RESTRAINT CONDITIONS
830 READ NRNOD:REM NUMBER OF RESTRAINED NODES
840 DIM NODRES(NRNOD,4)
860 FOR I=1 TO NRNOD
865 REM NODE NUMBER, RESTRAINS AGAINST W, THETA-X & THETA-Y
870 READ NODRES(I,1),NODRES(I,2),NODRES(I,3),NODRES(I,4)
880 NEXT I
881 REM ELASTIC RESTRAINT COEFFICIENTS
882 READ RAMAD
883 DIM TOTO1(RAMAD,2)
884 NNRESS=3*RAMAD
885 DIM CCOEFF(NNRESS,3)
886 EIRAG=ELMOD*B*(T^3)/12
887 FOR I=1 TO RAMAD
888 READ TOTO1(I,1),TOTO1(I,2)
889 NEXT I
890 FOR I=1 TO RAMAD
891 SHAB=TOTO1(I,1)
892 ADAD=TOTO1(I,2)
893 RAGA1=3*EIRAG/ADAD^3
894 RAGA2=3*EIRAG/ADAD^2
895 RAGA3=3*EIRAG/ADAD
896 SOSO1=3*SHAB-2
897 SOSO2=3*SHAB-1
898 CCOEFF(3*I-2,1)=SOSO1
899 CCOEFF(3*I-1,1)=SOSO1
900 CCOEFF(3*I,1)=SOSO2
901 CCOEFF(3*I-2,2)=SOSO1
902 CCOEFF(3*I-1,2)=SOSO2
903 CCOEFF(3*I,2)=SOSO2
904 CCOEFF(3*I-2,3)=RAGA1
905 CCOEFF(3*I-1,3)=RAGA2
906 CCOEFF(3*I,3)=RAGA3
907 NEXT I
909 REM INITIAL DISPLACEMENT EIGENVECTOR
915 READ NDIS:REM NUMBER OF NODES WITH GIVEN INITIAL DISP.
920 REM READ NODE NUMBER, DISPLACEMENT W, THETA-X, THETA Y
930 FOR I=1 TO NDIS
940 READ NODD,R0((NODD-1)*3+1),R0((NODD-1)*3+2)
```

```
945 READ RO((NODD-1)*3+3)
950 NEXT I
970 REM NSTIF=NUMBER OF STIFFENERS
980 READ NSTIF:DIM STIFFEN(NSTIF,3)
990 FOR I=1 TO NSTIF
1000 READ STIFFEN(I,1),STIFFEN(I,2),STIFFEN(I,3)
1010 REM LONGITUDINAL POINT NUMBER, WIDTH, THICKNESS
1020 NEXT I
1040 DIM KSI(4),ETA(4)
1050 KSI(1)=-1:KSI(2)=-1:KSI(3)=1:KSI(4)=1
1060 ETA(1)=-1:ETA(2)=1:ETA(3)=-1:ETA(4)=1
1070 REM SAMPLING POINTS & WEIGHTS
1080 IF SOLUT=1 THEN 1120
1090 DIM XSP(3),YSP(3),WSPX(3),WSPY(3)
1100 XSP(1)=-.7745967:XSP(2)=0:XSP(3)=.7745967
1105 YSP(1)=XSP(1):YSP(2)=XSP(2):YSP(3)=XSP(3)
1110 WSPX(1)=.5555556:WSPX(2)=.8888889:WSPX(3)=.5555556
1112 WSPY(1)=WSPX(1):WSPY(2)=WSPX(2):WSPY(3)=WSPX(3)
1115 GOTO 1155
1120 DIM XSP(3),YSP(9),WSPX(3),WSPY(9)
1130 XSP(1)=-.7745967:XSP(2)=0:XSP(3)=.7745967
1140 YSP(1)=-.9681602:YSP(2)=-.8360311:YSP(3)=-.6133714
1142 YSP(4)=-.3242534:YSP(5)=0:YSP(6)=-YSP(4)
1144 YSP(7)=-YSP(3):YSP(8)=-YSP(2):YSP(9)=-YSP(1)
1146 WSPX(1)=.5555556:WSPX(2)=.8888889:WSPX(3)=.5555556
1148 WSPY(1)=.0812744:WSPY(2)=.1806482:WSPY(3)=.2606107
1150 WSPY(4)=.3123471:WSPY(5)=.3302394:WSPY(6)=WSPY(4)
1152 WSPY(7)=WSPY(3):WSPY(8)=WSPY(2):WSPY(9)=WSPY(1)
1154 REM COEFFICIENTS FOR SIMPSON'S RULE
1155 DIM COEFS(5)
1156 COEFS(1)=1/3:COEFS(2)=4/3:COEFS(3)=2/3:COEFS(4)=4/3
1157 COEFS(5)=1/3
1158 REM COEFFICIENTS FOR TRAPEZOIDAL RULE
1159 DIM COEF(5)
1160 COEF(1)=.5:COEF(2)=1:COEF(3)=1:COEF(4)=1:COEF(5)=.5
1165 REM ***************************************************
1170 REM MAIN ALGORITHM
1190 IF SOLUT=1 THEN 2230
1200 GAMMA=1:GOSUB 2660
1230 CLS:PRINT "ELASTIC SOLUTION:  Mcr =";lAMBDA;"Mp"
1260 REM NORMALIZED BUCKLED SHAPE, EIGENVECTOR R()
1300 PRINT:PRINT "Normalized buckled shape"
1310 PRINT:PRINT "NODE              Z        THETA-X      THETA-Y"
1320 PRINT "-----------------------------------------"
1330 FOR I=1 TO NUMNP
1340 PRINT USING "###";I;
1350 PRINT "    ";
1360 PRINT USING "##.##^^^^";R((I-1)*3+1);
1370 PRINT "   ";
1380 PRINT USING "##.##^^^^";R((I-1)*3+2);
1390 PRINT "   ";
```

```
1400 PRINT USING "##.##^^^^";R((I-1)*3+3)
1405 IF INT((I-15)/20)=((I-15)/20) THEN 1408
1406 GOTO 1410
1408 PRINT:INPUT"PRESS ENTER TO CONTINUE ...";AZ:CLS
1410 NEXT I
1420 PRINT:INPUT"PRESS ENTER TO CONTINUE ...";AZ
1430 REM PLOT BUCKLED SHAPE
1450 CLS:SCREEN 2:KEY OFF
1460 REM NORMALIZED BUCKLED SHAPE SO THAT W-MAX = 1.0
1470 DIM RNORM(NEQ)
1480 ZMAXX=0
1490 FOR I=1 TO NEQ
1500 IF ABS(R(I))>ZMAXX THEN ZMAXX=ABS(R(I)):IMAXX=I
1510 NEXT I
1520 FOR I=1 TO NEQ:RNORM(I)=R(I)/R(IMAXX):NEXT I
1530 LINE(40,70)-(600,70)
1532 LOCATE 1,23:PRINT"NORMALIZED BUCKLED SHAPE, PLAN VIEW"
1534 IF SOLUT=1 THEN 1546
1536 LOCATE 3,23
1538 PRINT"Mcr =";:PRINT USING "##.####";LAMBDA;:PRINT" Mp"
1545 GOTO 1550
1546 LOCATE 3,23
1548 PRINT"Mcr =";:PRINT USING "##.####";GAMMA;:PRINT" Mp"
1550 REM PLOT EACH LONGITUDINAL DIVISION
1560 FOR I=1 TO NEL
1570 X1=XLONG(I):X2=XLONG(I+1)
1580 XX1=X1/XLONG(NLONG)*560+40:XX2=X2/XLONG(NLONG)*560+40
1590 FOR J=XX1 TO (XX2-PLOTINC) STEP PLOTINC
1600 REM TOP FLANGE
1610 ETA=1:GOSUB 1930
1620 REM MIDDLE OF WEB
1630 ETA=0:GOSUB 1930
1640 REM BOTTOM FLANGE
1650 ETA=-1:GOSUB 1930
1660 NEXT J
1670 NEXT I
1680 REM PLOT FLANGES AND WEB SYMBOLS
1690 FOR I=2 TO NLONG-1
1700 J=XLONG(I)/XLONG(NLONG)*560+40
1710 X1=XLONG(I):X2=XLONG(I+1)
1720 REM TOP FLANGE
1730 ETA=1:GOSUB 2090
1740 LINE(XPLOT-2,YPLOT+1)-(XPLOT+2,YPLOT-1)
1750 REM MIDDLE OF WEB
1760 ETA=0:GOSUB 2090
1770 LINE(XPLOT,YPLOT-1)-(XPLOT,YPLOT+1)
1780 REM BOTTOM FLANGE
1790 ETA=-1:GOSUB 2090
1800 LINE(XPLOT-2,YPLOT-1)-(XPLOT+2,YPLOT+1)
1810 NEXT I
1820 REM LEGEND
```

```
1830 LINE(170,124)-(270,124):LINE(218,125)-(222,123)
1840 LINE(170,140)-(270,140):LINE(220,139)-(220,141)
1850 LINE(170,156)-(270,156):LINE(218,155)-(222,157)
1860 LINE(170,172)-(270,172)
1870 LOCATE 16,40:PRINT"TOP FLANGE"
1880 LOCATE 18,40:PRINT"MIDDLE OF WEB"
1890 LOCATE 20,40:PRINT"BOTTOM FLANGE"
1900 LOCATE 22,40:PRINT"INITIAL POSITION"
1901 LOCATE 23,1
1929 END
1930 REM PLOT BUCKLED SHAPE ROUTINE
1940 XPLOT=J:GOSUB 1980:XPLOT1=XPLOT:YPLOT1=70-ZZ*25
1950 XPLOT=J+PLOTINC:GOSUB 1980:XPLOT2=XPLOT:YPLOT2=70-ZZ*25
1960 LINE(XPLOT1,YPLOT1)-(XPLOT2,YPLOT2)
1970 RETURN
1980 REM COMPUTE BUCKLED SHAPE WITH INTERPOLATION FUNCTIONS
1990 SUM=0
2000 FOR K=1 TO 4
2010 KSI=(XPLOT-(XX1+XX2)/2)/((XX2-XX1)/2)
2020 KSI0=KSI*KSI(K):ETA0=ETA*ETA(K)
2025 SOKR1=RNORM((I-1)*6+(K-1)*3+1)*(ETA0+1)
2030 SUM=SUM+(KSI0+1)*(2+KSI0+ETA0-KSI^2-ETA^2)*SOKR1
2035 SOKR2=RNORM((I-1)*6+(K-1)*3+2)*(ETA0-1)
2040 SUM=SUM+HP/2*ETA(K)*(KSI0+1)*(ETA0+1)^2*SOKR2
2045 SOKR3=(KSI0-1)*(ETA0+1)*RNORM((I-1)*6+(K-1)*3+3)
2050 SUM=SUM-(X2-X1)/2*KSI(K)*(KSI0+1)^2*SOKR3
2060 NEXT K
2070 ZZ=SUM/8
2080 RETURN
2100 SUM=0
2110 KSI=-1
2120 FOR K=1 TO 4
2130 KSI0=KSI*KSI(K):ETA0=ETA*ETA(K)
2135 SOKR4=(ETA0+1)*RNORM((I-1)*6+(K-1)*3+1)
2140 SUM=SUM+(KSI0+1)*(2+KSI0+ETA0-KSI^2-ETA^2)*SOKR4
2145 SOKR5=(ETA0-1)*RNORM((I-1)*6+(K-1)*3+2)
2150 SUM=SUM+HP/2*ETA(K)*(KSI0+1)*(ETA0+1)^2*SOKR5
2155 SOKR6=(ETA0+1)*RNORM((I-1)*6+(K-1)*3+3)
2160 SUM=SUM-(X2-X1)/2*KSI(K)*(KSI0+1)^2*(KSI0-1)*SOKR6
2170 NEXT K
2180 ZZ=SUM/8
2190 XPLOT=J
2200 YPLOT=70-ZZ*25
2210 RETURN
2220 REM **************************************************
2230 REM ALGORITHS FOR EIGENVALUE SOLUTION, INELASTIC
2270 REM Shift=EIGENVALUE SHIFT
2340 GAMMA=GAMMA0:GOSUB 2660
2360 LAMPP0=LAMBDA-GAMMA0
```

```
2370 PRINT GAMMA,LAMBDA
2372 IF GAMMA0=.01 THEN 2382
2374 IF LAMPP0<0 THEN 2380
2378 GOTO 2382
2380 PRINT:PRINT"Mcr/Mp < LOWER LIMIT GAMMA0":END
2382 IF LAMPP0<0 THEN PRINT:PRINT"Mcr = 0":END
2400 GAMMA=GAMMA1:GOSUB 2660
2410 LAMPP1=LAMBDA-GAMMA1
2420 PRINT GAMMA,LAMBDA
2424 IF GAMMA1=.99 THEN 2432
2426 IF LAMPP1>0 THEN 2430
2428 GOTO 2432
2430 PRINT:PRINT "Mcr/Mp > UPPER LIMIT GAMMA1":END
2432 IF LAMPP1>0 THEN PRINT:PRINT "Mcr = Mp":END
2440 IF LAMPP0*LAMPP1>0 THEN PRINT"ERROR":STOP
2450 REM LAMBDA FOR GAMMA2 AT MID-INTERVAL
2460 GAMMA2=(GAMMA0+GAMMA1)/2
2470 GAMMA=GAMMA2:GOSUB 2660
2480 LAMPP2=LAMBDA-GAMMA2
2490 PRINT GAMMA,LAMBDA
2500 IF LAMPP2=0 THEN 2580
2510 IF LAMPP0*LAMPP2<0 THEN 2540
2520 LAMPP0=LAMPP2:GAMMA0=GAMMA2
2530 GOTO 2550
2540 LAMPP1=LAMPP2:GAMMA1=GAMMA2
2550 REM CHECK CONVERGENCE
2560 IF ABS(GAMMA1-GAMMA0)/ABS(GAMMA1) <.01 THEN 2580
2570 GOTO 2450
2580 REM FINAL LOAD INTENSITY; END OF PROGRAM
2600 GAMMA=GAMMA2
2610 CLS:PRINT"INELASTIC SOLUTION:  Mcr =";GAMMA;"Mp"
2640 GOTO 1260:REM PLOT BUCKLED SHAPE
2650 REM ************************************************
2660 REM FORM ELEMENT STIFFNESS MATRICES
2730 FOR I=1 TO NNLOAD:LOADV(I)=NLOADV(I,2)*GAMMA:NEXT I
2740 REM SHEAR DIAGRAM FOR GIVEN LOAD INTENSITY
2750 FOR I=1 TO NEL:SHEAR(I,1)=GAMMA*SHDIA(I,1)
2755 SHEAR(I,2)=GAMMA*SHDIA(I,2):NEXT I
2760 REM MOMENT DIAGRAM FOR GIVEN LOAD INTENSITY
2780 FOR I=1 TO NLONG:BEND(I)=GAMMA*MOMDIA(I):NEXT I
2800 FOR I=1 TO NLONG
2810 M=ABS(BEND(I))
2850 IF SOLUT=0 THEN 2880
2860 IF (ABS(M*HP/D)/SSX+ABS(RESIDF(1)))>FY THEN 2920
2870 IF (ABS(M*HP/D)/SSX+ABS(RESIDF(5)))>FY THEN 2920
2880 REM NO YIELDING
2900 ET(I)=(M/SSX)*HP/D/ELMOD:EC(I)=-ET(I)
2910 GOTO 3400
2920 REM CHECK IF MOMENT EXCEEDS PLASTIC MOMENT
2930 REM COMPUTE PLASTIC MOMENT
2940 IF M>MOPL THEN PRINT"PLASTIC MOMENT IS EXCEEDED":STOP
```

```
2980 CURV0=M/ELMOD/(1.2*IBEAM)
2990 CURV1=M/ELMOD/(.05*IBEAM)
3010 CURV=CURV0
3030 GOSUB 3420
3050 GOSUB 3980
3060 MMD0=MMD
3080 CURV=CURV1
3100 GOSUB 3420
3120 GOSUB 3980
3130 MMD1=MMD
3140 IF MMD0*MMD1>0 THEN PRINT"ERROR":STOP
3150 CURV2=(CURV0+CURV1)/2
3180 CURV=CURV2
3200 GOSUB 3420
3220 GOSUB 3980
3230 MMD2=MMD
3240 IF MMD2=0 THEN 3320
3250 IF MMD0*MMD2<0 THEN 3280
3260 CURV0=CURV2:MMD0=MMD2
3270 GOTO 3290
3280 CURV1=CURV2:MMD1=MMD2
3290 REM CHECK TOLERANCE
3300 IF ABS(CURV0-CURV1)/ABS(CURV1)<.01 THEN 3320
3310 GOTO 3150
3320 ET(I)=ET:EC(I)=EC
3400 NEXT I
3410 GOTO 4050
3420 YBAR0=T:YBAR1=D-T
3460 REM EVALUATE TOTAL AXIAL FORCE FOR YBAR0
3470 YBAR=YBAR0:GOSUB 3660:P0=AXIALF
3480 REM EVALUATE TOTAL AXIAL FORCE FOR YBAR1
3490 YBAR=YBAR1:GOSUB 3660:P1=AXIALF
3500 IF P0*P1>0 THEN PRINT"ERROR":STOP
3510 YBAR2=(YBAR0+YBAR1)/2
3530 YBAR=YBAR2:GOSUB 3660
3540 P2=AXIALF
3550 IF P2=0 THEN 3630
3560 IF P0*P2<0 THEN 3590
3570 P0=P2:YBAR0=YBAR2
3580 GOTO 3600
3590 P1=P2:YBAR1=YBAR2
3600 REM CHECK TOLERANCE
3610 IF ABS(YBAR0-YBAR1)/ABS(YBAR1)<.01 THEN GOTO 3630
3620 GOTO 3510
3630 YBARF=YBAR2
3650 RETURN
3660 REM SUBROUTINE, TOTAL AXIAL FORCE
3670 REM EXTENT OF YIELDING
3680 GOSUB 3720
3690 REM TOTAL AXIAL FORCE IN SECTION
3700 GOSUB 3920
```

```
3710 RETURN
3720 REM STRAINS
3730 REM ECP, ETP ARE STRAINS AT EXTREME FIBERS
3740 ETP=CURV*D/(1+(D-YBAR)/YBAR)
3750 ECP=-ETP*(D-YBAR)/YBAR
3760 REM EC, ET ARE STRAINS AT FLANGE MID-FIBERS
3770 EC=ECP*(D-YBAR-T/2)/(D-YBAR):ET=ETP*(YBAR-T/2)/YBAR
3920 REM SUBROUTINE, COMPUTE TOTAL AXIAL FORCE IN SECTION
3922 REM 9-POINT TRAPEZOIDAL RULE, FLANGES
3924 AXIALC=0:AXIALT=0:FOR KKJ=1 TO 5
3925 STRESSCC=ELMOD*EC+RESIDF(KKJ)
3926 IF STRESSCC<-FY THEN STRESSCC=-FY
3927 STRESSTT=ELMOD*ET+RESIDF(KKJ)
3928 IF STRESSTT>FY THEN STRESSTT=FY
3930 AXIALC=AXIALC+STRESSCC*B/8*T*COEF(KKJ)
3935 AXIALT=AXIALT+STRESSTT*B/8*T*COEF(KKJ)
3940 NEXT KKJ:AXIALC=2*AXIALC:AXIALT=2*AXIALT
3941 REM AXIAL FORCE, WEB, TRAPEZOIDAL RULE
3943 SUMW=0:FOR KKJ=1 TO 5
3945 SSTRAIN=ET+(KKJ+3)/8*(EC-ET)
3946 STRESSW=ELMOD*SSTRAIN+RESIDW(KKJ)
3947 IF ABS(STRESSW)>FY THEN STRESSW=SGN(STRESSW)*FY
3948 SUMW=SUMW+COEF(KKJ)*HP/8*W*STRESSW
3949 NEXT KKJ:AXIALW=SUMW
3951 SUMW=0:FOR KKJ=1 TO 5
3952 SSTRAIN=EC+(KKJ+3)/8*(ET-EC)
3953 STRESSW=ELMOD*SSTRAIN+RESIDW(KKJ)
3954 IF ABS(STRESSW)>FY THEN STRESSW=SGN(STRESSW)*FY
3955 SUMW=SUMW+COEF(KKJ)*HP/8*W*STRESSW:NEXT KKJ
3959 AXIALW=AXIALW+SUMW
3960 AXIALF=AXIALC+AXIALT+AXIALW
3970 RETURN
3980 REM BENDING MOMENT ABOUT MID-FIBER OF BOTTOM FLANGE
3990 MM=AXIALC*HP
3991 REM MOMENT CONTRIBUTION, WEB, SIMPSON'S RULE, 9 POINTS
3993 SUMW=0:FOR KKJ=1 TO 5
3995 SSTRAIN=ET+(KKJ+3)/8*(EC-ET)
3996 STRESSW=ELMOD*SSTRAIN+RESIDW(KKJ)
3997 IF ABS(STRESSW)>FY THEN STRESSW=SGN(STRESSW)*FY
3998 SUMW=SUMW+COEFS(KKJ)*HP/8*W*STRESSW*((KKJ+3)*HP/8)
3999 NEXT KKJ
4000 MM=MM+SUMW
4002 SUMW=0:FOR KKJ=1 TO 5
4003 SSTRAIN=EC+(KKJ+3)/8*(ET-EC)
4004 STRESSW=ELMOD*SSTRAIN+RESIDW(KKJ)
4005 IF ABS(STRESSW)>FY THEN STRESSW=SGN(STRESSW)*FY
4006 SUMW=SUMW+COEFS(KKJ)*HP/8*W*STRESSW*((5-KKJ)*HP/8)
4007 NEXT KKJ
4008 MM=MM+SUMW
4010 MMD=-MM-M
4020 RETURN
```

```
4040 REM ******************************************************
4050 REM STRUCTURAL STIFFNESS, FLANGES
4090 ERASE KV,KGV:DIM KV(TOTA),KGV(TOTA)
4100 FOR I=1 TO NLONG
4110 IFC(I)=0:IFT(I)=0:FOR KKJ=1 TO 5
4111 AXZZC=1:AXZZT=1:STRESSCC=ELMOD*EC(I)+RESIDF(KKJ)
4112 STRESSTT=ELMOD*ET(I)+RESIDF(KKJ)
4113 IF SOLUT=0 THEN 4116
4114 IF STRESSCC<-FY THEN AXZZC=0
4115 IF STRESSTT>FY THEN AXZZT=0
4116 SOKR7=((KKJ-1)*B/8)^2*AXZZC
4117 IFC(I)=IFC(I)+ELMOD*COEFS(KKJ)*B/8*T*SOKR7
4118 SOKR8=((KKJ-1)*B/8)^2*AXZZT
4119 IFT(I)=IFT(I)+ELMOD*COEFS(KKJ)*B/8*T*SOKR8
4120 NEXT KKJ
4125 IFC(I)=2*IFC(I):IFT(I)=2*IFT(I)
4130 JFC(I)=SHMOD*B*T^3/3
4150 JFT(I)=SHMOD*B*T^3/3
4170 ENC(I)=0:BETAC(I)=0
4180 ENT(I)=0:BETAT(I)=0
4190 FOR J=1 TO 5
4195 STRESSCC=ELMOD*EC(I)+RESIDF(J)
4197 STRESSTT=ELMOD*ET(I)+RESIDF(J)
4199 IF SOLUT=0 THEN 4204
4200 IF STRESSCC<-FY THEN STRESSCC=-FY
4203 IF STRESSTT>FY THEN STRESSTT=FY
4204 ENC(I)=ENC(I)+COEF(J)*B/8*T*STRESSCC
4206 ENT(I)=ENT(I)+COEF(J)*B/8*T*STRESSTT
4208 BETAC(I)=BETAC(I)+COEFS(J)*B/8*T*STRESSCC*((J-1)*B/8)^2
4210 BETAT(I)=BETAT(I)+COEFS(J)*B/8*T*STRESSTT*((J-1)*B/8)^2
4360 NEXT J
4370 ENC(I)=2*ENC(I):BETAC(I)=2*BETAC(I)
4380 ENT(I)=2*ENT(I):BETAT(I)=2*BETAT(I)
4390 NEXT I
4430 FOR I=1 TO NEL
4440 PRINT"[K] flanges",I
4450 LE=XLONG(I+1)-XLONG(I)
4470 IF BEND(I)<0 THEN 4510
4480 IFI=IFT(I):IFJ=IFT(I+1)
4490 JFI=JFT(I):JFJ=JFT(I+1)
4500 GOTO 4530
4510 IFI=IFC(I):IFJ=IFC(I+1)
4520 JFI=JFC(I):JFJ=JFC(I+1)
4530 GOSUB 4560
4550 GOTO 4730
4560 KEF(1,1)=(6*IFI+6*IFJ)/LE^3
4590 KEF(1,3)=(-4*IFI-2*IFJ)/LE^2
4600 KEF(1,4)=(-6*IFI-6*IFJ)/LE^3
4610 KEF(1,6)=(-2*IFI-4*IFJ)/LE^2
4620 KEF(2,2)=(JFI/2+JFJ/2)/LE
4630 KEF(2,5)=(-JFI/2-JFJ/2)/LE
```

```
4640 KEF(3,3)=(3*IFI+IFJ)/LE
4650 KEF(3,4)=(4*IFI+2*IFJ)/LE^2
4660 KEF(3,6)=(IFI+IFJ)/LE
4670 KEF(4,4)=(6*IFI+6*IFJ)/LE^3
4680 KEF(4,6)=(2*IFI+4*IFJ)/LE^2
4690 KEF(5,5)=(JFI/2+JFJ/2)/LE
4700 KEF(6,6)=(IFI+3*IFJ)/LE
4720 RETURN
4730 REM ADD TO GLOBAL VECTOR KV()
4740 FOR II=1 TO 2:FOR JJ=II TO 2
4750 FOR KK=1 TO 3:FOR LL=1 TO 3
4760 REM IKKE,JKKE ARE ADDRESSES IN ELEMENT MATRIX
4770 REM IKK, JKK ARE ADDRESSES IN GLOBAL MATRIX
4780 IKKE=(II-1)*3+KK
4790 JKKE=(JJ-1)*3+LL
4800 IF IKKE>JKKE THEN 4860
4810 IKK=((I-1)*2+(II-1)*2)*3+KK
4820 JKK=((I-1)*2+(JJ-1)*2)*3+LL
4830 REM KGLOBAL=ADDRESS IN GLOBAL VECTOR
4840 GOSUB 9670
4850 KV(KGLOBAL)=KV(KGLOBAL)+KEF(IKKE,JKKE)
4860 NEXT LL:NEXT KK:NEXT JJ:NEXT II
4880 IF BEND(I)>=0 THEN 4920
4890 IFI=IFT(I):IFJ=IFT(I+1)
4900 JFI=JFT(I):JFJ=JFT(I+1)
4910 GOTO 4940
4920 IFI=IFC(I):IFJ=IFC(I+1)
4930 JFI=JFC(I):JFJ=JFC(I+1)
4940 REM FORM 6x6 MATRIX
4950 GOSUB 4560
4960 REM ADD TO GLOBAL VECTOR
4970 FOR II=1 TO 2:FOR JJ=II TO 2
4980 FOR KK=1 TO 3:FOR LL=1 TO 3
5010 IKKE=(II-1)*3+KK
5020 JKKE=(JJ-1)*3+LL
5030 IF IKKE>JKKE THEN 5090
5040 IKK=((I-1)*2+1+(II-1)*2)*3+KK
5050 JKK=((I-1)*2+1+(JJ-1)*2)*3+LL
5070 GOSUB 9670
5080 KV(KGLOBAL)=KV(KGLOBAL)+KEF(IKKE,JKKE)
5090 NEXT LL:NEXT KK:NEXT JJ:NEXT II
5100 NEXT I
5110 REM ***************************************************
5120 REM STRUCTURAL STIFFNESS, STIFFENERS
5140 FOR I=1 TO NSTIF
5160 IFS=STIFFEN(I,2)^3*STIFFEN(I,3)/12
5170 JFS=STIFFEN(I,2)*STIFFEN(I,3)^3/3
5190 REM FORM 6x6 MATRIX
5210 KEFS(1,1)=12*ELMOD*IFS/HP^3
5220 KEFS(1,2)=6*ELMOD*IFS/HP^2
5230 KEFS(1,4)=-12*ELMOD*IFS/HP^3
```

```
5240 KEFS(1,5)=6*ELMOD*IFS/HP^2
5250 KEFS(2,2)=4*ELMOD*IFS/HP
5260 KEFS(2,4)=-6*ELMOD*IFS/HP^2
5270 KEFS(2,5)=2*ELMOD*IFS/HP
5280 KEFS(3,3)=SHMOD*JFS/HP
5290 KEFS(3,6)=-SHMOD*JFS/HP
5300 KEFS(4,4)=12*ELMOD*IFS/HP^3
5310 KEFS(4,5)=-6*ELMOD*IFS/HP^2
5320 KEFS(5,5)=4*ELMOD*IFS/HP
5330 KEFS(6,6)=SHMOD*JFS/HP
5340 REM ADD TO GLOBAL MATRIX
5350 FOR II=1 TO 2:FOR JJ=II TO 2
5360 FOR KK=1 TO 3:FOR LL=1 TO 3
5370 IKKE=(II-1)*3+KK
5380 JKKE=(JJ-1)*3+LL
5390 IF IKKE>JKKE THEN 5440
5400 IKK=((STIFFEN(I,1)-1)*2+(II-1))*3+KK
5410 JKK=((STIFFEN(I,1)-1)*2+(JJ-1))*3+LL
5420 GOSUB 9670
5430 KV(KGLOBAL)=KV(KGLOBAL)+KEFS(IKKE,JKKE)
5440 NEXT LL:NEXT KK:NEXT JJ:NEXT II
5450 NEXT I
5460 REM ****************************************************
5470 REM GEOMETRIC STIFFNESS, FLANGES
5490 FOR I=1 TO NEL
5500 PRINT"[Kg] FLANGES",I
5510 LE=XLONG(I+1)-XLONG(I)
5530 IF BEND(I)<0 THEN 5562
5531 NI=ENT(I):BETAI=BETAT(I)
5532 IF BEND(I+1)<0 THEN 5550
5540 NJ=ENT(I+1):BETAJ=BETAT(I+1):GOTO 5554
5550 NJ=ENC(I+1):BETAJ=BETAC(I+1)
5554 NIJ=(NI+NJ)/2:BETAIJ=(BETAI+BETAJ)/2
5560 GOTO 5590
5562 NI=ENC(I):BETAI=BETAC(I)
5565 IF BEND(I+1)>=0 THEN 5580
5570 NJ=ENC(I+1):BETAJ=BETAC(I+1):GOTO 5584
5580 NJ=ENT(I+1):BETAJ=BETAT(I+1)
5584 NIJ=(NI+NJ)/2:BETAIJ=(BETAI+BETAJ)/2
5590 REM FORM 6x6 MATRIX
5600 GOSUB 5620
5610 GOTO 5730
5620 KGEF(1,1)=NIJ/LE
5650 KGEF(1,4)=-NIJ/LE
5660 KGEF(2,2)=BETAIJ/LE
5670 KGEF(2,5)=-BETAIJ/LE
5680 KGEF(4,4)=NIJ/LE
5690 KGEF(5,5)=BETAIJ/LE
5710 RETURN
5720 REM ADD TO GLOBAL VECTOR
5730 FOR II=1 TO 2:FOR JJ=II TO 2
```

```
5740 FOR KK=1 TO 3:FOR LL=1 TO 3
5770 IKKE=(II-1)*3+KK
5780 JKKE=(JJ-1)*3+LL
5790 IF IKKE>JKKE THEN 5850
5800 IKK=((I-1)*2+(II-1)*2)*3+KK
5810 JKK=((I-1)*2+(JJ-1)*2)*3+LL
5830 GOSUB 9670
5840 KGV(KGLOBAL)=KGV(KGLOBAL)+KGEF(IKKE,JKKE)
5850 NEXT LL:NEXT KK:NEXT JJ:NEXT II
5870 IF BEND(I)<0 THEN 5910
5880 NI=ENC(I):BETAI=BETAC(I)
5882 IF BEND(I+1)<0 THEN 5892
5890 NJ=ENC(I+1):BETAJ=BETAC(I+1):GOTO 5894
5892 NJ=ENT(I+1):BETAJ=BETAT(I+1)
5894 NIJ=(NI+NJ)/2:BETAIJ=(BETAI+BETAJ)/2
5900 GOTO 5930
5910 NI=ENT(I):BETAI=BETAT(I)
5912 IF BEND(I+1)>=0 THEN 5922
5920 NJ=ENT(I+1):BETAJ=BETAT(I+1):GOTO 5924
5922 NJ=ENC(I+1):BETAJ=BETAC(I+1)
5924 NIJ=(NI+NJ)/2:BETAIJ=(BETAI+BETAJ)/2
5930 GOSUB 5620
5950 REM ADD TO GLOBAL VECTOR
5960 FOR II=1 TO 2:FOR JJ=II TO 2
5970 FOR KK=1 TO 3:FOR LL=1 TO 3
6000 IKKE=(II-1)*3+KK
6010 JKKE=(JJ-1)*3+LL
6020 IF IKKE>JKKE THEN 6080
6030 IKK=((I-1)*2+1+(II-1)*2)*3+KK
6040 JKK=((I-1)*2+1+(JJ-1)*2)*3+LL
6060 GOSUB 9670
6070 KGV(KGLOBAL)=KGV(KGLOBAL)+KGEF(IKKE,JKKE)
6080 NEXT LL:NEXT KK:NEXT JJ:NEXT II
6090 NEXT I
6100 REM ***************************************************
6110 REM GEOMETRIC STIFFNESS OF VERTICAL LOADS & REACTIONS
6145 FOR I=1 TO NNLOAD
6155 QET=NLOADV(I,3)-HP/2:IF QET<0 THEN QET=0
6156 QEB=NLOADV(I,3)+HP/2:IF QEB>0 THEN QEB=0
6160 KGD(2,2)=0:KGD(5,5)=0
6170 KGD(1,1)=LOADV(I)*(NLOADV(I,3)-QET-QEB)/HP^2
6172 KGD(1,4)=-KGD(1,1)
6174 KGD(4,4)=KGD(1,1)
6190 KGD(2,2)=KGD(2,2)+LOADV(I)*QEB
6195 KGD(5,5)=KGD(5,5)+LOADV(I)*QET
6198 REM ADD TO GLOBAL VECTOR KGV()
6210 FOR II=1 TO 6:FOR JJ=II TO 6
6220 IKK=(NLOADV(I,1)-1)*6+II
6230 JKK=(NLOADV(I,1)-1)*6+JJ
6240 GOSUB 9670
6250 KGV(KGLOBAL)=KGV(KGLOBAL)+KGD(II,JJ)
```

```
6260 NEXT JJ:NEXT II
6270 NEXT I
6280 REM ************************************************
6290 REM STRUCTURAL ELEMENT STIFFNESS MATRIX, WEB
6330 FOR I=1 TO NEL
6340 PRINT"[K] web",I
6350 GOSUB 6380
6360 NEXT I
6370 GOTO 7130
6380 AA=(XLONG(I+1)-XLONG(I))/2
6410 BB=HP/2
6500 REM GAUSS INTEGRATION
6510 REM CLEAR KEW
6520 ERASE KEW:DIM KEW(12,12)
6530 JGAUSS=3:KGAUSS=3:IF SOLUT=1 THEN JGAUSS=3:KGAUSS=9
6540 FOR J=1 TO JGAUSS
6550 FOR K=1 TO KGAUSS
6570 KSI=XSP(J):ETA=YSP(K)
6590 WEIGH=WSPX(J)*WSPY(K)
6600 IF SOLUT=0 THEN YIEL=0:GOTO 6660
6620 YIEL=0
6622 IF BEND(I)<0 THEN 6636
6624 KORAN1=ELMOD*(EC(I)-ET(I))*((ETA+1)/2)
6630 STRESL=RESIDWW(K)+ELMOD*ET(I)+KORAN1:GOTO 6640
6636 KORAN2=(ET(I)-EC(I))*((ETA+1)/2)
6638 STRESL=RESIDWW(K)+ELMOD*EC(I)+ELMOD*KORAN2
6640 IF BEND(I+1)<0 THEN 6644
6641 KORAN3=ELMOD*(EC(I+1)-ET(I+1))*((ETA+1)/2)
6642 STRESR=RESIDWW(K)+ELMOD*ET(I+1)+KORAN3:GOTO 6646
6644 KORAN4=ELMOD*(ET(I+1)-EC(I+1))*((ETA+1)/2)
6645 STRESR=RESIDWW(K)+ELMOD*EC(I+1)+KORAN4
6646 SIGX=STRESL*(.5-KSI/2)+STRESR*(.5+KSI/2)
6648 IF ABS(SIGX)>FY THEN YIEL=1
6660 REM CONSTITUTIVE MATRIX D()
6680 EETT=ELMOD:GGTT=SHMOD:IF YIEL=1 THEN EETT=0
6690 D(1,1)=EETT*W^3/12/(1-NU^2)
6695 D(1,2)=EETT*W^3/12/(1-NU^2)*NU
6700 D(2,1)=D(1,2):D(2,2)=D(1,1)
6710 D(3,3)=GGTT*W^3/12
6720 REM [B] MATRIX
6730 FOR JJ=1 TO 4
6740 KI=KSI(JJ):EI=ETA(JJ):K0=KSI*KSI(JJ):E0=ETA*ETA(JJ)
6750 KK=(JJ-1)*3
6755 KORAN5=2*(K0+1)*(E0+1)
6760 B(1,KK+1)=-1/8/AA^2*(2*KI*(E0+1)*(KI-2*KSI)-KORAN5)
6765 KORAN6=4*AA*KI^3*(K0+1)*(E0+1)
6770 B(1,KK+3)=1/8/AA^2*(2*AA*KI^3*(K0-1)*(E0+1)+KORAN6)
6780 B(2,KK+1)=-1/8/BB^2*(2*EI*(K0+1)*(EI-2*ETA)-KORAN5)
6785 KORAN7=4*BB*EI^3*(K0+1)*(E0+1)
6790 B(2,KK+2)=-1/8/BB^2*(2*BB*EI^3*(K0+1)*(E0-1)+KORAN7)
6795 KORAN8=KI*EI*(2+K0+E0-KSI^2-ETA^2)
```

```
6797 KORAN9=KI*(E0+1)*(EI-2*ETA)+(K0+1)*EI*(KI-2*KSI)
6800 B(3,KK+1)=2/8/AA/BB*(KORAN8+KORAN9)
6805 KORIA1=2*BB*EI^2*KI*(E0^2-1)+BB*EI^2*KI*(E0+1)^2
6810 B(3,KK+2)=2/8/AA/BB*KORIA1
6815 KORIA2=2*AA*KI^2*EI*(K0^2-1)+AA*KI^2*EI*(K0+1)^2
6820 B(3,KK+3)=-2/8/AA/BB*KORIA2
6830 NEXT JJ
6850 FOR JJ=1 TO 12:FOR KK=1 TO 3:SUM=0:FOR LL=1 TO 3
6860 SUM=SUM+B(LL,JJ)*D(LL,KK)
6870 NEXT LL:E(JJ,KK)=SUM:NEXT KK:NEXT JJ
6880 REM [E] [B] MATRIX PRODUCT, PUT IN [F]
6890 FOR JJ=1 TO 12:FOR KK=1 TO 12:SUM=0:FOR LL=1 TO 3
6900 SUM=SUM+E(JJ,LL)*B(LL,KK)
6910 NEXT LL:F(JJ,KK)=SUM:NEXT KK:NEXT JJ
6940 FOR JJ=1 TO 12:FOR KK=1 TO 12
6950 KEW(JJ,KK)=KEW(JJ,KK)+AA*BB*WEIGH*F(JJ,KK)
6960 NEXT KK:NEXT JJ
6970 NEXT K:NEXT J
6980 REM ADD TO GLOBAL VECTOR
6990 FOR II=1 TO 4:FOR JJ=II TO 4
7000 FOR KK=1 TO 3:FOR LL=1 TO 3
7030 IKKE=(II-1)*3+KK
7040 JKKE=(JJ-1)*3+LL
7050 IF IKKE>JKKE THEN 7110
7060 IKK=((I-1)*2+(II-1))*3+KK
7070 JKK=((I-1)*2+(JJ-1))*3+LL
7090 GOSUB 9670
7100 KV(KGLOBAL)=KV(KGLOBAL)+KEW(IKKE,JKKE)
7110 NEXT LL:NEXT KK:NEXT JJ:NEXT II
7120 RETURN
7130 REM GEOMETRIC STIFFNESS MATRIX WEB ******************
7150 FOR I=1 TO NEL
7160 PRINT"[Kg] WEB",I
7170 GOSUB 7200
7180 NEXT I
7190 GOTO 7910
7200 REM SUBROUTINE; GEOMETRIC STIFFNESS ELEMENT MATRIX
7210 AA=(XLONG(I+1)-XLONG(I))/2:BB=HP/2
7220 REM CLEAR KGEW
7230 ERASE KGEW:DIM KGEW(12,12)
7240 REM GAUSS INTEGRATION
7250 FOR J=1 TO JGAUSS
7260 FOR K=1 TO KGAUSS
7270 KSI=XSP(J):ETA=YSP(K):REM NATURAL COORDINATES
7280 WEIGH=WSPX(J)*WSPY(K)
7290 REM STRESSES AT SAMPLING POINTS
7300 REM SIGMA-X
7310 IF BEND(I)<0 THEN 7350
7320 KORIA3=ELMOD*(EC(I)-ET(I))*((ETA+1)/2)
7340 STRESL=RESIDWW(K)+ELMOD*ET(I)+KORIA3:GOTO 7390
7350 KORIA4=ELMOD*(ET(I)-EC(I))*((ETA+1)/2)
```

```
7355 STRESL=RESIDWW(K)+ELMOD*EC(I)+KORIA4
7390 IF BEND(I+1)<0 THEN 7410
7395 KORIA5=ELMOD*(EC(I+1)-ET(I+1))*((ETA+1)/2)
7400 STRESR=RESIDWW(K)+ELMOD*ET(I+1)+KORIA5:GOTO 7460
7410 KORIA6=ELMOD*(ET(I+1)-EC(I+1))*((ETA+1)/2)
7420 STRESR=RESIDWW(K)+ELMOD*EC(I+1)+KORIA6
7460 SIGX=STRESL*(.5-KSI/2)+STRESR*(.5+KSI/2)
7461 IF SOLUT=0 THEN 7480
7462 IF ABS(SIGX)>FY THEN SIGX=SGN(SIGX)*FY
7470 REM TAU-XY; CONSTANT SHEAR STRESS OVER WEB HEIGHT
7480 TAUXYL=SHEAR(I,1)/HP/W:TAUXYR=SHEAR(I,2)/HP/W
7490 TAUXY=TAUXYL*(.5-KSI/2)+TAUXYR*(.5+KSI/2)
7494 SIGY=0
7504 FOR JJ=1 TO 4
7505 KI=KSI(JJ):EI=ETA(JJ):K0=KSI*KSI(JJ):E0=ETA*ETA(JJ)
7506 KK=(JJ-1)*3
7520 M(1,KK+1)=1/4/AA*KI*(E0+1)
7530 M(2,KK+1)=1/4/BB*EI*(K0+1)
7554 NEXT JJ
7556 REM FORM MATRIX [SIGM] 4x4 OF STRESSES
7557 SIGM(1,1)=SIGX:SIGM(1,2)=TAUXY:SIGM(2,1)=TAUXY
7558 SIGM(2,2)=SIGY
7562 FOR II=1 TO 12:FOR JJ=1 TO 2:SUM=0:FOR KK=1 TO 2
7564 SUM=SUM+M(KK,II)*SIGM(KK,JJ)
7566 NEXT KK:MTS(II,JJ)=SUM:NEXT JJ:NEXT II
7572 FOR II=1 TO 12:FOR JJ=1 TO 12:SUM=0:FOR KK=1 TO 2
7574 SUM=SUM+MTS(II,KK)*M(KK,JJ)
7576 NEXT KK:MTSM(II,JJ)=SUM:NEXT JJ:NEXT II
7590 REM ADD CONTRIBUTION TO ELEMENT MATRIX
7610 FOR II=1 TO 12:FOR JJ=II TO 12
7620 KGEW(II,JJ)=KGEW(II,JJ)+MTSM(II,JJ)*WEIGH
7630 NEXT JJ:NEXT II
7710 NEXT K
7720 NEXT J
7740 FOR II=1 TO 12:FOR JJ=II TO 12
7745 KGEW(II,JJ)=KGEW(II,JJ)*AA*BB*W:NEXT JJ:NEXT II
7760 REM ADD TO GLOBAL VECTOR
7770 FOR II=1 TO 4:FOR JJ=II TO 4
7780 FOR KK=1 TO 3:FOR LL=1 TO 3
7810 IKKE=(II-1)*3+KK
7820 JKKE=(JJ-1)*3+LL
7830 IF IKKE>JKKE THEN 7890
7840 IKK=((I-1)*2+(II-1))*3+KK
7850 JKK=((I-1)*2+(JJ-1))*3+LL
7870 GOSUB 9670
7880 KGV(KGLOBAL)=KGV(KGLOBAL)+KGEW(IKKE,JKKE)
7890 NEXT LL:NEXT KK:NEXT JJ:NEXT II
7900 RETURN
7910 REM EIGENVALUE ROUTINE ********************************
7920 REM INVERSE ITERATION, WITH EIGENVALUE SHIFTING
7930 REM ADD (FIXED) RESTRAINT CONDITIONS TO [K]
```

```
7940 FOR I=1 TO NRNOD
7960 FOR J=1 TO 3
7970 IKK=(NODRES(I,1)-1)*3+J:JKK=IKK
7980 GOSUB 9670
7990 RESTRAI=NODRES(I,J+1)
8000 IF RESTRAI=-1 THEN RESTRAI=1E+15:REM FIXED RESTRAINT
8010 KV(KGLOBAL)=KV(KGLOBAL)+RESTRAI
8020 NEXT J:NEXT I
8022 REM ADD ELASTIC RESTRAINT COEFFICIENTS
8023 FOR I=1 TO NNRESS
8024 IKK=CCOEFF(I,1):JKK=CCOEFF(I,2):GOSUB 9670
8025 KV(KGLOBAL)=KV(KGLOBAL)+CCOEFF(I,3)
8026 NEXT I
8040 FOR J=1 TO TOTA:KGV(J)=KGV(J)/GAMMA:NEXT J
8070 FOR I=1 TO TOTA:KBAR(I)=KV(I)+SHIFT*KGV(I):NEXT I
8100 FOR I=1 TO TOTA:KINV(I)=KBAR(I):NEXT I
8110 GOSUB 8960
8130 REM INVERSE ITERATION ROUTINE
8140 REM LAMBDA=EIGENVALUE; LAMBDAP=SHIFTED EIGENVALUE
8150 LAMBDA0=1E+20
8170 REM R0() IS INITIAL ASSUMED DISPLACEMENT EIGENVECTOR
8180 FOR I=1 TO NEQ:R(I)=R0(I):NEXT I
8200 ERASE Y:DIM Y(NEQ)
8210 FOR I=1 TO NEQ
8220 JLIM1=1:JLIM2=I+HBW-1
8230 IF I>HBW THEN JLIM1=I-HBW+1
8240 IF I>NEQ-HBW THEN JLIM2=NEQ
8250 FOR J=JLIM1 TO JLIM2
8260 IKK=I:JKK=J
8270 IF JKK<IKK THEN IKK=J:JKK=I
8280 GOSUB 9670
8290 Y(I)=Y(I)+KGV(KGLOBAL)*R(J)
8300 NEXT J
8310 NEXT I
8320 YYS=0
8340 FOR I=1 TO NEQ
8350 YYS=YYS+Y(I)*Y(I)
8360 NEXT I
8370 YABS=SQR(YYS)
8400 FOR I=1 TO NEQ
8410 Z(I)=Y(I)/YABS
8420 NEXT I
8440 GOSUB 9250
8450 REM RAYLEIGH QUOTIENT
8480 ERASE Y:DIM Y(NEQ)
8490 FOR I=1 TO NEQ
8500 JLIM1=1:JLIM2=I+HBW-1
8510 IF I>HBW THEN JLIM1=I-HBW+1
8520 IF I>NEQ-HBW THEN JLIM2=NEQ
8530 FOR J=JLIM1 TO JLIM2
8540 IKK=I:JKK=J
```

```
8550 IF JKK<IKK THEN IKK=J:JKK=I
8560 GOSUB 9670
8570 Y(I)=Y(I)+KGV(KGLOBAL)*R(J)
8580 NEXT J
8590 NEXT I
8620 ERASE VX:DIM VX(NEQ)
8630 FOR I=1 TO NEQ
8640 JLIM1=1:JLIM2=I+HBW-1
8650 IF I>HBW THEN JLIM1=I-HBW+1
8660 IF I>NEQ-HBW THEN JLIM2=NEQ
8670 FOR J=JLIM1 TO JLIM2
8680 IKK=I:JKK=J
8690 IF JKK<IKK THEN IKK=J:JKK=I
8700 GOSUB 9670
8710 VX(I)=VX(I)+KBAR(KGLOBAL)*R(J)
8720 NEXT J
8730 NEXT I
8750 PROD1=0
8760 FOR I=1 TO NEQ
8770 PROD1=PROD1+R(I)*VX(I)
8780 NEXT I
8800 PROD2=0
8810 FOR I=1 TO NEQ
8820 PROD2=PROD2+R(I)*Y(I)
8830 NEXT I
8850 LAMBDAP=-PROD1/PROD2
8860 LAMBDA1=LAMBDAP+SHIFT
8870 PRINT "lambda=";LAMBDA1
8880 REM CHECK CONVERGENCE
8890 IF ABS(LAMBDA1-LAMBDA0)/ABS(LAMBDA1)<.001 THEN 8920
8900 LAMBDA0=LAMBDA1
8910 GOTO 8320
8920 LAMBDA=LAMBDA1
8950 RETURN
8960 REM CROUT REDUCTION ROUTINE
8990 FOR J=2 TO NEQ
9010 I1=2
9020 IF J>HBW THEN I1=J-HBW+2
9030 FOR I=I1 TO J
9040 SUM=0
9060 K1=1
9070 IF J>HBW THEN K1=J-HBW+1
9080 FOR K=K1 TO I-1
9100 IKK=K:JKK=I
9110 GOSUB 9670:AKI=KINV(KGLOBAL)
9130 IKK=K:JKK=J
9140 GOSUB 9670:AKJ=KINV(KGLOBAL)
9160 IKK=K:JKK=K
9170 GOSUB 9670:AKK=KINV(KGLOBAL)
9180 SUM=SUM+AKI*AKJ/AKK
```

```
9190 NEXT K
9200 IKK=I:JKK=J:GOSUB 9670
9210 KINV(KGLOBAL)=KINV(KGLOBAL)-SUM
9220 NEXT I
9230 NEXT J
9240 RETURN
9250 FOR I=2 TO NEQ
9270 SUM=0
9290 K1=1
9300 IF I>HBW THEN K1=I-HBW+1
9310 FOR K=K1 TO I-1
9330 IKK=K:JKK=I
9340 GOSUB 9670:AKI=KINV(KGLOBAL)
9360 IKK=K:JKK=K
9370 GOSUB 9670:AKK=KINV(KGLOBAL)
9380 SUM=SUM+AKI*Z(K)/AKK
9390 NEXT K
9400 Z(I)=Z(I)-SUM
9410 NEXT I
9440 ERASE R:DIM R(NEQ)
9450 IKK=NEQ:JKK=NEQ
9460 GOSUB 9670
9470 R(NEQ)=Z(NEQ)/KINV(KGLOBAL)
9480 FOR I=NEQ-1 TO 1 STEP -1
9490 SUM=0
9510 J2=NEQ
9520 IF J>HBW THEN J2=HBW+I-1
9530 IF J2>NEQ THEN J2=NEQ
9540 FOR J=I+1 TO J2
9560 IKK=I:JKK=J
9570 GOSUB 9670:AIJ=KINV(KGLOBAL)
9580 SUM=SUM+AIJ*R(J)
9590 NEXT J
9610 IKK=I:JKK=I
9620 GOSUB 9670:AII=KINV(KGLOBAL)
9630 R(I)=(Z(I)-SUM)/AII
9640 NEXT I
9650 RETURN
9660 REM ***************************************************
9670 REM SUBROUTINE, ADDRESSES IN GLOBAL VECTORS
9680 IF IKK>JKK THEN 9720
9690 IF JKK>HBW THEN 9710
9700 KGLOBAL=IKK+JKK*(JKK-1)/2:GOTO 9720
9710 KGLOBAL=HBW*(HBW+1)/2+(JKK-HBW-1)*HBW+IKK-(JKK-HBW)
9720 RETURN
9730 REM DATA STATEMENTS ***********************************
9731 REM SOLUTION TYPE (ELASTIC=0, INELASTIC=1)
```

```
9732 DATA 0
9740 REM CROSS-SECTIONAL DIMENSIONS
9750 DATA 353,128,10.7,6.5
9760 REM NUMBER OF MAIN DIFFERENT LONGITUDINAL DIVISIONS
9770 DATA 3
9772 REM NUMBER OF SUBDIVISIONS, SUBDIVIDING INTERVAL
9775 DATA 6,500
9776 DATA 7,1000
9777 DATA 3,500
9800 REM MATERIAL PROPERTIES
9810 DATA 2E5,300,0.3
9820 REM RESIDUAL STRESSES
9821 REM FLANGES
9822 DATA 200,100,40,20,10
9824 REM WEB
9826 DATA -180,-170,-130,-40,200
9840 REM LOADS AND REACTIONS DATA
9850 DATA 8
9852 DATA 1,-48.5625E3,30
9854 DATA 1,-48.5625E3,231.9
9866 DATA 5,139.617E3,-176.5
9868 DATA 8,-24.2813E3,231.9
9870 DATA 10,-24.2813E3,231.9
9872 DATA 12,-24.2813E3,231.9
9874 DATA 14,127.4765E3,-176.5
9876 DATA 17,-97.125E3,0
9880 REM BENDING MOMENT AT ONE LONGIUDINAL POINT
9890 DATA 1,0
9898 REM SHIFT, GAMMA0, GAMMA1
9899 DATA 0.2,0,0
9900 REM NODAL RESTRAINTS
9901 DATA 7
9902 data 2,0,1E7,0
9903 data 10,-1,0,0
9905 data 16,0,1E7,0
9906 data 20,0,1E7,0
9909 data 24,0,1E7,0
9912 DATA 27,-1,0,0
9915 DATA 28,-1,0,0
9923 REM GENERAL RESTRAINTS
9924 DATA 4
9926 DATA 2,55.35
9928 DATA 16,55.35
9930 DATA 20,55.35
9932 DATA 24,55.35
9980 REM INITIAL DISPLACEMENT EIGENVECTOR
9981 DATA 1
9985 DATA 1,1,0,0
10000 REM STIFFENERS
10010 DATA 1
10012 DATA 5,128,10
```

Appendix B

WORKED EXAMPLE

Consider the beam with two overhangs shown in Fig. B.1. The beam geometry, loading and restraint conditions are also shown in that Figure. The dimensions of the W360x39 cross section used as well as the residual stress distribution are given in Fig. B.2. The mesh idealization which was used is shown in Fig. B.3 where the longitudinal point numbers are indicated by circles and nodal point numbers are also given. For a quick approximate estimate of the buckling load, an elastic solution is sought with a small value of the shift. This solution is used afterwards to estimate the best values of shift, lower and upper bounds to be used with the inelastic solution.

B.1 Preliminary calculations to prepare input data

1. Determine the plastic moment from the nominal dimensions, neglecting the fillets:

The plastic modulus Z_x:

$$Z_x = bt(d-t) + \frac{(d-2t)^2 t_w}{4}$$

$$= 128\text{x}10.7(353 - 10.7) + \frac{(353 - 2\text{x}10.7)^2\text{x}6.5}{4} = 647.5\text{x}10^3 \text{ mm}^3$$

$$M_p = Z_x\ F_y = 647.5\text{x}10^3\text{x } 300 = 194.2\text{x}10^6 \text{N.mm}$$

2. The value of P corresponding to a maximum negative moment, which occurs at left column, equals to the plastic moment is:

$$P = \frac{M_p}{2 \times 2000} = \frac{194.2 \times 10^6}{2 \times 2000} = 48.56 \times 10^3 \text{ N}$$

3. For lateral restraint above the top flange:

The distance, hh, between the centroid or middle surface of top flange and the point of lateral restraint (within which a fictitious 2-node element is introduced).

hh = 50 + 5.35 = 55.35 mm

B.2 Input data

1. Solution type: SOLUT

SOLUT = 0 for elastic.

SOLUT = 1 for inelastic.

An elastic solution is chosen as a first trial:

DATA 0

An inelastic solution is chosen in the final trial:

DATA 1

2. Cross-sectional dimensions: D,B,T,W.

DATA 353,128,10.7,6.5

3. Mesh characteristics

Number of longitudinal main divisions:

DATA 3

For each main division, in a left-right order along the beam, a data statement is expressed containing the number of subdivisions and their regular spacing:

DATA 6,500

DATA 7,1000

DATA 3,500

4. Material properties: elastic modulus (ELMOD), yield stress (FY) and Poisson's ratio (NU).

DATA 2E5,300,0.3

5. Residual stresses:

Flange ($(\sigma_{rf})_1$, $(\sigma_{rf})_2$, $(\sigma_{rf})_3$, $(\sigma_{rf})_4$, $(\sigma_{rf})_5$):

DATA 200,100,40,20,10

WEB ($(\sigma_{rw})_1$, $(\sigma_{rw})_2$, $(\sigma_{rw})_3$, $(\sigma_{rw})_4$, $(\sigma_{rw})_5$):

DATA -180,-170,-130,-40,200

6. Loads and reactions:

Number of loads and reactions:

DATA 8

The longitudinal point number where the force is applied, the force (positive upwards and negative downwards) and the height of application of the force above or below the shear centre (positive above and negative below):

DATA 1,-48.5625E3,30

DATA 1,-48.5625E3,231.9

DATA 5,139.617E3,-176.5

DATA 8,-24.2813E3,231.9

DATA 10,-24.2813E3,231.9

DATA 12,-24.2813E3,231.9

DATA 14,127.4765E3,-176.5

DATA 17,-97.125E3,0

7. Bending moment at a selected longitudinal point:

Longitudinal point number, bending moment (positive if causing tension on the bottom flange and negative otherwise):

DATA 1,0

8. Shift, lower bound and upper bound.

An elastic solution is first sought with a relatively small shift. The chosen values for upper and lower bounds are unimportant

DATA 0.2,0,0

After obtaining a value of $M_{cr}/M_p = 0.77$ an inelastic solution is sought with the following data statement:

DATA 0.7,0.6,0.99

9. Nodal restraints:

Number of restrained points:

DATA 8

For each restrained node enter the node number, restraint against lateral deflection, restraint against twisting rotation and restraint against rotation about the vertical axis. A value of -1 implies a fixed restraint and a value of 0 implies no restraint. An elastic (partial) restraint is specified simply by entering the actual restraint stiffness. The lateral restraint above nodes 2, 16, 20 and 24 will be considered in the next data section "General restraint". It is important to exclude these lateral restraint acting above the nodal points at this stage. It can be assumed that the torsional rotation angles above the nodes have the same values at these nodes. The elastic restraints against twisting applied above nodes 2, 10, 20 and 24 will therefore be specified at these nodes:

```
DATA 2,0,1E7,0

DATA 9,0,-1,0

DATA 10,-1,0,0

DATA 16,0,1E7,0

DATA 20,0,1E7,0

DATA 24,0,1E7,0

DATA 27,-1,0,0

DATA 28,-1,0,0
```

10. General restraints

Number of points restrained above the top flange.

DATA 4

For each restrained point, enter the node number nearest that point and the height of lateral restraint above the middle surface of top flange.

DATA 2,55.35

DATA 16,55.35

DATA 20,55.35

DATA 24,55.35

11. Initial displacement vector:

Number of nodes at which displacements are specified:

DATA 1

For each node, enter the specified normalized values for the lateral displacement, the rotation about the longitudinal axis, and the rotation about the vertical axis:

DATA 1,1,0,0

12. Stiffeners:

Number of stiffeners:

DATA 1

For each stiffener, enter the longitudinal point number at which the stiffener is used, the width of the stiffener, and its thickness:

DATA 5,128,10

B.3 Output data

1. Normalized buckling displacements at all nodes, given in Fig. B.4.

2. M_{cr}/M_p, given as 0.8986 in Fig. B.5.

3. Normalized buckled shape, given in Fig. B.5.

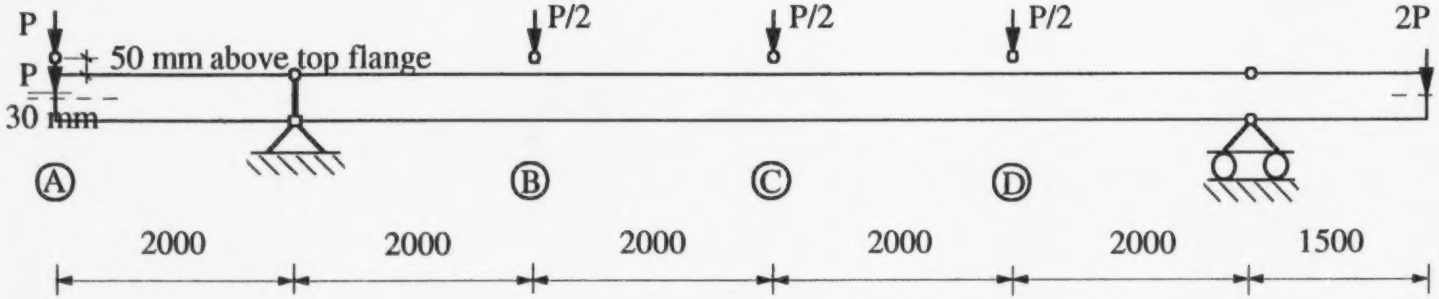
P
P
50 mm above top flange
30 mm
P/2
P/2
P/2
2P
Ⓐ
Ⓑ
Ⓒ
Ⓓ
2000
2000
2000
2000
2000
1500

Beam dimensions and loading configuration

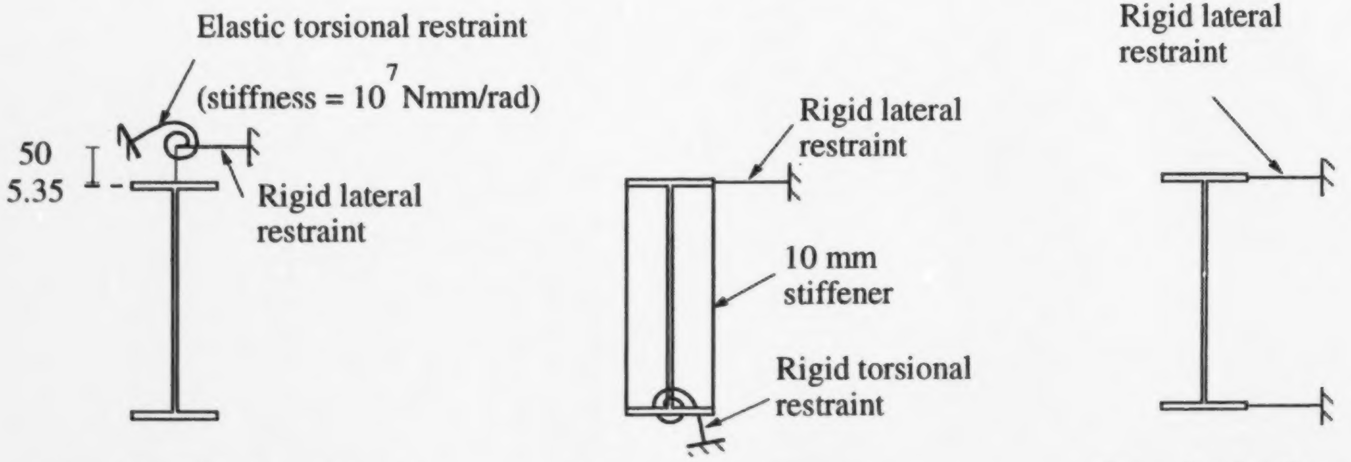
Elastic torsional restraint
(stiffness = 10^7 Nmm/rad)
50
5.35
Rigid lateral restraint
Rigid lateral restraint
10 mm stiffener
Rigid torsional restraint
Rigid lateral restraint

Restraint details at longitudinal points Ⓐ, Ⓑ, Ⓒ and Ⓓ

Restraint details at left support

Restraint details at right support

Fig. B.1 Beam with two overhangs

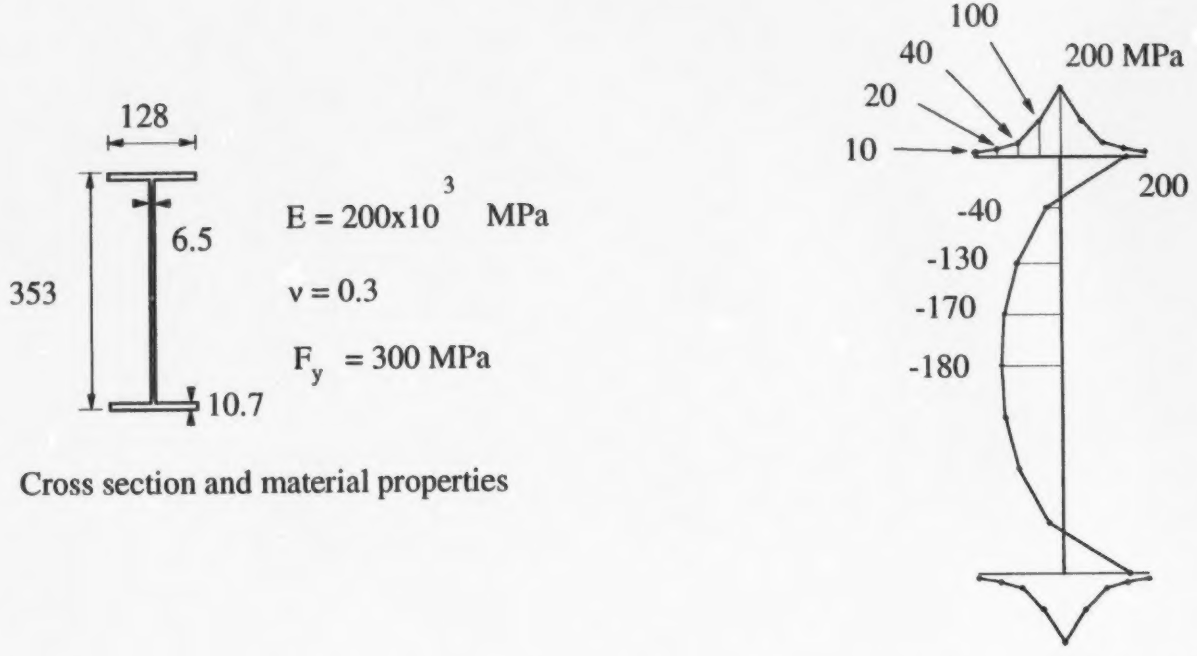
128
353
6.5
10.7
100
40
20
10
200 MPa
200
-40
-130
-170
-180

$E = 200\times10^{3}$ MPa

$\nu = 0.3$

$F_y = 300$ MPa

Cross section and material properties

Residual stress distribution

Fig. B.2 Cross-sectional dimensions, material properties and residual stresses

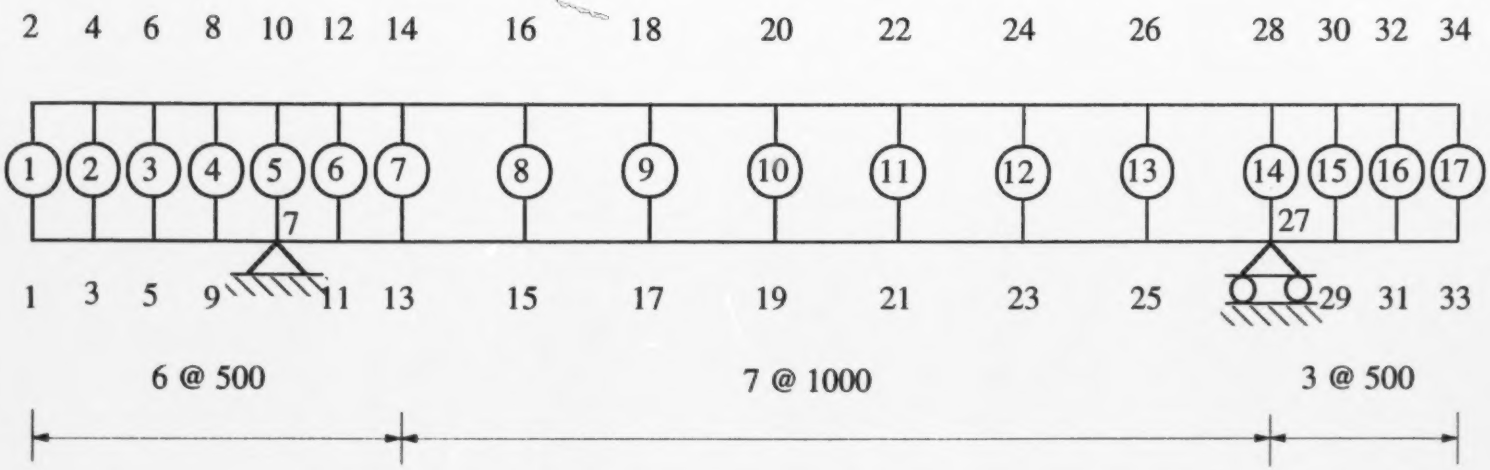
2 4 6 8 10 12 14 16 18 20 22 24 26 28 30 32 34
1 2 3 4 5 6 7 8 9 10 11 12 13 14 15 16 17
7
27
1 3 5 9 11 13 15 17 19 21 23 25 29 31 33
6 @ 500
7 @ 1000
3 @ 500

Fig. B.3 Mesh characteristics of worked example

```
INELASTIC SOLUTION:  Mcr = .8985937499999999 Mp

Normalized buckled shape

Node            Z               Theta-X           Theta-Y
-----------------------------------------------------------
  1        -7.27E-04          1.95E-06         -2.77E-07
  2        -6.71E-05          1.21E-06          3.51E-08
  3        -5.85E-04          1.57E-06         -2.99E-07
  4        -8.09E-05          1.36E-06          1.33E-08
  5        -4.22E-04          1.04E-06         -3.57E-07
  6        -7.63E-05          9.64E-07         -3.26E-08
  7        -2.26E-04          5.31E-07         -4.24E-07
  8        -4.87E-05          4.94E-07         -7.62E-08
  9         4.57E-07         -3.97E-15         -4.79E-07
 10        -4.06E-17         -2.04E-09         -1.23E-07
 11         2.33E-04         -5.38E-07         -4.39E-07
 12         5.32E-05         -5.17E-07         -3.78E-08
 13         4.32E-04         -1.07E-06         -3.50E-07
 14         6.79E-05         -1.03E-06         -2.16E-08
 15         6.77E-04         -1.82E-06         -1.41E-07

Press ENTER to continue ...?


 16         7.98E-05         -1.42E-06         -8.06E-09
 17         7.29E-04         -1.89E-06          2.65E-08
 18         8.54E-05         -1.88E-06          1.31E-09
 19         6.49E-04         -1.78E-06          1.17E-07
 20         7.62E-05         -1.37E-06          1.40E-08
 21         5.12E-04         -1.33E-06          1.55E-07
 22         6.02E-05         -1.34E-06          1.86E-08
 23         3.47E-04         -9.36E-07          1.73E-07
 24         4.19E-05         -7.48E-07          1.46E-08
 25         1.71E-04         -4.24E-07          1.77E-07
 26         2.90E-05         -4.22E-07          1.66E-08
 27         1.17E-17         -4.94E-09          1.58E-07
 28        -4.46E-17         -1.29E-08          4.47E-08
 29        -7.41E-05          1.39E-07          1.38E-07
 30        -2.58E-05          1.30E-07          5.56E-08
 31        -1.39E-04          2.48E-07          1.22E-07
 32        -5.39E-05          2.42E-07          5.59E-08
 33        -1.98E-04          3.11E-07          1.16E-07
 34        -8.14E-05          3.06E-07          5.46E-08
```

Fig. B.4 Normalized buckling displacements, predicted for the worked example

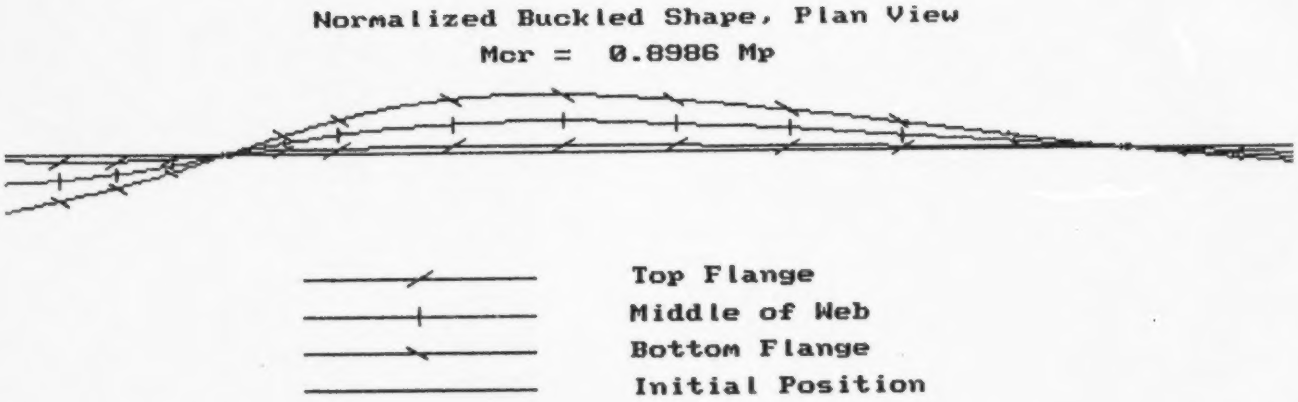

Fig. B.5 Normalized buckled shape, predicted for the worked example

Appendix C

BENDING STIFFNESS OF OPEN-WEB STEEL JOISTS

Fig. C.1 shows an open-web steel joist with a span length L and end panel length Lp. The top chord at both ends was assumed to extend a certain distance beyond the end of the the web member to account for the joist seat. This joist can be modelled as a beam with a moment of inertia I_1 for the central portion between end panels and a moment of inertia I_2, which is taken equal to that of the top chord member, for the end panel spans, as indicated in Fig. C.2. Applying an in-plane bending moment, M, at the end q, and assuming simply supported end conditions, the end rotation is given as

$$\text{[C.1]} \qquad \alpha_q = \frac{M}{3E I_1 L I_2}\left[I_1 L^2 - (I_1 - I_2)(L^2 - 3LL_p + 3L_p^2 - 2L_p^3/L)\right]$$

Because $I_1 >> I_2$ and $L >> L_p$, the expression for end rotation can be approximated as

$$\text{[C.2]} \qquad \alpha_q = \frac{M L_p}{E I_2}$$

Therefore, the in-plane bending stiffness of the open-web steel joist is obtained as

$$\text{[C.3]} \qquad K_B = \frac{M}{\alpha_q} = \frac{E I_2}{L_p}$$

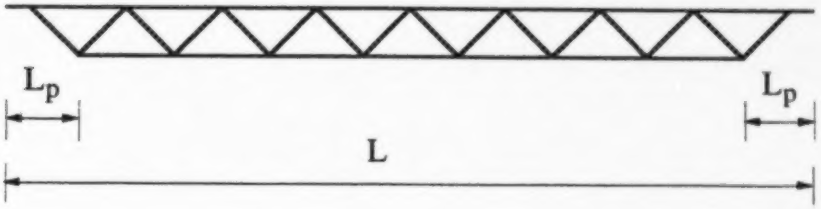

Fig. C.1 Open-web steel joist

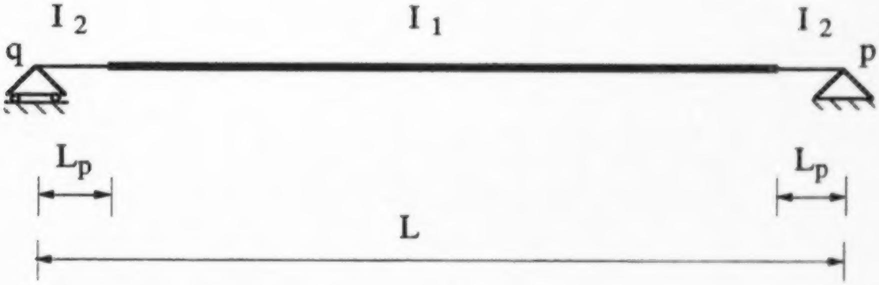

I_2
I_1
I_2
q
p
L_p
L_p
L

Fig. C.2 Equivalent beam model

Appendix D

The design procedures given in Chapter 7 for cantilever-suspended span beams are verified here for different cross sections under a variety of loading, geometry and restraint conditions. These verifications are given in Tables D.1, D.2, D.3 and D.4 for cases 1, 2 and 3 of beams with fork supports, and for the case of beams without fork supports, respectively. The yield stress and modulus of elasticity are taken as 300 MPa and 200000 MPa, respectively. The elastic values of M_{cr}/M_p are given in the tables for both the proposed design procedure and the finite element predictions. These elastic values were reduced according to the CSA standard CAN/CSA-S16.1-M89 (CSA 1989) using equation [7.26] to obtain the inelastic buckling capacities. The predicted/design ratios of the inelastic buckling capacities are given in the tables. The ratio P_1/P_2 shown on Tables D.2 and D.4 indicates the ratio of the load transferred to the cantilever tip from the suspended span, to the joist load applied at the top flange level within the cantilever span. It should be noted that the values of M_{cr} given in the tables refer to the maximum absolute moment along the beam.

Section	L, m	R	L_c/L	K_B	Elastic M_{cr}/M_p		Inelastic (S16.1)
				Nmm/rad.	Design	Predicted (FEM)	$\frac{\text{Predicted}}{\text{Design}}$
W310x39	6	0.6	0.25	6E7	3.097	3.285	1.00
W310x39	6	0.6	0.25	3E9	3.591	3.983	1.00
W310x39	6	1.0	0.25	3E9	4.062	4.917	1.00
W310x39	6	1.0	0.25	6E7	3.502	4.276	1.00
W310x39	6	1.6	0.25	6E7	3.713	5.454	1.00
W310x39	6	1.6	0.25	3E9	4.305	5.602	1.00
W310x39	6	1.6	0.17	3E9	6.398	6.501	1.00
W310x39	6	1.6	0.17	6E7	5.517	6.324	1.00
W310x39	6	1.0	0.17	6E7	4.720	5.018	1.00
W310x39	6	1.0	0.17	3E9	5.474	5.809	1.00
W310x39	6	0.6	0.17	3E9	4.044	4.291	1.00
W310x39	6	0.6	0.17	6E7	3.487	3.557	1.00
W310x39	9	1.0	0.17	6E7	4.540	4.162	1.00
W310x39	9	1.0	0.17	3E9	5.371	4.582	1.00
W310x39	9	1.0	0.25	3E9	3.410	3.633	1.00
W310x39	9	1.0	0.25	6E7	2.883	3.337	1.00

Table D.1 Verification of design procedure, Case 1

Section	L, m	R	L_c/L	K_B	Elastic M_{cr}/M_p		Inelastic (S16.1)
					Design	Predicted	$\frac{\text{Predicted}}{\text{Design}}$
				Nmm/rad.		(FEM)	
W360x39	9	0.6	0.25	6E7	1.787	1.673	0.99
W360x39	9	0.6	0.25	3E9	2.151	1.981	0.99
W360x39	9	1.0	0.25	3E9	2.432	2.379	1.00
W360x39	9	1.0	0.25	6E7	2.021	2.149	1.01
W360x39	9	1.6	0.25	6E7	2.143	2.475	1.00
W360x39	9	1.6	0.25	3E9	2.579	2.726	1.00
W360x39	9	1.6	0.17	3E9	3.831	3.753	1.00
W360x39	9	1.6	0.17	6E7	3.184	3.315	1.00
W360x39	9	1.0	0.17	6E7	2.724	2.702	1.00
W360x39	9	1.0	0.17	3E9	3.278	3.055	1.00
W360x39	9	0.6	0.17	3E9	2.422	2.261	1.00
W360x39	9	0.6	0.17	6E7	2.013	1.870	0.99
W360x39	9	0.6	0.17	1E15	2.420	2.272	1.00
W360x39	9	0.6	0.17	3E7	1.758	1.684	0.99
W360x39	9	0.6	0.25	3E7	1.563	1.514	0.99
W360x39	9	0.6	0.25	1E15	2.159	1.989	0.99

Table D.1 continued

Section	L, m	R	L_c/L	K_B	Elastic M_{cr}/M_p		Inelastic (S16.1)
				Nmm/rad.	Design	Predicted (FEM)	$\frac{\text{Predicted}}{\text{Design}}$
W410x39	9	0.6	0.17	6E7	1.670	1.663	1.00
W410x39	9	0.6	0.17	3E9	1.917	1.881	1.00
W410x39	9	1.0	0.17	3E9	2.595	2.786	1.00
W410x39	9	1.0	0.17	6E7	2.261	2.548	1.00
W410x39	9	1.6	0.17	6E7	2.642	3.057	1.00
W410x39	9	1.6	0.17	3E9	3.033	3.401	1.00
W410x39	9	1.6	0.25	3E9	2.041	2.545	1.01
W410x39	9	1.6	0.25	6E7	1.778	2.323	1.03
W410x39	9	1.0	0.25	6E7	1.678	2.039	1.04
W410x39	9	1.0	0.25	3E9	1.926	2.206	1.02
W410x39	9	0.6	0.25	3E9	1.703	1.678	1.00
W410x39	9	0.6	0.25	6E7	1.483	1.489	1.00
W410x39	10	1.0	0.17	1E15	2.440	2.835	1.00
W410x39	10	1.0	0.25	1E15	2.175	2.050	0.99
W410x39	10	1.0	0.25	3E7	1.410	1.704	1.04
W410x39	10	0.6	0.25	3E7	1.244	1.256	1.00

Table D.1 continued

Section	L, m	R	L_c/L	K_B Nmm/rad.	Elastic Design	M_{cr}/M_p Predicted (FEM)	Inelastic (S16.1) $\frac{\text{Predicted}}{\text{Design}}$
W410x39	7.5	0.6	0.25	3E7	1.484	1.711	1.03
W410x39	7.5	0.6	0.17	3E7	1.661	1.835	1.02
W410x39	7.5	0.6	0.17	1E15	2.130	2.184	1.00
W410x39	15	1.0	0.17	1E15	1.800	1.745	0.99
W460x74	12	0.6	0.25	6E7	1.718	1.721	1.00
W460x74	12	0.6	0.25	3E9	2.524	2.325	1.00
W460x74	12	1.0	0.25	3E9	2.855	2.853	1.00
W460x74	12	1.0	0.25	6E7	1.943	2.334	1.02
W460x74	12	1.6	0.25	6E7	2.060	2.628	1.01
W460x74	12	1.6	0.25	3E9	3.027	3.276	1.00
W460x74	12	1.6	0.17	3E9	4.497	4.470	1.00
W460x74	12	1.6	0.17	6E7	3.060	3.426	1.00
W460x74	12	1.0	0.17	6E7	2.618	2.864	1.00
W460x74	12	1.0	0.17	3E9	3.848	3.651	1.00
W460x74	12	0.6	0.17	3E9	2.843	2.639	1.00
W460x74	12	0.6	0.17	6E7	1.935	1.917	1.00

$n = 64$
$\mu = 1.002$
$V = 0.010$

Table D.1 continued

Section	L, m	R	L_c/L	P_1/P_2	K_B	Elastic M_{cr}/M_p		Inelastic (S16.1)
					Nmm/rad.	Design	Predicted (FEM)	Predicted / Design
W310x39	6	0.6	0.25	1	3E7	1.348	1.453	1.02
W310x39	6	1.0	0.25	1	3E7	1.543	1.577	1.01
W310x39	6	1.6	0.25	1	3E7	1.867	1.744	0.99
W310x39	9	0.6	0.25	1	3E8	1.808	1.803	1.00
W310x39	9	1.0	0.25	1	3E8	2.012	2.005	1.00
W310x39	9	1.6	0.25	1	3E8	2.286	2.133	1.00
W360x39	9	0.6	0.25	1	3E7	1.205	1.102	0.97
W360x39	9	1.0	0.25	1	3E7	1.331	1.253	0.98
W360x39	9	1.6	0.25	1	3E7	1.442	1.334	0.98
W360x39	6	0.6	0.25	1	3E7	1.128	1.180	1.01
W360x39	6	1.0	0.25	1	3E7	1.266	1.256	1.00
W360x39	6	1.6	0.25	1	3E7	1.463	1.357	0.98
W360x39	6	0.6	0.25	1	1E8	1.348	1.406	1.01
W410x39	12	1.6	0.25	2	3E9	1.241	1.367	1.03
W410x39	12	1.6	0.25	2	6E7	1.091	1.219	1.04
W410x39	12	1.6	0.17	1	6E7	1.091	1.134	1.01

Table D.2 Verification of design procedure, Case 2

Section	L, m	R	L_c/L	P_1/P_2	K_B Nmm/rad.	Elastic Design	M_{cr}/M_p Predicted (FEM)	Inelastic (S16.1) Predicted / Design
W410x39	9	0.6	0.25	1	3E7	0.814	0.888	1.04
W410x39	9	1.0	0.25	1	3E7	0.908	1.009	1.05
W410x39	9	1.6	0.25	1	3E7	1.036	1.058	1.01
W410x39	6	0.6	0.25	1	3E7	0.815	0.892	1.05
W410x39	6	1.0	0.25	1	3E7	0.933	0.971	1.02
W410x39	6	1.6	0.25	1	3E7	1.130	1.078	0.98
W410x39	12	0.6	0.25	1	6E7	0.906	0.967	1.03
W410x39	12	0.6	0.25	1	3E9	1.031	1.120	1.03
W410x39	12	0.6	0.25	2	3E9	1.031	1.157	1.04
W410x39	12	0.6	0.25	2	6E7	0.906	1.000	1.04
W410x39	12	1.0	0.25	2	6E7	0.989	1.114	1.04
W410x39	12	1.0	0.25	2	3E9	1.125	1.262	1.04
W410x39	12	1.0	0.25	1	3E9	1.125	1.207	1.02
W410x39	12	1.0	0.25	1	6E7	0.989	1.063	1.03
W410x39	12	1.6	0.25	1	6E7	1.091	1.151	1.02
W410x39	12	1.6	0.25	1	3E9	1.241	1.296	1.01

Table D.2 continued

Section	L, m	R	L_c/L	P_1/P_2	K_B Nmm/rad.	Elastic M_{cr}/M_p Design	Elastic M_{cr}/M_p Predicted (FEM)	Inelastic (S16.1) $\frac{\text{Predicted}}{\text{Design}}$
W410x39	12	1.6	0.17	1	3E9	1.241	1.277	1.01
W410x39	12	1.6	0.17	2	3E9	1.241	1.399	1.03
W410x39	12	1.6	0.17	2	6E7	1.091	1.239	1.04
W410x39	12	1.0	0.17	2	6E7	0.989	1.110	1.04
W410x39	12	1.0	0.17	2	3E9	1.125	1.269	1.04
W410x39	12	1.0	0.17	1	3E9	1.125	1.175	1.01
W410x39	12	1.0	0.17	1	6E7	0.989	1.032	1.02
W410x39	12	0.6	0.17	1	6E7	0.906	0.930	1.01
W410x39	12	0.6	0.17	1	3E9	1.031	1.084	1.02
W410x39	12	0.6	0.17	2	3E9	1.031	1.149	1.04
W410x39	12	0.6	0.17	2	6E7	0.906	0.983	1.04
W460x74	12	0.6	0.17	1	6E7	1.201	1.159	0.99
W460x74	12	0.6	0.17	1	3E9	1.765	1.613	0.98
W460x74	12	0.6	0.17	2	3E9	1.765	1.718	0.99
W460x74	12	0.6	0.17	2	6E7	1.201	1.223	1.01
W460x74	12	1.0	0.17	2	6E7	1.334	1.461	1.02

Table D.2 continued

Section	L, m	R	L_c/L	P_1/P_2	K_B	Elastic M_{cr}/M_p		Inelastic (S16.1)
					Nmm/rad.	Design	Predicted (FEM)	Predicted / Design
W460x74	12	1.0	0.17	2	3E9	1.961	1.936	1.00
W460x74	12	1.0	0.17	1	3E9	1.961	1.784	0.98
W460x74	12	1.0	0.17	1	6E7	1.334	1.353	1.00
W460x74	12	1.6	0.17	1	6E7	1.468	1.440	0.99
W460x74	12	1.6	0.17	1	3E9	2.157	1.953	0.99
W460x74	12	1.6	0.17	2	3E9	2.157	2.148	1.00
W460x74	12	1.6	0.17	2	6E7	1.468	1.569	1.02
W460x74	12	1.6	0.25	2	6E7	1.468	1.560	1.01
W460x74	12	1.6	0.25	2	3E9	2.157	2.137	1.00
W460x74	12	1.6	0.25	1	3E9	2.157	1.986	0.99
W460x74	12	1.6	0.25	1	6E7	1.468	1.446	1.00
W460x74	12	1.0	0.25	1	6E7	1.334	1.378	1.01
W460x74	12	1.0	0.25	1	3E9	1.961	1.849	0.99
W460x74	12	1.0	0.25	2	3E9	1.961	1.966	1.00
W460x74	12	1.0	0.25	2	6E7	1.334	1.474	1.03
W460x74	12	0.6	0.25	2	3E9	1.765	1.771	1.00

Table D.2 continued

Section	L, m	R	L_c/L	P_1/P_2	K_B Nmm/rad.	Elastic Design	M_{cr}/M_p Predicted (FEM)	Inelastic (S16.1) $\frac{\text{Predicted}}{\text{Design}}$
W460x74	12	0.6	0.25	2	6E7	1.201	1.261	1.01
W460x74	12	0.6	0.25	1	6E7	1.201	1.205	1.00
W460x74	12	0.6	0.25	1	3E9	1.765	1.692	0.99

$n = 67$
$\mu = 1.012$
$V = 0.020$

Table D.2 continued

Section	L, m	R	L_c/L	K_B Nmm/rad.	Elastic Design	M_{cr}/M_p Predicted (FEM)	Inelastic (S16.1) $\frac{\text{Predicted}}{\text{Design}}$
W310x39	6	0.6	0.25	6E7	1.665	1.646	1.00
W310x39	6	0.6	0.25	3E9	1.931	1.879	1.00
W310x39	6	0.6	0.17	6E7	1.876	1.855	1.00
W310x39	6	0.6	0.17	3E9	2.176	2.238	1.00
W310x39	6	1.0	0.17	6E7	2.171	2.058	0.99
W310x39	6	1.0	0.17	3E9	2.519	2.398	1.00
W310x39	6	1.0	0.25	6E7	1.760	1.756	1.00
W310x39	6	1.0	0.25	3E9	2.042	1.950	0.99
W310x39	6	1.6	0.25	6E7	1.863	1.893	1.00
W310x39	6	1.6	0.25	3E9	2.160	2.037	0.99
W310x39	6	1.6	0.17	3E9	2.800	2.601	1.00
W310x39	6	1.6	0.17	6E7	2.415	2.339	1.00
W310x39	9	1.0	0.17	6E7	1.691	1.771	1.01
W310x39	9	1.0	0.17	3E9	2.000	1.899	0.99
W310x39	9	1.0	0.25	3E9	1.554	1.413	0.98
W310x39	9	1.0	0.25	6E7	1.319	1.362	1.01

Table D.3 Verification of design procedure, Case 3

Section	L, m	R	L_c/L	K_B	Elastic	M_{cr}/M_p	Inelastic (S16.1)
				Nmm/rad.	Design	Predicted (FEM)	$\frac{\text{Predicted}}{\text{Design}}$
W360x39	6	0.6	0.25	6E7	1.114	1.258	1.04
W360x39	6	0.6	0.25	3E9	1.318	1.331	1.00
W360x39	6	0.6	0.17	3E9	1.632	1.576	0.99
W360x39	6	0.6	0.17	6E7	1.379	1.460	1.01
W360x39	6	1.0	0.17	6E7	1.569	1.581	1.00
W360x39	6	1.0	0.17	3E9	1.856	1.818	1.00
W360x39	6	1.0	0.25	3E9	1.395	1.422	1.01
W360x39	6	1.0	0.25	6E7	1.179	1.309	1.03
W360x39	6	1.6	0.25	6E7	1.216	1.374	1.04
W360x39	6	1.6	0.25	3E9	1.438	1.467	1.01
W360x39	6	1.6	0.17	3E9	2.002	1.943	0.99
W360x39	6	1.6	0.17	6E7	1.693	1.739	1.01
W360x39	9	1.0	0.17	6E7	1.196	1.250	1.01
W360x39	9	1.0	0.17	3E9	1.439	1.344	0.98
W360x39	9	1.0	0.25	3E9	1.035	0.999	0.99
W360x39	9	1.0	0.25	6E7	0.860	0.964	1.05

Table D.3 continued

Section	L, m	R	L_c/L	K_B	Elastic M_{cr}/M_p		Inelastic (S16.1)
				Nmm/rad.	Design	Predicted (FEM)	Predicted / Design
W410x39	8	0.6	0.25	6E7	0.812	0.839	1.02
W410x39	8	0.6	0.25	3E9	0.933	0.885	0.98
W410x39	8	0.6	0.17	3E9	1.146	1.097	0.98
W410x39	8	0.6	0.17	6E7	0.997	1.005	1.00
W410x39	8	1.0	0.17	6E7	1.143	1.166	1.01
W410x39	8	1.0	0.17	3E9	1.314	1.264	0.99
W410x39	8	1.0	0.25	3E9	0.992	0.941	0.98
W410x39	8	1.0	0.25	6E7	0.863	0.899	1.02
W410x39	8	1.6	0.25	6E7	0.889	0.926	1.02
W410x39	8	1.6	0.25	3E9	1.022	0.972	0.98
W410x39	8	1.6	0.17	3E9	1.412	1.357	0.99
W410x39	8	1.6	0.17	6E7	1.228	1.246	1.00
W410x39	12	1.0	0.25	6E7	0.596	0.617	1.04
W410x39	12	1.0	0.25	3E9	0.678	0.635	0.94
W410x39	12	1.0	0.16	3E9	0.939	0.891	0.98
W410x39	12	1.0	0.16	6E7	0.826	0.841	1.01

Table D.3 continued

Section	L, m	R	L_c/L	K_B	Elastic M_{cr}/M_p		Inelastic (S16.1)
				Nmm/rad.	Design	Predicted (FEM)	$\frac{\text{Predicted}}{\text{Design}}$
W460x74	12	1.0	0.17	3E8	1.542	1.518	1.00
W460x74	12	1.0	0.17	3E9	1.709	1.582	1.00
W460x74	12	1.0	0.25	3E9	1.240	1.177	0.98
W460x74	12	1.0	0.25	3E8	1.119	1.153	1.01
W460x74	12	0.6	0.17	3E8	1.436	1.374	0.99
W460x74	12	0.6	0.17	3E9	1.590	1.465	0.98
W460x74	12	0.6	0.25	3E8	1.089	1.109	1.01
W460x74	12	0.6	0.25	3E9	1.206	1.144	0.98
W460x74	12	1.6	0.17	3E8	1.657	1.634	1.00
W460x74	12	1.6	0.17	3E9	1.836	1.691	0.98
W460x74	12	1.6	0.25	3E9	1.271	1.210	0.99
W460x74	12	1.6	0.25	3E8	1.147	1.190	1.01

$n = 60$
$\mu = 1.000$
$V = 0.018$

Table D.3 continued

Section	L, m	R	L_c/L	P_1/P_2	K_B	Elastic M_{cr}/M_p		Inelastic (S16.1)
					Nmm/rad.	Design	Predicted (FEM)	$\frac{\text{Predicted}}{\text{Design}}$
W310x39	7.2	1.5	0.17	1	3E7	0.663	0.686	1.03
W310x39	7.2	1.5	0.17	1	3E9	0.875	0.967	1.04
W310x39	7.2	4.0	0.17	1	3E9	1.521	1.803	1.04
W310x39	7.2	4.0	0.17	1	3E7	1.152	1.257	1.03
W310x39	9.6	1.5	0.17	1	3E7	0.842	0.819	0.99
W310x39	9.6	1.5	0.17	1	3E9	1.116	1.123	1.00
W310x39	9.6	4.0	0.17	1	3E9	2.004	2.169	1.01
W310x39	9.6	4.0	0.17	1	3E7	1.512	1.545	1.01
W360x39	5.4	1.5	0.17	1	3E7	0.545	0.497	0.91
W360x39	5.4	1.5	0.17	1	3E9	0.721	0.719	1.00
W360x39	5.4	4.0	0.17	1	3E9	1.254	1.329	1.02
W360x39	5.4	4.0	0.17	1	3E7	0.810	0.888	0.97
W360x39	7.2	1.5	0.17	1	3E7	0.695	0.601	0.87
W360x39	7.2	1.5	0.17	1	3E9	0.940	0.851	0.96
W360x39	7.2	4.0	0.17	1	3E9	1.689	1.629	0.99
W360x39	7.2	4.0	0.17	1	3E7	1.248	1.104	0.96

Table D.4 Verification of design procedure, Beams without fork supports

Section	L, m	R	L_c/L	P_1/P_2	K_B Nmm/rad.	Elastic M_{cr}/M_p Design	Elastic M_{cr}/M_p Predicted (FEM)	Inelastic (S16.1) Predicted/Design
W410x39	14.91	1.5	0.17	1	3E7	0.612	0.604	0.99
W410x39	14.91	4.0	0.17	1	3E7	1.167	1.221	1.01
W410x39	9.94	1.5	0.17	1	3E7	0.479	0.496	1.04
W410x39	9.94	4.0	0.17	1	3E7	0.861	0.939	1.04
W410x39	9.94	4.0	0.17	1	3E9	1.074	1.287	1.07
W410x39	9.94	1.5	0.17	1	3E9	0.598	0.657	1.10
W410x39	9.94	1.5	0.25	1	3E9	0.598	0.708	1.16
W410x39	9.94	1.5	0.25	1	3E7	0.479	0.533	1.11
W410x39	9.94	4.0	0.25	1	3E7	0.861	0.996	0.96
W410x39	9.94	4.0	0.25	1	3E9	1.074	1.377	1.08
W410x39	9.94	1.5	0.17	2	3E7	0.479	0.524	1.09
W410x39	9.94	1.5	0.17	2	3E9	0.598	0.689	1.14
W250x39	6.27	1.5	0.17	1	3E7	1.295	1.128	0.96
W250x39	6.27	1.5	0.17	1	3E9	1.875	1.698	0.98
W250x39	6.27	4.0	0.17	1	3E9	3.366	3.225	1.00
W250x39	6.27	4.0	0.17	1	3E7	2.325	2.046	0.99

Table D.4 continued

Section	L, m	R	L_c/L	P_1/P_2	K_B Nmm/rad.	Elastic M_{cr}/M_p Design	Predicted (FEM)	Inelastic (S16.1) $\frac{\text{Predicted}}{\text{Design}}$
W410x39	12	1.5	0.25	1	3E7	0.556	0.574	1.03
W410x39	12	1.5	0.25	1	3E9	0.685	0.746	1.06
W410x39	12	1.5	0.25	2	3E9	0.685	0.760	1.07
W410x39	12	1.5	0.25	2	3E7	0.556	0.589	1.06
W410x39	12	1.5	0.17	1	3E7	0.556	0.549	0.99
W410x39	12	1.5	0.17	1	3E9	0.685	0.708	1.02
W410x39	12	1.5	0.17	2	3E9	0.685	0.731	1.04
W410x39	12	1.5	0.17	2	3E7	0.556	0.572	1.03
W410x39	12	4.0	0.17	1	3E7	1.015	1.072	1.02
W410x39	12	4.0	0.17	1	3E9	1.251	1.436	1.04
W410x39	12	4.0	0.17	2	3E9	1.251	1.471	1.04
W410x39	12	4.0	0.17	2	3E7	1.015	1.103	1.03
W410x39	12	4.0	0.25	1	3E7	1.015	1.121	1.04
W410x39	12	4.0	0.25	1	3E9	1.251	1.516	1.05
W410x39	12	4.0	0.25	2	3E9	1.251	1.541	1.05
W410x39	12	4.0	0.25	2	3E7	1.015	1.146	1.04

Table D.4 continued

Section	L, m	R	L_c/L	P_1/P_2	K_B Nmm/rad.	Elastic M_{cr}/M_p		Inelastic (S16.1)
						Design	Predicted (FEM)	$\frac{\text{Predicted}}{\text{Design}}$
W460x74	12	1.5	0.25	1	3E7	0.664	0.649	0.98
W460x74	12	1.5	0.25	1	3E9	1.158	1.117	0.99
W460x74	12	1.5	0.25	2	3E9	1.158	1.149	1.00
W460x74	12	1.5	0.25	2	3E7	0.664	0.680	1.02
W460x74	12	1.5	0.17	1	3E7	0.664	0.606	0.91
W460x74	12	1.5	0.17	1	3E9	1.158	1.048	0.97
W460x74	12	1.5	0.17	2	3E9	1.158	1.093	0.98
W460x74	12	1.5	0.17	2	3E7	0.664	0.643	0.97
W460x74	12	4.0	0.17	1	3E7	1.211	1.095	0.97
W460x74	12	4.0	0.17	1	3E9	2.112	2.062	1.00
W460x74	12	4.0	0.17	2	3E9	2.112	2.122	1.00
W460x74	12	4.0	0.17	2	3E7	1.211	1.134	0.98
W460x74	12	4.0	0.25	1	3E7	1.211	1.152	0.98
W460x74	12	4.0	0.25	1	3E9	2.112	2.184	1.00
W460x74	12	4.0	0.25	2	3E9	2.112	2.234	1.00
W460x74	12	4.0	0.25	2	3E7	1.211	1.188	0.99

Table D.4 continued

Section	L, m	R	L_c/L	P_1/P_2	K_B Nmm/rad.	Elastic Design	M_{cr}/M_p Predicted (FEM)	Inelastic (S16.1) $\frac{\text{Predicted}}{\text{Design}}$
W610x241	12	1.5	0.17	1	3E7	0.808	0.607	0.81
W610x241	12	1.5	0.17	1	3E9	1.926	1.659	0.97

$n = 66$
$\mu = 1.010$
$V = 0.055$

Table D.4 continued